

# ENABLING LOW VOLTAGE GRID VISIBILITY TO DETECT SAFETY HAZARDS

by

**Jacques Willem Wattel**



*Thesis presented in fulfilment of the requirements for the degree  
Master of Engineering (Research) in the Faculty of Engineering*

*at Stellenbosch University*

UNIVERSITEIT  
iYUNIVESITHI  
STELLENBOSCH  
UNIVERSITY

100

1918 · 2018

Supervisor: Dr. Johan Beukes

Co-Supervisor: Prof H. du T. Mouton

Department of Electrical & Electronic Engineering

**March 2017**

## **Declaration**

By submitting this thesis electronically I declare that the entirety of the work contained therein is my own, original work, that I am the sole author thereof (save to the extent explicitly otherwise stated), that reproduction and publication thereof by Stellenbosch University will not infringe any third party rights and that I have not previously in its entirety or in part submitted it for obtaining any qualification.

March 2018

J. Wattel

## Acknowledgements

I would like to thank my study leader and mentor Dr. Johan Beukes for allowing me to learn from his vast experience as an engineer. Thank you for the continual support and guidance during this project.

I would like to thank my co-supervisor Prof. Toit Mouton for all his patience and support over the years that I have had the opportunity to know him. Thank you for all the great memories and the cakes in the office, it will never be forgotten.

I would like to thank Dr. Males Tomlinson for his contribution, advice and guidance during this project.

I would like to thank my parents, Peter and Geer Wattel, for their continual support during my student years and all the sacrifices that they have made for me to be able to do this work.

I would like to thank all my Stellenbosch engineering friends who made this road so much easier, including but not restricted to: Wernich Raats, Cornel Verster, Pieter van der Lugt and Mariet Venter.

## Abstract

The low voltage (LV) network poses various hazards to humans and animals. In rural and deep rural areas the risk of electrocution and fire hazard is augmented, largely due to overhead conductors being used and illegal connections, with fatalities occurring each year on South Africa's rural networks. The aim of this thesis is to investigate the possibility of detecting such hazards by employing smart meters and smart grid infrastructure.

Four main hazard categories were identified as having the highest likelihood to the loss of life on Eskom's rural LV distribution network. The hazards include:

1. PEN conductor failure.
2. LV earth electrode conductor high impedance failure.
3. Unaccounted current flow.
4. Earth leakage protection not operational.

A model of each hazard is discussed and a possible detection method is proposed. An experimental setup of an LV feeder was built to verify the feasibility of the proposed detection methods. Experimental smart meters from Texas Instruments with ZigBee capabilities were installed at each customer installation and at the MV/LV transformer. The meters send measurement data to a data concentrator. The data concentrator was used to capture, store, manage and visualize data gathered from the smart meters. The thesis covers the hardware and software development that was done on the smart meters and data concentrator.

Hazards were imposed on the experimental network to simulate each hazardous condition and the associated detection methods were evaluated.

Lastly, the concept to monitor the feeder loop impedance using smart meters is introduced which provides an additional hazard detection parameter, providing an indication of the overall 'health' of a feeder. Experimental results showed that the feeder loop could successfully be measured using smart meters.

## Abstrak

Die laespanningnetwerk hou verskeie gevare in vir mense en diere. Die gevare is verhoog in landelike en diep landelike gebiede a.g.v hoofsaaklik oorhoofse geleiers wat gebruik word en die groot hoeveelheid onwettige konneksies. Elke jaar word verkseie sterftes vermeld a.g.v die gevare. Die hoof doel van die navorsing is om te bepaal of die gevare suksesvol bespeur kan word met die gebruik van slim meters en die slim kragnetwerk infrastruktuur.

Vier hoof gevaar kategorieë was geïdentifiseer wat die hoogste gevaar inhou op Eskom se landelike laespanningnetwerke. Die gevare sluit die volgende in:

1. Breek van die PEN geleier.
2. Laespannings aardelektrode hoë impedansie fout.
3. Onverklaarde stroomvloei.
4. Aardlek beskerming buitewerking.

'n Model van elke gevaar is bespreek en 'n moontlike deteksie metode is voorgestel. 'n Experimentele opstelling van 'n laespanningvoerder was gebou om die lewensvatbaarheid van die deteksie metodes te verifieer. Experimentele slim meters van Texas Instruments met ZigBee kommunikasie was geïnstaleer by elke kliënt se installasie en by die transformator. Die meters stuur meting data na 'n data konsentrator wat die data stoor, verwerk en vertoon op 'n webblad. Die tesis behandel die hardeware en sagteware ontwerp van die slim meters en data konsentrator.

Die geïdentifiseerde gevare was geïnduseer op die experimentele netwerk om die deteksie metodes te evalueer met behulp van die slim meters en data konsentrator.

Laastens, is die konsep om die voerder impedansie met behulp van slim meters te bepaal, voorgestel. Dit bied 'n addisionele gevaar deteksie parameter wat 'n goeie beraming gee van die algehele 'gesondheid' van 'n voerder. Eksperimentele resultate het gewys dat die voerder impedansie suksesvol bepaal kan word met die slim meters.

# Contents

<b>DECLARATION .....</b>	<b>II</b>
<b>ACKNOWLEDGEMENTS .....</b>	<b>III</b>
<b>ABSTRACT .....</b>	<b>IV</b>
<b>ABSTRAK .....</b>	<b>V</b>
<b>CONTENTS.....</b>	<b>VI</b>
<b>LIST OF TABLES.....</b>	<b>XI</b>
<b>LIST OF FIGURES .....</b>	<b>XII</b>
<b>PUBLICATIONS .....</b>	<b>XVII</b>
<b>LIST OF ACRONYMS AND ABBREVIATIONS .....</b>	<b>XVIII</b>
<b>CHAPTER 1 INTRODUCTION .....</b>	<b>1</b>
1.1. BACKGROUND.....	1
1.2. THESIS STRUCTURE .....	2
<b>CHAPTER 2 HAZARD IDENTIFICATION ON THE RURAL LV NETWORK .....</b>	<b>4</b>
2.1. INTRODUCTION .....	4
2.2. OVERVIEW OF THE RURAL LV NETWORK IN SOUTH AFRICA.....	4
2.3. LV EARTHING SCHEMES .....	6
2.3.1. <i>IEC system earthing identification code</i> .....	6
2.3.2. <i>LV earthing arrangements in South Africa</i> .....	7
2.3.3. <i>Earthing requirements for TN-C-S system</i> .....	8
2.4. REPRESENTATION OF HAZARDS ON THE LV NETWORK DIAGRAM .....	9
2.4.1. <i>Identified LV hazards</i> .....	10
2.5. HAZARD MODEL DEVELOPMENT .....	11
2.5.1. <i>PEN conductor failure</i> .....	11
2.5.2. <i>LV earth electrode conductor high impedance failure</i> .....	13
2.5.3. <i>Unaccounted current flow</i> .....	14
2.5.4. <i>Earth leakage protection not operational</i> .....	17
2.6. HAZARD DETECTION MECHANISMS.....	18
2.6.1. <i>PEN conductor failure</i> .....	20
2.6.2. <i>Transformer LV earth electrode conductor high impedance failure</i> .....	23
2.6.3. <i>Unaccounted current flow</i> .....	24
2.6.4. <i>Earth leakage protection not operational</i> .....	25
2.7. CONCLUSION .....	26

<b>CHAPTER 3 SMART METER OVERVIEW AND COMPONENTS .....</b>	<b>27</b>
3.1. INTRODUCTION .....	27
3.2. SMART GRID OVERVIEW .....	27
3.3. SMART METERING DEVELOPMENT IN ESKOM .....	28
3.3.1. <i>Eskom standard for smart metering architecture and communication protocols</i> .....	29
3.4. COMMUNICATION TECHNOLOGY ON LV FEEDERS .....	31
3.4.1. <i>G3- PLC specification</i> .....	31
3.4.2. <i>ZigBee specification</i> .....	32
3.5. CONCLUSION .....	36
<b>CHAPTER 4 SMART METER HARDWARE DEVELOPMENT .....</b>	<b>37</b>
4.1. INTRODUCTION .....	37
4.2. TEXAS INSTRUMENTS SMART METER OVERVIEW .....	37
4.3. SYSTEM DIAGRAMS.....	38
4.3.1. <i>High-level interface</i> .....	39
4.4. MEASUREMENT CIRCUITRY .....	40
4.4.1. <i>Voltage measurements</i> .....	41
4.4.2. <i>Current measurements</i> .....	41
4.5. CONNECTIONS TO A TEST SETUP .....	43
4.6. GPS MODULE .....	44
4.7. LCD DISPLAY .....	44
4.8. VIEW METER READINGS ON A PC .....	46
4.9. METER CALIBRATION .....	47
4.9.1. <i>Voltage and current gain calibration:</i> .....	48
4.9.2. <i>Active power gain calibration</i> .....	49
4.9.3. <i>Phase correction calibration</i> .....	49
4.10. METER ACCURACY .....	50
4.11. CONCLUSION .....	51
<b>CHAPTER 5 SMART METER SOFTWARE DEVELOPMENT .....</b>	<b>52</b>
5.1. INTRODUCTION .....	52
5.2. CODE COMPOSER STUDIO DEVELOPMENT ENVIRONMENT .....	52
5.2.1. <i>Overview</i> .....	52
5.2.2. <i>Setting up the project in CCS</i> .....	53
5.3. SOFTWARE DEVELOPMENT .....	54
5.3.1. <i>Overview</i> .....	54
5.3.2. <i>Foreground process</i> .....	54
5.3.3. <i>Background process</i> .....	59
5.3.4. <i>GPS interrupt service routine state machine</i> .....	63

5.3.5.	<i>ZigBee communications management</i> .....	68
5.4.	TEXAS INSTRUMENTS CC2530-ZNP IMPLEMENTATION .....	72
5.4.1.	<i>CC2530 evaluation module</i> .....	72
5.4.2.	<i>CC2530-ZNP physical interface</i> .....	73
5.4.3.	<i>SPI configuration</i> .....	74
5.4.4.	<i>Flashing CC2530EM with new firmware</i> .....	75
5.5.	CONCLUSION .....	75
<b>CHAPTER 6 DATA CONCENTRATOR HARDWARE DEVELOPMENT.....</b>		<b>77</b>
6.1.	INTRODUCTION .....	77
6.2.	HIGH-LEVEL OVERVIEW .....	77
6.3.	HARDWARE DESIGN .....	79
6.3.1.	<i>Computer module</i> .....	79
6.3.2.	<i>Power circuitry</i> .....	81
6.3.3.	<i>USB to UART expansion and ethernet</i> .....	82
6.3.4.	<i>USB boot circuitry</i> .....	83
6.3.5.	<i>XBee ZigBee radio</i> .....	85
6.3.6.	<i>GSM/GPRS module</i> .....	88
6.3.7.	<i>GPS module/ Real-time clock (RTC)</i> .....	93
6.3.8.	<i>Standard Raspberry Pi header</i> .....	94
6.3.9.	<i>RS-232 interface</i> .....	95
6.3.10.	<i>CAN bus</i> .....	96
6.3.11.	<i>PCB design</i> .....	97
6.4.	CONCLUSION .....	98
<b>CHAPTER 7 DATA CONCENTRATOR SOFTWARE DEVELOPMENT .....</b>		<b>99</b>
7.1.	INTRODUCTION .....	99
7.2.	COMPUTER MODULE LINUX FLASH PROCEDURE.....	99
7.2.1.	<i>Linux terminal steps used to flash the eMMC over USB from a Linux PC</i> .....	100
7.3.	REMOTE CONNECTION TO DATA CONCENTRATOR.....	100
7.3.1.	<i>SSH connection to data concentrator</i> .....	100
7.3.2.	<i>FTP connection to data concentrator</i> .....	101
7.4.	XBEE MODEM .....	101
7.4.1.	<i>XCTU</i> .....	102
7.4.2.	<i>XBee AT commands</i> .....	103
7.4.3.	<i>API protocol</i> .....	104
7.4.4.	<i>Python XBee library</i> .....	107
7.5.	SQLITE .....	108
7.5.1.	<i>SQLite overview</i> .....	108
7.5.2.	<i>Data concentrator SQL database</i> .....	108

7.6.	PYTHON SCRIPTS .....	109
7.6.1.	<i>The Python programming language</i> .....	110
7.6.2.	<i>Python Script to receive data frames</i> .....	110
7.6.3.	<i>Python script to determine unaccounted current flow</i> .....	112
7.6.4.	<i>PEN conductor failure Python script</i> .....	113
7.6.5.	<i>Transformer LV earth electrode failure Python script</i> .....	115
7.6.6.	<i>Meter watchdog Python script</i> .....	116
7.7.	THE LV SAFETY WEB INTERFACE .....	117
7.7.1.	<i>Common gateway interface (CGI)</i> .....	117
7.7.2.	<i>Apache web server</i> .....	118
7.7.3.	<i>The web interface</i> .....	119
7.7.4.	<i>Hosting the website on the internet</i> .....	120
7.8.	CONCLUSION .....	122
<b>CHAPTER 8 PRACTICAL SETUP AND EXPERIMENTAL RESULTS .....</b>		<b>123</b>
8.1.	INTRODUCTION .....	123
8.2.	EXPERIMENTAL SETUP .....	123
8.3.	PEN CONDUCTOR FAILURE .....	127
8.3.1.	<i>Prepaid meter: alternative solution</i> .....	127
8.3.2.	<i>Smart meter proposed solution</i> .....	129
8.4.	LV EARTH ELECTRODE CONDUCTOR HIGH IMPEDANCE FAILURE .....	132
8.5.	UNACCOUNTED CURRENT FLOW .....	135
8.6.	EARTH LEAKAGE PROTECTION NOT OPERATIONAL .....	137
<b>CHAPTER 9 PERMANENT LOOP IMPEDANCE ASSESSMENT AND EXPERIMENTAL RESULTS .....</b>		<b>138</b>
9.1.	INTRODUCTION .....	138
9.2.	LOOP IMPEDANCE CALCULATION USING COMPLETE FEEDER CURRENT AND VOLTAGE MEASUREMENTS 138	
9.3.	LOOP IMPEDANCE CALCULATION USING CURRENT AND VOLTAGE CHANGES AT METERS .....	139
9.3.1.	<i>Mathematical Proof</i> .....	141
9.4.	LOOP IMPEDANCE CALCULATION ERRORS AND SIMULATION RESULTS .....	143
9.5.	LOOP IMPEDANCE SOFTWARE IMPLEMENTATION .....	148
9.6.	PRACTICAL LOOP IMPEDANCE MEASUREMENTS .....	149
9.6.1.	<i>Actual feeder loop impedance</i> .....	150
9.7.	FEEDER LOOP IMPEDANCE EXPERIMENTAL RESULTS .....	151
9.7.1.	<i>Experimental results - Single switching load</i> .....	151
9.7.2.	<i>Experimental results - Multiple switching loads</i> .....	156
9.8.	CONCLUSION .....	162

<b>CHAPTER 10 CONCLUSIONS</b> .....	<b>164</b>
10.1. CONCLUSION .....	<b>ERROR! BOOKMARK NOT DEFINED.</b>
10.2. FUTURE WORK.....	165
<b>REFERENCES</b> .....	<b>166</b>
<b>APPENDIX A. GPS NMEA DATA</b> .....	<b>171</b>
A.1 BACKGROUND.....	171
A.2 NMEA MESSAGE SENTENCES .....	171
A.3 HARDWARE INTERFACE .....	171
A.4 NMEA MESSAGE DATA STRUCTURE .....	172
A.5 NMEA MESSAGE EXAMPLE .....	172
<b>APPENDIX B. SCHEMATICS OF TEXAS INSTRUMENTS SMART METER</b> .....	<b>173</b>

## List of tables

Table 1: Maximum permissible LV system earth resistance values.....	9
Table 2: Smart Grid communication levels.....	28
Table 3: ZigBee OSI Model [25].....	33
Table 4: GPS connection to smart meter .....	44
Table 5: Displayed parameters [28] .....	45
Table 6: Meter current measurement accuracy.....	50
Table 7: Meter voltage measurement accuracy .....	51
Table 8: Measurement message header structure .....	71
Table 9: Measurement message body .....	71
Table 10: GPS location message header.....	71
Table 11: GPS location message body .....	71
Table 12: MSP430F67791a to CC2530-ZNP interconnect.....	73
Table 13: Data concentrator communication interfaces .....	79
Table 14: Communication interfaces on Raspberry Pi computer module and model B+ .....	81
Table 15: Comparison between XBee Series 1 and Series 2 [49].....	86
Table 16: Associate LED status [49] .....	88
Table 17: Signals of the SIM interface [50] .....	92
Table 18: Standard Raspberry Pi Header [54] .....	95
Table 19: Basic API frame structure [49].....	105
Table 20: Commonly used API mode frame types [49] .....	106
Table 21: API format for AT commands [49] .....	106
Table 22: Key SQLite commands [60] .....	108
Table 23: Data concentrator SQLite database tables .....	109
Table 24: Commonly used NMEA Data Types.....	171

## List of figures

Figure 1: Example of a low population density, rural electrification installation with an overhead MV spur and single-phase LV feeder (near Tsolo, Eastern Cape, South Africa) .....	5
Figure 2: Typical rural electrical distribution network for rural electrification .....	5
Figure 3: TN-S system: Single-phase customer connection from a three-phase feeder .....	7
Figure 4: TN-C-S system: Single-phase customer connection from a three-phase feeder .....	8
Figure 5: Simplified diagram showing the main components in a typical LV network .....	9
Figure 6: Typical Eskom LV network with hazards indicated .....	10
Figure 7: Typical Eskom LV network with updated hazard locations .....	11
Figure 8: Circuit representing broken PEN conductor failure.....	12
Figure 9: Circuit representing LV earth electrode conductor high impedance failure .....	13
Figure 10: Stolen LV earth electrode conductor of a pole top transformer.....	14
Figure 11: Circuit representing phase conductor exposed and reachable from earth .....	15
Figure 12: Circuit representing PEN conductor short-circuited with phase conductor without line protection.....	16
Figure 13: Circuit representing phase conductor and PEN conductor exposed and reachable hazard .....	17
Figure 14: Circuit representing earth leakage protection not operational.....	18
Figure 15: Circuit showing the smart meters installed at the transformer and a customer .....	19
Figure 16: PEN conductor failure model for a single-phase customer connection with the prepaid meter solution .....	23
Figure 17: NRS 049 AMI Architecture [19] .....	29
Figure 18: Eskom open standard & protocols layout [20] .....	30
Figure 19: Typical ZigBee mesh network with the three device types .....	34
Figure 20: Top view of the three phase EVM with components highlighted [28].....	38
Figure 21: Typical per-phase connections of an electricity meter [28] .....	39
Figure 22: 3-Phases 4-wire star connection using MSP430F67791a MCU [28] .....	40
Figure 23: Voltage inputs analog front end [28].....	41
Figure 24: Current transformers of the meter [28] .....	42
Figure 25: Current inputs analog front end [28].....	42
Figure 26: Top View of the EVM showing the voltage input terminals [28] .....	43
Figure 27: Front View of the EVM showing the three phase current input terminals [28].....	43
Figure 28: LCD display of smart meter [28].....	45
Figure 29: GUI configuration file – changing the com port [28].....	46
Figure 30: GUI window [28] .....	47
Figure 31: Results window [28].....	47
Figure 32: Calibration factors window [28] .....	48

Figure 33: Manual calibration window [28] .....	49
Figure 34: Project folder .....	53
Figure 35: E-meter software main foreground process .....	56
Figure 36: E-meter software background process [28].....	60
Figure 37: Zero-crossing detection for frequency measurement [28] .....	62
Figure 38: Flow diagram for energy indicator pulse generation [28].....	63
Figure 39: GPS interrupt service routine state machine .....	65
Figure 40: GPS message start state .....	66
Figure 41: GPS data state .....	67
Figure 42: GPS checksum state .....	67
Figure 43: GPS message end state .....	68
Figure 44: Software flow diagram for the ZigBee communications manager.....	69
Figure 45: CC2530EM [33] .....	72
Figure 46: CC2530 interface.....	73
Figure 47: SPI initialization code using the EUSCI_B interface.....	75
Figure 48: CC-Debugger with SoC-battery board and CC2530EM [39].....	75
Figure 49: Data concentrator block diagram .....	78
Figure 50: Raspberry PI computer module [42].....	80
Figure 51: Conventional Raspberry PI model B+ [43] .....	80
Figure 52: Computer Module I/O Board [44] .....	81
Figure 53: Dual channel DC-DC step-down converter .....	82
Figure 54: USB to UART interface .....	83
Figure 55: FSUSB42 analogue symbol [47] .....	84
Figure 56: USB selection switch .....	84
Figure 57: USB boot enable.....	85
Figure 58: Digi-International XBee pro series 2B ZigBee module [49].....	87
Figure 59: Schematic representation of XBee pro series 2B for the data concentrator.....	87
Figure 60: LP3856-ADJ typical application [50].....	89
Figure 61: ESR curve for output capacitor (with 10uF tantalum input capacitor) [50] .....	90
Figure 62: TC63i GSM/GPRS Module [50] .....	91
Figure 63: TC63i U.FL-R-SMT antenna connector [50].....	91
Figure 64: TC63i integration clip [50] .....	91
Figure 65: UART voltage conversion .....	92
Figure 66: 2.9 V linear regulator.....	93
Figure 67: Adafruit GPS module with integrated real-time clock [53].....	93
Figure 68: RS-232 MAX3232E line driver .....	96
Figure 69: MCP25625 CAN controller with integrated transceiver.....	97
Figure 70: Completed data concentrator board.....	98

Figure 71: XBee explorer adapter [58] .....	102
Figure 72: XCTU software interface [59] .....	103
Figure 73: Python script to receive and store measurements .....	112
Figure 74: Python script to calculate unaccounted current flow .....	113
Figure 75: Python script to capture values required to detect a single-phase PEN conductor failure .....	114
Figure 76: Python script to capture values required to detect a dual phase PEN conductor failure .....	115
Figure 77: Python script to capture values required to detect a transformer LV earth electrode failure .....	116
Figure 78: Meter watchdog Python script .....	117
Figure 79: CGI architecture diagram .....	118
Figure 80: LV Safety web interface .....	120
Figure 81: NAT operation .....	121
Figure 82: LV lab model schematic – single-phase system .....	124
Figure 83: LV lab model schematic – dual phase system .....	125
Figure 84: Lab experimental setup with a 1:1 dual or single-phase isolation transformer supplying three customers .....	126
Figure 85: Lab experimental setup showing single customer installation .....	126
Figure 86: Diagram of the single-phase experimental setup .....	128
Figure 87: Single phase system experimental results ( $VM1$ top and $VH$ bottom) .....	128
Figure 88: Diagram of the dual-phase experimental setup .....	129
Figure 89: Dual phase system experimental results ( $VM1$ top and $VM2$ bottom) .....	129
Figure 90: Single-phase system experimental results .....	131
Figure 91: Dual phase system experimental results .....	132
Figure 92: Experimental setup used for LV earth electrode high impedance failure .....	132
Figure 93: Transformer secondary live current and transformer LV earth electrode current .....	134
Figure 94: Ratio between transformer live current and transformer LV earth electrode current .....	134
Figure 95: Experimental Setup used for phase conductor and PEN conductor exposed and reachable .....	135
Figure 96: Transformer live current and current unbalance .....	136
Figure 97: Percentage current unbalance .....	136
Figure 98: Line diagram illustrating the complete measurement technique .....	139
Figure 99: Graphical representation of delta current calculation .....	140
Figure 100: Graphical representation of delta current calculation ignoring the sample in which the switching event falls .....	141
Figure 101: Mathematical representation .....	142
Figure 102: Simple circuit model to illustrate measurement error .....	143

Figure 103: Norton equivalent circuit of simple circuit model in Figure 102 .....	143
Figure 104: Reduces simplified circuit model with $Z_L$ removed .....	144
Figure 105: Phasor diagrams illustrating the simplified measurement technique .....	145
Figure 106: Power Factory single-line diagram to simulate the current and voltage change technique.....	146
Figure 107: Power Factory outputs for calculating the impedance from current and voltage changes at meter 4.....	147
Figure 108: Power Factory outputs for calculating the loop impedance from current and voltage changes at meter 4 with damaged conductor.....	148
Figure 109: Loop impedance calculation flow diagram.....	149
Figure 110: Experimental setup used to evaluate network impedance.....	150
Figure 111: Voltage and current change used to calculate impedance of experimental feeder	150
Figure 112: Line impedance of $10\ \Omega$ ( $Z_{L3}$ ) switched out and in of the feeder with a constant load of $0.43\ \text{A}$ and a switching load of $4.78\ \text{A}$ .....	152
Figure 113: Line impedance of $1\ \Omega$ ( $Z_{L2}$ ) switched in and out of the feeder with a constant load of $0.43\ \text{A}$ and a switching load of $4.78\ \text{A}$ .....	153
Figure 114: Line impedance increased in steps of approximately $1\ \Omega$ ( $Z_{L3}$ ) with a constant load of $0.43\ \text{A}$ and a switched load of $4.78\ \text{A}$ .....	154
Figure 115: Line impedance of $1\ \Omega$ ( $Z_{L2}$ ) switched in and out of the feeder with a constant load of $4.4\ \text{A}$ and a switched load of $4.78\ \text{A}$ .....	154
Figure 116: Line impedance of $1\ \Omega$ ( $Z_{L2}$ ) switched in and out of the feeder with a constant load of $4.4\ \text{A}$ and a switched load of $0.7\ \text{A}$ .....	155
Figure 117: Line impedance of $1\ \Omega$ ( $Z_{L2}$ ) switched in and out of the feeder with a constant load of $4.4\ \text{A}$ and a switched load of $0.3\ \text{A}$ .....	155
Figure 118: Impedance measured with $Z_{2s}$ switching at 4 second intervals and $Z_{1s}$ switching at 20 second intervals.....	157
Figure 119: Impedance measured with $Z_{2s}$ switching at 4 second intervals and $Z_{1s}$ switching at 20 second intervals.....	158
Figure 120: Impedance measured with loads $Z_{2s}$ and $Z_{1s}$ switching at random intervals between 5 and 15 seconds .....	159
Figure 121: Statistical representation of impedance data in Figure 120. 64% of the data measured lies between $1.8\ \Omega$ and $2\ \Omega$ .....	160
Figure 122: Impedance measured with loads $Z_{2s}$ and $Z_{1s}$ switching at random intervals between 5 and 15 seconds. Line impedance $Z_{L2}$ was switched in to the feeder .....	161
Figure 123: Statistical representation of impedance data in Figure 122. As expected most data points lie around $1.9\ \Omega$ and $2.9\ \Omega$ .....	162
Figure 124: Smart Meter Schematics (1 of 4) [28].....	173

Figure 125: Smart Meter Schematics (2 of 4) [28].....	174
Figure 126: Smart Meter Schematics (3 of 4) [28].....	175
Figure 127: Smart Meter Schematics (4 of 4) [28].....	176
Figure 128: Data Concentrator Schematics (1 of 7) .....	177
Figure 129: Data Concentrator Schematics (2 of 7) .....	178
Figure 130: Data Concentrator Schematics (3 of 7) .....	179
Figure 131: Data Concentrator Schematics (4 of 7) .....	180
Figure 132: Data Concentrator Schematics (5 of 7) .....	181
Figure 133: Data Concentrator Schematics (6 of 7) .....	182
Figure 134: Data Concentrator Schematics (7 of 7) .....	183

## Publications

### Conference papers

- J.W. Wattel, D.M. Tomlinson, J. Beukes, “*Possible Solutions to the Loss of Neutral in Low Voltage Rural Networks in South Africa*”, 2016 SAUPEC
- J.W. Wattel, D.M. Tomlinson, J. Beukes, T. Mouton “*Enabling Low Voltage Visibility to Detect Hazards on Rural Distribution Networks*”, 2017 UPEC Greece

## List of acronyms and abbreviations

ABC	Aerial Bundled Conductor
AC	Alternating Current
ACD	Appliance Control Device
ADC	Analogue-to-Digital Converter
AMI	Advance Metering Infrastructure
CIU	Customer Interface Unit
CPOC	Customer Point of Connection
CPU	Central Processing Unit
DC	Direct Current
DNP3	Distributed Network Protocol v.3
DNS	Domain Name System
DDNS	Dynamic Domain Name System
EVM	Evaluation Module
G3-PLC	Third Generation Power Line Communication
GPRS	General Packet Radio Service
GPS	Global Positioning System
HAN	Home Area Network
HRC	High Rupturing Capacity
IP	Internet Protocol
ISP	Internet Service Provider
Kbps	Kilobits per second
KBps	Kilobytes per second
kW	Kilowatts
LCD	Liquid Crystal Display
LV	Low Voltage
Mbps	Megabits per second
MBps	Megabytes per second

MDMS	Meter Data Management System
MHz	Megahertz
MV	Medium Voltage
N	Neutral
NAN	Neighbourhood Area network
NAT	Network Address Translation
NECRT	Neutral Earthing Compensators with Resistors and Auxiliary Transformers
NMEA	National Marine Electronics Association
OS	Operating System
OSI	Open System Interconnection
PAN	Personal Area Network
PE	Protective Earth
PEN	Protective Earth Neutral
PME	Protective Multiple Earthing
PLC	Power Line Communication
RCD	Residual Current Device
RF	Radio Frequency
SOC	System on Chip
SSH	Secure Shell
T-N-S	Terra Neutral Separate
T-N-CS	Terra Neutral Combined Separate
TI	Texas Instruments
UART	Universal Asynchronous Receiver/Transmitter
USB	Universal Serial Bus
VPN	Virtual Private Network
WAN	Wide Area Network

# CHAPTER 1

## INTRODUCTION

### 1.1. BACKGROUND

Smart Metering and Smart Grid is an ever-evolving field and the number of smart meters being installed is increasing rapidly. This thesis examines the possibility to use these technologies to identify hazards on the low voltage (LV) network.

“In general, a hazard is a situation that poses a level of threat to life, health, property, and environment. Most hazards are dormant or potential, with only a theoretical risk of harm; however, once a hazard becomes active, it can create an emergency situation. A hazardous situation that has come to pass is called an incident. Hazard and possibility interact together to create risk” [1].

Most of the hazards on the low voltage networks are currently undetectable with the typical protection mechanisms that Eskom employs on such installations.

The objective of hazard risk management on LV networks is to report the hazard rather than the incident. Traditionally hazard report mechanisms on these networks have been limited to overcurrent protection at the transformer and at the pole-top boxes. The accumulation of small leakage currents does not allow for the management of residual current devices implemented on LV networks before the point of supply using traditional technology.

In this project, smart meters with ZigBee radio frequency (RF) communication capabilities will be located at the LV side of the medium voltage (MV) to LV transformer and at the customer. By having these metering points, it will be possible to detect various hazards. Four hazard categories have been found prominent on Eskom’s network, each hazard is discussed with a model of the hazard, and possible detection methods are proposed and evaluated.

The measurement data sent from the various smart meters is received by a data concentrator via a ZigBee RF link. The data received is stored, processed and display graphically on a web interface. This thesis covers the development done on the smart meter and the data concentrator, covering the hardware and software of each.

Lastly, a new capability is introduced which allows the smart meter to measure the loop impedance from the customer to the MV/LV transformer. The concept to measure the loop impedance of a feeder using a smart meter has not been introduced in literature. It provides an additional measurement to detect a possible deteriorating or broken neutral or live conductor.

## 1.2. THESIS STRUCTURE

This thesis is structured as follows:

- Chapter 2 start with background on the earthing schemes used in South Africa. An Eskom working group identified nine hazards by analysing fault and fatality reports. These nine hazards were further reduced to three hazard categories. Hazards originating from the medium voltage grid were excluded from this study. The hazards identified are illustrated schematically and discussed in this chapter. A possible detection method for each hazard is also discussed. The detection methods make use of smart meters with ZigBee communication located at the customer and a smart meter located at the MV/LV transformer.
- Chapter 3 gives an overview of the smart grid and its various components focusing on third generation power line communication (G3-PLC) and ZigBee RF.
- Chapter 4 covers the hardware of the Texas Instrument smart meter used in this project. The specifications and capabilities of the meter is discussed and the hardware changes required for this project.
- Chapter 5 covers the software development done on the meter. The meters were supplied with source code developed in TI's proprietary IAR workbench. The code was ported to code composer studio as it is open source. The software did not incorporate the required code to send data using the add-on ZigBee modem. It was added and is also discussed in this chapter.
- Chapter 6 gives a detailed overview of the data concentrator that was designed and built. A data concentrator was required to capture the measurements sent over ZigBee from the meters. The data concentrator was designed around a Linux computer module. Various communication mediums were added, some only for future use. Finally, the printed circuit board (PCB) was designed and populated.
- Chapter 7 covers the data concentrator's software development. Python was used as the primary programming language of choice. Python scripts were written to receive, store and analyse the data. A web server, hosted on the data concentrator was also developed to provide a graphical presentation of the data received.
- Chapter 8 finally shows a model LV feeder that was built to experimentally evaluate the system, with three smart meters located at three simulated customers connections and a meter located at a transformer. This chapter continues with experimental results obtained for each fault condition.
- Chapter 9 presents the concept of using the smart meters to measure the LV feeder loop impedance, for the detection of a deteriorating live or neutral conductor. The developed meter software is discussed and experimental results are shown for various

cases. The idea to measure the loop impedance originated towards the end of this project, therefore it is written as a standalone chapter.

## **CHAPTER 2**

### **HAZARD IDENTIFICATION ON THE RURAL LV NETWORK**

#### **2.1. INTRODUCTION**

Most of the hazards on the low voltage network are currently undetectable with the protection systems that Eskom and municipalities employ. These hazards can only be detected once they become active and create an emergency situation.

This chapter presents the reader with an overview of the rural LV network typically used in South Africa and the different types of earthing schemes. It is followed by the representation of the various hazards that might exist on an Eskom LV network. Each hazard is discussed and a possible detection method is proposed.

#### **2.2. OVERVIEW OF THE RURAL LV NETWORK IN SOUTH AFRICA**

In 2015, 85.3% of households in South Africa had access to electricity of which about 12% (6.4 million) lived in rural areas [2]. This is the result of the South African government's electrification programme for universal access to electricity that aims to provide electricity to even the most remote parts of the country. As such, these areas are often sparsely populated as shown in Figure 1.

The typical rural distribution network topology for residential electrification consists of a three-phase medium voltage (MV) backbone feeder with dual-phase MV spurs that branch off. These MV feeders can sometimes stretch for hundreds of kilometres to reach deep-rural settlements. Eskom uses 22 kV system technology primarily for new network installations in rural areas, as well as 11 kV technology in older urban environments. The use of 33 kV on the MV networks is seen in rare cases. Earthing through neutral earthing compensators with resistors and auxiliary transformers (NECRT) are used for earth fault protection on MV feeders, which limit the earth fault current nominally to 350 A [3].

The LV network typically consists of single or dual-phase MV/LV transformers with bare-wire or aerial-bundled-conductor (ABC) overhead LV feeders. Single-phase concentric cables (airDac) are used as service cable between the pole top box and the customer's point of supply. A depiction of a rural distribution network is shown in Figure 2. Three-phase MV/LV transformers are not commonly used for the electrification of deep-rural settlements due to the very low population density and as such, only single and dual phase transformers will be assessed in this report.



Figure 1: Example of a low population density, rural electrification installation with an overhead MV spur and single-phase LV feeder (near Tsolo, Eastern Cape, South Africa)

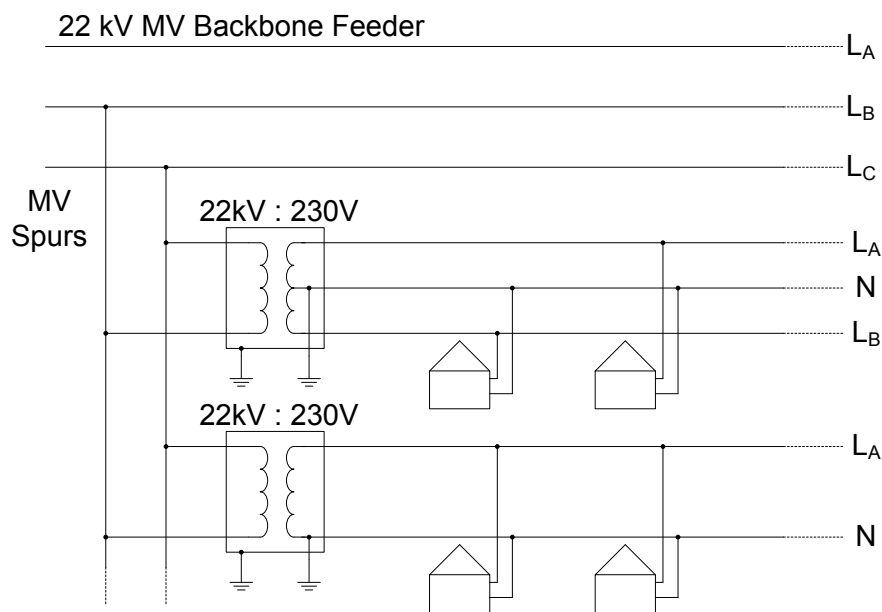


Figure 2: Typical rural electrical distribution network for rural electrification

On Eskom's network, the LV system is earthed per South African national standard (SANS) 10292 [4] (Code of Practice for the Earthing of LV Distribution Systems). Earth electrodes with maximum earth impedance values of  $30 \Omega$  and  $70 \Omega$  for the LV and MV side of the transformer respectively, should be used.

## 2.3. LV EARTHING SCHEMES

An understanding of the LV earthing schemes used in South Africa is necessary to identify the possible hazards that can be present on the LV network.

### 2.3.1. IEC system earthing identification code

The international standard IEC 60364-1 [5] is used to specify two letter codes to identify various types of earthing schemes. These identification codes have been adopted by SANS 10292 [4] for local use. It also defines three families of earthing arrangements. The following rules govern the use of letter codes:

- The first letter indicates how the source side usually at the transformer, is earthed.
- The second letter indicates how the device side at the customer, is earthed.

The letters used in this standard are as follows:

**T – Terra** – French word for Earth. It means a direct connection of a point to earth.

**I – Isolation** – It means that no point is connected to earth or connection is through a high impedance.

**N – Neutral** – Earth connection is supplied from the source side via the network, either as a separate protective earth (PE) or as a combination with the neutral known as the protective earth neutral (PEN) conductor.

There are three families proposed by IEC based on a combination of the above letters:

- Terra Neutral (TN)
- Terra Terra (TT)
- Isolation Terra (IT)

The TN earthing scheme is subdivided further depending on the arrangement of the neutral and protective conductors. This subdivision is denoted by further letters:

**C – Combined** - Neutral and protective functions on the LV distributor and in the consumer's installation are combined in a single conductor.

**S – Separate** – Neutral and protective functions on the LV distributor and in the consumer's installation are separate conductors.

**C-S – Combined-Separate** – Neutral and protective functions on the LV distributor are combined in a single conductor and separated in the customer's installation.

The three subdivisions of TN networks are:

- Terra Neutral Separate (TN-S)
- Terra Neutral Combined (TN-C)

- Terra Neutral Combined-Separate (TN-C-S)

### 2.3.2. LV earthing arrangements in South Africa

The South African national standard (SANS) 10292 [4] governs the earthing schemes of LV networks in South Africa, which advocates the application of TN-C-S or TN-S earthing systems.

#### 2.3.2.1. *TN-S system*

The TN-S system uses two separate conductors for the PE and N which are connected and solidly earthed at the MV/LV transformer. Although widely implemented in South-Africa the TN-S system is no longer used for rural electrification where overhead conductors are used, due to the cost of having the additional PE conductor over long distances. Eskom and municipalities are still using this system on their cable networks, with the outer armouring of the cable used as the PE conductor. Another disadvantage of this system is that a broken PE conductor may go unnoticed until an earth fault occurs, at which the earth fault protection will not operate. Figure 3 shows the TN-S system for a single-phase customer from a three-phase feeder.

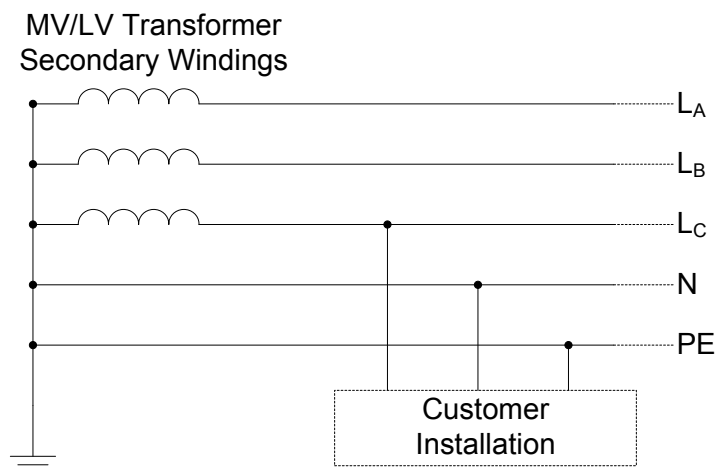


Figure 3: TN-S system: Single-phase customer connection from a three-phase feeder

#### 2.3.2.2. *TN-C-S system*

The TN-C-S system combines the PE and N conductors into a single PEN conductor. At the MV/LV transformer, the single PEN conductor is connected to the LV neutral and is earthed with an earth electrode. At the customer's point of connection, before the earth leakage protection device, the PEN conductor is split into separate N and PE conductors. Figure 4 shows a TN-C-S system with a single-phase customer connection from a three-phase feeder. For dual and single-phase feeders, the earthing topology will remain the same. Eskom and many municipalities in South-Africa have standardised on the TN-C-S earthing scheme for all new overhead electrification installations. The integrity of the PEN conductor is of vital importance in this system as dangerous voltages might appear on the supply earth terminal

and thus on metal earthed appliances. This aspect will be further explored later in this chapter and thesis.

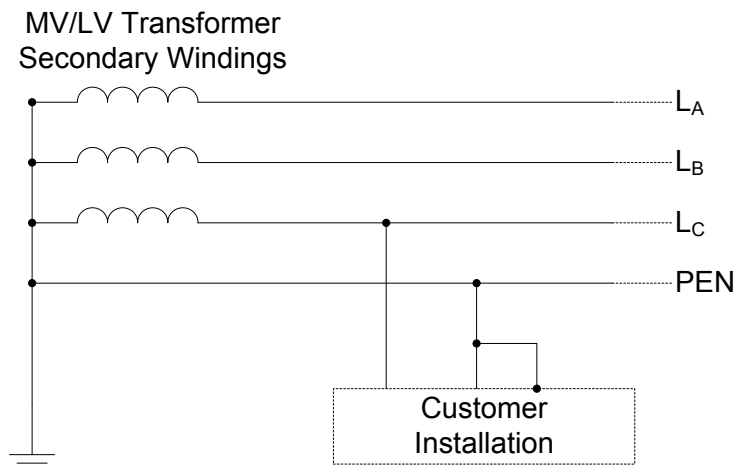


Figure 4: TN-C-S system: Single-phase customer connection from a three-phase feeder

### 2.3.3. Earthing requirements for TN-C-S system

The following is a summary of the earthing requirements for a TN-C-S system as specified in SANS 10292 [4]:

- The source transformer shall always be earthed to ensure an earth return path back to the supply. The design of the transformer earth is based on results from soil resistivity tests.
- The source MV/LV transformer earthing may be combined, provided that the medium-voltage source resistance does not exceed 3  $\Omega$ .
- In most cases the overall resistance exceeds 3  $\Omega$  in which case the MV equipment earth electrode and the LV neutral earth electrode shall be kept separate. A suitably rated surge arrester should be installed between the transformer tank (which is connected to MV earth) and LV neutral to prevent an overvoltage insulation breakdown between the MV and LV windings of the transformer.
- The LV neutral earth electrode should be at least 5 m from the MV earth electrode.
- With separate earth electrodes, the total resistance of the LV source earth should be such that in the event of breakdown between MV and LV transformer windings, the MV protection will operate. To achieve this condition, the earth resistance values in Table 1 should be attempted. Eskom should ensure that the main earth fault protection would operate in the event of an insulation breakdown between the medium-voltage and low-voltage sides.

Table 1: Maximum permissible LV system earth resistance values

Transformer Primary Voltage (kV)	LV Earth Resistance Value ( $\Omega$ )
6.6	15
11	30
22	70

- All metalwork that is accessible from ground level and that forms part of the LV distributor external to the substation, shall be bonded to the distributor PEN conductor.

#### 2.4. REPRESENTATION OF HAZARDS ON THE LV NETWORK DIAGRAM

Figure 5 shows the main components of a typical LV network as used by Eskom for rural electrification. Earthing is provided to customers by means of the TN-C-S system. As discussed in section 2.3.2.2 the system makes use of a combined PEN conductor up to the service connection panel. The cable is split into a PE and N conductor for sensitive earth fault protection by means of an earth leakage device, also known as a residual current device (RCD), set to 30 mA trip level. The RCD will trip if an unbalance, greater than 30 mA, between the net Live (L) and N conductor current is detected. This breaker also provides over current protection of 20 A.

Surge arrestors between the live conductor and transformer tank (connected via MV earth to ground) are used to provide a return path back to earth under overvoltage conditions. A surge arrester is installed between the MV and LV earth electrodes to prevent overvoltage insulation breakdown between the MV and LV windings of the transformer under overvoltage conditions.

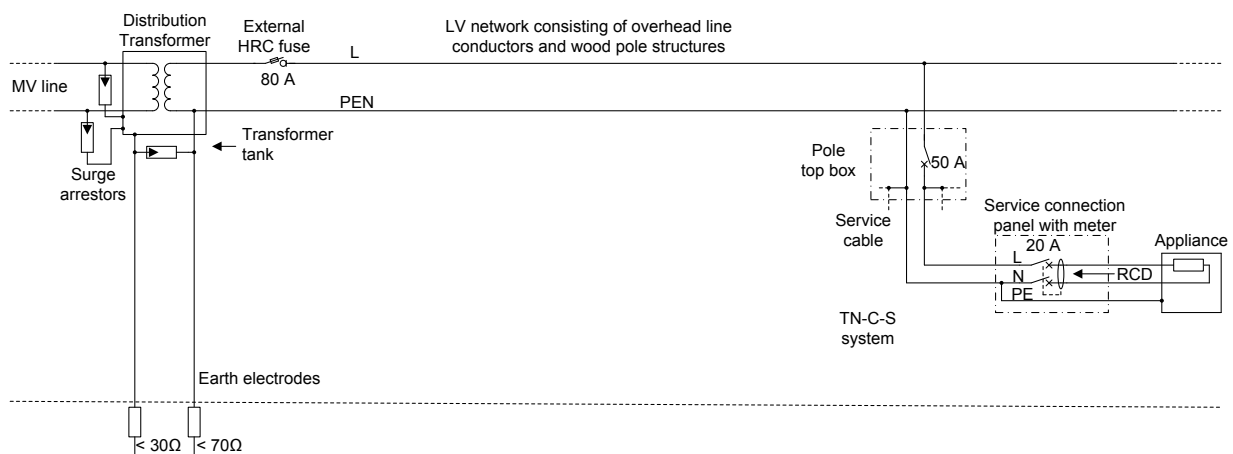


Figure 5: Simplified diagram showing the main components in a typical LV network

Pole mounted service distribution boxes are used to tap from the LV overhead conductor. The pole top box is fitted with 50 A miniature circuit breakers (MCB) on all of Eskom's networks as

specified in Eskom's Distribution Specification – Part 8 [6]. The specification states that the breaker should be DIN rail mounted and rated at 230 V with a short circuit breaking capacity of 5 kA.

High rupturing capacity (HRC) fuses are installed on the LV side of the transformer as shown in Figure 5 to provide overcurrent protection. HRC fuses can carry short circuit current for a certain period before it blows [7]. It allows for a fault condition to clear itself in a certain time frame. All LV HRC fuses on the Eskom distribution network must comply with the requirements of SANS 60269-2 [8].

#### 2.4.1. Identified LV hazards

An investigation was done by an Eskom working group into the causes of fatalities on the Eskom LV network. Nine hazards were identified with the highest occurrence and fatality rate. These hazards, as presented in Figure 6, are as follows:

1. Phase conductor and transformer tank short-circuited
2. MV earth and LV earth conductors short-circuited
3. LV earth electrode conductor high impedance failure
4. PEN conductor high impedance failure
5. Phase conductor exposed and reachable from earth
6. PEN conductor short-circuited with phase conductor without line protection
7. Phase conductor and PEN conductor exposed and reachable
8. Earth leakage protection not operational
9. MV to LV short circuit

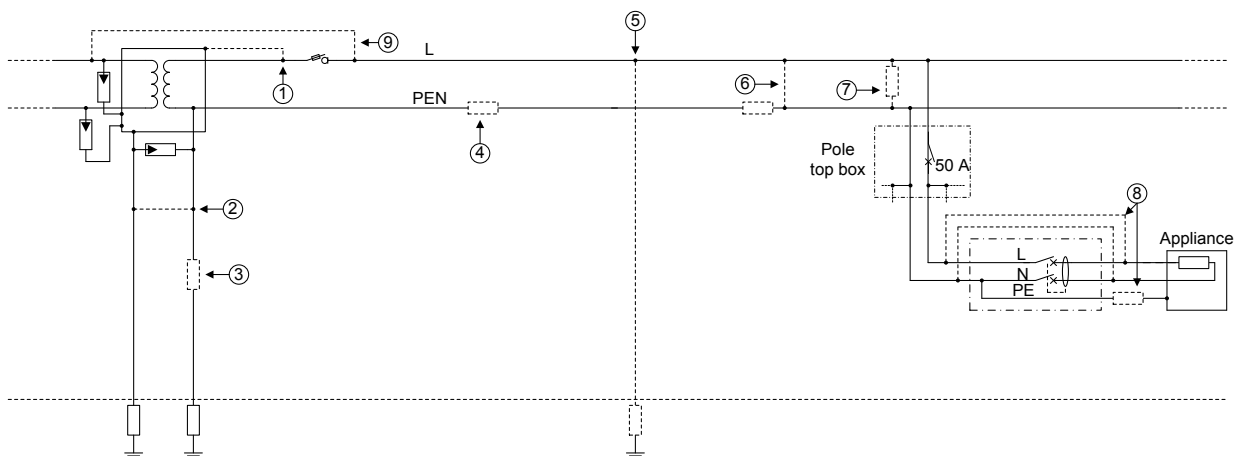


Figure 6: Typical Eskom LV network with hazards indicated

It was decided that the hazards originating from the MV side and protected from the MV protection system should not fall within the scope of this project. This includes hazard 2 and 9.

Hazard 1 has a very low-risk factor and is also excluded from this study. Hazards 5,6 and 7 are all examples of unaccounted current flow and thus grouped together under this single hazardous condition.

This results in a reduction of the identified hazards to the following four hazard categories:

1. PEN conductor failure
2. LV earth electrode conductor high impedance failure
3. Unaccounted current flow
  - a. Phase conductor exposed and reachable from earth
  - b. PEN conductor short-circuited with phase conductor without line protection
  - c. Phase conductor and PEN conductor exposed and reachable
4. Earth leakage protection not operational

These hazards are exploited further in the following section by creating an incident model of each hazard and examining possible detection methods of each. Figure 7 shows the updated LV network diagram with the reduced hazards.

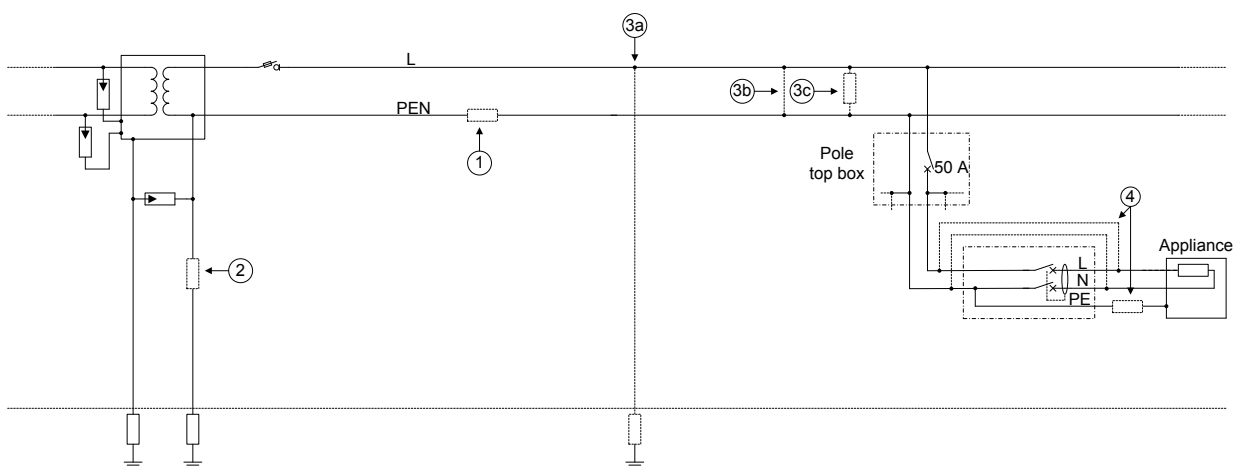


Figure 7: Typical Eskom LV network with updated hazard locations

## 2.5. HAZARD MODEL DEVELOPMENT

Basic models of each hazardous condition are used to identify the potential hazards that exist. The following section gives a description of each hazard and its corresponding circuit model.

### 2.5.1. PEN conductor failure

The PEN conductor failure of a single-phase connection can be modelled by the simplified circuit diagram in Figure 8. The voltage  $V_{TL}$  represents the MV/LV transformer secondary voltage and the earth electrode at the transformer is given by the impedance  $Z_{LVE}$ . The LV feeder impedance is not considered. The PEN conductor is split at the customer's installation into separate neutral and earth conductors. The appliances are modelled as a single

impedance  $Z_A$  with the accompanying voltage difference  $V_A$ . The appliance impedance is enclosed at earth potential. This represents the exposed conductive parts of the appliance that are bonded to earth through the PE and PEN conductors to the earth electrode at the transformer. A human touching the appliance is modelled by the impedance  $Z_H$ .

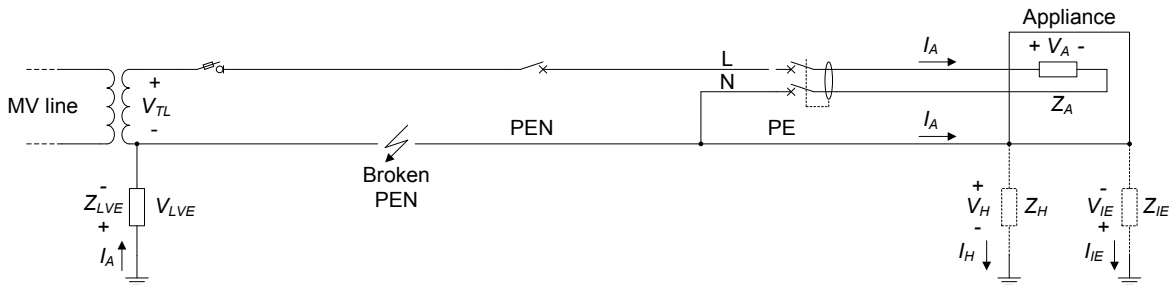


Figure 8: Circuit representing broken PEN conductor failure

The impedance  $Z_{IE}$  represents the incidental earth connection that is created between the exposed conductive parts of appliances and earth. A geyser's piping and a fridge standing on a damp floor are typical examples. This impedance is typically in the kilo-ohm range.

From Figure 8 it is evident that when the PEN conductor is broken, bonding is lost to earth and no conventional return path exists for the load current  $I_A$ . As such, the voltage  $V_A$  across the appliances will be zero and the neutral (N) conductor, the protective earth (PE) conductor and all bonded exposed conductive parts of any appliance will be at the phase voltage (230 V) – even when turned off. If a person, represented by impedance  $Z_H \approx 1 \text{ k}\Omega$ , should touch an appliance the person will provide a return path for the current via earth and could be electrocuted. In this case the RCD will not operate since the live and neutral current will remain balanced.

The hazard is further impacted by the combined load impedance  $Z_A$ . If all appliances will be turned off the touch hazard will be temporarily removed. Conversely, if sufficiently low-impedance loads are turned on, a touch hazard is established. Using the current loop represented by  $I_A$ , the hazard voltage is calculated as follows:

$$V_H = V_{TL} - I_A Z_A - I_A Z_{LVE} \quad (2.5.1)$$

The incidental earth impedance is ignored in this calculation as the impedance is usually much greater than that of a human touching a live appliance.

Rural households are typically protected with a 20 A main circuit breaker at the customers installation. By assuming a maximum load current of  $I_A = 20 \text{ A}$ , the minimum appliance impedance is approximated  $Z_A = 11.5 \Omega$ . The typical human touch impedance is approximately  $Z_H \approx 1 \text{ k}\Omega$ , which is substantially higher than the appliance impedance. For a transformer LV earth impedance  $Z_{LVE} \approx 70 \Omega$ , it can be approximated that  $V_H \approx V_{TL}$ .

If the minimum current for a human fatality is 30 mA, the required load impedance to cause a fatality is:

$$\begin{aligned} Z_A &= \frac{V_{TL}}{I_A} - Z_H - Z_{LVE} \\ &= \frac{230 \text{ V}}{30 \text{ mA}} - 1 \text{ k}\Omega - 70 \Omega \\ &= 6.6 \text{ k}\Omega \end{aligned} \quad (2.5.2)$$

which is equivalent to an appliance with a power rating of 8 W.

### 2.5.2. LV earth electrode conductor high impedance failure

The LV earth electrode high impedance failure of a single-phase installation can be modelled by the simplified diagram in Figure 9. The appliance is an electric stove which does not require earth leakage protection per SANS 10142:2017 [9] due to possible nuisance tripping of the RCD.

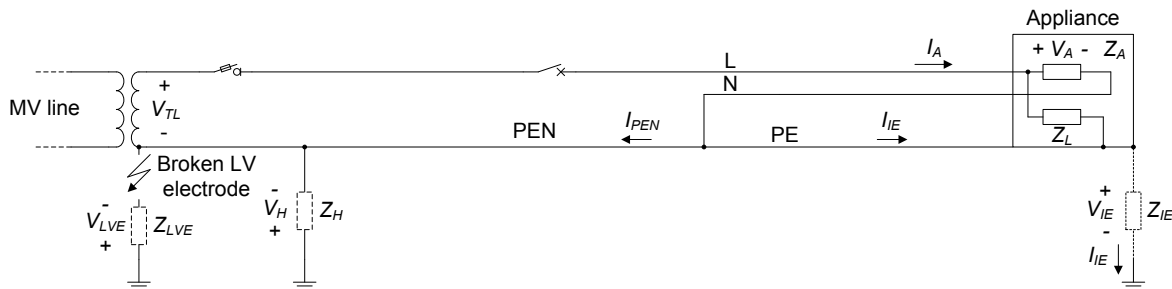


Figure 9: Circuit representing LV earth electrode conductor high impedance failure

The impedance  $Z_L$  represents a leakage impedance to the chassis of the stove which has a typical impedance in the order of  $Z_L \approx 1 \text{ k}\Omega$ . A broken earth electrode conductor would result in the loss of bonding of the PEN and the PE conductors. There must be two earth connections to create a hazard. Assume  $Z_H \approx 1 \text{ k}\Omega$  representing a person with  $Z_{IE}$  creating a return path. The following fatal current would flow:

$$\begin{aligned} I &= \frac{230 \text{ V}}{1 \text{ k}\Omega + 1 \text{ k}\Omega + 1 \text{ k}\Omega} \\ I &= 76.67 \text{ mA} \end{aligned} \quad (2.5.3)$$

The human would be exposed to a voltage of:

$$\begin{aligned} V_H &= I \times Z_H \\ V_H &= 77 \text{ V} \end{aligned} \quad (2.5.4)$$

The touch hazard will also be present on the PEN conductor and appliances of other customers connected to the same feeder.

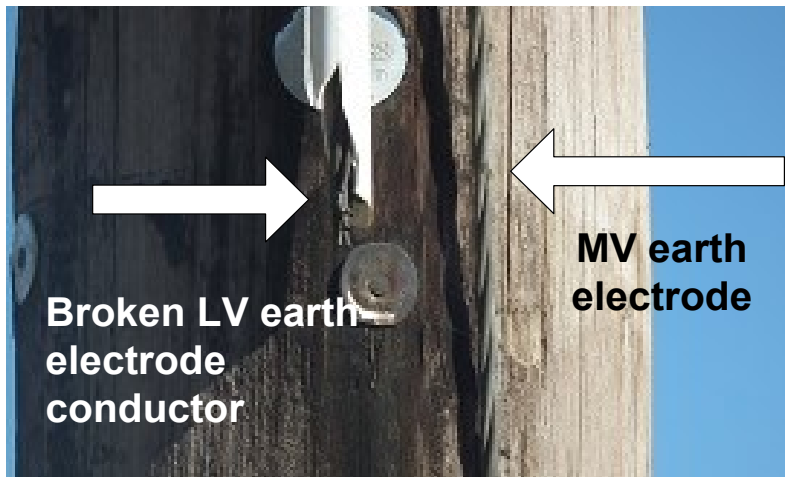


Figure 10: Stolen LV earth electrode conductor of a pole top transformer

Figure 10 shows a stolen LV earth electrode conductor of a pole top transformer. The electrode is placed in a PVC pipe to avoid short circuiting with the MV earth electrode. Earth electrodes are considered easy targets for cable theft which is a big problem in South Africa. A person touching the broken electrode is at risk of being electrocuted by completing the earth return path back to the transformer. The hazard may also present itself over a period of time with the LV earth electrode gradually becoming a high impedance.

### 2.5.3. Unaccounted current flow

The following three hazards are categorised under the unaccounted current flow condition. They represent conditions where current is *lost* in the network. Each hazard and its corresponding circuit model is given below:

#### 2.5.3.1. *Phase conductor exposed and reachable from earth*

The phase conductor exposed and reachable from earth hazard is modelled with the simplified circuit diagram in Figure 11. Examples of this hazard are insulator on a pole failure, a low-hanging conductor, structures making contact with conductors, etc.

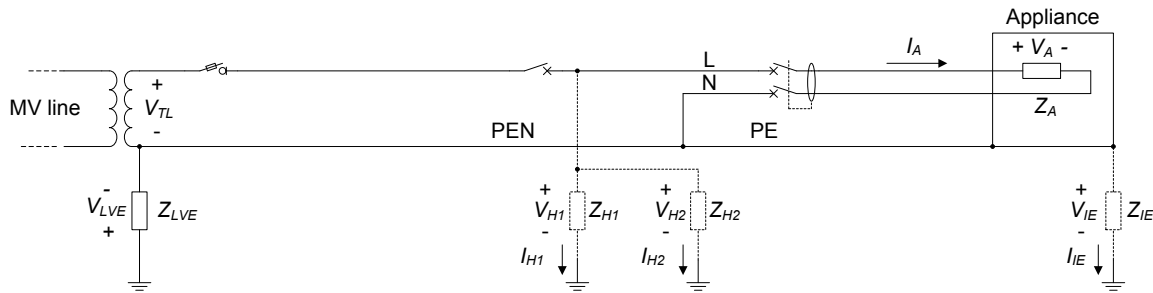


Figure 11: Circuit representing phase conductor exposed and reachable from earth

The hazard may have a low impedance to earth or high impedance. In Figure 11,  $Z_{H1}$  represents the impedance of the pole and earth in the case of a pole-top insulator failure. A hazard will only be present on poles with a low impedance to earth. The pole impedance would be negligible and the potential at the top of the pole would appear at the entry to earth. If a person or animal would make contact to the pole at this entry point, impedance in the range of 1 k $\Omega$  is added in parallel to the earth impedance to form the hazard impedance  $Z_{H2}$ . Since the contact impedance of a human or animal is high compared to the earth impedance, it can be neglected. By assuming the pole has an impedance to earth equal to the LV earth electrode impedance,  $Z_{LVE}$  the lethal voltage can be calculated as follows.

$$V_{H1} = V_{TL} \frac{Z_{H1}}{Z_{H1} + Z_{LVE}} = 230 \frac{70}{70 + 70} = 115 \text{ V} \quad (2.5.5)$$

Low hanging conductors, structures making contact with conductors only have  $Z_{H1}$  and  $Z_{LVE}$  in circuit and is treated in exactly the same way.

Depending on where the problem on the network is either the 50 A pole top breaker or the 80 A fuse will act as protection. This breaker will only operate when the total earth impedance is less than:

$$Z_{LVE} + Z_{H1} = \frac{V_{TL}}{I_{H1}} = \frac{230}{50} = 4.6 \text{ } \Omega \quad (2.5.6)$$

A second touch potential hazard is possible on customer appliances if the fault current caused by a line fault, represented by  $Z_{H1}$ , causes the PEN voltage to rise due to the fault current returning to the transformer via the LV earth electrode. By assuming the hazard impedance  $Z_{H1}$  has an impedance to earth equal to the LV earth electrode impedance the PEN conductor is raised with respect to ground as follows:

$$V_{PEN} = -V_{LVE} = V_{TL} \frac{Z_{LVE}}{Z_{H1} + Z_{LVE}} = 230 \frac{70}{70 + 70} = 115 \text{ V} \quad (2.5.7)$$

Although wood pole leakage currents can cause fires on MV structures, it is unlikely to happen on LV, since there would likely be insufficient energy. Other material making contact can,

however, present a fire hazard as long as the impedance is not lower than  $4.6 \Omega$  when the transformer fuse will blow. At this point the power consumed can be as high as:

$$P_{H1} = I_{H1}V_{H1} = 50 \times 230 = 11.5 \text{ kW} \quad (2.5.8)$$

### 2.5.3.2. PEN conductor short-circuited with phase conductor without line protection protection

PEN conductor short-circuited with phase conductor without line protection hazard can be caused, as an example, when a customer service cable, that has a coaxial structure, is nailed down to a support structure when the original fittings became loose. This hazard is modelled with the simplified circuit diagram in Figure 12.

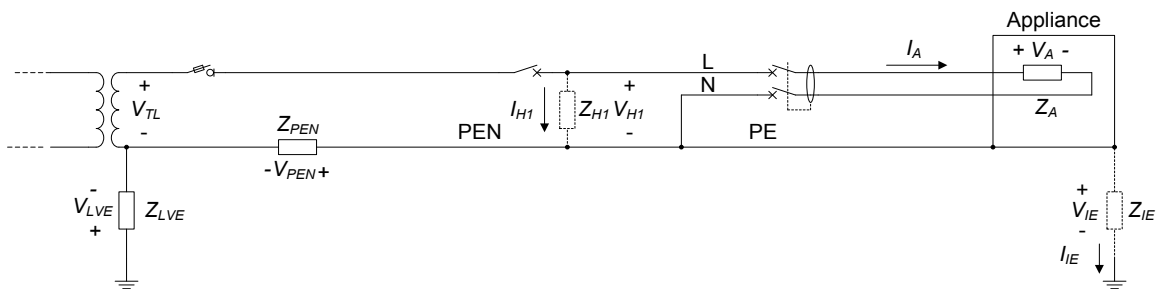


Figure 12: Circuit representing PEN conductor short-circuited with phase conductor without line protection

A nail through a coaxial cable can either short out the inner live conductor to the outer PEN conductor or cause enough damage to the insulation that high impedance is formed between the conductors. A proper bonding would cause a current to flow that is only governed by the line impedance that would be greater than the pole top circuit breaker rating (assumed to be 50 A). A situation would be hazardous when the impedance  $Z_{H1}$  is high enough to cause the breaker not to trip, or:

$$Z_{H1} > \frac{V_{TL}}{I_{H1}} = \frac{230}{50} = 4.6 \Omega \quad (2.5.9)$$

Such an incident will not create any hazardous voltages to customers on any equipment caused by the rise in voltage on the PEN conductor  $V_{H2}$ . When the hazard impedance  $Z_{H1}$  is low, the contact of a structure with the live conductor will cause an exposed and reachable from earth hazard.

Before the pole top breaker trip, the power dissipated in the damaged service cable insulation can be as high as:

$$P_{H1} = I_{H1}V_{H1} = 50 \times 230 = 11.5 \text{ kW} \quad (2.5.10)$$

This is enough power to create a hot spot in the cable that would cause combustion to material in contact with it.

If, however, the PEN conductor is also damaged it can have a higher impedance than the short circuit. The PEN conductor voltage on the customer side of the fault will now be close to the line voltage magnitude.

### 2.5.3.3. Phase conductor and PEN conductor exposed and reachable

The phase conductor and PEN conductor exposed and reachable hazard is shown in Figure 13. In this case, contact is made between the live conductor and the PEN conductor. This condition is worse than the previous one since there is a low impedance path back to the transformer and the body making contact is the only significant impedance in the current loop.

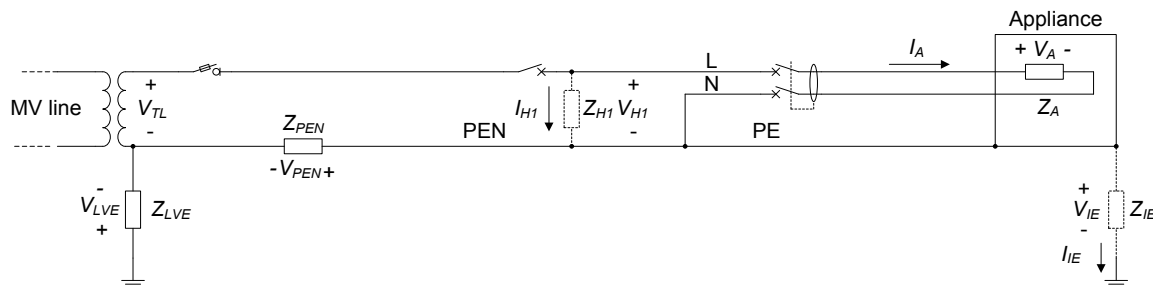


Figure 13: Circuit representing phase conductor and PEN conductor exposed and reachable hazard

A body ( $Z_{H1}$ ) with a typical impedance of 1 k $\Omega$  between the live and PEN conductors would cause the following fatal current:

$$I_{H1} = \frac{V_{TL}}{Z_{H1}} = 0.23 \text{ A} \quad (2.5.11)$$

If combustible material makes contact with exposed conductors a fire hazard is formed. Again, before the pole top breaker trip, the power dissipated in the damaged service cable insulation can be as high as:

$$P_{H1} = I_{H1}V_{H1} = 50 \times 230 = 11.5 \text{ kW} \quad (2.5.12)$$

### 2.5.4. Earth leakage protection not operational

This hazard can have a number of causes, such as an illegal connection (a connection directly to the network with no earth leakage included), a bypassed meter (hence the earth leakage is also bypassed), a faulty earth leakage breaker, unsafe wiring (only if the earth leakage is also not operational), etc. The hazard can be modelled with the simplified circuit diagram in Figure 14.

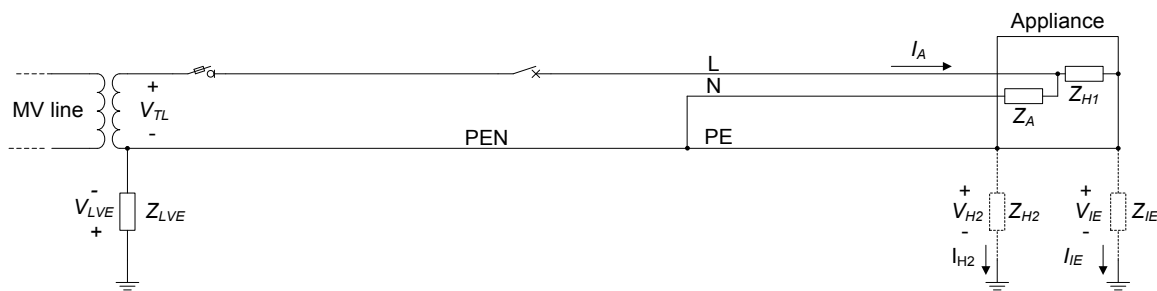


Figure 14: Circuit representing earth leakage protection not operational

In these connections, the PEN conductor is not split to create an earth terminal. Any appliance with a metal casing has insulation impedance between the internal circuit and the enclosure  $Z_{H1}$ . In most cases this impedance is high and probably only capacitive, but it can also be low, especially with dirt and moisture contamination present. Examples of appliances that can have low insulation impedance are electrical stoves. To prevent nuisance tripping these appliances do not need to be fed through an earth leakage breaker, but still need to be properly earthed. A fatal hazard becomes active when the body of a person or animal touches the casing of an appliance that is not properly earthed. Such a hazard has high impedance, i.e. in the range of 1 k $\Omega$ . By assuming the insulation impedance has the same value, the hazard voltage can be estimated as follows:

$$V_{H2} = V_{TL} \frac{Z_{H2}}{Z_{H2} + Z_{H1}} = 230 \frac{1000}{1000 + 1000} = 115V \quad (2.5.13)$$

Only the 80 A fuse or the 50 A breaker is in the circuit and such a low impedance incident will not cause them to operate.

It is also possible that the appliance insulation is damaged that would cause a low impedance to the enclosure. In such a case, the hazard voltage will reach values much closer to the line voltage. If under these conditions a low impedance contact to earth is formed much higher current can flow up to a point where the 80 A fuse or 50 A breaker would operate. By assuming a short circuit between the live conductor and the enclosure the total line voltage would appear across the hazard. Depending on the hazard impedance current up to 50 A can flow without protection operation. The power dissipated by the hazard in such a case would be:

$$P_{H1} = I_{H1} V_{H1} = 50 \times 230 = 11.5 \text{ kW} \quad (2.5.14)$$

Such high-power dissipation would cause a fire in a very short duration.

## 2.6. HAZARD DETECTION MECHANISMS

In this section, the possible methods for detecting the identified hazards on the LV distribution network are discussed. The primary focus is on the use of network visibility to detect the

identified hazards. Smart meters are currently used to manage revenue control and in some cases, demand side management is applied.

The typical smart meter is equipped with a microprocessor and measurement circuits for measuring the voltage and current at the customer's point of connection. These measurements are processed by the smart meter to extract revenue data. The data is communicated back to the utility by way of a communication link to a data concentrator or server. This may be via a radio connection such as GPRS over a cell phone network, a Wi-Fi connection, ZigBee connection or a physical connection such as power line communication (PLC). ZigBee RF communication is used in this evaluation and will be further discussed in Chapter 3. The smart meter is therefore not only a meter but also a data gathering device that can provide valuable insight for detecting possible hazards.

In addition to smart meters at customers, the use of a smart transformer is also required to detect hazards. A smart transformer has the capability, like a smart meter, to take various measurements and send these measurements to a data concentrator. In this project, a smart meter located on the low voltage side of a regular MV/LV transformer is used to represent a smart transformer. If the system is not equipped with a smart transformer, a smart meter can be installed at the LV side of the transformer.

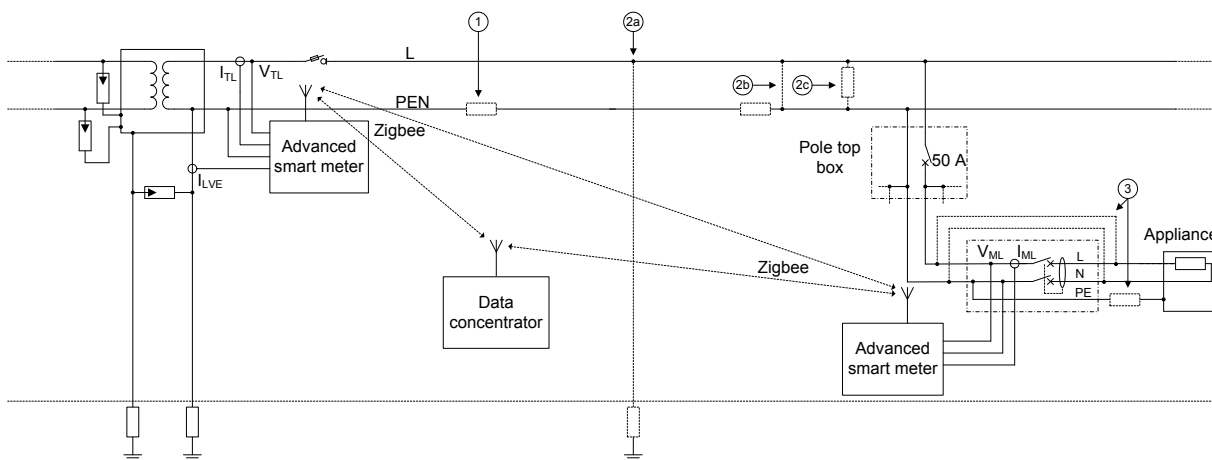


Figure 15: Circuit showing the smart meters installed at the transformer and a customer

The schematic diagram in Figure 15 shows a simplified model of an electrification transformer with a single-phase feeder and a typical TN-C-S customer connection. The measurements taken at the transformer are: the LV earth conductor current  $I_{LVE}$ , the phase conductor current  $I_{TL}$  and the LV phase-to-neutral voltage  $V_{TL}$ . The measurements taken at the customer are: The live-to-neutral voltage  $V_{ML}$  and the live conductor current  $I_{ML}$ .

The detection mechanisms of each hazard and possible solutions are discussed below:

### 2.6.1. PEN conductor failure

This section examines existing solutions and their practical consideration for the South African environment. The first solution presented makes use of network visibility with the topology as seen in Figure 15. An alternative solution is also proposed that makes use of existing prepaid meter technology.

If the PEN conductor fails with a high impedance or open circuit between the customer's point of connection and the shared PEN conductor, the only other current return path is through the earth. This creates a hazardous condition where a dangerous voltage level may be present on the chassis of the customer appliances.

It was first considered that the failure can be detected with the smart meter by using the current measurements  $I_{ML}$  and  $I_{PE}$ . It was assumed that if the earth return current corresponds with the live conductor current with phase and with a similar amplitude, it can be classified as a broken PEN conductor. However, this solution is severely limited. If the PEN conductor fails at a point that is shared by multiple customers, the PE current measurement would not be an accurate reflection since the earth return consists of the combined earth impedances of all the customers connected to the isolated section of the PEN conductor. This solution is further limited by the fact that the PEN conductor can have a lethal voltage as a result of other customers, while no current is measured on the live conductor.

Furthermore, if the PEN conductor fails on a dual-phase feeder, a neutral voltage offset of up to 230 V may be induced due to load unbalance. In this case, the customer may not only experience a shock hazard on the PE conductor, but the live-neutral voltage may reach levels up to 460 V which may damage appliances or even cause a fire.

#### 2.6.1.1. *PEN conductor failure existing solutions*

This section examines existing solution from literature to mitigate a PEN conductor failure.

##### **Protective multiple earthing**

According to British Standards (BS 7430:2011) [10], which deals with the earthing of electrical installations in the United Kingdom, TN-C-S systems are required to use protective multiple earthing (PME). The PME system implements multiple earths along the PEN conductor which ensures that, should the PEN conductor become an open-circuit, any exposed conductive parts will remain close to the earth potential through a combined distributed earth. Generally, the PME system requires an earth electrode at each customer's point of supply. Although SANS 10292 does not require PME, many municipalities have opted to use this scheme where customers are supplied by underground feeders. Where lightning protection systems (LPS) are installed, the South African standard for the protection against lightning, SANS 62305-4 [11], requires a suitable earth-termination system and bonding network at the customer installation.

This requires that the PE conductor of the electrical installation be bonded to the earth-termination system of the LPS. For PME to be effective, the combined earth impedance on the feeder after the fault location should be low enough to limit the voltage rise of the open PEN conductor.

This system, however, is not effective for rural electrification for a number of reasons. 1) Rural areas typically have a low population density, which may not provide sufficient combined earth impedance for a particular feeder. 2) South Africa is geographically diverse with often poor soil conductivity that varies greatly between regions and seasons. 3) Earth conductors are considered “easy targets” by criminals and are often stolen after installation, making the PME system unreliable. 4) If sufficient earth impedance should exist, customers may continue to use the compromised supply without reporting it – especially when the primary loads are LED lights and electronic appliances with low consumption that can accept a wide input-voltage range. For a 20 A main circuit breaker to operate, a return path impedance of less than 11.5  $\Omega$  is required. However, the Eskom Distribution Standard for earthing specifies that an LV earth impedance at the transformer may vary between 10  $\Omega$  and 70  $\Omega$  depending on the MV voltage and protection setting. It can therefore not be guaranteed that the return path via earth will provide a sufficiently low impedance for the customer’s circuit breaker to operate if they continue to use the compromised supply.

### **Phase-to-neutral voltage monitoring**

It is recommended that an electronic circuit breaker configuration be used that monitors the phase-to-neutral voltage and operates during overvoltage conditions. In addition, such a circuit breaker should estimate the neutral point voltage shift for three-phase systems and operate if the neutral point voltage rises above a certain threshold. This solution provides a cost-effective way to mitigate the risk of neutral voltage rise in dual and three-phase systems, but not single-phase systems. In the case of single-phase systems, the live-to-neutral potential will experience an undervoltage rather than an overvoltage.

### **PEN-to-earth voltage monitoring**

It is further argued in [12] that a device that monitors the voltage between the PEN conductor and earth would provide better protection. SANS 10142-1 [9] requires that the supplier be notified when the neutral voltage exceeds 25 V and the installation be disconnected when it exceeds 50 V. Although the author does not elaborate on any functional details, it is assumed that such a device will use a dedicated, non-current-carrying earth electrode as the measurement reference to earth.

This solution is not ideal for rural electrification because the integrity of any earth electrode cannot be guaranteed.

### **2.6.1.2. Proposed solution: Smart meters and communication**

This solution makes use of the smart meter topology as seen in Figure 15. Smart meters provide additional visibility, automated fault reporting as well as avoiding nuisance tripping. The PEN conductor failure can be detected by an over or undervoltage condition between the live and neutral conductors at the customer's premises on a dual phase system. A customer on a single-phase system will only experience an undervoltage. By continually monitoring the voltage at the transformer and at the customer the utility can avoid nuisance tripping by adjusting the detection parameters, e.g. feeder is overloaded. This solution is further explored in this report and a trial implementation is done using smart meters and a data concentrator with ZigBee wireless communications.

### **2.6.1.3. Alternative proposed solution: Prepayment meter as a protection device**

An alternative solution to the problem makes use of existing prepayment meters as a device to protect the customer against dangerous over and undervoltage conditions.

The rural electrification installations are typically fitted with an electricity control unit (ECU), a type of electronic prepayment meter that is installed in the home and that includes an RCD and a 20 A circuit breaker. No additional distribution board is installed and wall outlets and lights are directly supplied from the ECU. Due to meter tampering and electricity theft, Eskom and municipalities have moved to implement split meters in many new installations. These meters consist of a metering unit that is placed at the pole top outside of the customer installation and a customer interface unit (CIU) that is placed inside the home. Wireless ZigBee or PLC technology is typically used to communicate between the two units.

Both types of meters typically have a microcontroller, a user interface, a relay or contactor to disconnect the live conductor when the credit is depleted, an analogue front-end to measure the live-to-neutral voltage and current, and non-volatile memory to store consumption and user credit. This provides most of the hardware that is needed to implement protection against PEN conductor failures.

By replacing the existing contactor in the meter with a dual-pole contactor or adding an additional single-pole contactor and changing the firmware, the meter can be programmed to act as a voltage window comparator and circuit breaker that can disconnect both the live and PEN conductors. The circuit diagram is shown in Figure 16. This will allow the meter to completely isolate the customer during hazardous conditions.

In single-phase systems, an undervoltage will be present during a PEN conductor failure whereas with dual-phase systems an under or overvoltage, up to the line-to-line voltage of 460 V, may occur. The South African standard for power quality NRS 0480-2 [13] specifies a maximum voltage deviation of  $\pm 10\%$  from the nominal 230 V under normal conditions. It also



sudden increase in the ratio can imply a broken LV earth electrode, while a gradual increase in the ratio measured over time might signal an earth electrode deteriorating and becoming a high impedance. A trend in the ratio must be determined over time to more accurately determine if an electrode is starting to fail. This increases the certainty of detecting such a hazardous condition.

### **2.6.3. Unaccounted current flow**

These hazards are grouped together as they share the same detection mechanism. Each is discussed in more detail below:

#### **2.6.3.1. *Phase conductor exposed and reachable from earth***

When a conductor is exposed and reachable from earth, a current path is created that returns via earth back to the transformer through the transformer LV earth electrode.

The first hazard is local to the exposed phase conductor. Examples of such a hazard includes a broken pole-top insulator or a broken and exposed phase conductor that is touching the ground, a tree, fence or other structure. In the case of a broken pole-top insulator, the pole provides a conductive path via earth back to the LV earth electrode. The impedance of the pole may vary depending on the material, treatment, moisture conditions and the presence of a lightning earth conductor. If no earth conductor is present or the pole is not well earthed it may pose a touch hazard if someone standing on the ground should touch the pole. This same principle applies when a broken phase conductor touches a tree, fence or other structure.

The second hazard occurs when the phase conductor has a low impedance connection to earth. This would cause a rise in the PEN conductor voltage which would cause a touch hazard on all customer appliances. This hazard is similar to the hazard when the phase conductor is short-circuited with the transformer tank. The only differences are that the conductor may have a higher impedance to earth and that the return path is only via the LV earth conductor.

A possible solution to detect this hazardous condition is to do current balancing. By comparing the current delivered by the transformer to the sum of all currents at the customer installation, the current imbalance would indicate that power is being lost in the network. It would, however, not be possible to distinguish between an illegal connection or the other hazards in this category. It will give an indication that a hazard exists on the network and allow an operator to investigate.

The current comparison requires accurate time stamped data, which can be achieved by time syncing the measurements taken at the transformer with the customer meters measurements using global positioning system (GPS). GPS capabilities in the meters are therefore a requirement.

### **2.6.3.2. *PEN conductor short-circuited with phase conductor without line protection***

This hazard causes a short circuit current to return via the PEN conductor back to the transformer without passing any customer meter. This condition does not create dangerous voltages at the customer's installation but does create a fire hazard if the fault impedance is low enough allowing substantial current to flow, but still low enough not to be detected by line protection.

This hazard can also be detected by using current balancing, it would however again not be possible to distinguish between an illegal connection and this hazard.

### **2.6.3.3. *Phase conductor and PEN conductor exposed and reachable***

When the phase and PEN conductor are exposed and reachable, a touch hazard is created that would allow a limited amount of current to return via the PEN conductor.

This situation generally does not produce dangerous voltages at the customer's point of connection but creates a fatal touch hazard at the exposed conductors. However, if the touch hazard results in a fault impedance that is low enough, the same hazardous condition is created as discussed in Section 2.6.3.2.

This hazard can be detected in the same way as an exposed earth conductor to earth. It would not be possible to distinguish between an illegal connection and this hazard, but it would provide an indication that a hazard is present.

### **2.6.4. Earth leakage protection not operational**

The earth leakage protection can become non-operational for a number of reasons:

- The RCD device becomes non-operational due to electromechanical failure.
- The meter is bypassed due to electricity theft and no longer operational.

To detect an RCD device that has failed, a self-diagnostic feature should be added to the RCD device that can be used by the smart meter to determine the functional state of the RCD. The smart meter should send a warning message to the data concentrator if the RCD is believed to be faulty.

If the meter is bypassed completely and rendered inactive, the loss of communication can be used as an indicator that the meter is no longer functional. In this case, it could be assumed that the earth leakage is no longer operational.

Adding battery backup to the meter, to keep the meter active for a certain time period when bypassed, will provide a more accurate indication that the meter is bypassed. The GPS location of the meter will provide the operator with an accurate location of the bypassed meter.

Furthermore, when the meter is bypassed or illegal connections are made, a current unbalance between the transformer phase current measurement and the sum of the meter current measurements will exist. If a current imbalance is detected, it can be assumed that no functional earth leakage is installed for known connections and/or that illegal connections are present.

## **2.7. CONCLUSION**

This chapter presented the reader with background on the earthing schemes used in South Africa. Various hazards are still undetectable by Eskom on the LV network and these hazards, as identified by an Eskom working group, are discussed. Initially, 9 hazards were identified, but it was decided that hazards originating from the MV side of the MV/LV transformer should be ignored. This reduced the hazards to four hazard categories. Basic circuit models were used to identify the potential hazard that might exist. Each hazard is discussed and a potential hazard detection method is proposed using smart meters located at the LV side of the transformer and at each customer. A data concentrator will be used to gather, store and process the measurements received.

To identify the various hazards discussed in this chapter voltage and current monitoring is required at the LV side of the transformer and at the customers. These should all be communicated to a central data concentrator.

Smart meters with adaptable firmware and communication capabilities as well as a data concentrator is therefore required. GPS is also a necessity on the meters and data concentrator to accurately timestamp the measurements sent to the data concentrator and for incident location purposes.

## CHAPTER 3

### SMART METER OVERVIEW AND COMPONENTS

#### 3.1. INTRODUCTION

This chapter presents an overview of the smart meter concept and the technologies that have been implemented in South Africa. The smart meter is a component of the smart grid. A smart meter differs from a prepaid meter in that it incorporates communication to send usage data to a back-end system of the utility. The two main communication technologies, ZigBee RF and power line communication (PLC) that have been used on LV feeders in industry, are discussed. The chapter concludes with a detailed discussion on the ZigBee communications protocol that has been implemented in this project.

#### 3.2. SMART GRID OVERVIEW

The term smart grid refers to an intelligent electricity network. A smart grid can intelligently integrate the actions of all users connected to it to efficiently deliver sustainable, economic and secure electricity supplies [15]. Innovative products and services are employed to intelligently monitor and control an electricity network.

Smart grids are a rapidly evolving field with new technologies such as distributed generation and electric vehicles introducing new problems and challenges to manage the electrical network. New smart technologies are, however, becoming available to meet these challenges. By intelligently monitoring and controlling demand and supply of various loads and generators the utilities can ensure a more efficient, reliable and sustainable grid. Each device on the network is given the ability to measure, gather data and communicate to a central location. This gives the utility the ability to control an individual component out of millions of components [16].

The communication layer of the smart grid architecture is key to enable a smart grid. Greater visibility into the grid can only be achieved with reliable communication between the various communication layers that can be represented by a multi-layer architecture. The architecture incorporates various levels of data processing. This architecture comprises of the following architecture, which is classified by data rate and coverage range [17]:

- Home area network (HAN)
- Neighbourhood area network (NAN)
- Wide area network (WAN)

An HAN application includes home automation. This relates to the communication between appliances and smart meters located at a customer's premises. It does not require high data rates and communication distances are over short distances of up to 100 m.

A NAN is the communication between smart meters, data concentrators and field devices such as distribution automation. It requires larger amounts of data to be sent over longer distances from meters to a centrally located data concentrator.

A WAN represents the highest level of the communication hierarchical structure. Data points from various data concentrators are communicated back to a master station which analyses the data to make informed decisions. Communication distances of up to 100 km are required.

Table 2 shows a summary of the smart grid communication levels with the various technologies used in each level.

Table 2: Smart Grid communication levels

Level	Coverage range	Example technologies
Home area network	Up to 100 m	ZigBee, PLC (HomePlug), WiFi, Z-Wave
Neighbourhood area network	Up to 10 km	ZigBee Mesh, PLC, WiMAX, GPRS, ADSL
Wide area network	Up to 100 km	GPRS, Satellite

### 3.3. SMART METERING DEVELOPMENT IN ESKOM

This section presents an overview of the smart metering progress of Eskom.

Eskom initiated an Advanced metering infrastructure (AMI) pilot project to comply with this regulation. AMI refers to the entire smart metering system from the enterprise level down to the end device or smart meter located at a customer. It enables the collection of measurements, analyses and controls energy usage by enabling data to be transmitted over a two-way communications network [18]. The advanced metering infrastructure deployed in South Africa is governed by a national standard NRS 049 [19]. The standard was prepared by the Electricity suppliers liaison committee as for use by South African electricity supply authorities. The standard was accepted by the industry and the first revision published in 2008 by the SABS. The latest revision was released in 2016.

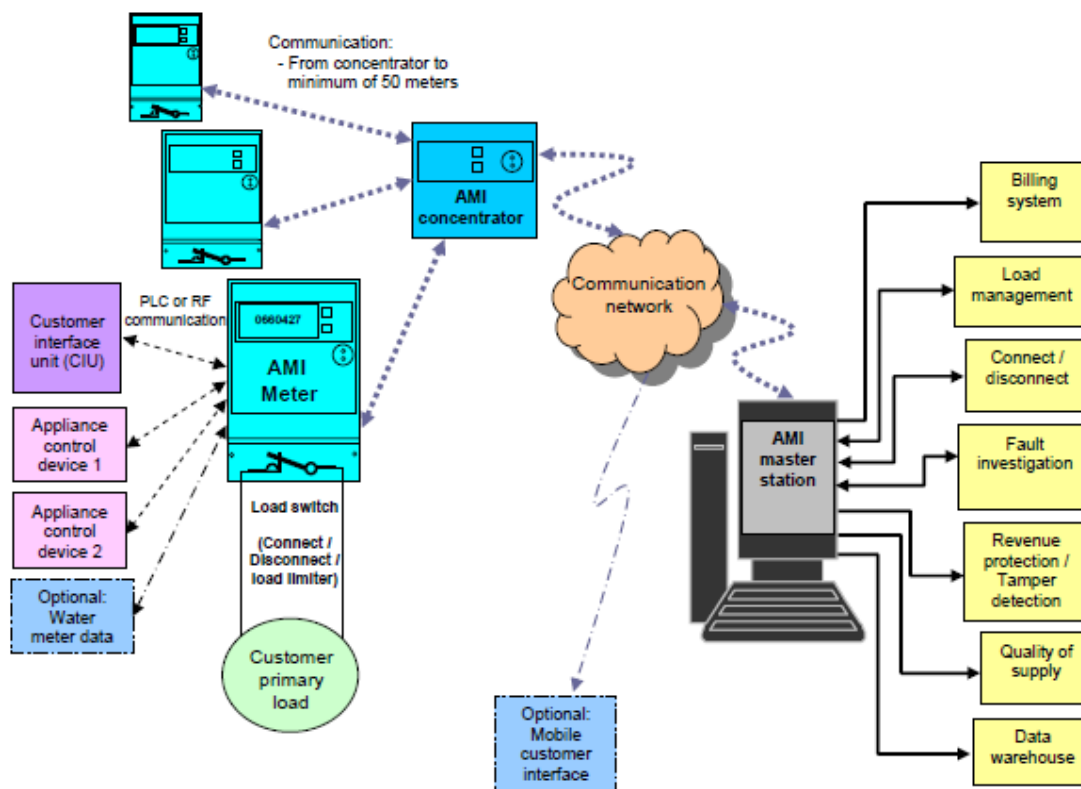


Figure 17: NRS 049 AMI Architecture [19]

Figure 17 shows the AMI architecture as specified in NRS 049 [19]. Eskom adopted this architecture to implement its own AMI solution. The Eskom standard for adopted open protocol for advanced smart metering [20] architecture is shown in Figure 18.

### 3.3.1. Eskom standard for smart metering architecture and communication protocols

The diagram in Figure 18 depicts an overview of the various standards and protocols to be adopted for meters and metering field devices. The diagram also depicts the companion specification, Interoperable device interface specification (IDIS), to be employed to ensure true interoperability and interchangeability between various manufacturers.

It was decided by Eskom to adopt internationally accepted open protocols (preferably endorsed by the IEC) to ensure a larger pool of manufacturers where smart meters and field devices can be sourced from. Therefore, Eskom decided to standardise on the device language message specification (DLMS) with companion specification for energy meter (COSEM), G3 PLC (where PLC is used) protocols and other HAN protocols, which are in accordance with NRS 049 [19].

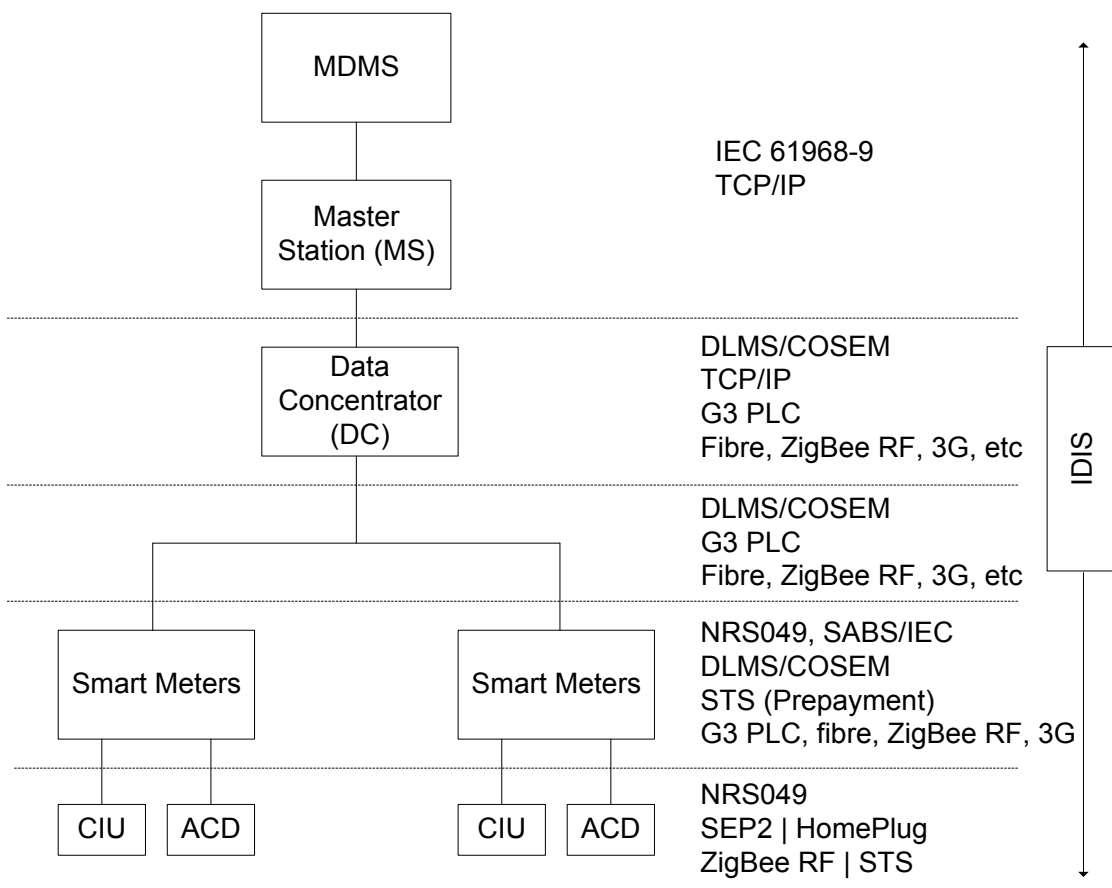


Figure 18: Eskom open standard & protocols layout [20]

The following describes the various abbreviations used in Figure 18.

**MDMS: Meter Data Management System** - Back end system which performs long term data storage and data management. The AMI master stations report mostly usage and events data to this system. Currently, Eskom uses two of these systems: transmission MDMS and Eskom MDMS, but plans are set to integrate the two systems into a common system.

**AMI Master Station:** Collects data and sends control data and configuration instructions to AMI field devices. It also sends data to the MDMS system.

**Data Concentrators:** Manages communications between the AMI Master Station and various smart meters associated with that concentrator. Is it also capable of processing data and only report specific usage and events data to the master station.

**Smart Meters:** Field device usually installed at a customer's premises which provide traditional metering functionality with remote communication capabilities. The communication standard used is usually PLC or ZigBee RF.

**CIU:** Normally located inside a customer's premises, these devices display a range of information to the customer such as energy consumed, the rate of consumption, demand rate etc., which it receives from the smart meter.

**ACD: Appliance Control Device** – Located inside a customer’s premises, these devices act in a similar fashion as the traditional “ripple” controllers with added communication to the smart meter.

Communication required for this study are between the meters and data concentrator. For this the Eskom adopted communication standards specify the use of either G3-PLC or ZigBee RF. The following section will examine the use of both on LV feeders giving the advantages and disadvantages of both.

### **3.4. COMMUNICATION TECHNOLOGY ON LV FEEDERS**

This section gives an overview of G3-PLC and ZigBee RF specifications which are the two major communication technologies used on low voltage feeders in the smart grid environment.

#### **3.4.1. G3- PLC specification**

This section examines the G3-PLC specification starting with an overview of power line communication in general and moving to more detail regarding the G3 protocol.

##### **3.4.1.1. Power line communication overview**

PLC utilises existing power lines as a communication channel making it a very powerful alternative as no extra fibre, telephone or additional cable should be installed. Power lines were, however, not initially designed to carry higher frequency communication signals resulting in various technical challenges.

PLC can broadly be grouped into two main categories narrowband PLC and broadband PLC.

Broadband PLC makes use of higher frequency (1.8 – 250 MHz) and higher bit rates (up to hundreds of Mbps) but has the drawback of reduced communication distance. Broadband PLC is thus not used in the smart grid environment as communication distance is of high importance. Due to the higher frequencies, broadband PLC easily interferes with other radio communication and is restricted in many countries. Broadband PLC is most often used in the home environment to interconnect computers and peripherals such as WiFi extenders.

Narrowband PLC operates at lower frequencies in the kilohertz range (3 – 500 kHz) at reduced data rates but has the advantage of longer communication distances of up to several kilometres, which can be extended by using repeaters.

##### **3.4.1.2. G3-PLC protocol**

The Eskom adopted protocol G3-PLC protocol operates in the narrowband frequency range. It is the latest industry standard available and was developed specifically for the smart grid vision. The G3-PLC alliance claims high reliability, high transfer speeds and the ability to cross transformers making it the ideal communication platform to use on an existing powerline grid

[21]. The G3 standard is also the only solution supporting the IPv6 addressing in the CENELEC frequency range. This will allow addressing of virtually an unlimited number of endpoints and allows easy integration with the internet of things development [22].

G3-PLC is uniquely identified over other PLC standards and protocols by the use of orthogonal frequency multiplexing (OFDM) in the physical layer which makes efficient use of the spectrum. Two data checks are performed to ensure data reliability. Mesh routing protocol is also supported to determine the best path between remote network nodes [23].

In congested cities or urban areas, the MV lines usually run up to a sub-station room, where depending on the load, a few transformers can exist [24]. These substations typically house a data concentrator with each transformer. Communication to meters situated on the LV network can, therefore, be easily established without the need to cross a transformer. This is, however, not the case for rural areas, due to the low population density a transformer (usually aerial pole mounted) typically serves only a few customers. By placing a data concentrator at each transformer will have high-cost implications. The ability of PLC to cross these transformers will have an economic benefit.

An evaluation of the ability of G3-PLC to cross a MV/LV transformer was done in [24] where it was concluded, by field trials, that G3-PLC can communicate at distances greater than one kilometre on the MV lines, then cross a transformer into the LV grid and communicate with a smart meter at data rates greater than 50 Kbps.

### **3.4.2. ZigBee specification**

This section gives an overview of the ZigBee wireless specification.

ZigBee is a wireless specification developed in 1998, standardised in 2003 and revised in 2006 by the ZigBee *Alliance* who is also responsible for maintaining the protocol. ZigBee is based on the IEEE 802.15.4 standard which defines the operation of low-rate wireless personal area networks (LR-WPANS) and maintained by the 802.15.4 working group. The 802.15.4 protocol focuses on low-power, low-cost communication with devices in the nearby vicinity. It defines the lower network layers (physical and media access control layer) of the ZigBee open systems interconnection (OSI) model. (See Section 3.4.2.1).

ZigBee has a defined transfer speed of 250 Kbps or 31.25 KBps making it best suited for intermitted communications in applications not requiring high-bandwidth. ZigBee operates in the industrial, scientific and medical (ISM) radio band. In South-Africa and most jurisdictions worldwide, 2.4 GHz is used, while Europe uses 868 MHz and 915 MHz is used in USA and Australia.

ZigBee has the advantage of forming mesh networks defined in its network layer. Mesh networking topology allows any node to communicate with any other node, if not directly in range, but indirectly by relaying the message through additional nodes. Should a node lose connectivity the network will “self-heal” and form a new route to a target node.

### 3.4.2.1. ZigBee protocol architecture

The ZigBee protocol architecture or ZigBee stack is defined by its OSI model as seen in Table 3.

Table 3: ZigBee OSI Model [25]

	Simplified 5 layer OSI-model	ZigBee layer	Description
ZigBee Alliance	User application layer	ZigBee device objects (ZDO)	Application layer that provides device and service discovery features and advanced network management capabilities.
	Application layer	Application support sublayer (APS)	Application layer that defines various addressing objects including profiles, clusters, and endpoints.
	Network layer	Network	Adds routing capabilities that allow RF data packets to traverse multiple devices (multiple ‘hops’) to route data from source to destination (peer to peer).
IEEE 802.15.4	Data link layer	Media access control (MAC)	Manages RF data transactions between neighbouring devices (point to point). The MAC includes services such as transmission retry and acknowledgement management, and collision avoidance techniques (CSMA-CA).
	Physical layer	Physical (PHY)	Defines the physical operation of the ZigBee device including receive sensitivity, channel rejection, output power, the number of channels, chip modulation, and transmission rate specifications.

### 3.4.2.2. Addressing

ZigBee devices have two address types. A 64-bit *IEEE address* (also called *MAC address* or *extended address*) and a 16-bit *network address*.

- **IEEE device address (64-bit)**

The 64-bit address or MAC address is a globally unique address and is assigned to the device for its lifetime, set by the manufacturer during fabrication [26].

- **IEEE network address (16-bit)**

The 16-bit address is assigned to a device when it joins the network and changes every time a device joins a new network. It is used for identifying a device on a network [26]. The address 0x0000 is reserved for the coordinator. The 16-bit address can also change while the device is connected to a network should the following conditions occur:

- An address conflict is detected where two devices are found to have the same 16-bit address.
- A device temporarily loses connectivity from the network.

### 3.4.2.3. *Device types*

A ZigBee network consists of up to three device types that form a complete network. Figure 19 shows a typical ZigBee mesh network with the three device types i.e. Coordinator, Router and End-Device. Each type and its network function are discussed in more detail below:

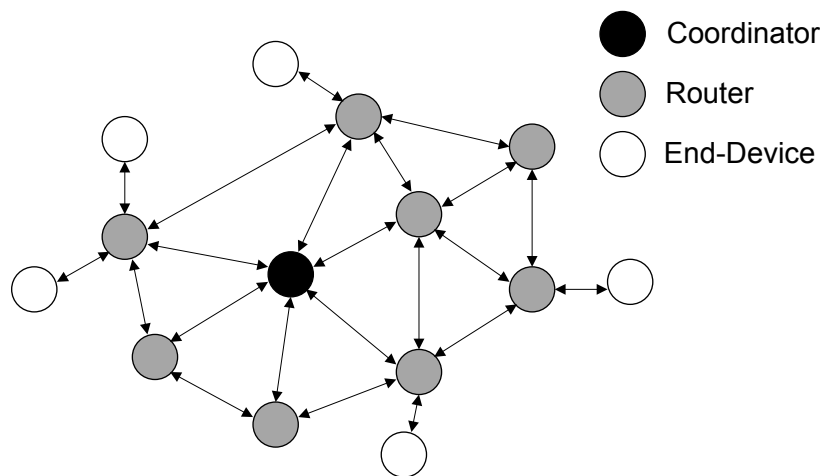


Figure 19: Typical ZigBee mesh network with the three device types

#### **Coordinator**

This is the device that “starts” a ZigBee network. It is the first device on the network. The coordinator scans the RF environment for an existing network, chooses a channel and a personal area network identifier (PAN ID) and then forms/starts the network [26].

The coordinator assigns network addresses to each router and end device that joins the network and is responsible for the managing this process. Security features of the network can optionally be configured in the coordinator's network settings.

Once the coordinator has started the network, it behaves like a router node. The continued operation of the ZigBee network does not depend on the coordinator due to ZigBee 'self-healing capabilities. A network will, therefore, continue to function if the coordinator node should fall away.

The device type is normally determined at compile-time via compile options.

### **Router**

A router is a full-featured ZigBee node. A router performs functions (i) allowing other devices to join the network (ii) multi-hop routing (iii) assisting in communication for its child battery-powered end devices. Routers are typically always active on the network, therefore, requiring more power [26].

### **End device**

The end device can be a battery powered device as it has no specific responsibility for maintaining the network infrastructure. It can therefore sleep and wake up as it chooses [26]. End devices are unable to allow other devices to join the network as is the case with routers.

#### **3.4.2.4. Personal area network ID**

ZigBee networks are known as Personal Area Networks or PANs. Each network has its own unique PAN ID. All devices on a specific network will share a common identifier. ZigBee devices can be preconfigured to join any network that is in range or to only join a network with a specific PAN ID.

ZigBee supports both a 64-bit and a 16-bit PAN ID. Both IDs are unique to a specific network. All devices on the same network must share both the same 64-bit and 16-bit identifier. This is to avoid network interference between multiple networks sharing the same channel and are within range of one another.

The 64-bit PAN ID was created by the *ZigBee Alliance* to resolve the potential that two networks share the same 16-bit PAN ID as only limited addressing space is available (65 535 possibilities). If a device has a preconfigure 64-bit PAN ID, it will only join a network with the same 64-bit PAN ID. If no 64-bit PAN ID has been preconfigured, a device will join any detected PAN ID and inherit the PAN ID of the network.

Devices such as routers and end devices are usually configured to join a detected network with any PAN ID if the 64-bit ID is valid.

#### **3.4.2.5. Stack profile**

The set of stack parameters that need to be configured to specific values, along with the above device type values, is called a *stack profile*. The parameters are defined by the ZigBee Alliance.

All devices on the same network must conform to the same stack profile, therefore be configured with the same stack parameters. Devices with different stack profiles will not be able to form a network.

The ZigBee Alliance has defined two standard stack profiles for the ZigBee – 2007 specification, ZigBee, and ZigBee PRO with the goal of promoting interoperability. All devices that conform to these stack profiles will be able to form a network even if they are from different vendors.

The stack profile identifier that a device conforms to is present in the beacon transmitted by that device. This enables a device to determine the stack profile of a network before joining to it. The network-specific stack profile has an ID of 0 while the ZigBee stack profile has ID of 1, and a ZigBee PRO stack profile has ID of 2 [27].

If a device of one profile (ex. ZigBee PRO) joins a network with a different profile (ex ZigBee-2007), it will join as a non-sleeping end device [26].

### **3.5. CONCLUSION**

This chapter presented an overview of smart meters and communication technologies used in a smart grid environment. G3-PLC and ZigBee RF communication technologies were discussed with the focus on ZigBee RF as it will be the communication medium of choice in the project. The following chapters will discuss the development of the smart meters and data concentrator.

## **CHAPTER 4**

### **SMART METER HARDWARE DEVELOPMENT**

#### **4.1. INTRODUCTION**

This section describes the smart meter development with GPS and ZigBee RF communication capabilities required to detect the various identified hazards. Two smart meter manufacturers were approached, but neither was willing to allow access to their proprietary software. A solution found was to purchase a development meter from Texas Instruments (TI). The meter was supplied with open source software and all schematics are freely available. The meter was designed to house a ZigBee modem, which slots onto the PCB. Software to implement the ZigBee communication was also available from Texas Instruments.

#### **4.2. TEXAS INSTRUMENTS SMART METER OVERVIEW**

The TI energy meter evaluation module (EVM) associated with this thesis implements the MSP430F67791a system-on-chip (SoC). A SoC relates to a microcontroller (MCU) in that both implement a central processing unit (CPU) and embedded memory. A SoC, however, is a complete solution with added peripherals designed for a specific task, as with the MSP430F67791a, which incorporates an analogue front-end consisting of seven independent 24-bit  $\Sigma\Delta$  analogue to digital converters (ADC) to accurately measure current and voltage. The MSP430F67791a forms part of the MSP430F67xx family, which are some of the latest metering SoCs currently available and widely used in the metering industry. The SoC is closely comparable to the SoCs used in industrial meters.

Figure 20 shows the top view of the EVM, and the locations of the various sections of the EVM based on functionality.

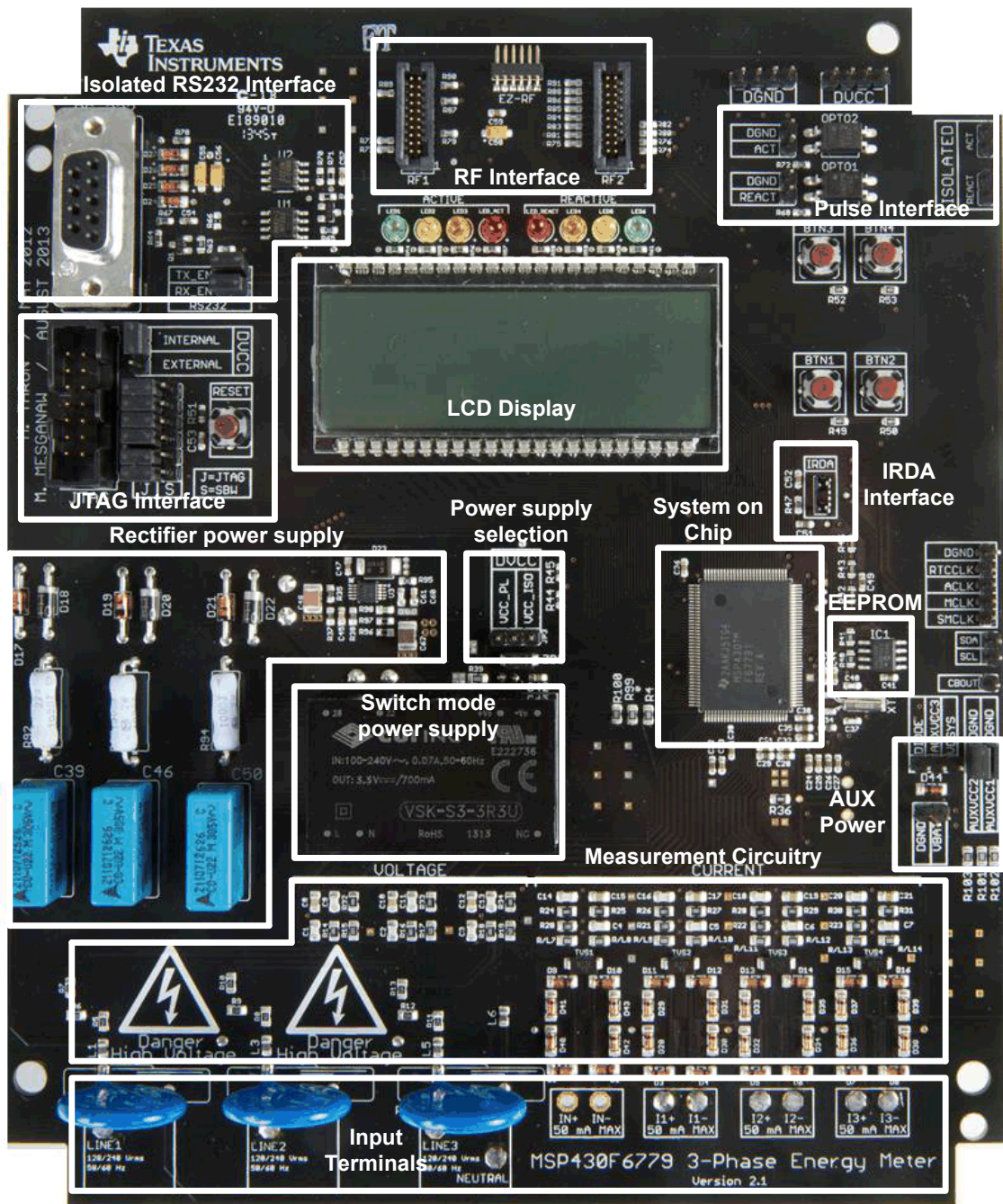


Figure 20: Top view of the three phase EVM with components highlighted [28]

### 4.3. SYSTEM DIAGRAMS

Figure 21 shows the typical connection for a single-phase electricity meter. For the multi-phase meter used, the connections in Figure 21 are duplicated for each phase. The AC voltages supported are 230V/460V at 50/60Hz to allow for over voltages that may be experienced by customers on dual phase feeders when a PEN conductor fails.

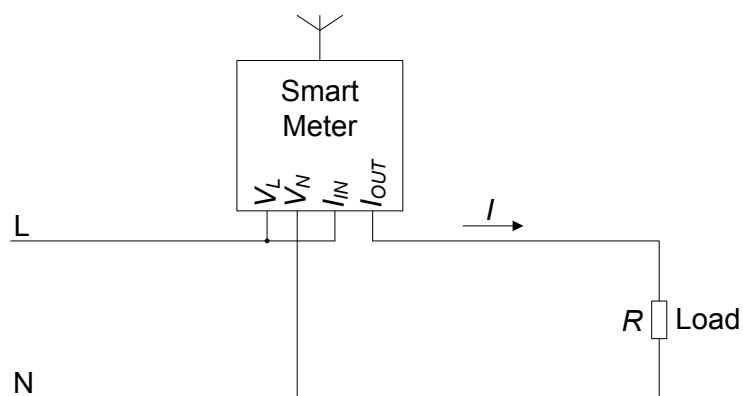


Figure 21: Typical per-phase connections of an electricity meter [28]

The following sections provide more information on the current and voltage measurement circuitry, ADCs, and other features of the EVM used.

#### 4.3.1. High-level interface

Figure 22 shows a block diagram of the TI smart meter which is based on the MSP430F67791a SoC. The meter was originally designed as a three phase-meter energy meter but only a single phase will be used in this implementation. The diagram shows the meter connected to a three-phase four wire star connection.

The meter has the capability to measure up to four currents but only three current transformers (CTs) were supplied with the meters. For this implementation on a single current measurement at a customer's premises and two current measurements at the MV/LV transformer is required. The CT has an associated burden resistor. The voltage across the burden resistors are measured by the sigma-delta ADC's to in turn calculate the current.

The voltage analog front end was designed to measure voltages of up to 460 V which can be measured at customers premises on a dual-phase feeder during a PEN conductor failure. The voltage was divided down to the range as accepted by the 24-bit sigma-delta ADC channels.

Pulse LED's on the meter are used to indicate the active and reactive power consumed. These LED's may also be used during active and reactive power calibration.

The MSP430F67791a MCU consist of a built-in liquid crystal display (LCD) controller, which can support up to an 8-input multiplexer display and 320 segments. In this design the LCD controller is configured to work in 4 input multiplexer mode using 160 segments [28].

Serial peripheral interfaces (SPI) can also be seen in Figure 22 that is used to communicate to the ZigBee modem, which slots onto the main board. Two universal asynchronous receiver/transmitter (UART) interfaces are used for calibration of the meter and output the current state of the ZigBee transmissions to a serial interface.

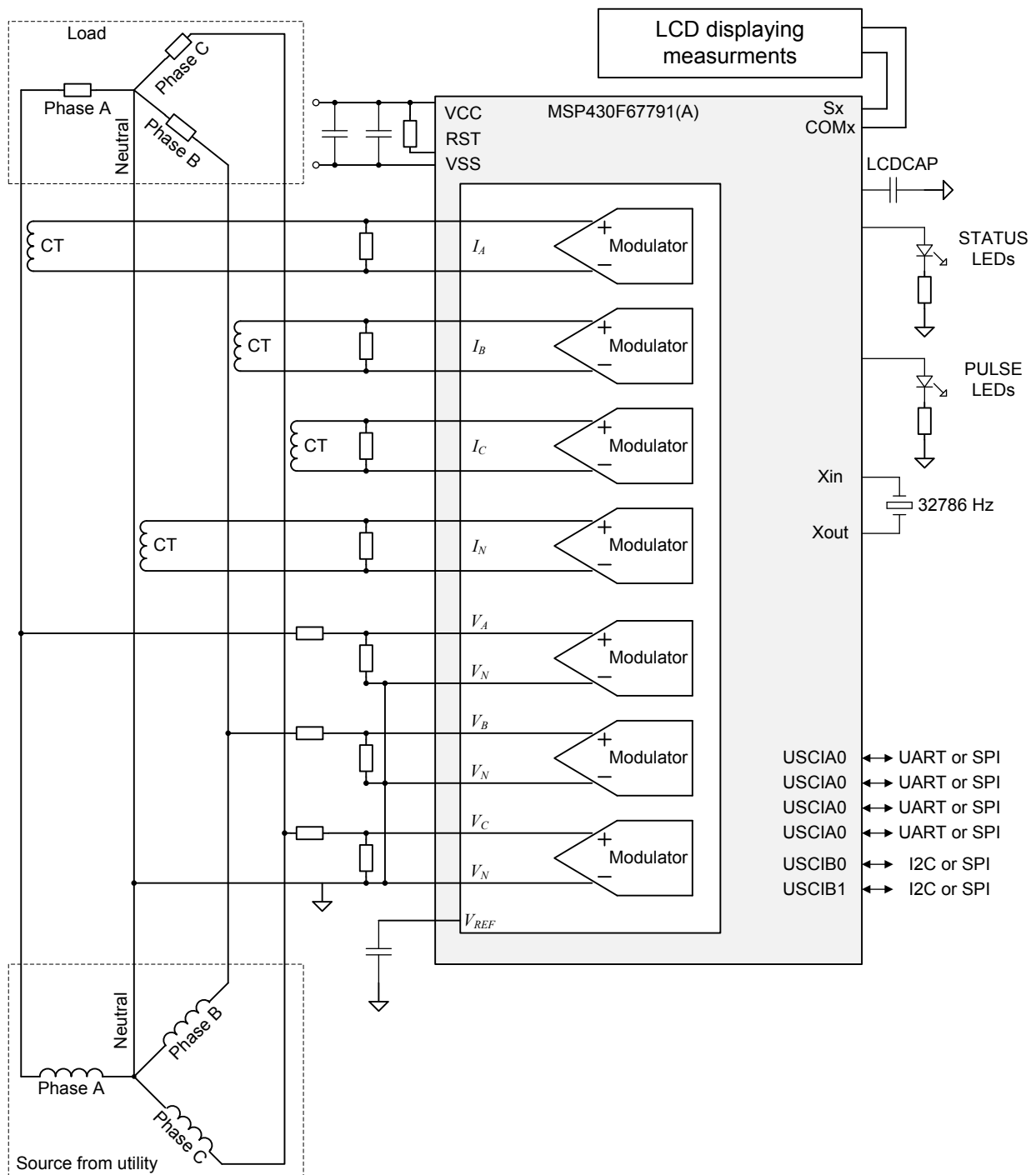


Figure 22: 3-Phases 4-wire star connection using MSP430F67791a MCU [28]

#### 4.4. MEASUREMENT CIRCUITRY

The MSP430F67791a SoC analogue front end has a fully differential architecture allowing negative voltage inputs. Therefore, AC signals can be connected directly without the need for level shifters. The maximum voltages at the pins may not exceed  $\pm 1$  V. The current and voltage measurements are scaled to meet this requirement. This section describes the analogue front end used for the voltage and current channels.

#### 4.4.1. Voltage measurements

On a dual-phase feeder, a phase-to-neutral unbalance may occur that could lead to a voltage as high as the dual-phase line-to-line voltage of 460 V. The design of the analog front was altered from the original design to allow for voltages of up to 460 V. Voltage measurements are scaled down to a range of 930 mV to allow for a 70 mV safety margin. This is done by the analogue front end, which consists of surge protection varistors followed by a simple voltage divider and RC low-pass filter that acts as an anti-alias filter.

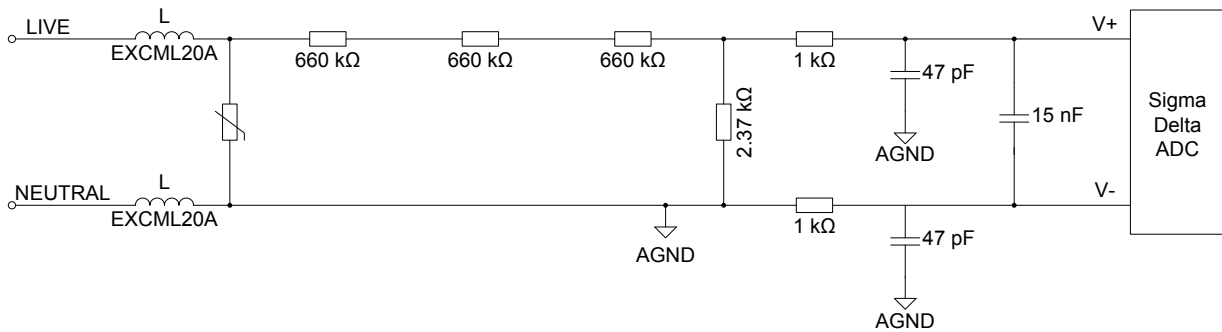


Figure 23: Voltage inputs analog front end [28]

Figure 23 shows the analogue front end for the voltage measurements for a maximum input voltage of 460 V. The voltage divider circuit consisting of three resistors in series and a single parallel resistor can be seen in the figure. The output voltage is calculated as follows:

$$\begin{aligned}
 V_{out} &= \frac{2.37k}{660k + 660k + 660k + 2.37k} \times V_{in} & (4.4.1) \\
 &= \frac{2.37k}{1982.37k} \times 460 \text{ V} \\
 &= 549 \text{ mV}
 \end{aligned}$$

The voltage is scaled to approximately  $549 \text{ mV}_{\text{rms}}$ , which is  $779 \text{ mV}_{\text{peak}}$ . This voltage measurement is within the SoC's ADC's analogue limit by a safety margin of greater than 15%. It allows for accurate measurement even during overvoltage conditions.

The meters were supplied with three 330 kΩ scaling resistors instead of the 660 kΩ resistors as the design of the meters were initially for a maximum voltage of 230 V. These were replaced by the 660 kΩ components.

#### 4.4.2. Current measurements

##### 4.4.2.1. Current transformers

Figure 24 shows the current transformers located in the meters. The CTs supplied with the meters has a primary rated current of 5 A with a secondary current of 2.5 mA resulting in a turns ratio of 1:2000. The CT's maximum allowable current is 100 A. No CT is supplied for the

neutral current, but can be added if required, but was not needed in this implementation as three current channels were sufficient.

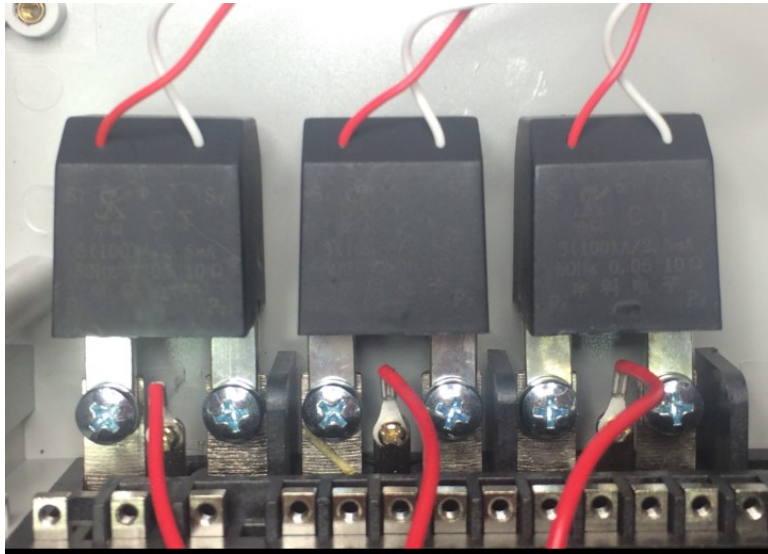


Figure 24: Current transformers of the meter [28]

#### 4.4.2.2. Analog front-end

Figure 25 shows the analogue front end used for the current measurements.

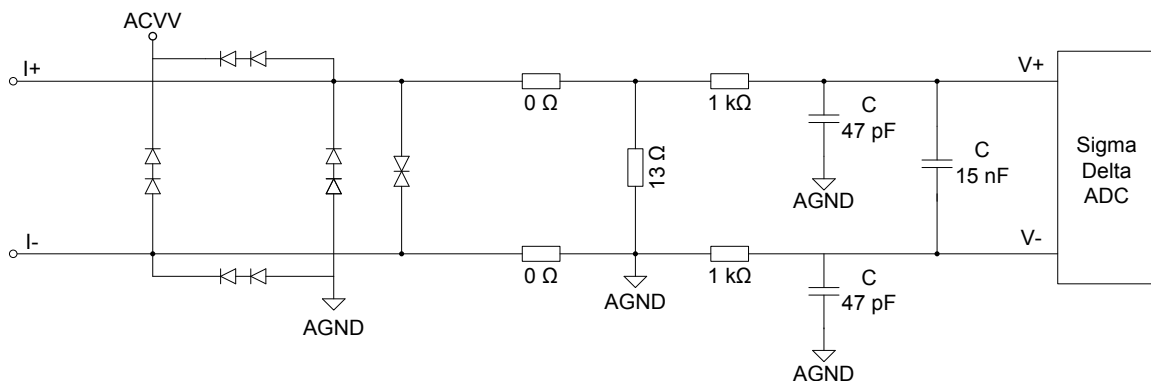


Figure 25: Current inputs analog front end [28]

The analogue front end for the current inputs was designed for a maximum input current of 100 A as supported by the CTs. With a turns ratio of 1:2000 the output secondary current is 50 mA. The design of the maximum peak input voltage is done for an output voltage of 919 mV<sub>peak</sub> or 649.83 mV<sub>rms</sub>. The burden resistor is calculated below to achieve the desired output voltage for a maximum current input:

$$\begin{aligned}
 R &= \frac{V}{I} & (4.4.2) \\
 &= \frac{649.83 \text{ mV}}{50 \text{ mA}} \\
 &= 13 \Omega
 \end{aligned}$$

The anti-aliasing circuitry, which consists of resistors and capacitors, follows the  $13\ \Omega$  burden resistor.

#### 4.5. CONNECTIONS TO A TEST SETUP

Figure 26 shows the top view of the meter indicating the voltage terminals  $V_A$ ,  $V_B$  and  $V_C$  correspond to the line voltages for phases A, B and C respectively. The voltage terminals should only be connected to the terminal that the three arrows are pointing to.  $V_N$  corresponds to the neutral voltage of the test AC source. A voltage input may not exceed 460 V.

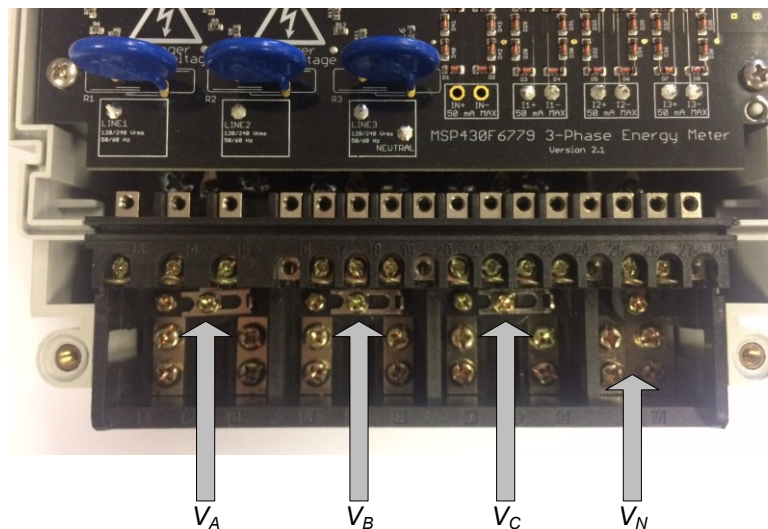


Figure 26: Top View of the EVM showing the voltage input terminals [28]

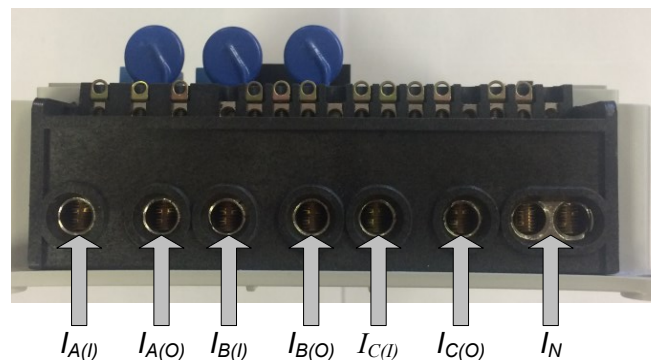


Figure 27: Front View of the EVM showing the three phase current input terminals [28]

Figure 27 shows the current input terminals.  $I_{A(I)}$  and  $I_{A(O)}$  correspond to the current input terminals for phase A,  $I_{B(I)}$  and  $I_{B(O)}$  correspond to the input terminals for phase B and,  $I_{C(I)}$  and  $I_{C(O)}$  correspond to the input terminals for phase C.

$V_N$  corresponds to the neutral voltage from the test setup. Even though the hardware and software supports the measurement of the neutral current, the EVMs obtained from TI does not

include a fourth current transformer connected to the fourth channel of the ADC. This could, however, be added if needed, but was not required in this project.

#### 4.6. GPS MODULE

An external GPS module was added to the smart meter to supply the meter with position and time data. The Adafruit GPS module is used which is similar to the module used on the data concentrator. See Section 6.3.7 for more information regarding the GPS module.

A UART serial connection is used to interface from the meter to the GPS module. The EZ-RF header on the meter is equipped with a UART port which is used. Only the TX pin of the GPS module is used as communication is only from the GPS module to the meter. Communication from the meter to the module is not required. Table 4 shows the connections between the meter and GPS module. The GPS outputs national marine electronics association (NMEA) packets, containing time and position information, to the meter which is interpreted by a state machine running on the meter. The software implementation to capture and interpret the NMEA packets can be seen in Section 5.3.4. Detail of the NMEA protocol can be found in APPENDIX B.

Table 4: GPS connection to smart meter

Adafruit GPS module	Texas Instruments smart meter
3.3V	DVCC (3.3V)
GND	DGND
TX	EZ-RF_RXD

#### 4.7. LCD DISPLAY

The liquid crystal display (LCD) of the meter scrolls through metering parameters approximately every two seconds. The meter cycles through the three phase measurements (A, B and C) displaying each metering parameter. For each parameter that is displayed a parameter symbol, the parameter's value and its corresponding phase is displayed. The symbol, value and phase is displayed in the LCD as shown in Figure 28.

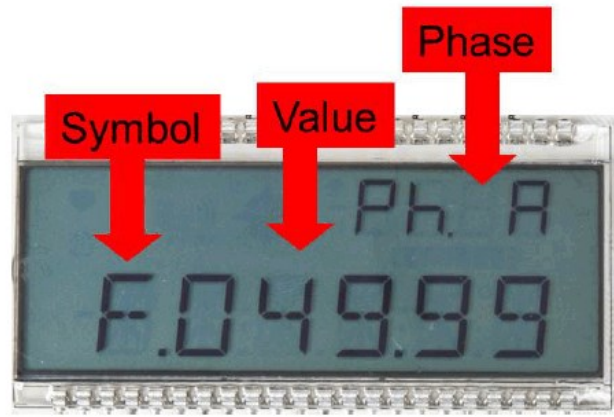


Figure 28: LCD display of smart meter [28]

Table 5 shows the different metering parameters, with their corresponding symbols, that is displayed on the LCD.

Table 5: Displayed parameters [28]

Parameter Name	Symbol	Units	Comments
Voltage		Volts (V)	--
Current		Amps (A)	
Active Power		Watt (W)	--
Reactive Power		Volt-Ampere Reactive (var)	--
Apparent Power		Volt-Ampere (VA)	--
Frequency		Hertz (Hz)	--
Power Factor		Constant between 0 and 1	<p>The characters  are used if the load is determined to be a capacitive load.</p> <p>The characters  are used if the load is determined to be an inductive load.</p>
Total Consumed Active Energy		100 "Tick"	Every 10 ticks increments the tenths place by 1.
Total Consumed Reactive Energy		100 "Tick"	Every 10 ticks increments the tenths place by 1.

#### 4.8. VIEW METER READINGS ON A PC

A Texas Instruments provided graphical user interface (GUI) is used to view the current meter readings on a windows computer as well as to calibrate the meter. This section will give an overview of the process to follow to install the GUI.

The calibrator can be downloaded from <http://www.ti.com/tool/TIDMTHREEPHASEMETER-F6779> and located in the /Source/GUI folder.

To run the GUI:

1. Connect the EVM (RS-232 port) to a PC via an RS-232 to USB converter cable.
2. Open the /Source/GUI folder and open calibration-config.xml in a text editor.
3. Change the port name field within the meter tag to the communication (COM) port connected to the meter.
4. In Figure 29 the field is changed to COM2. The COM port number can be found under the device manager on a Windows PC.

```

343 | <step current="25.000" phase="0.0" gain="1.0"/>
344 | <step current="30.000" phase="0.0" gain="1.0"/>
345 | <step current="35.000" phase="0.0" gain="1.0"/>
346 | <step current="40.000" phase="0.0" gain="1.0"/>
347 | <step current="45.000" phase="0.0" gain="1.0"/>
348 | <step current="50.000" phase="0.0" gain="1.0"/>
349 | <step current="55.000" phase="0.0" gain="1.0"/>
350 | </correction>
351 | </phase>
352 | <temperature/>
353 | <rtc/>
354 | </cal-defaults>
355 | <meter position="1">
356 | <port name="\\.\com2" speed="9600"/>
357 | </meter>

```

Figure 29: GUI configuration file – changing the com port [28]

5. Run calibrator.exe, if the COM port was configured correctly the GUI will open up. If the GUI connects correctly to the EVM, the top left button is green as in Figure 30. If there are problems with the connection the button is red. Click on the green button to view the meter measurements.

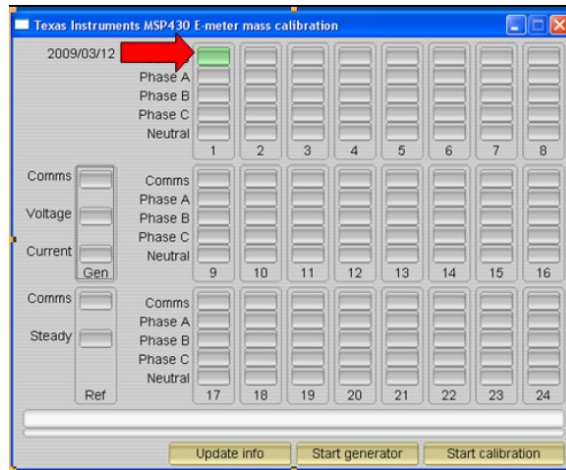


Figure 30: GUI window [28]

6. Selecting the green button in Figure 30 opens the results window as seen in Figure 31. The phase measurements as measured by the meter will be displayed.



Figure 31: Results window [28]

#### 4.9. METER CALIBRATION

Calibration is an important aspect of the performance of the meter as the components of each meter might differ slightly due to component tolerances. The key to calibration is a highly accurate AC source. An Omicron CMC256 [29] was used as it was available and can generate any desired voltage and current at a specified phase angle. This section gives more detail to the process of calibrating the meter.

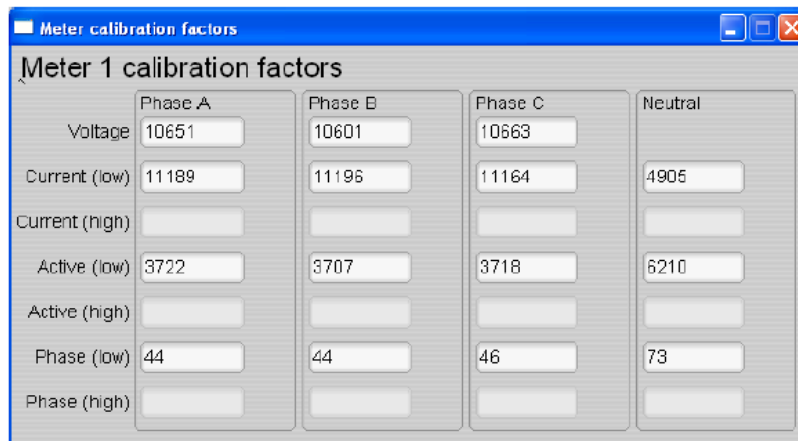
The GUI discussed in section 4.8, is also used for the calibration of the meter. The calibration process changed parameters of the software running on the meter. These parameters are called calibration factors. The following scaling factors are available, which can be altered during the calibration process:

- Voltage scaling factor
- Current scaling factor

- Power scaling factor
- Phase compensation factor

These scaling factors are used to convert the measured values to real-world values in volts, amps and watts [28].

Default calibration factors which can be found in the emeter-3ph-neutral-6779(A).h file of the meters software are loaded when the meter is flashed with the metering software. The GUI is used to alter these values during calibration. The calibration factors are stored in information memory, and therefore, will remain the same when the meter is restarted. The meter should, however, be recalibrated when it's flashed with new software. The meter calibration factors are saved by selecting the "Meter calibration factors" button shown in Figure 31. The final calibration parameters obtained can be used to change the default calibration factors in the emeter-3ph-neutral-6779(A).h file accordingly, to ensure the meter is calibrated correctly when re-flashed with a new version of the metering software.



	Phase A	Phase B	Phase C	Neutral
Voltage	10651	10601	10663	
Current (low)	11189	11196	11164	4905
Current (high)				
Active (low)	3722	3707	3718	6210
Active (high)				
Phase (low)	44	44	46	73
Phase (high)				

Figure 32: Calibration factors window [28]

#### 4.9.1. Voltage and current gain calibration:

The following describes the steps to follow to calibrate the voltage and current measurement of the meter [28]:

1. Open the GUI software supplied by TI.
2. Configure a source, such as an Omicron, to supply the meter with a specific voltage and current. Supply all the metering phases with the same voltage and current. Ensure there is a zero-degree phase shift between voltage and current. For example, 230V, 10A, 0° (PF = 1).
3. Select the "Manual cal" button in the GUI to open a meter error window as shown in Figure 33.

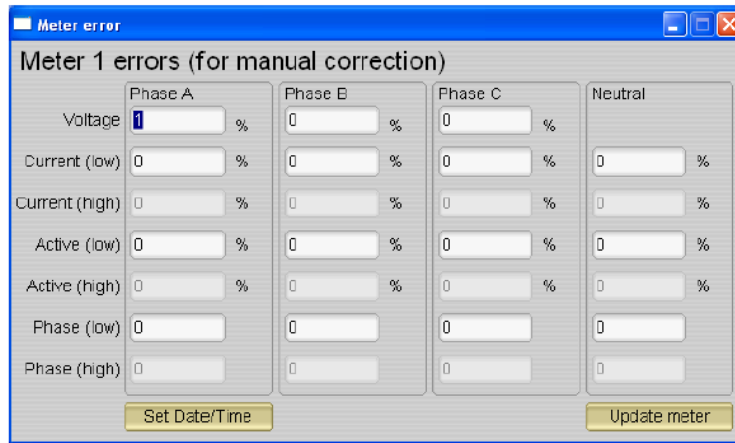


Figure 33: Manual calibration window [28]

- The correction values to enter into the voltage and current fields is calculated using equation 4.9.1. The value observed is the value as shown in the GUI software.

$$Correction (\%) = \left( \frac{value_{observed}}{value_{desired}} - 1 \right) \times 100 \quad (4.9.1)$$

- Enter the calculated correction percentages for all the voltages and currents in the corresponding “voltage and current (low) fields”. Negative values entered should include the negative sign.
- Select “Update meter” tab and see the observed values settle to the desired values. Repeat the process if the values are not perfectly calibrated yet.

#### 4.9.2. Active power gain calibration

The active power gain calibration process is similar to that of the voltage and current gain calibration process. Repeat the steps as described in section 4.9.1 by inputting a desired voltage and current with zero phase shift. Calculate the amount of active power injected by the source and calculate the correction percentage using equation 4.9.1. Enter the correction percentage into the active (low) field. Repeat this process until the error percentage is zero [28].

#### 4.9.3. Phase correction calibration

The following explains the process to follow to perform phase calibration. Each phase should be calibrated separately, repeating the steps for each phase.

Phase correction calibration is performed with the following steps: [28]

- Disable all phases that are not being calibrated by setting the current of these phases to zero.

2. Change only the phase that is being calibrated to a non-zero value on the AC supply (Omicron); typically,  $+60^\circ$  is chosen. The PC GUI will now display the new phase shift value in the “Phase V->I” field.
3. If the value is not close to the supplied phase-shift value, perform phase correction by following these steps:
  - a) Enter a small positive or negative integer value as an update for the Phase (Low) field in the Manual Calibration window (Figure 33).
  - b) Select ‘update meter’ and monitor the value of the “Phase V->I” field.
  - c) If the reading is not changed to the desired value, fine tune by increasing or decreasing the by a value of 1 based on Step 3a and 3b.
  - d) Change the phase shift to  $-60^\circ$  to verify that the meters measured value is still acceptable.

After calibration is completed the new calibration factors can be viewed by selecting the “Meter Calibration Factors” button of the GUI.

#### 4.10. METER ACCURACY

The accuracy of the meter was tested to provide an insight into the accuracy of the ADC and CTs. The results obtained can be seen in Table 6 and Table 7. The tests were conducted using an Omnicron 256 as the source. The results gathered is the final measurements as measured by the meter, thus it includes all the inaccuracies of the CTs and ADC. The meter proved to be very accurate with voltage errors of less than 1% and current errors smaller than 0.35% for currents above 10 mA. The percentage error shown in the tables are based on the average of the three phases.

Table 6: Meter current measurement accuracy

Input:	10 A	5 A	1 A	0.5 A	0.2 A	105 mA	15 mA	10 mA	1 mA
PH A	10.032	5.016	1.002	0.500	0.200	105 m	15 m	11 m	3 m
PH B	10.033	5.016	1.003	0.501	0.200	105 m	15 m	10 m	3 m
PH C	10.040	5.025	1.005	0.502	0.200	105 m	15 m	10 m	3 m
Average	10.035	5.019	1.0033	0.501	0.200	105 m	15 m	10.3 m	3 m
% Error	0.35 %	0.38 %	0.333%	0.2 %	0 %	0%	0%	3 %	200 %

Table 7: Meter voltage measurement accuracy

<b>Input:</b>	<b>115 V</b>	<b>110 V</b>	<b>100 V</b>	<b>100.1 V</b>	<b>80.5 V</b>
<b>PH A</b>	115.00	110.00	100.00	100.09	80.49
<b>PH B</b>	115.00	110.01	100.00	100.11	80.50
<b>PH C</b>	115.00	110.01	100.00	100.01	80.50
<b>Average</b>	115.00	110.01	100.00	100.07	80.497
<b>% Error</b>	<b>0 %</b>	<b>0.009 %</b>	<b>0 %</b>	<b>0 %</b>	<b>0.003 %</b>

#### 4.11. CONCLUSION

This section described the hardware development of the TI smart meter used for this project. The meters make provision for three voltage and current measurement inputs. The voltage analogue front end was altered to be able to measure dual phase line to line voltages of 460 V.

An external GPS module was added to the meters as GPS capabilities are not included as standard. The meters make provision for ZigBee modules capable of sending meter data. The following chapter will discuss the software development of the meter which was required for this project.

## CHAPTER 5

# SMART METER SOFTWARE DEVELOPMENT

### 5.1. INTRODUCTION

This chapter covers the software development for implementing a smart meter using the TI MSP430F67791a polyphase metering system-on-chip (SoC) microcontroller. In addition to the typical functions of existing off-the-shelf meters, this metering solution provides customizability that will allow the implementation of additional functionality that will enable research in detecting LV safety hazards.

The smart meter is intended to communicate to a data concentrator by using the industry standard IEEE802.15.4, ZigBee wireless protocol. The CC2530 SoC from TI has been selected and provides a single-chip solution for implementing ZigBee. This allows the MSP430F67791a SoC to focus on the metrology while the CC2530 maintains the ZigBee protocol stack.

TI has published a certified and open source implementation of the ZigBee protocol for the CC2530, called the Z-stack. Although the Z-stack source code is freely available, the pre-compiled Z-stack firmware is sufficient and no modifications were needed for the project.

In this chapter, the MSP430F67791a SoC software for implementing the metrology and managing the ZigBee communications with the CC2530 are discussed.

### 5.2. CODE COMPOSER STUDIO DEVELOPMENT ENVIRONMENT

#### 5.2.1. Overview

TI provides an integrated development environment (IDE) for use with its microcontrollers. This IDE is called Code Composer Studio (CCS) and is available for download free of charge from the TI website. The free version has a code size limit, which is sufficient for this work. CCS provides extensive development and debugging tools for programming the MSP430 series microcontrollers in the C language.

The original source code for the MSP430F67791a smart meter that was provided by TI was developed with the proprietary IAR Embedded workbench. IAR Embedded workbench is another software suite, similar to CCS, but requires a software license for each workstation. IAR does not follow the standard C language and makes use of adapted syntax to improve code optimisation during compile time. For this reason, code that was developed specifically for IAR optimisation will not compile in CCS unless the syntax is altered.

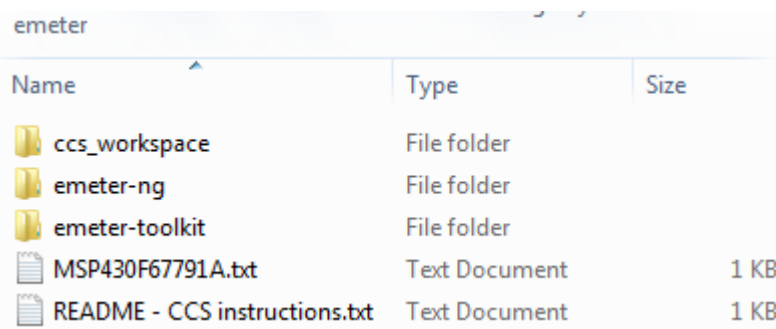
Due to the high costs involved in obtaining IAR software licenses (approximately R25 000 per license), it was decided to port the code base from IAR Embedded workbench to CCS. This

required the familiarisation with the differences between standard C and IAR adaptations and to correct those adaptations for CCS. The software was successfully ported from IAR to CCS and the next section will detail how the ported project can be imported into a new CCS installation. The porting of the code to CCS was done with the help of Dr. Males Tomlinson.

### 5.2.2. Setting up the project in CCS

Here it will be shown how to import the project into a new installation of CSS. The e-meter source code consists of two projects, the e-meter toolkit and the e-meter implementation. The e-meter toolkit provides common functions and sub-routines that are used throughout the e-meter implementation. Some of these functions and sub-routines are written in assembly language.

In the base folder, there are three subfolders, `ccs_workspace`, `emeter-ng` and `emeter-toolkit` as shown in Figure 34. The folder `ccs_workspace` contains the CCS project configuration files and the other two folders contain the actual source code.



Name	Type	Size
ccs_workspace	File folder	
emeter-ng	File folder	
emeter-toolkit	File folder	
MSP430F67791A.txt	Text Document	1 KB
README - CCS instructions.txt	Text Document	1 KB

Figure 34: Project folder

1. Start with a new CCS workspace. The workspace can be saved to any desired location.
2. From the menu bar, go to Project -> Import CCS Projects...
3. Under "Select search-directory", browse to the source code base folder in Figure 34.
4. The "emeter-toolkit" and "emeter-ng" projects should appear in the discovered projects list.
5. Highlight both projects
6. Uncheck: "Automatically import referenced projects found in the same search-directory"
7. Uncheck: "Copy projects into the workspace"
8. Click Finish

The two projects should now appear under the project explorer. For each of the two projects, highlight the project in the project explorer and:

1. From the menu bar select: Project -> Properties

2. Under: Resources - > Linked Resources, choose the “Path Variables” tab and select “New”.
3. Create a new path variable with the name “EMETER\_SOURCES” and point it to the source code base folder shown in Figure 34.

Both projects are now imported into the current CCS workspace, but the project files are not copied into the CCS workspace. The project configuration and source files remain in the source code base folder. If the base folder is moved, the “EMETER\_SOURCES” path variable just needs to be updated accordingly. This makes it easy to transport, backup and share the project.

### **5.3. SOFTWARE DEVELOPMENT**

#### **5.3.1. Overview**

The smart meter software described in this chapter is based on the example source code that is provided by TI for use with the MSP430F67791a metrology SoC and the EVM430 evaluation board. The source code has been ported from IAR embedded workbench to code composer studio, see Chapter 5.2, and has been adapted to suit the needs of this project. This chapter provides an overview of the implemented functionality with adaptations to the original code and documentation. For the original source code and documentation, see document SLAA577G [30].

#### **5.3.2. Foreground process**

The metrology software is split between two processes, a foreground process for tasks with a longer calculation time and a background process that is strictly timed and responsible for accumulating the measurement samples from the ADC. The foreground process is the main program loop that is executed upon device reset. The flow diagram of the foreground process is shown in Figure 35.

The background loop is responsible for accumulating voltage and current sample measurements at a rate of 4096 times per second. After a second of accumulation, the background loop indicates to the foreground loop that data is available for processing. A status flag indicates every time a data frame is ready for processing. A data frame consists of processed current, voltage, active energy, and reactive energy accumulated for one second. A counter keeps track of the number of samples captured, which can continually change as the software automatically synchronises with the grid frequency [28].

As shown in Figure 35 the foreground loop starts with a system reset followed by the setup of the peripheral hardware. After the hardware is setup is completed, the foreground process

checks for a notification from the background that a new data frame is available for processing. If data is available, the foreground loop calculates the respective r.m.s. values, active power, apparent power, reactive power, accumulated active and reactive energy, the mains frequency and the power factor. Thereafter, the LCD display is refreshed. The network impedance is then calculated using the voltage and current measurements, more detail can be found in Chapter 9 on this subject.

The foreground process is also responsible for updating the RTC of the meter with the latest timestamp received from the GPS. The state machine responsible for interpreting the NMEA packets received from the GPS module is explained in detail in section 5.3.4.

ZigBee data strings are then constructed in a structured manner to send to the data concentrator. Lastly, the ZigBee communications management is serviced and the process is returned to the beginning. The software to service ZigBee, calculate the impedance and update the RTC from the GPS data strings had to be additionally programmed.

Two things are worth noting here. Firstly, the ZigBee communications management is executed continuously when no data frame is ready for processing. Secondly, the foreground loop's total execution time should not exceed one second and may not skip any data frame sent from the background loop. The calculation time of the ZigBee communications management must, therefore, be restricted to allow the foreground loop keep to its timing schedule. To accomplish this, a multi-switch-case tasking scheme is implemented for the communications management.

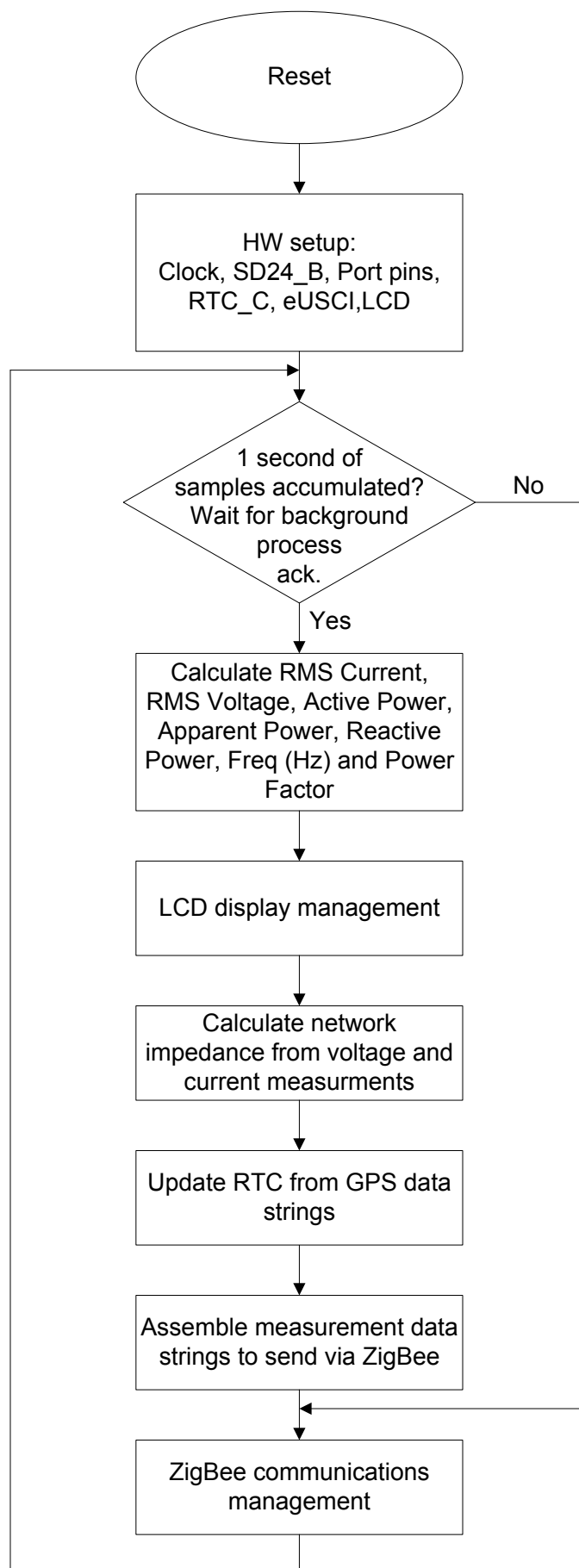


Figure 35: E-meter software main foreground process

### 5.3.2.1. Voltage and current measurements

The meter accumulates the voltage and current samples at a rate of 4096 samples per second using the 24-bit sigma-delta ADC channels. One second worth of samples are accumulated, thus when the sample counter reaches a value of 4096, and kept to obtain the r.m.s. values of the voltage and current. The assembly functions `div_sh48` and `div_ac_current` are used for calculating the r.m.s. measurements from the respective accumulated sample sets. Equations 5.3.1 and 5.3.2 are used to calculate the r.m.s. voltage and current from the accumulated samples

$$V_{RMS,\phi} = K_{v,\phi} \sqrt{\frac{\sum_{n=1}^{Sample\ count} v_{\phi}(n) * v_{\phi}(n)}{Sample\ count}} \quad (5.3.1)$$

$$I_{RMS,\phi} = K_{i,\phi} \sqrt{\frac{\sum_{n=1}^{Sample\ count} i_{\phi}(n) * i_{\phi}(n)}{Sample\ count}} \quad (5.3.2)$$

where  $\phi$  indicates the phase,  $v_{\phi}(n)$  is the respective phase voltage at sample instance  $n$ ,  $i_{\phi}(n)$  is the respective phase current at sample instance  $n$ , and  $K_{v,\phi}$  and  $K_{i,\phi}$  the respective scaling factors. Sample count is the number of samples in the given data frame which is usually 4096 but can change under certain conditions for example when no zero crossing is detected. Under this condition, the meter will collect up to a maximum of 4296 samples then force the foreground loop to calculate the r.m.s. values.

### 5.3.2.2. Power and energy measurements

Active and reactive power and active and reactive energy are calculated using one data frame worth of voltage and current samples. These samples are phase corrected by the background process and passed to the foreground process. The active and reactive and power are calculated in the foreground process as follows:

$$P_{ACT,ph} = K_{ACT,ph} \frac{\sum_{n=1}^{sample\ count} v(n) * i_{ph}(n)}{sample\ count} \quad (5.3.3)$$

$$P_{REACT,ph} = K_{REACT,ph} \frac{\sum_{n=1}^{sample\ count} v_{90}(n) * i_{ph}(n)}{sample\ count} \quad (5.3.4)$$

where,  $v_{90}(n)$  is the voltage sample at instant  $n$  shifted by  $90^{\circ}$  and  $K_{ACT,ph}$  and  $K_{REACT,ph}$  are the scaling factors for the active and reactive power respectively. The active and reactive energy is calculated from the active power by

$$E_{ACT,ph} = P_{ACT,ph} \times (Sample\ count) \quad (5.3.5)$$

$$E_{REACT,ph} = P_{REACT,ph} \times (Sample\ count) \quad (5.3.6)$$

As stated in [31] reactive power can be calculated in a meter using three possible methods. The time delay method has been implemented in the meter, which delays one of the waveforms by 90° (a quarter of a cycle) at the fundamental frequency. The reactive power is then obtained by multiplying the two waveforms. The major disadvantage of this method is the error introduced with frequency changes as the number of samples representing a quarter-cycle is no longer a constant [31].

In this implementation, the voltage waveform is shifted by 90°. The meter implements interpolation of two voltage samples, one sample slightly more than 90° before the current and another sample slightly less than 90° before the current to improve accuracy and reduce the effect of frequency changes as explained above. The reactive power is then obtained by multiplying the newly obtained voltage sample with the corresponding current sample.

After calculating the active and reactive power, each phase's apparent power is calculated by

$$P_{APP,ph} = \sqrt{(P_{ACT,ph})^2 + (P_{REACT,ph})^2} \quad (5.3.7)$$

and in addition to calculating the per-phase active and reactive power and energy, the cumulative sum of these parameters are calculated by

$$P_{ACT,Cumulative} = \sum_{ph=1}^3 P_{ACT,ph} \quad (5.3.8)$$

$$P_{REACT,Cumulative} = \sum_{ph=1}^3 P_{REACT,ph} \quad (5.3.9)$$

$$E_{ACT,Cumulative} = \sum_{ph=1}^3 E_{ACT,ph} \quad (5.3.10)$$

$$E_{REACT,Cumulative} = \sum_{ph=1}^3 E_{REACT,ph} \quad (5.3.11)$$

### 5.3.2.3. Power factor

The power factor is calculated after the active and apparent power have been calculated. The result is the absolute value of the power factor. To determine if the power factor is leading (current leads voltage) or lagging (current lags voltage) the software monitors the current waveform at each negative to positive zero crossing. If the current is below the voltage waveform, the current is lagging the voltage. If the current is above the waveform, the current is leading the voltage. Internal to the meter a leading power factor is represented by positive power factor, while a negative power factor represents a lagging power factor. The value of the power factor is determined by the background process as follows:

$$PF_{internal} = \begin{cases} \frac{P_{ACT}}{P_{APP}}, & \text{if capacitive load} \\ -\frac{P_{ACT}}{P_{APP}}, & \text{if inductive load} \end{cases} \quad (5.3.12)$$

### 5.3.3. Background process

The primary function of the background process is to take the voltage and current sample measurements from the ADC and accumulate these samples. The background process is an interrupt service routine (ISR) that is triggered by the sigma-delta ADC's interrupt. The ADC triggers at a fixed rate of 4096 samples per second, or approximately 82 samples per cycle. The square of the samples is accumulated and passed to the foreground process to calculate the r.m.s. voltage and current using formulas as in Section 5.3.2.1. Voltage samples are accumulated and stored in three 16-bit registers, which act as a single 48-bit register. Similarly, three 24-bit registers acting as a single 64-bit register is used to accumulate the current samples. This is done per phase for both the voltage and the current. The active power and reactive power are also accumulated in 64-bit registers.

The timing of the background process is critical and is timed by the interrupts of the ADC. Approximately one second worth of samples are accumulated, or 4096 samples. The background process waits for the first zero crossing of the voltage after 4096 samples have been accumulated to trigger the foreground process to process the data. If no zero crossing is detected after 4296 samples the background process automatically triggers the foreground process. While the foreground process calculates the final values of the r.m.s. voltage, r.m.s. current, active, reactive and apparent powers, active, reactive and apparent energy, frequency and power factor the background process is busy accumulating a new second worth of samples. It is therefore critical that the foreground process executes in under a second to ensure it is ready to process the new set of samples captured by the background process.

The calculation of the LED energy pulses, the grid frequency and the determination if the current leads or lags the voltage is also done by the background process.

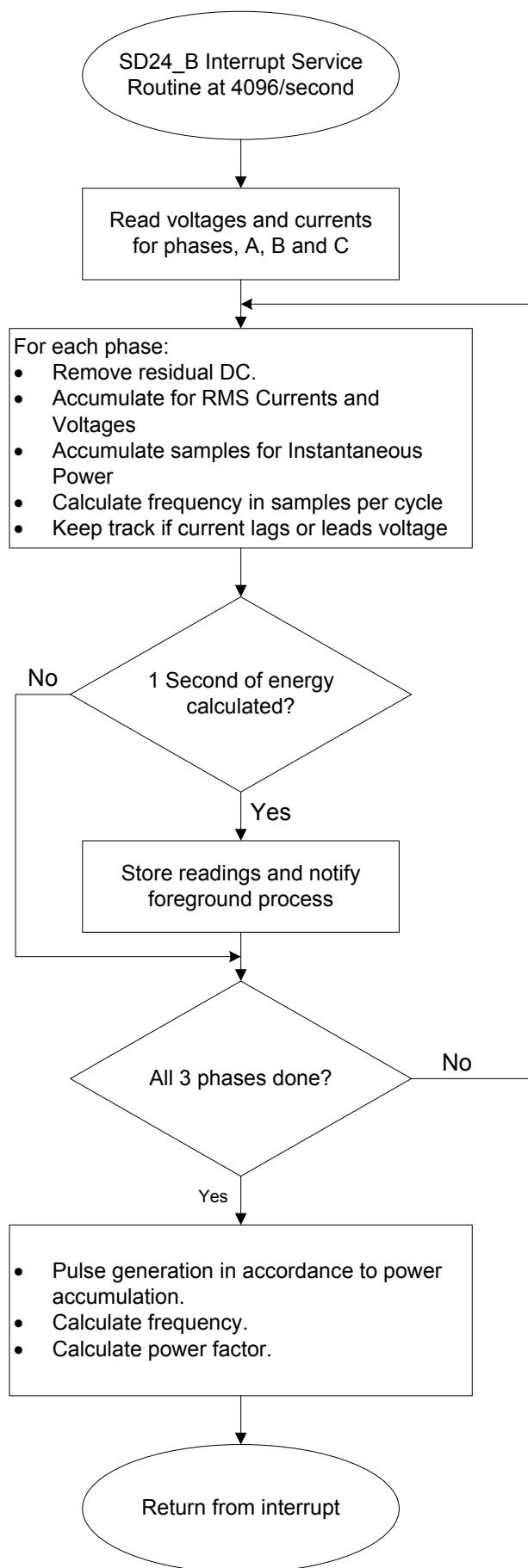


Figure 36: E-meter software background process [28]

### 5.3.3.1. Phase compensation on current measurement

An additional phase shift is introduced by the CTs on the current measurements. This relative phase shift between the voltage and current must be compensated for. The sigma-delta ADC include programmable delay registers ( $\Sigma\Delta 24PREx$ ) that can be used to compensate for the phase shift caused by the CTs. The resolution of the delay registers is a function of the input frequency ( $f_{IN} = 50\text{Hz}$ ), over-sampling ratio (OSR), and the sampling frequency ( $f_s = 4096$ ). The following formula is used to calculate the delay resolution:

$$DelayResolution_{DEG} = \frac{360^\circ \times f_{IN}}{OSR \times f_s} = \frac{360^\circ \times f_{IN}}{f_M} \quad (5.3.13)$$

For this meter, for an input frequency of 50 Hz, over-sampling ratio of 256, and sampling frequency of 4096, the resolution for every bit in the preload register is approximately  $0.017^\circ$  with a maximum of  $4.37^\circ$  (maximum of 255 steps). It is common practise to apply 128 steps of delay ( $2.17^\circ$ ) to all the phases and then adjust for each phase accordingly. Each phase can be adjusted by a maximum of  $\pm 2.17$ . The phase compensation is achieved by changing the value of the  $\Sigma\Delta 24PREx$  register in software for each phase.

### 5.3.3.2. Frequency measurement

As previously discussed, the background process is responsible for accumulating voltage and current samples. Zero cross detection is used to count the number of cycles in 1 second. After 1 second has passed, or a maximum of 4296 samples accumulated, the background process calculates the frequency as samples per mains cycle. The conversion to hertz is then done by the foreground process as follows:

$$f_{HZ} = \frac{\text{Sampling Rate} \left( \frac{\text{samples}}{\text{second}} \right)}{\text{Number of samples per cycle}} \quad (5.3.14)$$

To measure frequency, a straight-line interpolation between the zero crossing voltage samples is used. A process called linear interpolation is used to filter out noise spikes near the zero crossing. Figure 37 shows samples near a zero cross and the interpolation process. The process uses the rate of change of voltage samples to determine if a voltage samples is accurate. This will ensure that the two samples used for interpolation, are genuinely the samples just before and just after the zero cross.

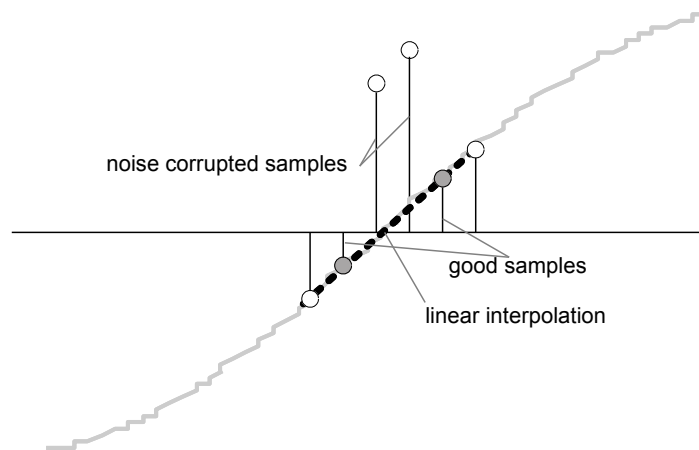


Figure 37: Zero-crossing detection for frequency measurement [28]

### 5.3.3.3. *LED pulse generation*

Most electricity meters generate light pulses proportionally to the rate at which electricity is being consumed. This gives the user a visual indication of the rate of consumption. Another key usage of the LED energy pulses is to calibrate the active and reactive power measurement of the meter. By using a reference power supply with a light emitter detector, the meter's active and reactive power measurements can be calibrated according to the power supplied by the reference power supply.

It is therefore critical that pulse generation is accurate. The meter uses the average power, as accumulated by the background loop and processed by the foreground loop, which is the equivalent of converting it to energy, to generate a pulse once a certain energy threshold is crossed. The amount of energy above this threshold is stored and a new energy value is added on top of this value in the next interrupt cycle.

The threshold, which determines the rate of the LED "tick" is a predefined constant. It is usually defined as the number of pulses per kWh. In this case the "tick" rate is set at 6400 pulses per kWh of active and reactive energies. The smart meter has 5 LEDs, three (LED1, LED2, LED3) correspond to the active energy consumed by phases A, B and C respectively, LED\_ACT indicates the cumulative three-phase active energy of the three phases and LED\_REACT indicates the cumulative three-phase reactive energy of the three phases.

The LED pulse rate can be set in software. Figure 38 shows the flow diagram for pulse generation.

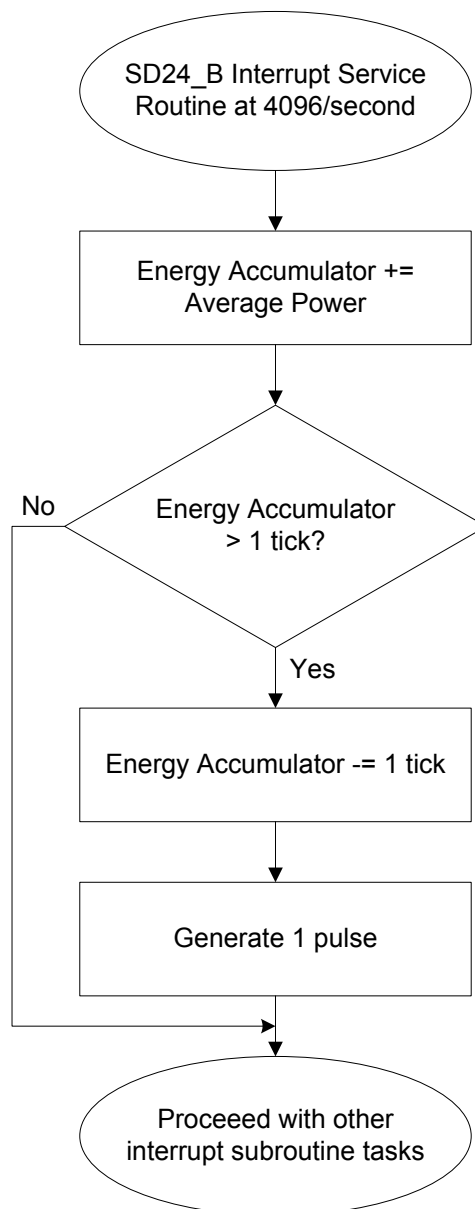


Figure 38: Flow diagram for energy indicator pulse generation [28]

#### 5.3.4. GPS interrupt service routine state machine

GPS data is captured in an interrupt service routine (ISR) state machine, which was added to the meter's software, as the original code did not make provision for GPS capability. GPS national marine electronics association (NMEA) data strings received over the serial UART port from the Adafruit GPS module triggers an ISR as soon as the first byte is received.

##### 5.3.4.1. *Interrupt service routine overview*

An ISR, also known as an interrupt handler, is a separate function which is triggered by an interrupt event such as an external input to a system. The MCU will stop executing the code that it is currently busy with in the foreground process and jump to a separate piece of code.

The interrupt handling code is often called an ISR [32]. When the ISR is finished, it will return to the foreground process that it was busy with no awareness that the code has been interrupted.

Interrupt service routines need to be kept as short and simple as possible to ensure the MCU can return to the main program in a timely manner. State machines are used to keep large and complicated service routines short and simple. The function to be performed by the ISR depends on the state of the application prior to the interrupt being triggered. This drastically reduces the execution time of the ISR as the MCU jumps directly to the specific state which requires execution by making use of a switch statement.

#### **5.3.4.2.        *GPS ISR state machine***

A four-state state machine is used to capture the NMEA GPS messages over a UART port shown in Figure 39. An explanation of the NMEA standard can be found in APPENDIX A. A flow diagram of each state is given in Figure 40 to Figure 43. A description of each state is given below:

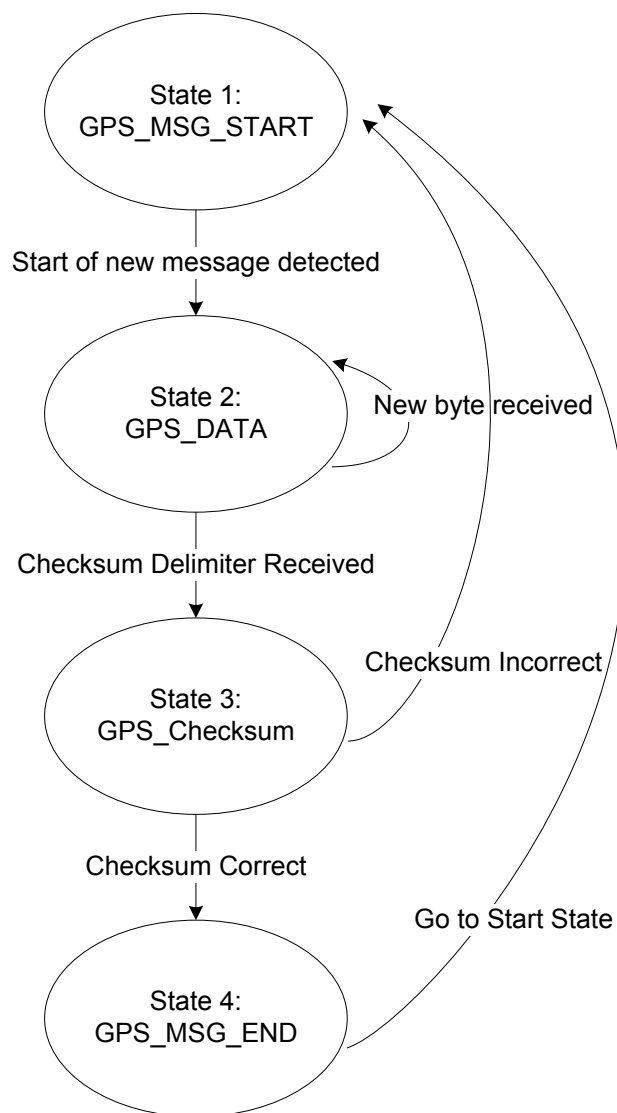


Figure 39: GPS interrupt service routine state machine

#### GPS message start state:

This state is entered upon the first-time trigger of the ISR. If the start delimiter of a GPS NMEA string is detected it is stored and the state variable is changed to the next state. If the byte received was not the start delimiter it will remain in the current state.

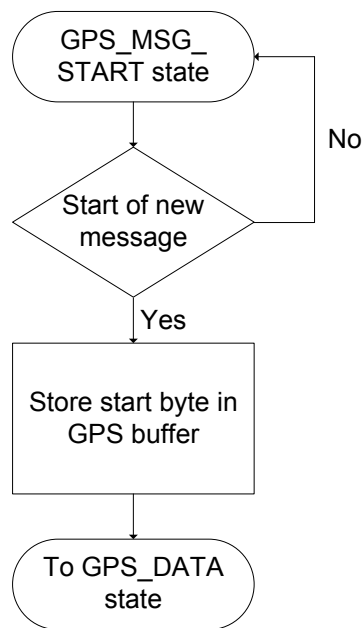


Figure 40: GPS message start state

**GPS data state:**

In this state, a check is done for the NMEA checksum delimiter. If it is received over the UART port the state variable is set to the GPS checksum state. If this condition is false another check is done to ensure there is space in the GPS buffer and the maximum possible string length has not been reached. If these conditions are both false, the data character received is stored in the GPS string buffer as it is part of the data of the NMEA data string.

**GPS checksum state:**

This state is reached if the checksum delimiter was received in the data state. In this state, a check is performed to the end of message character. If this character was not received it entails that the data received must be the value of the checksum character. This is typically a value of 73 but depends on the GPS message type. If the end of message character is received a check is performed to ensure the checksum value is correct. If incorrect the message is deleted from the buffer and the state variable changed to the first state. If the checksum value is correct the state variable is changed to the last state: GPS message end state.

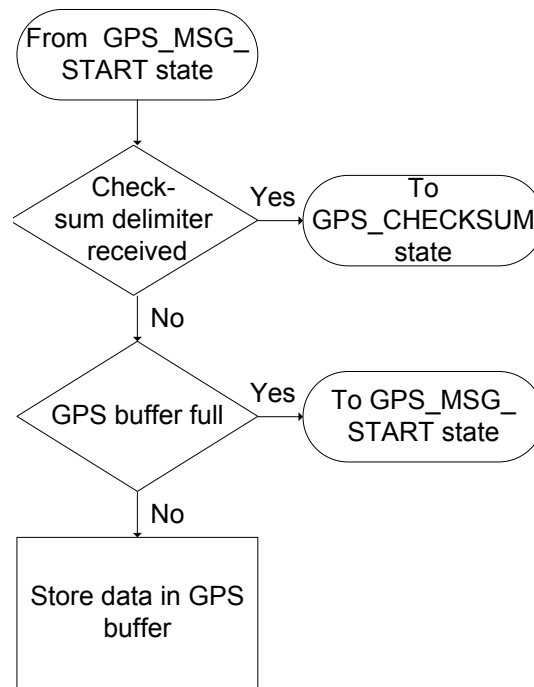


Figure 41: GPS data state

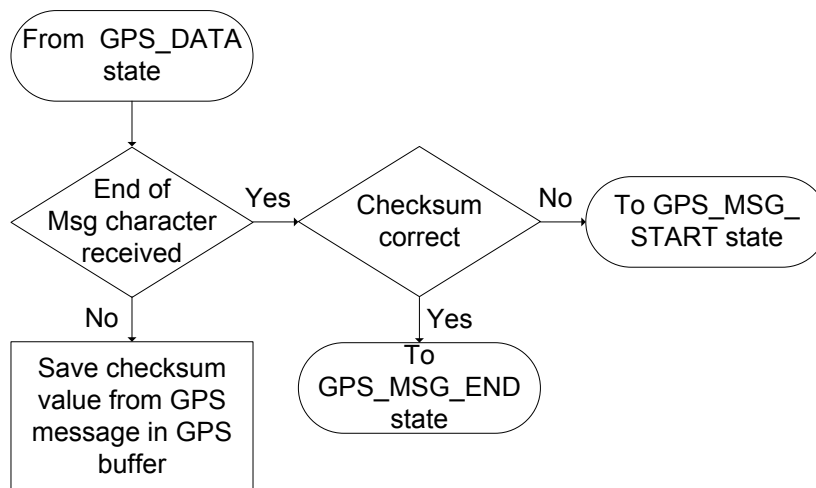


Figure 42: GPS checksum state

### GPS message end state:

In this state, the next expected character to be received over the UART port is the end of line character '\n'. A check is performed if this is the case, if it is false the state machine returns to the first state and the GPS message that has been received is ignored and deleted from the buffer. If the end of line character is received the GPS string, now complete in the GPS buffer, is analysed and stored in a specific data type buffer. Examples of the data types can be found in Table 24 of APPENDIX A. On completion, the state variable is reset to the first state.

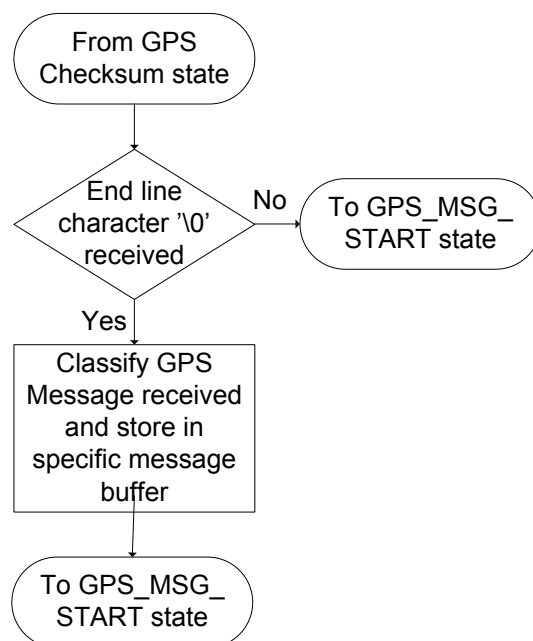


Figure 43: GPS message end state

### 5.3.5. ZigBee communications management

This section describes the software implementation on the smart meter that is used to manage the communication with the CC2530 ZigBee modem. Details about the CC2530 ZigBee modem, its physical and software interface is given in section 5.4. The software described in this section was not supplied with the meter and was written from scratch.

The ZigBee communications management subroutine is called from the foreground process as shown in Figure 35. It was shown that the foreground process is required to perform various calculations every second and that it may never skip a data frame or fall behind. To this end, the communications subroutine's execution time should be limited.

To keep to the timing constraints, a switch-case multi-tasking approach was followed where the communications subroutine is split into smaller subroutine steps. After each step is completed, the program returns to the foreground process to see if any new data has been passed on from the background loop. If a new data frame is available, the data is first processed before returning to the communications management subroutine to continue where it left off.

The main communications management process is depicted in the flow diagram in Figure 44. Upon reset, the process enters the modem initialization function. Here, the ZigBee modem parameters are configured and network details are specified. After initialization, the modem is configured to automatically connect to the specified network when it comes into range. The communications process monitors the modem for incoming messages or commands and the local transmit buffer for pending outgoing messages.

Incoming messages from the modem receive priority over outgoing messages from the meter. This is necessary to allow the meter to hold transmission when the modem loses the network connection. If the network connection is lost, the modem will send a message to the meter telling it that it has lost communication.

**Registers:**

**Network\_State:**  
 (0) Device not ready  
 (1) Seeking  
 (2) Connected

**TX\_buffer\_state:**  
 (0) No messages  
 (1) Pending send  
 (2) Pending confirm

**CC2530 SRDY pin:**  
 (0) New RX messages  
 (1) No RX message

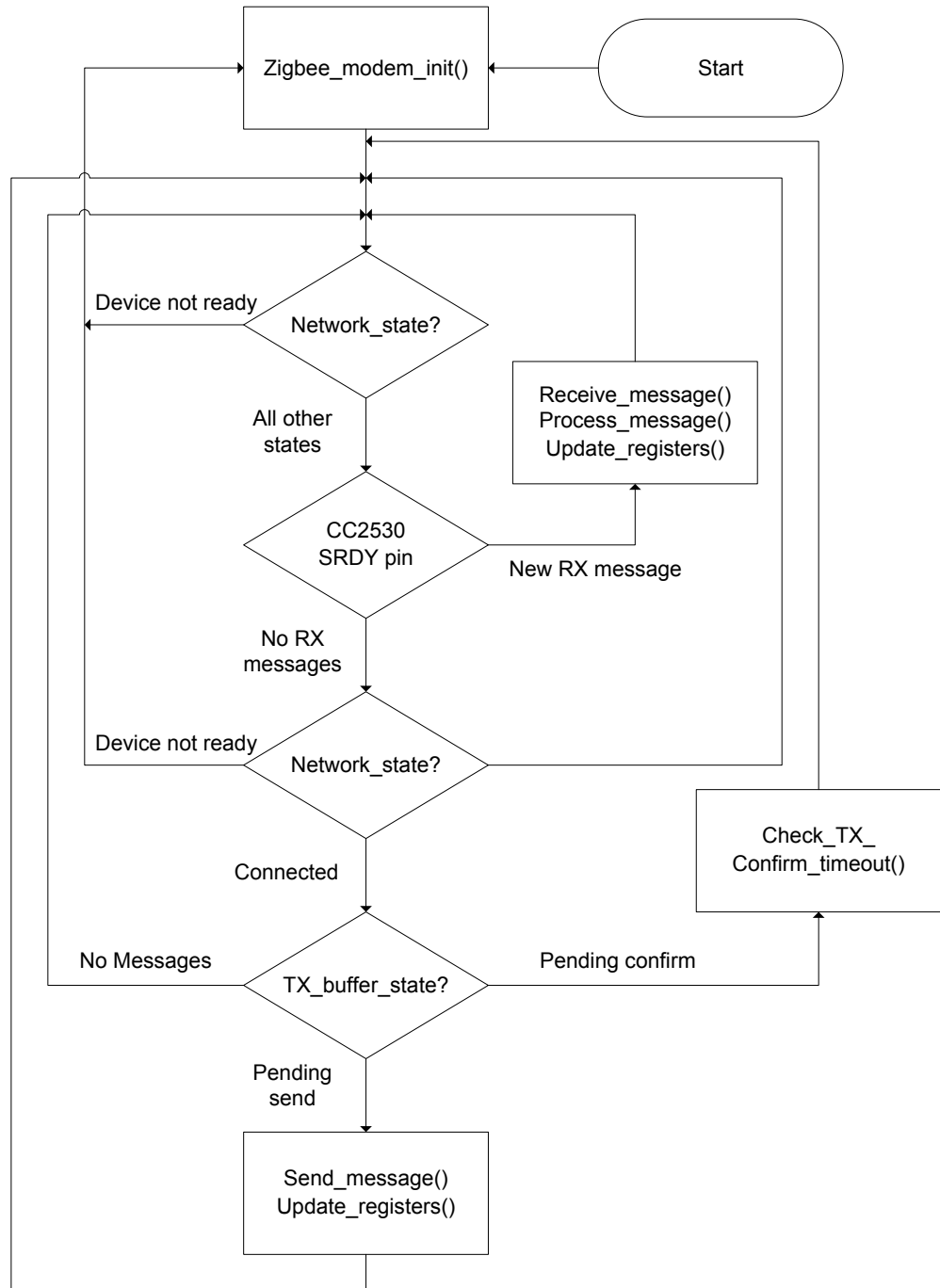


Figure 44: Software flow diagram for the ZigBee communications manager

The meter implements a transmit buffer, TX\_Buf, as a ring buffer for storing outgoing messages when the network connection is unavailable. Incoming messages from the data

concentrator are buffered on the modem, not on the meter. The meter reads one message at a time from the modem and processes that message before the next is read in. In addition to the transmit buffer, three register flags, `Network_state`, `TX_buffer_state` and `SRDY` are defined. `Network_state` is used to indicate the state of the network connection. `TX_buffer_state` is used to indicate the status of the transmit buffer and transmission success. `SRDY` (slave-ready) is used to indicate that the meter has a message to receive from the modem.

When a message is placed in the transmit buffer, `TX_buffer_state` indication is set to “pending send”. The communications manager will pass the message to the modem for transmission to the data concentrator. Upon receipt, the data concentrator will return a “confirm”. The meter will wait for the “confirm” before sending the next message in the buffer. If no “confirm” is received, a timeout function will resend the message. This resend process will continue until the message is successfully sent.

#### **5.3.5.1. ZigBee message data structure**

The meters were programmed to send three message types sequentially to the data concentrator. The first, a measurement message, containing the 1-minute aggregated meter readings with a GPS timestamp, are sent every minute for each channel. The second message type is a GPS location message which is GPS time-stamped containing the last known position of the meter. There are thus in total 4 messages sent to the data concentrator in a 1-minute interval basis. If the samples gathered in a one-minute time period do not fall between 58 and 62 an ID fail message with a body length of zero is sent instead of the normal measurement message.

The third message sent to the data concentrator is the calculated network impedance. The value is sent every second with a GPS timestamp.

Additional messages which are sent at random includes an under or overvoltage alarm condition as detected by the meters and a message indicating the return to a nominal voltage of 230 V.

Table 8 shows the message header structure for a measurement message and Table 9 shows the measurement message body containing the channel number of the measurements being sent and the various 1 minutes aggregated measurements. If a message ID fails condition should arise the body length is zero, and the `Message_ID_OK` byte is set to zero.

Table 8: Measurement message header structure

Byte	1	2	3	4	5	6	7	8	9	10 - 41
Value	0xFF	Seconds	Minutes	Hour	Day	Month	Year	Message ID OK	Message Body Length	Message Body (Table 8)

Table 9: Measurement message body

Byte	10	11 - 14	15 - 18	19 - 22	23 - 26	27 - 30	31 - 34	38 - 41
Value	Channel	Power factor	Power factor sign	Apparent power	Reactive power	Active power	Current	Voltage

Table 10 and Table 11 shows the GPS location message header body and the GPS location message body respectively. The GPS location message header contains a timestamp of when the location message is sent. The GPS location message body contains the latitude and longitude of the meter in degrees, minutes, seconds format.

Table 10: GPS location message header

Byte	1	2	3	4	5	6	7	8	10 - 15
Value	0xFF	Seconds	Minutes	Hour	Day	Month	Year	Message Body Length	Message Body (Table 10)

Table 11: GPS location message body

Byte	10	11	12	13	14	15
Value	Latitude degrees	Latitude minutes	Latitude seconds	Longitude degrees	Longitude minutes	Longitude seconds

## 5.4. TEXAS INSTRUMENTS CC2530-ZNP IMPLEMENTATION

This section describes how the ZigBee communication network is created with the smart meter as the host processor for the CC2530ZNP (ZigBee Network Processor). A CC2530EM (Evaluation Module) is used as the CC2530ZNP. The physical SPI interface between the MSP430 host processor on the meter and the CC2530EM is also discussed.

The CC2530-ZNP contains the core ZigBee PRO stack and exposes an API interface to the host processor (Smart Meter) for configuration of the stack and data transmission.

Application examples provided by TI is used as the basis of the application implementation on the host processor. These examples were written specifically for the CC2530ZNP, however, they are written for the IAR embedded workbench compiler, which was not available for use. Changes had to be made to the C code to be compiled in the open source IDE code composer studio.

### 5.4.1. CC2530 evaluation module



Figure 45: CC2530EM [33]

The CC2530EM is based upon TI's CC2530 RF integrated circuit and contains the necessary external components and matching filters. The module can be plugged into the smart meter used in this project which uses the MSP430F67791a MCU. The schematics of the evaluation module is freely available and can be found on the web [34].

The CC2530 on which the CC2530EM is based uses TI's second generation ZigBee/IEEE 802.15.4 compliant system-on-chip with an optimised 8051 MCU core. A radio for the 2.4GHz unlicensed band [35].

Additional information on the CC2530 can be found in the products folder on the web at [34] with datasheets, user guides, and application notes. Several of these documents were referenced during the implementation.

### 5.4.2. CC2530-ZNP physical interface

The CC2530-ZNP support SPI, UART and universal serial bus (USB) interfaces from a host processor. For this implementation, the SPI interface to the host processor on the meter is used as the meter's PCB is designed to only use the SPI interface to the ZigBee modem. Figure 46 shows a diagram of the interface with the CC2530 [36].

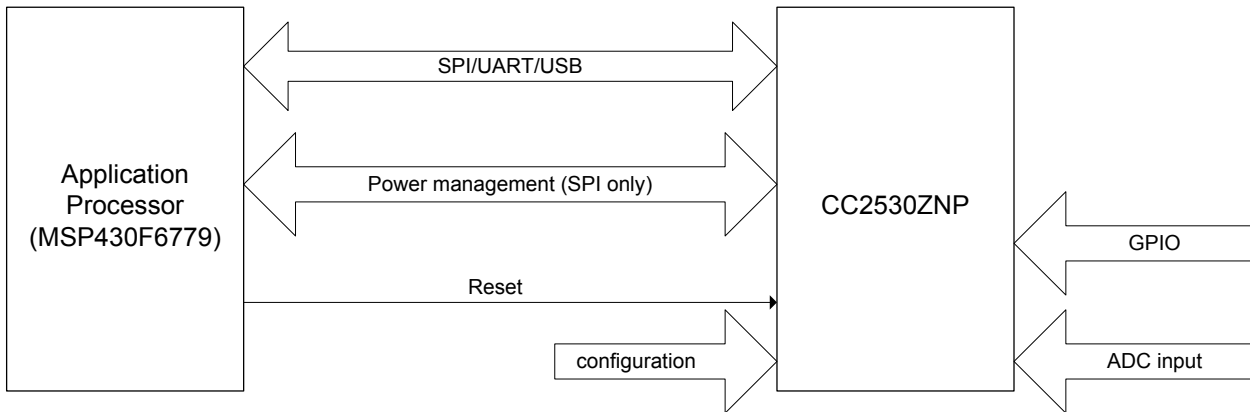


Figure 46: CC2530 interface

The CC2530-ZNP consists of two pin configurations, a main and alternative configuration. The specific configuration is selected with the CFG0 and CFG1 pins. The main configuration is used since the meter made provision for it. Table 12 shows the main pins configuration and pins used on the MSP430F67791a.

Table 12: MSP430F67791a to CC2530-ZNP interconnect

CC2530-ZNP signal	CC2530	MSP430	Direction (on C2530)
SS	P1_4	P2_1	IN
CLK	P1_5	P4_6	IN
MOSI	P1_6	P4_5	IN / OUT
MISO	P1_7	P4_4	OUT / IN
RESET	RESET_N	P11_2	IN
MRDY	P0_3	P4_1	IN
SRDY	P0_4	P11_1	OUT
CFG0	P1_2	NC	IN
CFG1	P2_0	P2_3	IN

Signal descriptions are given below:

- **MOSI/MISO/SS/CLK for SPI:** These are the standard signals used for SPI.
- **SRDY (Slave-Ready):** This signal is asserted by the CC2530 for power management and transaction control when using SPI transport. The application processor (MSP430) can use a regular GPIO pin to poll the status of this signal.
- **MRDY (Master-Ready):** This signal is asserted by the application processor for power management and transaction control when using SPI transport. This is typically hardwired to the SS pin and does not have to be controlled by a separate GPIO from the application processor.
- **RESET:** This signal is used by the application processor (MSP430F67791a) to reset the CC2530.
- **CFG0, CFG1:** These two signals are used to configure the CC2530ZNP. The CC2530ZNP reads this signal at power up and sets the appropriate pins configuration. In this implementation, the CFG0 pin is not used.

### 5.4.3. SPI configuration

#### 5.4.3.1. CC2530-ZNP

The following SPI configuration is supported by the CC2530ZNP [36]:

- SPI Slave
- Clock speed up to 4 MHz. It is found that the most reliable communication is achieved between 2 – 4 MHz.
- Clock polarity 0 and clock phase 0 on CC2530.
- Bit order MSB first.

#### 5.4.3.2. MSP430F67791a

The MSP430 on the meter is configured according to the SPI requirements as seen above. The Enhanced Universal Serial Communication Interfaces (eUSCI\_A and eUSCI\_B) both support serial communication in SPI mode. For the SPI interface to the CC2530EM the EUSCI\_B interface is used.

The *Enhanced Universal Serial Communication Interface (eUSCI) – SPI mode* [37] document is used with the setup of the SPI registers. The code below is used:

```
UCB1CTLW0 |= UCSWRST;           // **Put state machine in reset**
UCB1CTLW0 |= UCMST | UCSYNC | UCMSB; // 3-pin, 8-bit SPI master, Clock
UCB1CTLW0 |= UCSSEL_2;         // SMCLK source
UCB1BRW_L = 0x05;              // (17.17MHz / 5 = 3.43MHz)
UCB1BRW_H = 0;                 // (17.17MHz / 5 = 3.43MHz)
UCB1CTLW0 &= ~UCSWRST;        // **Initialize USCI state machine**
```



Figure 47: SPI initialization code using the EUSCI\_B interface.

This setup code can be found in the *hal\_cc2530znp\_target\_board.c* file.

#### 5.4.4. Flashing CC2530EM with new firmware

To upload new firmware to the CC2530EM the CC debugger is used. The SoC\_BB (system on chip battery board) is required to house the CC2530EM module [38]. Two AA-Batteries is used to supply power to the CC2530EM.



Figure 48: CC-Debugger with SoC-battery board and CC2530EM [39]

TI's smart RF flash programmer is the software required to flash new firmware onto the ZigBee evaluation module. This is an executable program and no installation is required. It can be downloaded directly from TI's website at [40].

The CC2530EM is flashed with ZNP hex files found in the installed z-stack folder. "Z\_STACK ENERGY" is used in this implementation and can be downloaded at [41]. The executable should be installed on a host PC. The installed directory "z-stack energy 1.1.0" consists of various sub-directories.

The required ZNP-hex file can be found at "z-stack energy 1.1.0/Projects/zstack/ZAP/ZNP-HexFiles".

## 5.5. CONCLUSION

This chapter discussed the software development done on the Texas Instruments smart meters. The meters were used as it satisfies the requirements needed for this project. The meters are supplied with factory software which was altered to compile in TI's open source IDE Code Composer. The meters support add-on ZigBee modules capable of sending data to

modems from other manufacturers. Additional software was written to handle the ZigBee communications. The meters send 1-minute aggregated measurements to the data concentrator. Should an overvoltage or undervoltage occur at any time the meter will send an alarm message to the data concentrator immediately. The following two chapters will discuss the development of the data concentrator.

## CHAPTER 6

### DATA CONCENTRATOR HARDWARE DEVELOPMENT

#### 6.1. INTRODUCTION

A data concentrator is developed which is used to gather and process measurement data received from the smart meters located at the transformer and customer installations. It uses the data and turns it into information on hazards.

The data concentrator that was developed is based on a Linux ARM development platform. The Raspberry Pi Compute Module is used as the development platform.

The data concentrators primary purpose is to receive data via a ZigBee link, process the data, identify fault conditions, and display the received data in graph format. It, therefore requires a ZigBee modem as well as a GSM/GPRS modem. Additional communication interfaces were also added to the board that will be required during development and possibly in future projects.

The chapter starts with a high-level overview of the hardware showing the interaction of each component on the board with the computer module. The latter sections describe each communication interface in more detail and the hardware used to implement each.

The software development completed on the data concentrator is discussed in the next chapter.

#### 6.2. HIGH-LEVEL OVERVIEW

This section gives a high-level overview of the data concentrator hardware design. Figure 49 shows a block diagram overview of the system with the computer module, the Raspberry Pi computer module, forming the core and communication links to the various communication interfaces of the board.

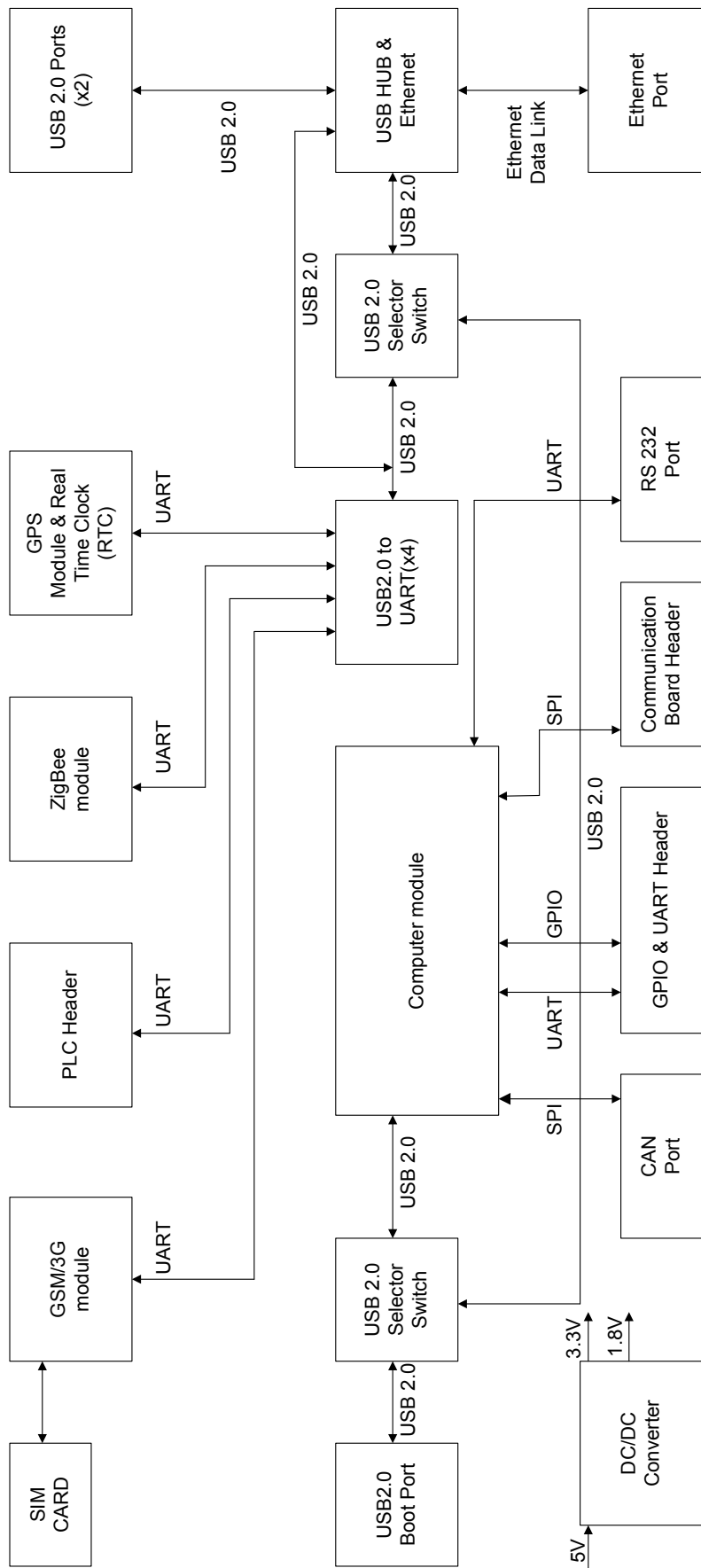


Figure 49: Data concentrator block diagram

The data concentrator consists of the following communication interfaces/protocols:

Table 13: Data concentrator communication interfaces

Communication interface	Functionality/Purpose
ZigBee	Receive measurement data from smart meters.
GSM/GPRS	Send data to the master station via the DNP3 protocol. (Future Implementation)
GPS	Get the position of data concentrator in the field and to sync the Linux system time to the GPS provided time.
USB Ports(2x)	Used during development to upload data to the Linux development board.
Ethernet Port	Used during development to enable internet access on the Linux development board.
RS232 Port	Future use.
CAN Bus	Future use.
UART Pins	Used during development to gain access to the Linux command files.
GPIO Pins	Future use.

### 6.3. HARDWARE DESIGN

This section gives an in-depth view of the complete hardware design of the data concentrator board looking at each section shown in Figure 49 individually.

#### 6.3.1. Computer module

The Raspberry PI compute module is a computer module and is used as the central computer of the data concentrator board. The computer module is based on the same Broadcom BCM2835 processor as a conventional Raspberry PI computer. It also consists of 512 MB of RAM and 4 GB of embedded multimedia card (eMMC) flash memory used as storage which fulfils the same purpose as an SD card on a conventional Raspberry PI.



Figure 50: Raspberry PI computer module [42]



Figure 51: Conventional Raspberry PI model B+ [43]

The flash memory of the computer module is connected directly to the processor on the board, with all the remaining interfaces available for custom use via the connector pins. The module slots into a standard DDR2 SODIMM or small outline dual in-line memory module connector. This ensures that the full flexibility of the BCM2835 SoC is available for development use.

Table 14 shows the interfaces available on the computer module as well as the conventional Raspberry PI Model B+. From Table 14 it can be seen that additional interfaces are available on the computer module that makes it ideal for a communications development board.

Table 14: Communication interfaces on Raspberry PI computer module and model B+

Interface	Computer model	Model B+
Universal asynchronous receiver/transmitter (UART)	2	1
Serial Peripheral Interface (SPI)	3	1
I2C	2	1
General Purpose Input/Output (GPIO)	47	17
Universal Serial Bus (USB)	1	1
Pulse-Width Modulation (PWM)	2	1

The Raspberry PI computer module was released with the computer module I/O board as shown in Figure 52 which is a simple, open-source, breakout board into which a computer module slots. The schematic of the board is freely available and is used as a template for the design of the data concentrator. The board as standard only provides a USB-port, HDMI connector, camera connectors and GPIO pins.



Figure 52: Computer Module I/O Board [44]

The power circuitry design, as well as the USB-boot circuitry design from the I/O board, is used for the data concentrator.

### 6.3.2. Power circuitry

The hardware design of the communication board is done based on the computer module I/O board as the schematics are freely available. The required voltages on the board for the computer module and external components are 5V, 3.3V and 1.8V. The board is powered by a 5V DC supply connected via a terminal block.

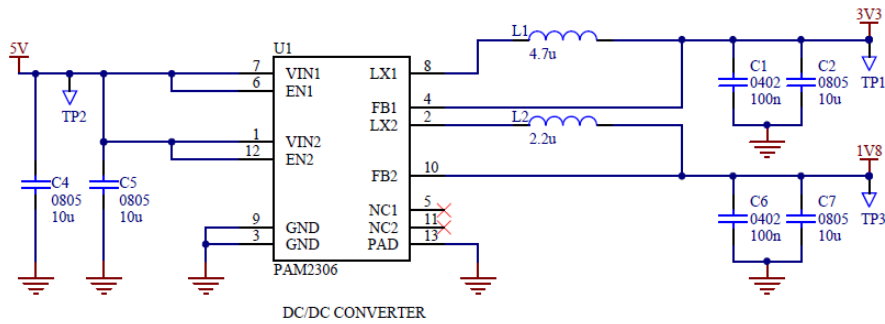


Figure 53: Dual channel DC-DC step-down converter

The PAM2306 (Figure 53) is used as the main supply converter for the board. It is an efficient dual PWM step down current mode, DC-DC converter. Each channel can supply 1 A of current, and consumes only 40  $\mu$ A of quiescent current [45].

### 6.3.3. USB to UART expansion and ethernet

The data concentrator required up to six internal UARTs to interface the computer module with all the communication interfaces available on the board. As the computer module only consists of two UARTs it was decided to make use of the single USB line on the computer module to communicate with the various communication modules. Using a USB hub (LAN9514) the single USB line of the computer module was split into 4 USB lines and an additional Ethernet port, which will be required during development [46].

A USB-to-quad UART converter is used to provide the additional 4 UARTs that is required. Figure 54 shows the topology that was designed and implemented.

USB selector 1 as seen in Figure 54 is used to enable the USB port by selecting between the dedicated USB port and the USB and UART expansion circuitry. The USB boot port is used to flash the computer module with a Linux distribution image.

USB selector 2 is added to enable or disable the USB hub. It is added to ensure the USB to UART converter can still function even if a problem should occur with the USB hub. Bypassing the USB hub will, however, result in the disconnecting of the USB ports and Ethernet port on the data concentrator.

The solution proved to be very effective as no problems were found with using the four UART ports as well as the USB ports and ethernet port simultaneously.

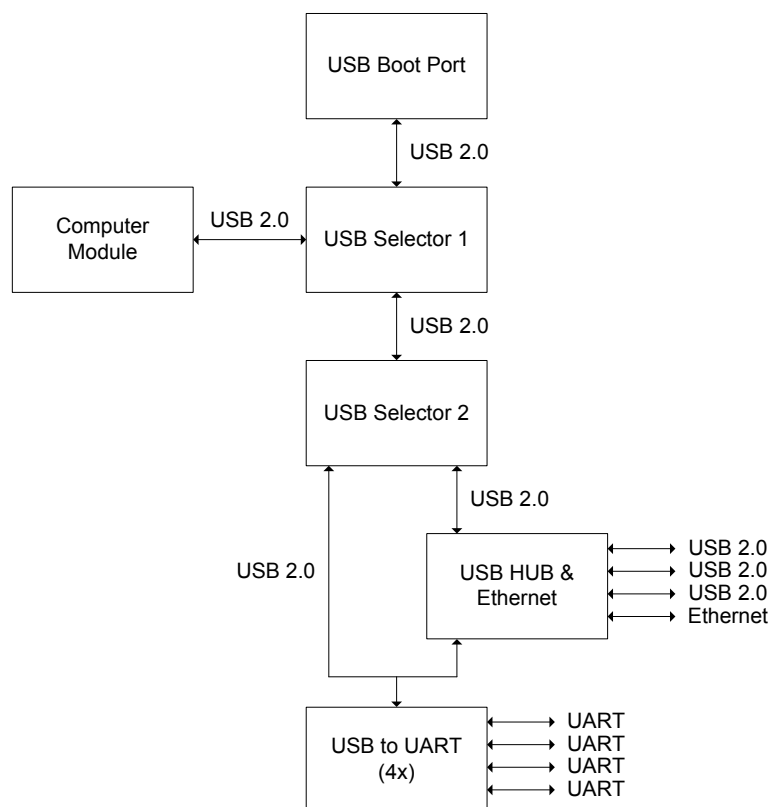


Figure 54: USB to UART interface

### 6.3.4. USB boot circuitry

The following describes the USB boot circuitry used to flash the eMMC memory of the computer module with a Linux distribution operating system.

#### 6.3.4.1. *USB 2.0 selection switch*

A bi-directional USB selection switch (FSUSB42) is used to switch between the dedicated USB boot port and a USB hub (Figure 55). The design is similar to that of the computer module I/O board.

The FSUSB42 is a double-pole, double throw switch, which is optimised for switching between any combinations of high-speed (480 Mbps) of full-speed (12 Mbps) sources. It meets all the requirements of USB 2.0 and features a wide bandwidth (720 MHz) that exceeds the required bandwidth [47].

The device is powered by a  $V_{CC} = 3.3\text{ V}$  supply voltage. The data lines (D+/D-) are switched between HSD1+/HSD1- and HSD2+/HSD2- by applying an active low and active high to the select pin (SEL) respectively.

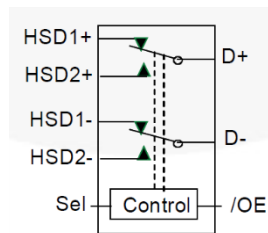


Figure 55: FSUSB42 analogue symbol [47]

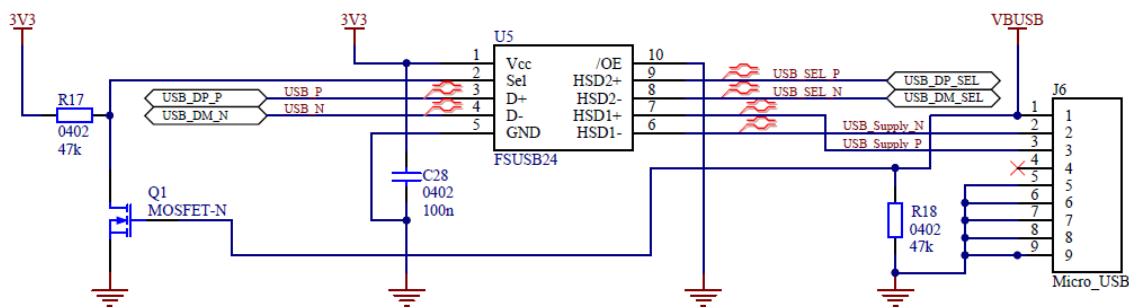


Figure 56: USB selection switch

Figure 56 shows the schematic design for the USB selection switch as implemented on the data concentrator. Data lines D+/D- are connected to the computer module's USB data lines. The multiplexed source input 1 data lines (HSD1+/HSD1-) are connected to the micro USB boot port, with the multiplexed source input 2 data lines (HSD2+/HSD2-) connected to the USB hub circuitry. The not switch enable pin (/OE) is connected to ground to enable the selection switch pin (SEL).

The selection switch pin is connected to the drain of an n-channel MOSFET transistor. The drain pin is by default pulled high through a pull-up resistor, which disables the USB boot port and enables the data lines to the USB hub. The USB boot port is enabled when a USB plug is inserted into the port. The 5V supply of the boot port will switch on the N-channel MOSFET transistor, pulling the SEL pin to ground, which enables the USB boot port data lines.

#### 6.3.4.2. Module booting and flashing the eMMC procedure and circuitry

This section describes the boot circuitry operating to flash an image onto the computer module.

When the computer module is initially powered up the BCM2835 will look for a file called `bootcode.bin` on the eMMC memory. If no `bootcode.bin` file is found, which is used to start the booting of the system, the device falls back to waiting for the file to be written over its USB port. A version of Linux can now be written onto the device, over USB, using the Linux software tool `rpiboot`. The software can be downloaded from [42].

If a new Linux OS needs to be flashed onto the module the module can be forced to boot from the USB port. This is done by holding the EMMC\_DISABLE\_N pin of the BCM2835 low for a couple of second to indicate to the processor to boot over USB.

Figure 57 shows the circuit to allow the flashing of the eMMC by forcing EMMC\_DISABLE\_N pin to ground. Jumper (J7), position 2-3, is intended for “USB boot-enabled“ and position 1-2 for “USB boot-disabled“. With the jumper in the USB boot enabled position a logic high will be present on the gate of transistor Q2 switching it on which will force EMMC\_DISABLE\_N to ground since transistor Q3 is also “on“ with a 1.8 V pull-up resistor on its gate terminal [48].

Once the computer module has finished booting over USB it needs to fall back to the eMMC device by releasing the USB EMMC\_DISABLE\_N pin. It is done automatically by the computer module by driving the GPIO47\_1V8 pin to ground, which was initially pulled up to 1.8 V as can be seen in Figure 57.

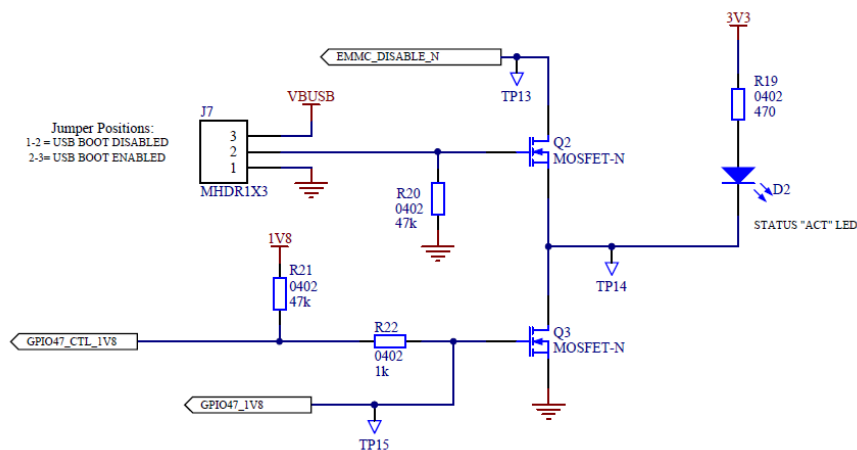


Figure 57: USB boot enable

### 6.3.5. XBee ZigBee radio

An XBee ZigBee radio from Digi International is used to provide ZigBee RF capabilities to the data concentrator. XBee module is used due to their low cost and their ability to operate within the ZigBee protocol. XBee is the radio brand created by Digi-International which supports a variety of protocols including ZigBee, 802.15.4, Wi-Fi etc. XBee and ZigBee are often mistaken for the same thing, which is not true. ZigBee is a standard communications protocol which is supported by the XBee radio brand. All devices of a specific brand which supports the ZigBee protocol can communicate with devices from another manufacturer also supporting the ZigBee protocol [49].

XBee features two main product ranges namely the series 1 and series 2 radios. The series 1 radios (also called XBee 802.15.4) only supports, as its name suggest, the 802.15.4 protocol and not the full ZigBee protocol stack as with series 2. Both series 1 and 2 includes a

professional (PRO) model. The professional model indicates an increase in the radio's maximum transmit power. Table 15 shows a summary of the main differences between the series 1 and 2 XBee models:

Table 15: Comparison between XBee Series 1 and Series 2 [49]

Model	XBee Series 1 (802.15.4)	XBee Series 2 (ZigBee)
Frequency	2.4 GHz	2.4 GHz
Maximum line-of-sight range	XBee 802.15.4: 90 m XBee PRO 802.15.4: 1.6 km	XBee ZigBee: 1.2 km XBee PRO ZigBee: 3.2 km
Data Rate	250 Kbps	250 Kbps
Communication protocol	802.15.4	ZigBee
Max. transmit power	1 mW (0 dBm)	XBee ZigBee: 6.3 mW (8 dBm) XBee PRO ZigBee: 63 mW (18 dBm)
Max. receiver sensitivity	XBee 802.15.4: -92 dBm XBee PRO 802.15.4: -100 dBm	XBee ZigBee: -102 dBm XBee PRO ZigBee: -101 dBm
Max. current consumption (transmitting)	XBee 802.15.4: 45 mA XBee PRO 802.15.4: 215 mA	XBee ZigBee: 59 mA XBee PRO ZigBee: 120 mA
Max. current consumption (receiving)	XBee 802.15.4: 50 mA XBee PRO 802.15.4: 55 mA	XBee ZigBee: 42 mA XBee PRO ZigBee: 45 mA
Max. current consumption (sleeping)	< 10 $\mu$ A	< 1 $\mu$ A
Serial data interfaces	UART	UART, SPI

The XBee product range includes up to 30 different combinations of component hardware all supporting different transmit power levels, firmware protocol support and antenna options. The antenna options include U.FL, RPSMA, PCB and wire antennas. The option used on the data concentrator is the reverse polarity – subminiature version A (RPSMA) connector as seen in Figure 58 due to the antenna being very common and reliable. The connector can also easily be extended to an external housing by means of subminiature version A (SMA) extension cable.

The XBee pro-Series 2B from Digi-International (Figure 58) is an example of such a radio. It supports the full ZigBee protocol stack, which is essential to ensure interoperability with ZigBee

modems from other manufacturers. It is capable of communicating up to 3.2 km line-of-sight. This XBee-PRO model is used on the data concentrator (Product number: XBP24BZ7SIT-004).



Figure 58: Digi-International XBee pro series 2B ZigBee module [49]

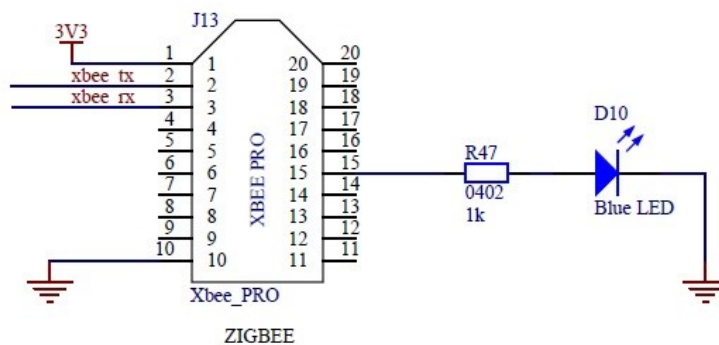


Figure 59: Schematic representation of XBee pro series 2B for the data concentrator

#### 6.3.5.1. Power supply

The XBee Series 2B module used for the data concentrator implementation requires a supply voltage of 2.7 – 3.6 V. The XBee is supplied with the 3.3 V supply available on the data concentrator board. The maximum current drawn is 120 mA at 3.3 V.

#### 6.3.5.2. Serial communication

The XBee module interfaces to a host device through a UART serial port. The module can communicate with a device using 3.3 V logic, or to any device through an appropriate voltage level translator such.

The module is interfaced to one of the USB to UART converter's available ports using only the transmit (TX/D<sub>IN</sub>) and receive (RX/D<sub>OUT</sub>) data lines. The XBee makes provision for a clear to send (CTS) line but is not used as it is only necessary when receiving large amounts of data. Figure 59 shows the data lines connected to pin 2 and 3 of the module.

### 6.3.5.3. Associate LED

The associate LED (pin 15) can provide an indication of the modules network status and diagnostic information. A LED is connected to pin 15 through a 1 k $\Omega$  current limiting resistor. The functionality is enabled by default in the device. Table 16 shows the various network associations for the various states of the associated LED.

Table 16: Associate LED status [49]

LED Status	Network Association
On, solid green	Joined, and network connection to Coordinator is working
On, 3 sec blink	Not joined
On, 1 sec blink	Trying to join a network
On, ¼ second blink	Joined, but connection to coordinator is not working

### 6.3.6. GSM/GPRS module

This section covers the hardware implementation of a GSM/GPRS module. The TC63i from Cinterion wireless modules is used as it is a surface mount module and has been used in previous projects. Software is available which will simplify the final implementation.

#### 6.3.6.1. Power Supply (LP3856-ADJ)

The TC63i module requires a supply voltage of between 3.2 V and 4.5 V, with a typical value of 3.8 V. Peak power of the supply should be 1.6 A. As the data concentrator only consists of a 3.3 V and 5 V supply an additional power supply is added specifically for the GPRS module.

The LP3856-ADJ 3 A Fast Response Ultra Low Dropout linear regulator from Texas Instruments is used. The regulator operates from a 2.5 V to 7 V input supply. The regulator is capable of supplying up to 3 A [50].

The 5 V board input supply is directly connected to the input of the regulator. A design choice is made to supply the TC63i module with a 4.2 V as it is well within its desired input range.

The typical application circuit used is shown in Figure 60.

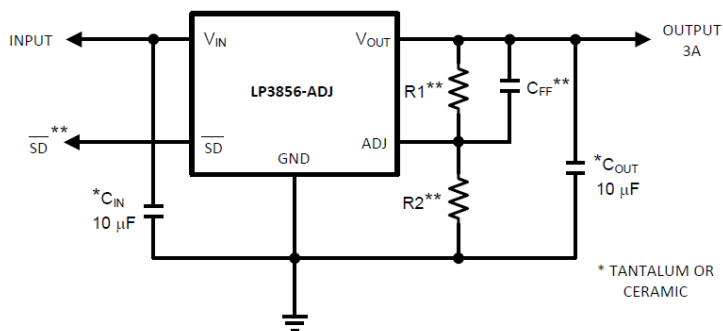


Figure 60: LP3856-ADJ typical application [50]

The only design that is done is the design of resistors  $R_1$  and  $R_2$ . The resistors determine the output voltage and is calculated below using the relationship given in the datasheet [27]. ( $V_{out} = 4.2\text{ V}$ )

$$V_{out} = 1.216 \times \left(1 + \frac{R_1}{R_2}\right) \quad (6.3.1)$$

$$\frac{R_1}{R_2} = 2.454$$

This result in the chosen resistors of:  $R_1 = 2.4\text{ k}\Omega$  and  $R_2 = 1\text{ k}\Omega$ .

The nSD pin is pulled high through a  $10\text{ k}\Omega$  resistor, permanently enabling the regulator.

### 6.3.6.2. Capacitor selection

#### Input Capacitor

The datasheets specify an input capacitor of  $10\text{ }\mu\text{F}$  to be used. Tantalum capacitors are preferred as to keep the output capacitor value smaller.

#### Output Capacitor

The minimum amount of output capacitance that can be used for stable operation is  $10\text{ }\mu\text{F}$ . Figure 61 shows the minimum and maximum ESR range for the output capacitor for stable operation of the regulator, assuming any output capacitor whose value is greater than  $10\text{ }\mu\text{F}$ . A  $10\text{ }\mu\text{F}$  capacitor is used in the final implementation.

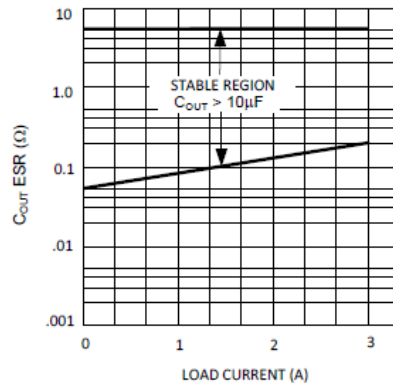


Figure 61: ESR curve for output capacitor (with 10uF tantalum input capacitor) [50]

### Feed forward capacitor

The feed forward capacitor ( $C_{FF}$ ) is used to add phase lead and improve loop compensation. The capacitance value depends on the value of the value of  $R_1$ . The capacitor should be designed such that the zero frequency is approximately 45 kHz. The capacitor is designed using the equation 6.3.2.

$$F_z = 45000 = \frac{1}{2 \times \pi \times R_1 \times C_{FF}} \quad (6.3.2)$$

$$C_{FF} = 3.54 \mu\text{F}$$

A Tantalum capacitor of 4.7  $\mu\text{F}$  was chosen for  $C_{FF}$ .

#### 6.3.6.3. TC63i module

The TC63i is an embedded GSM module by Cinterion with Quad Band GSM and Remote SIM Access (RSA) support. RSA enables TC63i to use a remote SIM card, of any network provider, via its serial interface. An embedded module is chosen as it simplifies the communication board, allows for a more compact design and enhances the reliability of the GPRS communication. The TC63i module uses an 80-pin board-to-board connector used to connect the module to the computer module. Figure 62 shows the module.

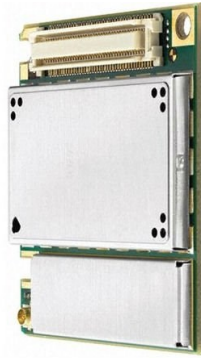


Figure 62: TC63i GSM/GPRS Module [50]

#### 6.3.6.4. **TC63i housing and antenna:**

The TC63i easily integrates onto a PCB using the integration clip. The integration clip is designed to withstand vibration pulling forces of 150 N which makes it a secure mounting solution for the TC63i module.

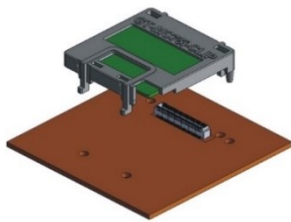


Figure 63: TC63i U.FL-R-SMT antenna connector [50]



Figure 64: TC63i integration clip [50]

Figure 64 shows the location of the U.FL-R-SMT antenna connector. The RF interface has an impedance of  $50\ \Omega$ . The external antenna must be matched properly to achieve best performance regarding radiated power, DC-power consumption, modulation accuracy and harmonic suppression.

The recommended antenna installation is to use the U.FL antenna connector from Hirose assembled on the component side of the PCB.

#### 6.3.6.5. **SIM interface**

The integrated processor of the TC63i has an integrated SIM interface compatible with the ISO 7816 IC Card standard. Six pins on the 80-pin board-to-board connector are reserved for the SIM interface. The SIM interface supports both 3 V and 1.8 V SIM cards.

The TC63i has the capability to detect whether a SIM card is inserted into the SIM card holder. The CCIN signal serves to detect whether a SIM card is present. A SIM card holder with a SIM card detect switch is required to take advantage of this feature.

Table 17: Signals of the SIM interface [50]

Signal	Description
CCGND	Separate ground connection for SIM card to improve EMC.
CCCLK	Chipcard clock, various clock rates can be set in the baseband processor.
CCVCC	SIM supply voltage.
CCIO	Serial data line, input and output.
CCRST	Chipcard reset, provided by the baseband processor.
CCIN	Input on the baseband processor for detecting a SIM card tray in the holder.

#### 6.3.6.6. Serial interface

The TC63i supports two UART interfaces. The first, ASC0 is an 8-wire unbalanced, asynchronous modem interface. The second UART is a 4-wire unbalanced, asynchronous modem interface ASC1. The significant levels are 0 V (for logic low) and 2.9 V (for logic high). Only the 8-wire UART on the GSM module will be used.

As of the above mentioned electrical characteristic of the UART interface, a buffer is inserted to level shift the signals coming from the FT4232HL USB to quad UART IC. Figure 65 shows the configuration and voltage level conversion used for the serial UART communication to the GSM module.

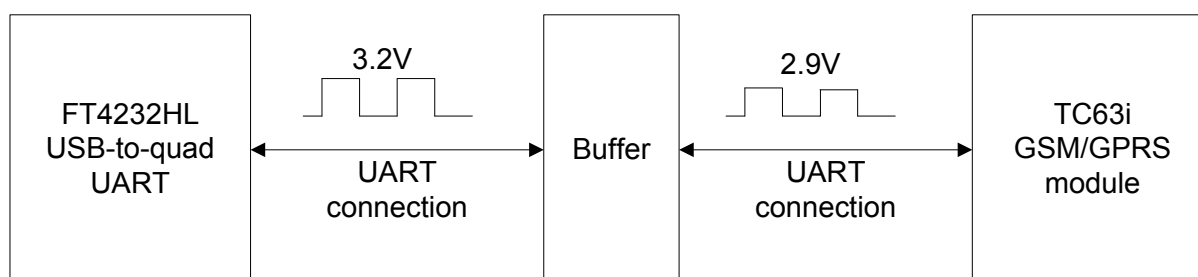


Figure 65: UART voltage conversion

The 74LCX541 low voltage octal buffer/line driver is used to convert the voltage levels from the UART on the FT4232HL. The FT4232HL outputs 3.2 V for a logical high but the maximum logical high input accepted by the GSM module is 3.05 V [51]. The buffer outputs its supply

voltage as a logical high. An additional supply voltage for the buffer of  $V_{cc} = 2.9\text{ V}$  is therefore required.

The NCP582 linear low-dropout regulator with a fixed output voltage of  $2.9\text{ V}$  is used as the supply for the buffer. The regulator has a low dropout voltage of  $220\text{ mV}$  at  $150\text{ mA}$  and accepts an input voltage of up to  $6.5\text{ V}$  [52]. Figure 66 shows the schematic of the regulator.

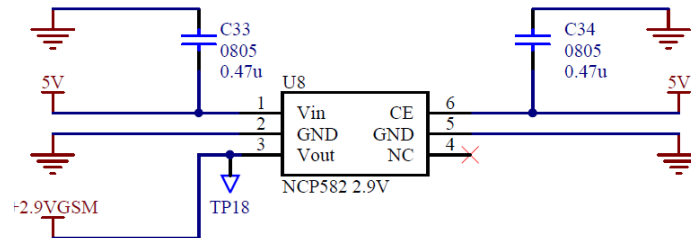


Figure 66: 2.9 V linear regulator

#### 6.3.6.7. *TC63i and UART buffer schematic:*

See Appendix A5 for the schematic of the TC63i GSM/GPRS module as well as the UART buffer schematic.

#### 6.3.7. **GPS module/ Real-time clock (RTC)**

A GPS location is required to obtain the location of the data concentrator in the field. The GPS data will also be used to synchronise GPS time on the Linux computer module. It was decided to use the GPS breakout board from Adafruit as it is a complete solution and ideal for development purposes. The GPS breakout board also includes a built-in RTC, which will supply time to the Linux system when the GPS signal is lost. As soon as a GPS signal is found, the RTC will synchronise itself to the GPS provided time automatically [53].

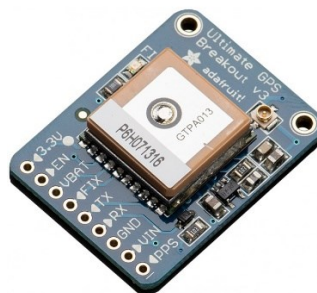


Figure 67: Adafruit GPS module with integrated real-time clock [53]

Figure 67 shows Adafruit's GPS module which is built around the MTK3339 chipset, which is a high-quality GPS module that can track up to 22 satellites on 66 channels, has a high-

sensitivity receiver (-165 dB tracking), and a built-in antenna. The module is also capable to interface with a 3 V active GPS antenna via the u.FL connector [53].

The breakout GPS can be powered from 3.3 – 5 V. It interfaces with the computer module using a UART from the USB to UART expansion. A CR1220 coin cell is added to the bottom of breakout board to keep the RTC running during a power failure and allows for GPS warm start, enabling quick satellite detection.

### **6.3.8. Standard Raspberry Pi header**

A standard 40-pin J8 header as found on the conventional Raspberry PI Model B+ is added to the data concentrator. This is to add additional functionality to the board and enhance the expandability for future use.

The header includes power outputs (5 V, 3.3 V & GND) an SPI, I2C and UART interface as well as 17-GPIO pins. Table 18 shows a pinout of the header as found on the data concentrator board:

Table 18: Standard Raspberry Pi Header [54]

Function/GPIO	J8 Header		Function/GPIO
3.3 V	1	2	5 V
GPIO2(I2C1_SDA)	3	4	5 V
GPIO3(I2C1_SCL)	5	6	GND
GPIO4	7	8	GPIO14(UART_TXD)
GND	9	10	GPIO15(UART_RXD)
GPIO17	11	12	GPIO18
GPIO27	13	14	GND
GPIO22	15	16	GPIO23
3.3 V	17	18	GPIO24
GPIO10(SPI_MOSI)	19	20	GND
GPIO9(SPI_MISO)	21	22	GPIO25
GPIO11(SPI_SCLK)	23	24	GPIO8(SPI_CE0)
GND	25	26	GPIO7(SPI_CE1)
GPIO0(ID_SD)	27	28	GPIO2(ID_SC)
GPIO5	29	30	GND
GPIO6	31	32	GPIO12
GPIO13	33	34	GND
GPIO19	35	36	GPIO16
GPIO26	37	38	GPIO20
GND	39	40	GPIO21

### 6.3.9. RS-232 interface

As the computer module only supports a mini-UART (only RX and TX lines) with voltage levels between 0 V and 3.3 V an electrical interface is needed to convert the voltage levels to meet the RS-232 requirements to create a mini RS-232 port.

The MAX3232E device is used to implement the RS232 level conversion of the electrical signals between the computer module and the serial port. It consists of two line drivers, two line receivers and a dual charge pump circuit. The device meets the requirements of TIA/EIA-232-F

and provides the electrical interfaces needed between the asynchronous communication controller and the serial port connector [55].

The IC operated at CMOS voltages for pre CMOS compatibility, requiring only 3.3 V. It supports a supply input range of between 3 V and 5.5 V. The 3.3 V supply available on the communications board is used to power the board.

The chip uses charge-pump capacitors to boost the output data line voltages to meet the RS232 specifications. Charge-pump capacitors C16, C17, C18 and C19 are all electrolytic, requiring special attention to their polarity. The minimum value of the charge-pump capacitors is 0.1  $\mu\text{F}$  when powered by a 3.3 V supply [55].

Figure 68 shows the schematic used to implement the MAX3232E line driver. The Rx\_RS232 and Tx\_RS232 lines connect to one of the two UARTs available directly on the computer module.

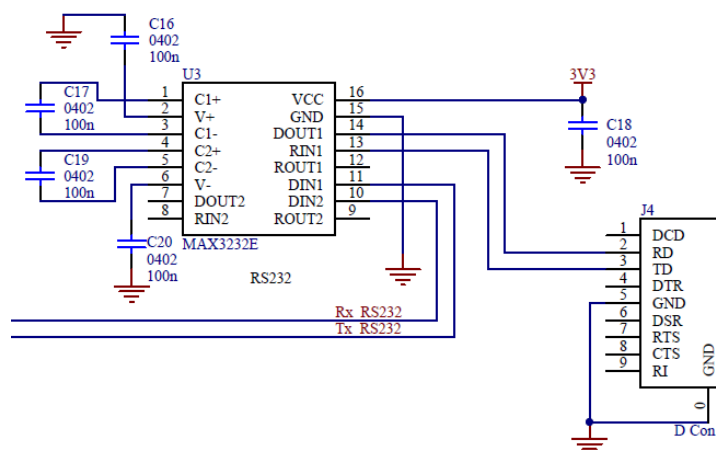


Figure 68: RS-232 MAX3232E line driver

### 6.3.10. CAN bus

The CAN bus implementation is done using the MCP25625 chip from TI. This chip is specifically chosen as it combines the CAN controller as well as transceiver into a single package. General features of the MCP25625 include the following [56]:

- Stand-alone CAN2.0B controller with integrated transceiver and serial peripheral interface (SPI).
- Up to 1 Mbps (High-Speed) operation.
- Up to 10 MHz SPI clock speed.
- Interfaces directly with microcontrollers with 2.7 V to 5.5 V I/O.

A typical CAN solution consists of a CAN controller that implements the CAN protocol, and a CAN transceiver that serves as the interface to the physical CAN bus. The MCP25625

integrates both the CAN controller and transceiver. Therefore, it is a complete CAN solution that can be easily added to a microcontroller with an SPI interface.

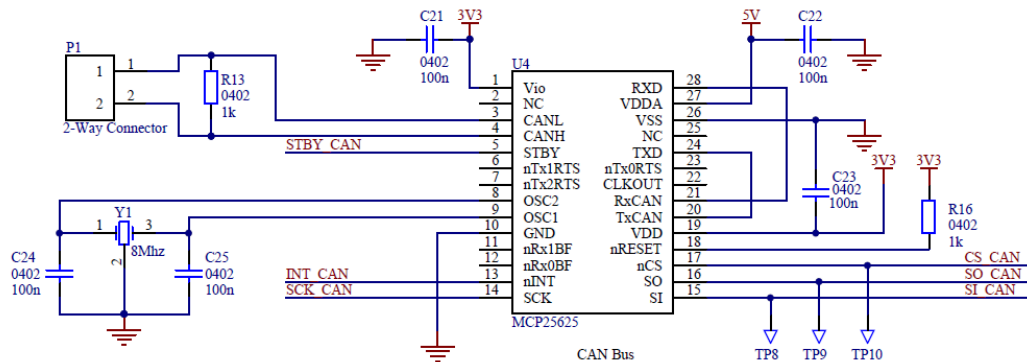


Figure 69: MCP25625 CAN controller with integrated transceiver

Figure 69 shows the schematic for the MCP25625 CAN controller and transceiver.  $V_{DDA}$  supplies the CAN transceiver and is connected to the required 5 V.  $V_{DD}$ ,  $V_{IO}$  is the digital supply for the CAN controller, connected to 3.3 V.

The TxD and RxD pins of the CAN transceiver must be externally connected to the TxCAN and RxCAN pins of the CAN controller.

The SPI interface of the computer module is used to configure and control the CAN controller over the MOSI, MISO, CS and SCK lines (SPI interface). The interrupt pin of the MCP25625 signals an interrupt to the microcontroller and is connected to a GPIO pin of the computer module.

The usage of the nRxXBF and nTxXRTS is optional since the functions of the pins can be accessed through SPI. They are therefore not used in this implementation. The nRESET pin is pulled up to  $V_{DD}$  of the MCP25625 using a 10 k $\Omega$  resistor [56].

The CAN+ and CAN- lines are connected to a header for external connection, with a 120  $\Omega$  resistor between the lines as required by the CAN bus standard.

### 6.3.11. PCB design

Altium Designer was used to design the PCB of the data concentrator. The board was made in China by PCBWay as the cost was less compared to local companies and the time from order to delivery was only one week.

The components were populated and each piece of hardware individually tested. Figure 70 shows the completed PCB with all the components.



Figure 70: Completed data concentrator board

#### 6.4. CONCLUSION

This chapter discussed the hardware development of the data concentrator. The data concentrator is based around a Linux computer module manufactured by Raspberry PI. The main function of the data concentrator is to capture incoming messages from the meters over a ZigBee link. The data concentrator has GPS capabilities to update the Linux system time and GSM capabilities to send alarm conditions to a central head end system.

## CHAPTER 7

# DATA CONCENTRATOR SOFTWARE DEVELOPMENT

### 7.1. INTRODUCTION

This chapter documents the software development done on the data concentrator. The data concentrator can receive data from the smart meters via a ZigBee link, storing the data in a MySQL database and processing the data to detect possible fault conditions on an experimental LV network. Various Linux processes and third-party Linux software packages that were used is discussed.

A web server is hosted on the data concentrator to view the incoming measurement data in graph format on a website. A graph associated with each hazardous condition is displayed on the website. Additional features on the website include an embedded google map to view the location of the meters in near real time. The website also displays the time elapsed since last communications was received from a specific meter.

### 7.2. COMPUTER MODULE LINUX FLASH PROCEDURE

This section explains the procedure to follow to flash the data concentrator's computer module with a distribution of Linux. The Raspbian distribution is used as the operating system on the data concentrator. It is based on the Debian Linux operating system, which is used by millions around the world but has been modified to be compatible with the ARM processor used by Raspberry PI [57].

The flashing of the data concentrator board is similar to that of the computer module I/O board with a computer module inserted.

A USB tool is available on github which allows a host PC running Linux to write the BCM2835 boot code over USB to the module with the USB selection jumper in the USB boot enabled position. On the data concentrator board, this is done by placing jumper "J6" in the "EN" position.

"With the USB boot enabled the BCM2835 will wait for a file called "bootcode.bin" which is squirted down the USB to the BCM2835. This will then execute the second stage boot process that normally looks for a file called config.txt and start.elf on the SD card and loads start.elf (or whatever version of start is required depending on the settings in config.txt)" [17].

"With usbbootcode.bin it re-enumerates as a device (but this time with a serial number of 1 to distinguish the second stage from the primary boot) and waits for a message packet from the host. After the message packet, it receives the data (the length is in the message packet). It then checks the length of the downloaded information (should be an .elf file either msd.elf or

buildroot.elf), if the length is greater than the size of the elf file, it assumes the rest of the data is an FAT16 image of a file system as created using the Raspberry Pi buildroot target raspberrypi\_defconfig” [35].

### 7.2.1. Linux terminal steps used to flash the eMMC over USB from a Linux PC

- Clone this onto an Ubuntu Linux machine:
  - `git clone --depth=1 https://github.com/raspberrypi/tools`
  - `cd tools/usbboot`
  - `sudo apt-get install libusb-1.0-0-dev`
  - `make`
  - `sudo make install`
  - `sudo rpiboot`
- Checkout the upstream buildroot from git:
  - `git clone git://git.buildroot.net/buildroot`
- Patch the Pi patches:
  - `cd buildroot`
  - `patch -p1 < ../tools/usbboot/buildroot.patch`
  - `make raspberrypi_defconfig`
  - `make`
- Run:
  - `sudo rpiboot tools/usbboot/usbbootcode.bin tools/usbboot/buildroot.elf`  
`buildroot/output/images/fatimage`

When the image is finished written to the eMMC flash a reboot is required to boot from the internal flash of the computer module. The data concentrator should now start with a fresh Linux installation.

## 7.3. REMOTE CONNECTION TO DATA CONCENTRATOR

Access to the data concentrator’s Linux OS is obtained via the SSH (secure shell) and FTP (file transfer protocol) protocols. The SSH protocol is used to open a remote Linux terminal window and the FTP protocol is used to copy files from a device such as a Windows PC to the data concentrator’s internal memory.

### 7.3.1. SSH connection to data concentrator

The following steps show how to open a Linux terminal window of the data concentrator via a remote SSH connection:

1. Connect the data concentrator to the same network (router) as the device/computer used to gain access to the data concentrator by connecting an ethernet cable from the router to the data concentrator's ethernet port. The router will automatically assign an IP address to the data concentrator if it is setup as a dynamic host configuration protocol (DHCP) server.
2. Obtain the IP address assigned to the data concentrator by the router. If using a network router, the router's web-based setup page can be used by entering the IP address of the router in a web browser.
3. Open an SSH client such as on the remote computer and enter the data concentrator's IP address. Putty is an open source SSH client program which can be used on a Windows PC.
4. A terminal window will open requesting a username and password. Enter the username and password found below to gain access to the filesystem:
  - a) Username: *pi*
  - b) Password: *raspberrry*

### 7.3.2. FTP connection to data concentrator

To copy files to the DC the FTP protocol is used. The following steps shows how to open a remote FTP connection:

1. Repeat Steps 1 & 2 of the remote SSH connection to obtain the IP of the data concentrator.
2. Open an FTP client such as FileZilla. (Open source software)
3. Enter the following details:
  - a) IP: IP address as assigned by the network to the data concentrator.
  - b) Username: *pi*
  - c) Password: *raspberrry*
  - d) Port: 22

A remote FTP connection will open and the files on the data concentrator can be accessed.

### 7.4. XBEE MODEM

The following section describes the software configuration of the XBee ZigBee and the libraries used to interface with the modem from the Linux data concentrator board.

### 7.4.1. XCTU

A configuration tool XCTU, available for download from DIGI's website, used for updating the firmware of the XBee modem and configuring the modules parameters. XCTU has the capability to do the following:

- Update modules firmware over a serial connection from a personal computer.
- Read or write configuration parameter on a local device.

#### 7.4.1.1. *XBee explorer*

A XBee explorer adapter (Figure 71) is used to interface with a XBee from a Windows or Linux computer. It enables the XCTU software to communicate to the modem to update firmware and configure parameters. The explorer uses a FTDI chip to convert the USB data lines from a computer's USB port to UART serial data lines. A XBee modem slots on the provided header of the Explorer.



Figure 71: XBee explorer adapter [58]

#### 7.4.1.2. *Firmware update*

The XBee modems can be configured with various versions of firmware from a specific product family and function set. The product family can be found below the device. The function set indicates the various device types which consist of a coordinator, router, and end-device which the XBee modem can be configured with. For each device type, the option is given between the application programming interface (API) and attention (AT) function set.

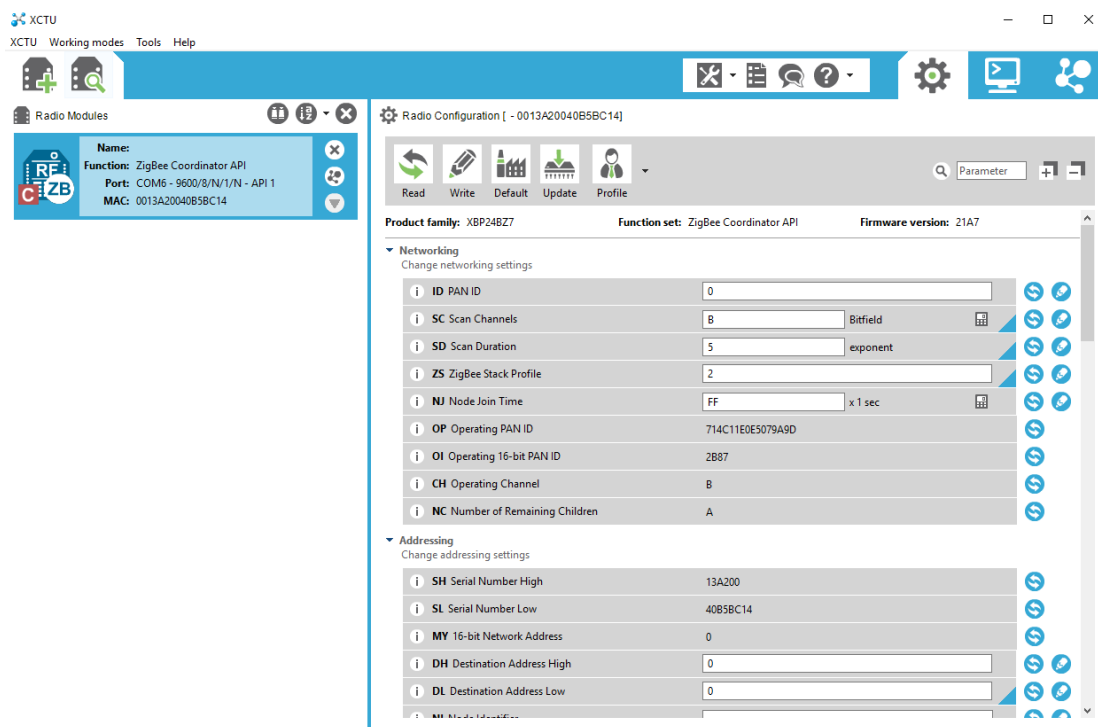


Figure 72: XCTU software interface [59]

New firmware can be flashed on the modem by selecting the correct function set and firmware version and selecting *update* on the XCTU interface. For the data concentrator, the following firmware specifications were used in this project:

- Product family: XBP24BZ7
- Function set: ZigBee coordinator API
- Firmware Version: 21A7 (The latest version available)

Before the firmware is written to the modem the correct configuration parameters should be inserted in the various fields.

#### 7.4.1.3. XBee configuration parameters

The XBee modem used on the data concentrator was flashed with the configuration parameters as shown in Figure 72. The important configuration parameter to note is the ZigBee stack profile, which should be changed to “2” to enable communication to devices from other manufacturers.

#### 7.4.2. XBee AT commands

The Xbee makes use of AT commands for local communication to the modem over a serial connection. AT commands are instructions used to control a modem. AT is the abbreviation of attention. Every AT command starts with “AT” or “at” followed by the actual command. For example, on the XBee modems, the command “ATID” will assign a new PAN address to the

modem. For the XBee modems AT commands are mostly used for setup of the device and the same configuration parameters can be set as in XCTU. Only AT-configured XBees are able to be configured using AT commands. Radios configured in API mode will not accept AT commands. Various network indications can also be read by using AT commands.

#### **7.4.2.1. Command mode and transparent mode**

All XBee ZigBee radios communicate between one another in the same way or using the same protocol. XBees can, however, communicate in very different ways using their local serial connection. Radios configured to use application programming interface (API) mode implements a XBee specific protocol (See Section 7.4.3). XBee radios configured for “AT” commands constantly switch between two modes:

##### **Transparent mode**

In transparent mode, the radio simply passes the data through to the other radios in the network just as it was received over its serial port. The same happens when the data is received, it is sent out through the serial port exactly as it was received.

##### **Command mode**

Command mode is used to send AT-commands directly to the XBee radio to alter its configuration or change the configuration parameters.

#### **7.4.3. API protocol**

API operations are provided to allow communication with other devices through a UART port. Data is sent and received in a predefined structured way as specified by the API. “An API is simply a set of standard interfaces created to allow one software program to interact with another. The goal of API-mode communications is to transmit highly structured data quickly, predictably, and reliably” [49]. The data is structured in such a way to allow checks to be performed on the data received to determine if data was lost or got corrupted during the sending and receiving process, just as in any other protocol.

XBee implements its own standard API protocol over the serial port to allow a host device such as a Raspberry PI or personal computer to effectively communicate with the modem.

##### **7.4.3.1. XBee API protocol**

To use the XBee API a firmware function sets name ending in API should be flashed on the XBee modem using the XCTU software as in section 7.4.1. The following section gives more detail into the API protocol used to communicate with the modem. The XBee API frame consists of a series of bytes, each building on the information already transmitted. Table 19 shows the basic API frame structure used for the XBee API:

Table 19: Basic API frame structure [49]

Start delimiter	Length		Frame data	Checksum
<i>Byte 1</i>	<i>Byte 2</i>	<i>Byte 3</i>	<i>Byte 4 ... Byte n</i>	<i>Byte n +1</i>
0x7E	MSB	LSB	API-specific structure	Single byte

**Start delimiter:** Indicates the start of a new incoming message. For the XBee API, 0x7E is used.

**Length:** The overall length of the data frame sent.

**Frame data:** See the XBee API frame data section.

**Checksum:** Used to test data integrity. For the XBee API, the checksum is calculated by adding all the bytes, not including the delimiter and length bits and only keeping the lowest 8 bits of the sum. The sum should equal 0xFF if the data integrity is correct.

#### **7.4.3.2. XBee API frame data**

The XBee API frame data contains the core of the information sent to the modem. Various different frame types/structures are used to send and receive different types of messages to and from the modem. Each frame structure contains substructures containing the different kinds of data types which will be sent to and received from the XBee modem. The XBee API specifies a frame type for each type of message sent or received. Table 20 shows the most commonly used frame types with their identification value.

AT commands can be sent via API frames to configure a radio over the local UART connection. The same AT commands used for AT configured modems can be used for XBees which are configured with API firmware. The AT command API frame is used as an example of the API frames used to communicate with a local radio configured in API mode. Table 21 shows the API format used for sending AT commands to a local radio. The frame specific data structure will change depending on the type of message sent or received from the XBee radio. A full description of the API format for each type of message can be found in [49].

Table 20: Commonly used API mode frame types [49]

Frame type	Description
0x08	AT command (immediate)
0x09	AT command (queued)
0x17	Remote Command Request
0x88	AT command response
0x8A	Modem Status
0x10	TX request
0x8B	TX response
0x90	RX received

Table 21: API format for AT commands [49]

Frame fields		Offset	Example	Description
Start delimiter		0	0x7E	
Length		MSB 1	0x00	Number of bytes between the length and the checksum.
		LSB 2	0x04	
Frame-specific data	Frame type	3	0x08	Indicates the frame data type that is sent.
	Frame ID	4	0x52	Identifies the UART data frame for the host to correlate with a subsequent ACK (acknowledgment). If set to 0, no response is sent.
	AT commands	5	0x4E (N)	The command name – two ASCII characters that identify the AT command.
		6	0x4A (J)	
Parameter value (optional)			If present, indicates the requested parameter value to set the given register. If no characters present, the register is queried.	
Checksum		7	0x0D	0xFF – the 8-bit sum of bytes from offset 3 to this byte.

The other frame types shown in Table 20 follows a similar pattern to the API format for AT commands. An example of each of the API frame types can be found in [49].

#### 7.4.4. Python XBee library

Python-XBee is a Python library providing an implementation of the XBee serial communications API. It provides a semi-complete implementation of the XBee binary API protocol which allows a user to send and receive data to XBee modems without having to deal with the raw data of the various API formats.

The library is compatible with XBee 802.15.4 (series 1) and XBee ZigBee (series 2) radios in API mode, supporting either normal or PRO XBee modules. The library is thus compatible with the series 2 PRO radio used for the data concentrator.

To enable the library for XBee ZigBee (series 2) radios the following line of code is to be changed:

```
xbee = XBee(Serial_Port,escaped=True)

to:

xbee = ZigBee(Serial_Port,escaped=True)
```

##### 7.4.4.1. Dependencies

###### PySerial

The library encapsulates the access for the serial port. It allows a user to easily access the serial port on a device to send and receive data across a serial port.

##### 7.4.4.2. Receiving a data frame in API format

The XBee library method `xbee.wait_read_frame()` is used to receive a string of incoming data containing the ZigBee message data received from the XBee module over a UART connection in API format. The function waits for incoming data from the module, interprets the data, and outputs data fields in a Python dictionary type.

A Python dictionary type is similar to an array but is capable of storing different value types, accessed by key rather than by index. Individual fields which can be accessed are shown below as specified by the XBee Python library:

**Source\_addr\_long:** The 64-bit mac address of the ZigBee modem of a specific meter.

**Rf\_data:** Actual data string sent from the meter.

**Source\_addr:** The 16-bit network address of the meter ZigBee modem.

## 7.5. SQLITE

A SQLite database was used on the data concentrator to store the data received. This section provides more detail regarding SQLite and the database implementation on the data concentrator.

### 7.5.1. SQLite overview

The SQLite database was developed in 2000 by Richard Hipp. Today it is the most widely deployed database engine in the world, with many browsers, operating systems and embedded systems making use of this database. SQLite is a lighter version of the more traditional database engines such as MySQL, PostgreSQL etc. SQLite emphasises economy, efficiency, reliability independence and simplicity making it an ideal choice to use of the Raspberry PI based data concentrator. SQLite offers all the complex queries of these more high-end databases with a limited *alter table* function, as it can't modify or delete columns [60].

Structured query language (SQL) is a programming language used to modify or insert new data into a database. Its syntax is similar to English allowing the user to easily insert data into or modify a database. SQL commands can be used inside a Python script allowing for programs to alter or insert data into the database while running.

Some key SQLite commands used in the data concentrator is shown in Table 22.

Table 22: Key SQLite commands [60]

SQLite command	Function
CREATE TABLE	Creates a new table
DROP TABLE	Deletes a table
INSERT	Inserts value into a specified table
SELECT	Fetch data from a table
UPDATE	Modify existing records in a table
DELETE	Delete existing records from a table

### 7.5.2. Data concentrator SQL database

A SQLite database was created to store incoming data and act as a communication channel between the processes storing the data and the processes reading from the database. The database contains various database tables, a table for each meter where all the data received from a specific meter is stored and a table for each fault condition monitored. The data required

to analyse a specific fault condition is read from the meter specific database table and stored in the fault specific database table, from which it can be analysed by specific Python scripts.

Table 23 shows the various tables contained in the database and their specific function:

Table 23: Data concentrator SQLite database tables

Database name	Function
meter0_ph3	Stores all the time stamped data received from meter 0 for phase 3 located at the transformer.
meter0_ph2	Stores all the time stamped data received from meter 0 for phase 2 located at the transformer.
meter0_ph1	Stores all the time stamped data received from meter 0 for phase 1 located at the transformer.
meter1_ph3	Stores all the time stamped data received from meter 1 for phase 3 located at house 1.
meter1_ph1	Stores all the time stamped data received from meter 1 for phase 2 located at house 1.
meter3_ph3	Stores all the time stamped data received from meter 3 for phase 3 located at house 3.
meter3_ph1	Stores all the time stamped data received from meter 3 for phase 1 located at house 3.
current_balancing	Stores current measurements from meter 0, 1 and 3.
lv_earth_high_impedance	Stores phase 2 & 3 current measurements of meter 0 located at the transformer.
pen_failure_single_phase	Stores phase 2 current of meter 0 located at the transformer and meter 3 voltage.
pen_failure_dual_phase	Stores voltage measurements of meter 1 and 3.
impedance	Stores impedance values received from meters 0,1,2 and 3.

## 7.6. PYTHON SCRIPTS

The following documents the Python script development that took place for the data concentrator.

Various Python scripts were written to achieve the desired functions of the data concentrator. The scripts functions include the capturing of the incoming data strings received over the ZigBee link from the meters and inserting the data into the desired database tables. Additional

scripts were written to read from these tables to create fault specific database tables with the information from various meters that are required to detect a specific fault condition.

### 7.6.1. The Python programming language

Python was conceived in the late 1980s and first released by its designer, Dutchman Guido Van Rossum, in February 1991. Python is often viewed as a scripting language but is, in fact, a general programming language, with support for object-orientated programming including user-defined classes. In Python, variables do not need to be declared before they are assigned, but the type-checking is done at runtime by the interpreter, unlike other programming languages where it is done during the compilation step [61].

What makes Python so popular around the world is its extensive standard library and third-party modules that are available, most of which are open source. The Python package index (PYPI) contains the official repository of all third-party software for Python and contains over 92 000 packages [62]. These packages include but is not limited to the following functionality:

- Graphical user interface
- Databases
- Networking
- Text Processing
- Image Processing
- Web Development

Another major appeal of Python is its ability to make seemingly complicated tasks very easy, and realisable with very little code. An example of this is its ability to manipulate strings with very easy of use [61].

### 7.6.2. Python Script to receive data frames

The main Python script *receive\_samples.py*, represented by the flow diagram shown in Figure 73 is used to receive the data incoming from the meters. This script runs continually waiting for incoming data and parses the data when received. The Python dictionary field *source\_addr\_long* containing the 64-bit MAC address of the sender modem is used to identify the meter from which the data originates. The *rf\_data* dictionary field contains the data string received from the meter.

The meters send a message for each phase and a single location message every second. For each phase the message contains all the one minute averaged measurements for the specific phase together with a timestamp provided by the meter's real time clock that has been synchronised with the GPS provided timestamp. After each phase's data has been sent by the

meter a location message is sent containing the GPS location of the meter. Each meter, therefore, sends in total four consecutive messages every second.

The *receive\_samples.py* script continually waits for a new data frame received over the UART port. As a new frame is received the *rf\_data* data field contains the new data string received from the meter. A first check is done to interpret the message type which was received. This is done by checking the length of the *rf\_data* field.

The various data fields are extracted from the data frame by splitting the data after each 8 bytes. Each 8 bytes contains a specific measurement such as voltage, current, real power, date, time etc. Individual 8-byte strings are converted to integer types to be stored in the SQL database. This is all done by the *parse\_data* function in the Python script *receive\_samples.py*.

A *storeval* function lastly stores the data received and parsed, in a meter and phase specific database table. See section 7.5.2 for a full list of the database tables.

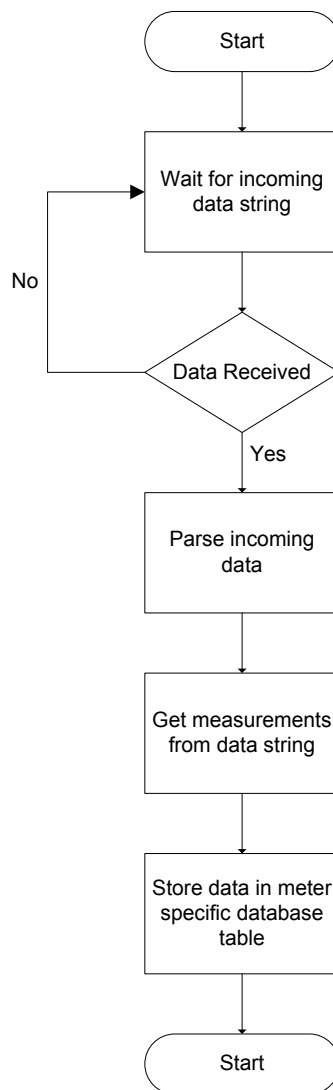


Figure 73: Python script to receive and store measurements

### 7.6.3. Python script to determine unaccounted current flow

Figure 74 shows the flow diagram of a Python script to read entries from three-meter tables in a SQL database. The script is shown in Figure 73 executed concurrently with *receive\_samples.py*.

The script starts by determining the current date and time to determine the next expected measurements to be read. The date and time are captured from the Linux system time, which is synchronised with GPS provided time.

The script continually waits for new data to enter into the meter database tables. As soon as a new entry is entered into the meter database tables it is read by the script and marked as read in the meter table. If an entry from each table has been read, and they are all at the expected time instance (a time offset of 20 secs is allowed), current balancing is performed. Current balancing is done by subtracting the current measured by meter 1 and meter 3 from the current

measured by meter 0 located at the transformer. The unaccounted current percentage is also calculated and both values are stored in the *current\_unbalance* database table.

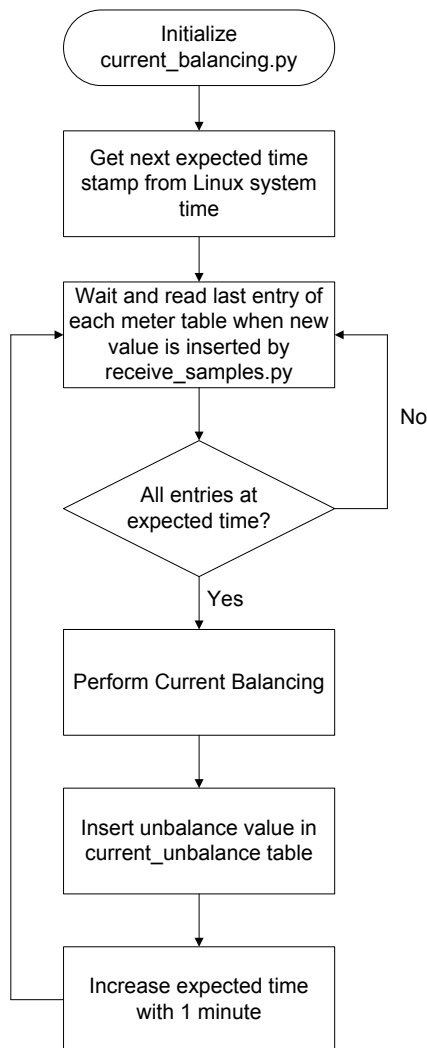


Figure 74: Python script to calculate unaccounted current flow

The next expected time of the entries to be read from the meter tables is now increased by 1 minute and the script returns to waiting for new data to be entered into the meter tables.

#### 7.6.4. PEN conductor failure Python script

##### 7.6.4.1. *Single-phase*

Figure 75 shows the Python script used to capture the entries from the required meter tables and insert the measurements into the *pen\_failure* table. As discussed, a voltage measurement is required to detect a possible PEN conductor failure. The voltage from meter 3 is therefore captured. An increase in the current returning to the transformer via the LV earth electrode can also be an indication of a possible PEN failure. The LV earth electrode current of the transformer is therefore also required, which is measured by phase 2 of meter 0 located at the transformer.

The scripts follow a similar sequence as with the unbalanced current detection discussed in section 7.6.3. It waits for a new entry into meter 0 and meter 3 tables, reads these entries when detected, and inserts the voltage from meter 3 and the phase 2 current from meter 0 into the *pen\_failure* database table.

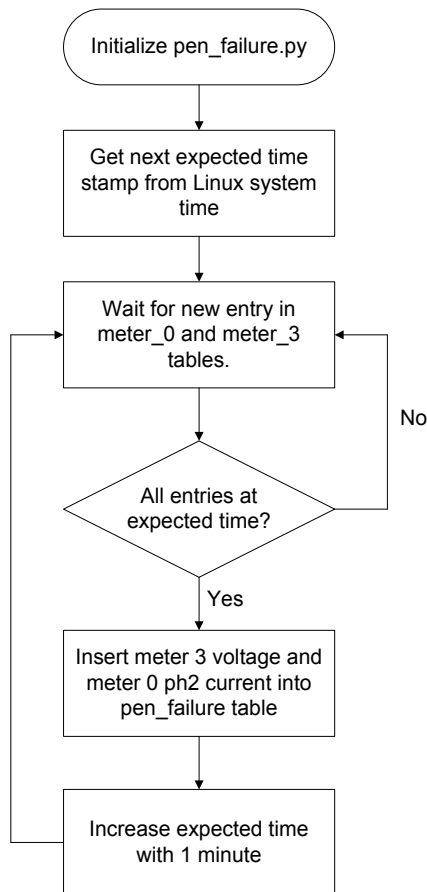


Figure 75: Python script to capture values required to detect a single-phase PEN conductor failure

#### 7.6.4.2. Dual phase

Figure 76 shows the Python script to capture the required entries to detect a possible PEN conductor failure on a dual phase system. A broken PEN conductor can be detected by continually monitoring the voltage at the customer's point of connection. A PEN failure on a dual phase system will result in customers on one phase experiencing an overvoltage while customers on the other phase experiencing an undervoltage. The Python script, therefore, captures voltage readings from two meters on different phases. The script is similar to that of the single-phase system, with voltage being read from meter 1 and meter 3 located at customer installation 1 and 3 respectively.

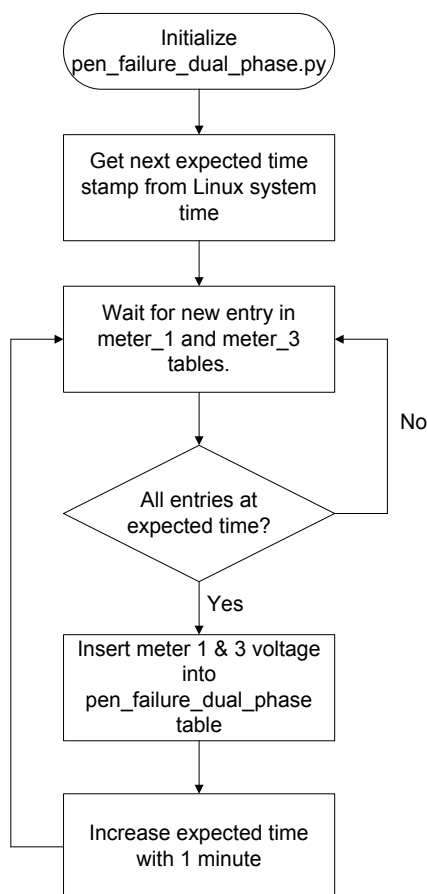


Figure 76: Python script to capture values required to detect a dual phase PEN conductor failure

#### 7.6.5. Transformer LV earth electrode failure Python script

The script used to capture the table entries to detect a possible LV earth electrode failure can be seen in Figure 77. A similar script is used as the others explained above. To detect a transformer LV earth electrode failure, the current through the earth electrode is measured. A sudden decrease in the LV earth electrode current can indicate a possible failure of the electrode. The ratio between the transformer live current and electrode current is used to give a good indication of a possible indication of an electrode failure. A sudden increase in the ratio of electrode current over live current can also be used to indicate an electrode failure.

The required table entries are the live current and the LV earth electrode current of the transformer measured by meter 0 phase 3 and 2 respectively. These values are stored in *lv\_earth\_electrode\_failure* database table.

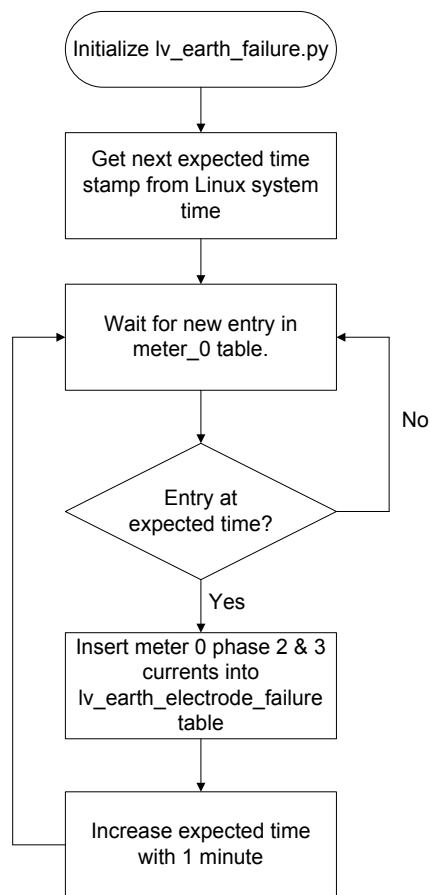


Figure 77: Python script to capture values required to detect a transformer LV earth electrode failure

#### 7.6.6. Meter watchdog Python script

A watchdog Python script was written to detect a loss in communication from a meter. A loss in communication from the meter could indicate a variety of reasons including a bypassed meter. It is, therefore, important to monitor the time since last communication was made with a meter.

The Python script starts by acquiring the Linux system time, which is synchronised to GPS provided time. The latest meter entries are now captured from the meter database tables. The timestamps of these entries are compared to the Linux system time to determine the time elapsed since last meter messages were received. These calculated values for each meter are inserted into a *meter\_watchdog* database table. The values in this table are overwritten every minute as only the latest reading is of value. The script now waits for 1 minute as the messages from the meters are sent in 1-minute intervals. Figure 78 shows a flow diagram of the Python script written.

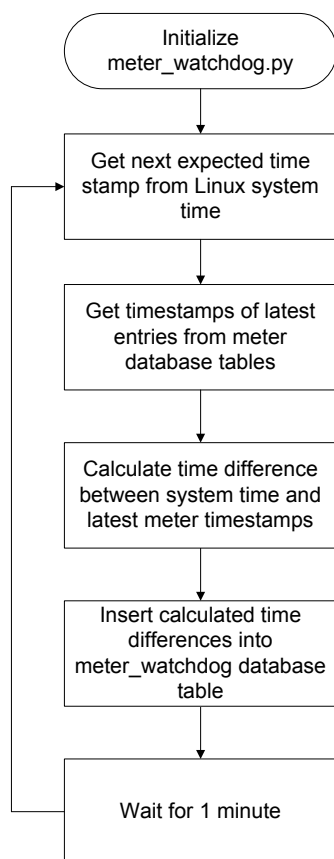


Figure 78: Meter watchdog Python script

The time difference values in minutes are displayed on the LV safety website which is discussed in section 7.7.

## 7.7. THE LV SAFETY WEB INTERFACE

An LV Safety website was developed to view the data captured from the meters in near real time. As the data concentrator does not incorporate a display output to view the meter data received, a website hosted on the data concentrator is used. Graphs of the data stored in the SQLite database is plotted to give a graphical representation of the various hazardous conditions. The development of the website is explained in this section.

### 7.7.1. Common gateway interface (CGI)

To display the website developed, a common gateway interface was used. CGI is a set of standards which define how information is exchanged between a web server and a custom script [63]. With normal web browsing to a specific URL or web address, a browser contacts the specific HTTP (Hypertext transfer protocol) web server hosting the website and demands the filename. The filename, if found by the web server, is sent to the browser requesting the file and displayed by the browser.

It is however also possible to configure a web server to execute a program and return the output generated instead of just sending back a specific file. This function is called a CGI and the programs executed are called CGI scripts. The CGI program can be a Python script, Perl script, Shell script, C or C++ program or any language that allows it to be executed [63].

HTML (HyperText markup language) is a plain document that does not change. CGI is, therefore, distinguishable from standard HTML in that it executes in real time and output dynamic information.

CGI is often used when a database needs to be queried. A CGI script can be written, which when executed, transmits information to the database engine and then receive results and displays them in a web browser. The link between the database and the user is known as the gateway, which is where the CGI standard originated from. Figure 79 shows the CGI architecture.

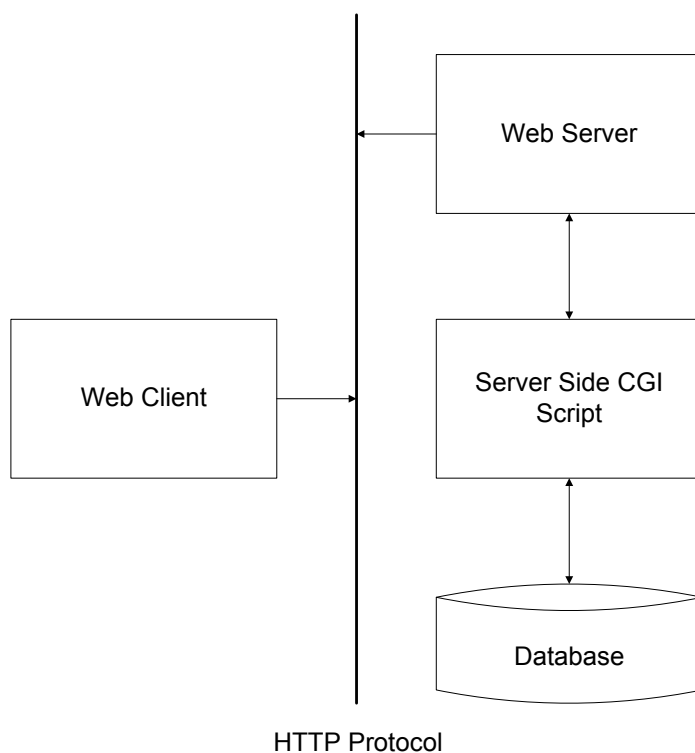


Figure 79: CGI architecture diagram

As Python has been readily used to capture the measurement and access the SQLite database it was decided to make use of a Python script as the CGI program.

### 7.7.2. Apache web server

To host the website and execute the Python CGI program a web server was required. Apache web server was used as it is the most commonly used web server on Linux systems. Web servers are used to serve web pages requested by client computers using a web browser.

Apache 2.0 was installed on the data concentrator and configured to execute Python CGI scripts.

### **7.7.3. The web interface**

The web interface was created primarily to view the data received by the data concentrator from the smart meters in graph format. Single or multiple graphs were created for each hazardous condition. Python was used as the scripting language generating HTML and JavaScript to be processed by a browser.

The website layout shows multiple tabs on the top of the website. It allows the client to view results obtained for each hazardous condition. A locations tab displays an embedded google maps chart of the last received location of the meters in the field. Figure 80 shows a screenshot of the main web interface with the Google maps chart showing the locations of the meters. The location plotted is gathered from the last location message received from a specific meter.

#### **7.7.3.1. *Time elapsed since last meter communications***

The website displays the time elapsed since data was last received from a specific meter as shown in Figure 80. The Python CGI script reads the time elapsed data from the *meter\_watchdog* database table and displays it on the website. It allows for the easy monitoring of lost communications with a meter. Times longer than 5 – 10 minutes could possibly indicate a faulty or bypassed meter, broken communication link or a power outage in the area.

## LV Safety Project

Project Description

Hazard 1

Hazard 2

Hazard 3

Hazard 4

Hazard 5

Hazard 6

Hazard 7

Hazard 8

Hazard 9

Gallery

Location of Meters

### LV Safety Project Description

The LV safety project stream objective is to find new methods to detect safety hazards on the LV network. Utilities employ advances in processing and communication technologies to improve network operation. Devices that employ these technologies are often referred to as smart. The current emphasis on the LV safety project is to demonstrate the feasibility of using smart meters and smart transformers to detect hazards.

### Time elapsed since last meter communications (In Minutes):

Meter 0: Meter 1: Meter 3:

278 42 41

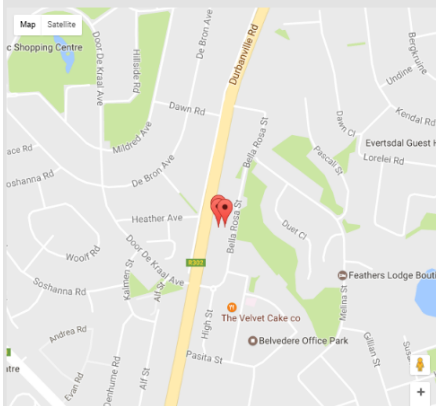


Figure 80: LV Safety web interface

### 7.7.3.2. Graphs

The various graphs on the homepage of the website are used to view the data received during the experiments performed. This allows for a clear visual indication if such a hazard will be detectable. The graphs were drawn using Google charts. It provides a user-friendly way to view data in a browser. It was created with JavaScript and executed by the Python CGI script. Google chart libraries were added to the Python script which is called during execution of the script. All Google charts are viewable in any browser supporting HTML5. The graphs are shown in the experimental results chapter.

### 7.7.3.3. Authentication

The LV Safety website includes authentication to allow only desired users to view the website. The Apache utility *htpasswd* was used to create a password file which Apache uses to authenticate users. The utility creates a hidden file called *.htpasswd* within the */etc/apache2* configuration directory. A username and password is set in this file and Apache was configured to check this file before serving the protected website. When browsing to the LV Safety website a pop-up will appear asking to provide a username and password.

The website can be viewed by browsing to <http://lvsafety.duckdns.org/cgi-bin/webgui.py>

### 7.7.4. Hosting the website on the internet

The following describes the process followed to publish the LV Safety web server, which is hosted on the data concentrator, onto the global internet to be accessible by anyone from

anywhere. The understanding of network address translation (NAT), port forwarding and dynamic domain name system (DDNS) was required.

#### 7.7.4.1. **Network address translation (NAT)**

A single IP address is assigned to each customer by the internet service provider (ISP). This results in only one computer being able to connect to the internet at any given time. To overcome this problem a router running a NAT gateway is used. A NAT gateway allows a single IP address on the internet to be shared by multiple computers on a local network.

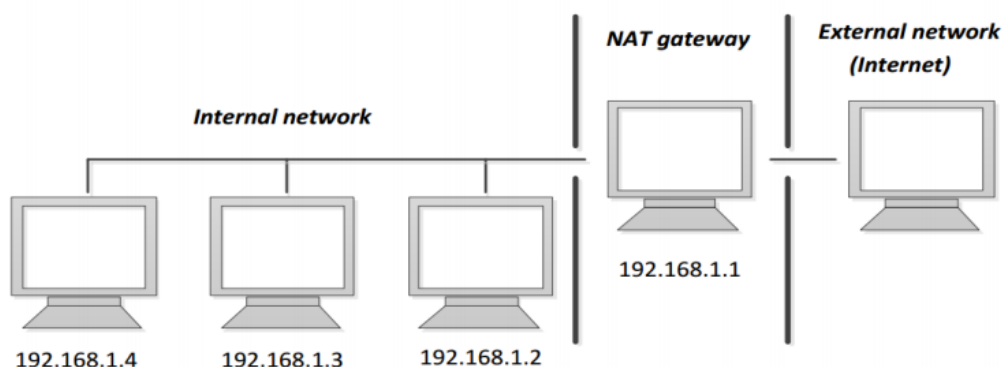


Figure 81: NAT operation

Figure 81 shows the typical NAT operation. A gateway is created for multiple computers on an internal network to access the internet through the use of a single IP address. The network interface is either another computer or a router. A router has built-in NAT capabilities and assigns a IP address to each computer on the local network. The router using NAT, multiplexes traffic from the local network and transmits as if it was coming from a single IP address.

#### 7.7.4.2. **Port forwarding**

NAT allows for request from the internal network to an outside network such as the internet, but does not allow for external computers to access computers on the internal local network. A web browser trying to access the lvsafety website, which is hosted on the internal network, will not be allowed access. To overcome this problem, NAT provides an application called port forwarding.

Port forwarding allows external requests access to a private local network. All incoming traffic on a specific port will be forwarded to a specified local IP address. On a router, the unique port is linked to an internal IP address and stored in the NAT gateway's port mapping table.

All web pages are fetched over port 80. Port 80 on the router to which the data concentrator connects has therefore been forwarded. All incoming HTTP requests on port 80 will automatically be forwarded to the data concentrator's IP address on the internal network. A

static IP address has assigned to the data concentrator to prevent breaking this link. The internal network behind the routers firewall is now accessible to allow traffic on port 80.

#### **7.7.4.3. DDNS**

All internet address or domain names represent IP addresses. The translation between the domain names as entered by a user in a web browser is translated to a specific IP address by an internet service called domain name system (DNS). AS an example, the web address [www.myexample.co.za](http://www.myexample.co.za) might translate to the web address 198.103.456.5. Domain names of websites are used instead of IP addresses as they are easier to remember than IP addresses.

A router's public IP address is dynamic, meaning it changes frequently. This will result in the website hosted by a webserver on a router's network not being accessible as the domain name will no longer point to the correct IP address. A dynamic DNS (DDNS) addresses the problem by allowing a dynamic address to act as a static address. Various DDNS providers are available which provides software that points the domain name created by the user to the public IP address of the user's router. Whenever the public IP address of the router is changed the software will update the DDNS providers database to the new IP address of the router. This will ensure that a domain name remains accessible even when it's IP address has changed.

Duck DNS was used to create a domain name for the LV safety website. It is a free service which will point a DNS (sub-domains of duckdns.org) to an IP address of your choice. A free client script from Duck DNS was installed on the data concentrator which periodically (usually every 5 minutes) updates the Duck DNS server with the latest external IP address of the router.

A domain name for the LV safety website was registered on Duck DNS which is <http://lvsafety.duckdns.org>

#### **7.8. CONCLUSION**

This chapter discussed the software development done on the data concentrator. The data concentrator makes use of a Python script to receive the incoming ZigBee messages. The measurements received are stored in meter specific MySQL database tables. Various Python scripts were written to read measurements required to detect specific fault conditions from the meter database tables. These measurements are stored in fault specific database tables. From these tables, the data is plotted on a website in graph format to detect possible hazardous conditions.

## CHAPTER 8

### PRACTICAL SETUP AND EXPERIMENTAL RESULTS

#### 8.1. INTRODUCTION

In this chapter, the practical setup and experimental results obtained are discussed. The chapter starts with an overview of a scale model of a LV network and continues to results obtained for each fault condition as discussed in Chapter 2.

#### 8.2. EXPERIMENTAL SETUP

A LV feeder experimental setup was built to simulate the various hazards identified in Chapter 2. The feeder was built to simulate an actual feeder as closely as possible. The schematic diagram of the experimental setup can be seen in Figure 82 and Figure 83 for the single and dual phase respectively. A 1:1 isolation transformer is used to represent a MV/LV transformer as no MV supply was available. A smart meter is located at the transformer to measure the live-to-neutral voltage at the transformer, the transformer live current and the MV and LV earth electrode currents as shown on the schematics.

Figure 84 shows the complete lab setup built according to the schematic in Figure 82 and Figure 83. Three distribution board installations were used to represent three customer installations. Figure 85 shows a single customer installation. The live and PEN conductors are tapped from the feeder line running to the customer's point of supply. From the point of supply, the neutral is split into a PE and N conductors running to the customer's point of connection (POC) as shown in the schematics. A typical distribution board is used, equipped with a RCD. A two-pole contactor is added in parallel to the RCD, to bypass the RCD, simulating an earth leakage protection failure condition. The smart meters as seen in Figure 84 measures the live current and live to neutral voltage at the customers POC. A breaker with a resistor is used to simulate an appliance chassis making contact with earth. An optional earth electrode can also be switched into the circuit to evaluate the effect of an earth electrode at a customer's premises.

Breakers were used to break certain conductors or switch in resistors to simulate the various hazardous conditions as discussed in Section 2.4 to 2.6. The breaker and resistors associated with each hazardous condition are indicated in the schematics.

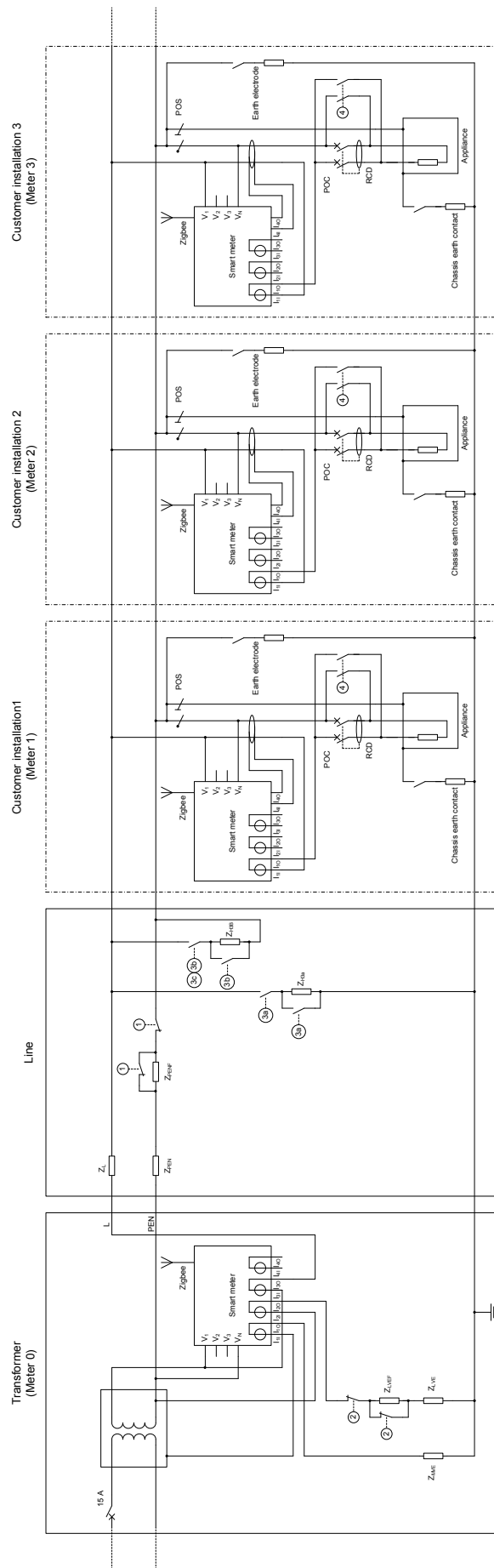


Figure 82: LV lab model schematic – single-phase system

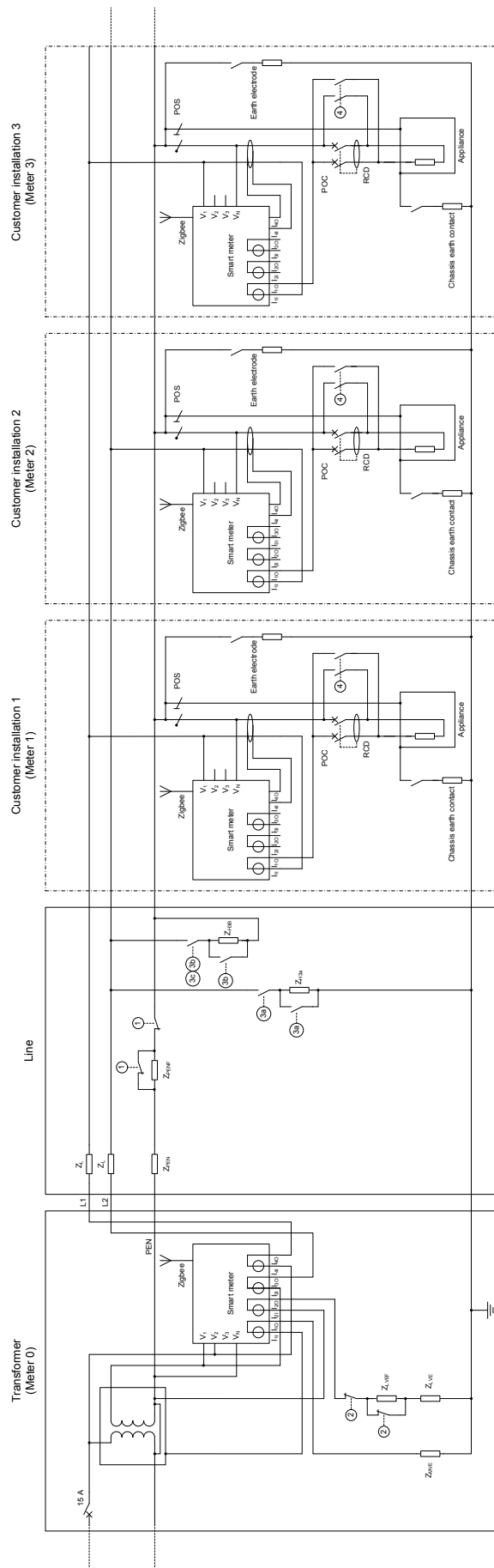


Figure 83: LV lab model schematic – dual phase system



Figure 84: Lab experimental setup with a 1:1 dual or single-phase isolation transformer supplying three customers

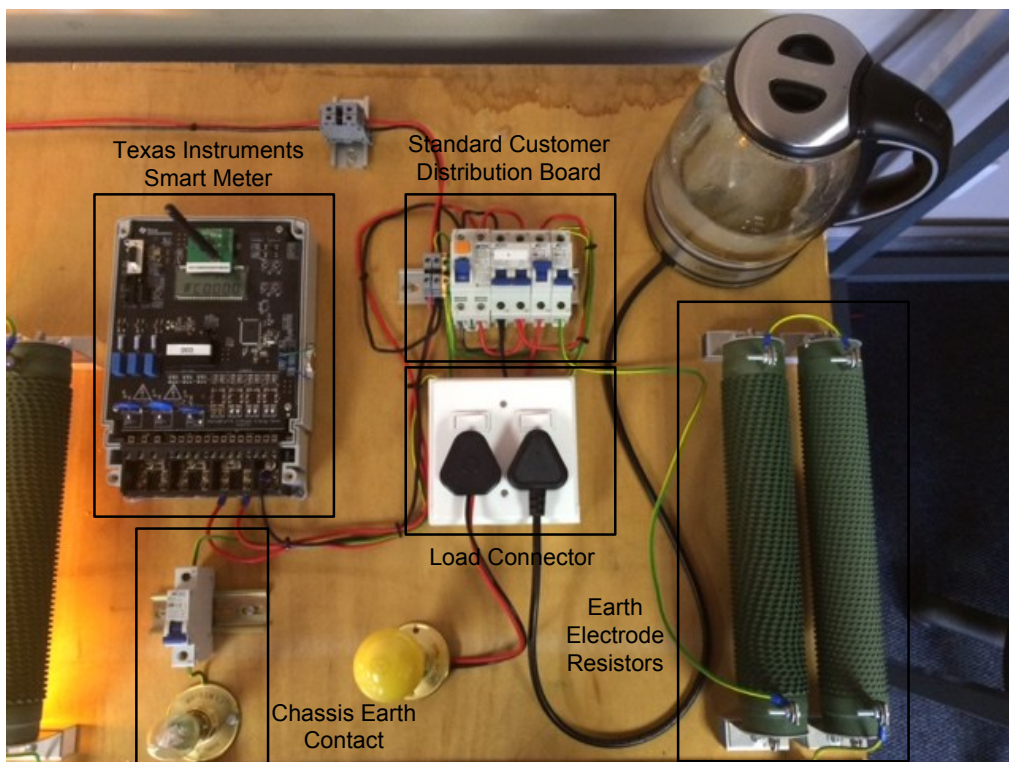


Figure 85: Lab experimental setup showing single customer installation

### 8.3. PEN CONDUCTOR FAILURE

Two solutions were proposed to detect and mitigate the hazard associated with a broken PEN conductor. The first is to use a prepaid meter to isolate the customer during an over or under voltage condition. The second is to make use of the smart meters discussed in this report to send voltage measurements to the experimental data concentrator to detect a possible break in the PEN conductor.

#### 8.3.1. Prepaid meter: alternative solution

The first solution makes use of prepaid meters to detect a possible break in the PEN conductor. A PEN conductor failure will result in an undervoltage on single-phase systems and an over or undervoltage on dual phase systems.

The proposed meter action as discussed in Section 2.6.1.3 is represented by a voltage comparator relay and a dual-pole contactor to open the live and neutral conductors during an over or undervoltage condition.

A combined over and undervoltage monitoring relay (Rhomberg A-Line AP 224) is used to simulate the voltage measurement function of the prepaid meter. This unit is specifically chosen as it is capable of measuring voltages up to 525 V. A dual phase unbalance condition can result in an overvoltage of up to the line-to-line voltage of 460 V. Other key features incorporated in the device is a start-up, trip and a 3-minute recovery delay. A recovery delay is key as to avoid the contactor jittering.

A four-pole contactor (ABB AF09(Z)) is used to break the live and neutral if an under or overvoltage is detected by the voltage monitoring relay. The contactor makes use of an electronic coil allowing low operating voltages, which are required during an undervoltage condition. The relay is capable of operating from 24 – 500 V.

Two experiments were performed to validate the proposed solution for both a single and dual phase system. The circuit used and results obtained for both solutions are discussed below:

##### 8.3.1.1. *Experiment 1: single phase system*

Figure 86 shows the experimental setup for a single-phase feeder with one customer connection. A kettle with a 27  $\Omega$  load impedance and a metallic chassis was used as the appliance.

The experimental results of a PEN conductor failure and subsequent protection are shown in Figure 87. During stage 1, the PEN conductor is intact and the load is switched on. No touch voltage  $V_H$  is observed. At stage 2 the PEN conductor becomes an open circuit,  $V_A$  falls away and a hazardous touch voltage  $V_H = 230$  V is observed. During stage 3 the protection relay opens the meter contactor and the hazardous touch voltage is cleared. This shows that by

disconnecting both the live and PEN conductors inside the meter a customer installation can be made safe during a PEN conductor failure.

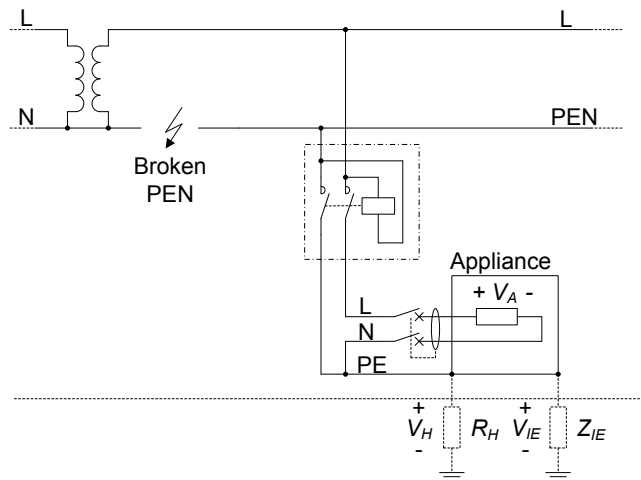


Figure 86: Diagram of the single-phase experimental setup

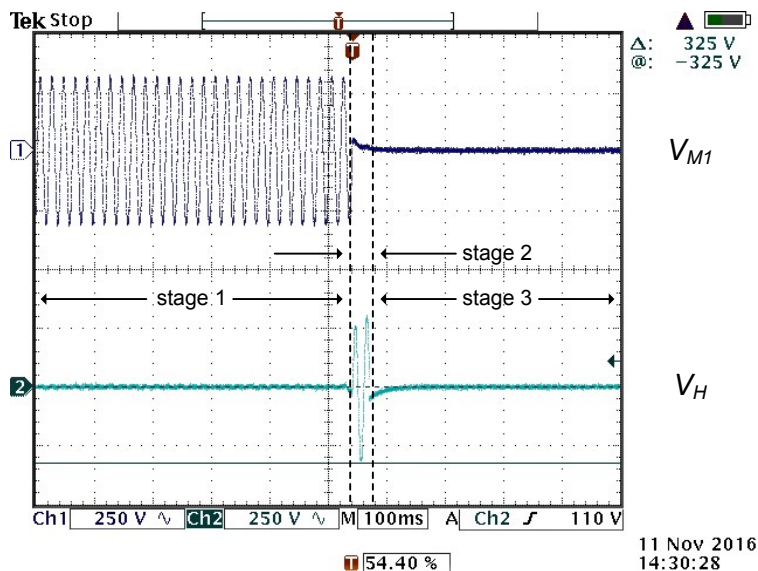


Figure 87: Single phase system experimental results ( $V_{M1}$  top and  $V_H$  bottom)

### 8.3.1.2. Experiment 2: dual phase systems

Figure 88 shows the experimental setup of a dual-phase feeder with a single customer connection at each phase. When the PEN conductor becomes an open circuit, a phase-to-neutral voltage unbalance may occur that could lead to a voltage as high as the dual-phase line-to-line voltage of 460 V or as low as 0 V. The appliance load  $Z_{A1}$  is 27  $\Omega$  and  $Z_{A2}$  is 44  $\Omega$ . The experimental results are shown in Figure 89. Initially, during stage 1, the PEN conductor is intact and both appliance 1 voltage ( $V_{A1}$ ) and appliance 2 voltage ( $V_{A2}$ ) is nominal. In stage 2, the PEN conductor becomes an open circuit,  $V_{A1}$  experiences an undervoltage of 174 V and  $V_{A2}$  an overvoltage of 286 V. At stage 3, the meter contactors are opened and both customer

installations are made safe. The reaction time (stage 2) was extended in the test to better show the unbalance.

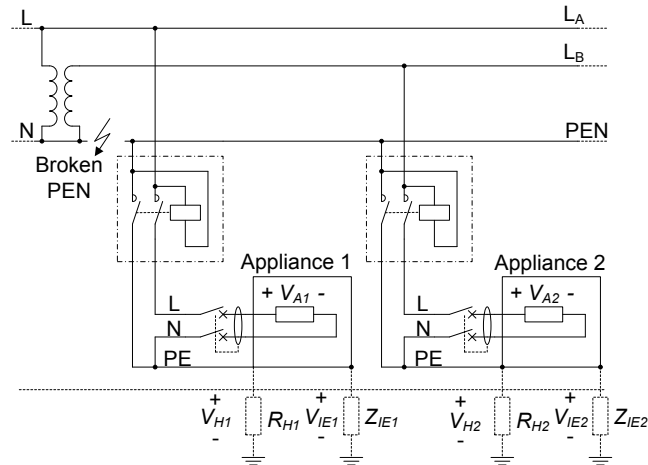


Figure 88: Diagram of the dual-phase experimental setup

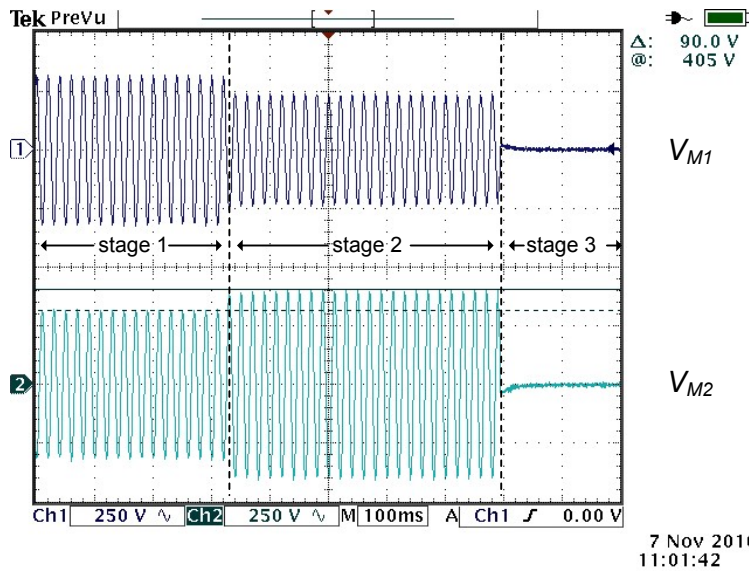


Figure 89: Dual phase system experimental results ( $V_{M1}$  top and  $V_{M2}$  bottom)

### 8.3.2. Smart meter proposed solution

As discussed in section 2.6.1 a customer installation on a single-phase system will experience an undervoltage and a customer on a dual-phase system will experience either an over or undervoltage depending on the load balancing of the phases of the transformer. The experiments discussed in section 8.3.1 is repeated with similar circuits with the contactors and voltage monitoring relays removed.

### **8.3.2.1. Experiment 1: single phase system**

A similar experimental setup is used as shown in Figure 86. An incidental earth impedance ( $Z_{IE}$ ) of 1 k $\Omega$  is used. A 1200 W load is connected resembling the appliance which has an impedance ( $Z_A$ ) of 44  $\Omega$ .

The experimental results obtained are shown in Figure 90. Initially, during stage 1, the PEN conductor is intact and the appliance voltage is nominal. During stage 2 the PEN conductor is broken. The appliance experiences an undervoltage as indicated by meter 3 voltage in Figure 90. The only return path present is via earth back to the transformer. The current returned via earth through the LV earth electrode at the transformer is measured. As expected the earth return current increases during stage 2. The LV earth electrode current is shown in milliampere. The appliance voltage measured on the chassis of the appliance during stage 2 was 202 V. During stage 3 the broken PEN conductor is restored with the voltage and earth return current returning to nominal.

A PEN conductor failure on a single-phase system can, therefore, be detected by measuring primarily the voltage at various customers. If multiple meters on a single LV feeder measures an undervoltage, a possible break in the PEN conductor can be concluded. As a secondary measure, the earth return current through the transformer's LV earth electrode can be monitored. A sudden increase in the earth return current can indicate a possible PEN conductor failure. This is however not a definitive indication of a sudden increase in load current or a new installation with a low impedance earth return path can also cause a sudden increase in the earth return current.

By continually monitoring both the voltage at the customers and the voltage at the transformer a distinction can be made between transformer overloading and a possible PEN conductor failure.

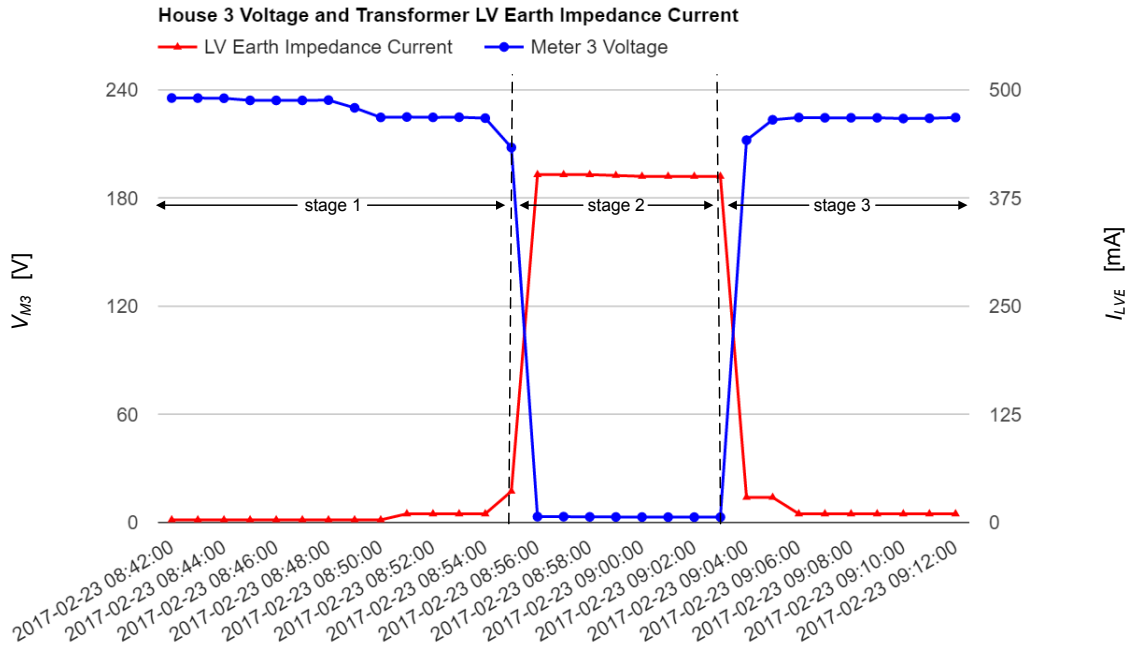


Figure 90: Single-phase system experimental results

### 8.3.2.2. Experiment 2: dual phase system

A similar setup was used as shown in Figure 88. The appliance loads  $Z_{A1}$  of  $27 \Omega$  and  $Z_{A2}$  of  $44 \Omega$  is similar as in the previous dual phase experiment. The graph in Figure 91 shows the measurements received from the two meters at the customer installation which are supplied from different phases. During stage 1 the PEN conductor is intact and the voltages on both phases are close to nominal with the appliances switched on. A difference in voltage is seen between the phase which can be explained due to the different loading on each phase. During stage 2 the PEN conductor is broken and the full line-to-line voltage of 460 V is present across both appliances. The line-to-line voltage is divided across the two appliances with meter 3 measuring an overvoltage of 290 V and meter 1 an undervoltage of 160 V. The remaining 10 V is lost due to a  $1 \Omega$  line impedance. During stage 3 the broken PEN conductor is restored with the voltages on both phases returning to nominal.

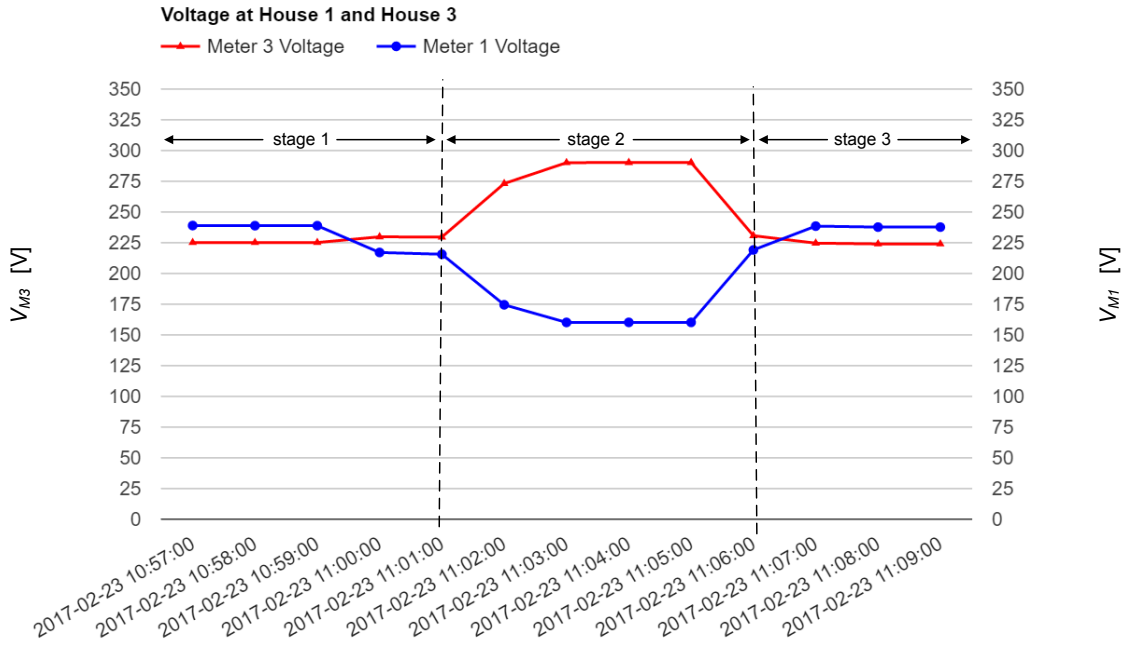


Figure 91: Dual phase system experimental results

#### 8.4. LV EARTH ELECTRODE CONDUCTOR HIGH IMPEDANCE FAILURE

As discussed in section 2.6.2 a LV earth electrode conductor high impedance failure can be detected by continually measuring the secondary current and the LV earth electrode current of the MV/LV transformer. This section shows practical measurements taken on the experimental setup discussed in section 8.2.

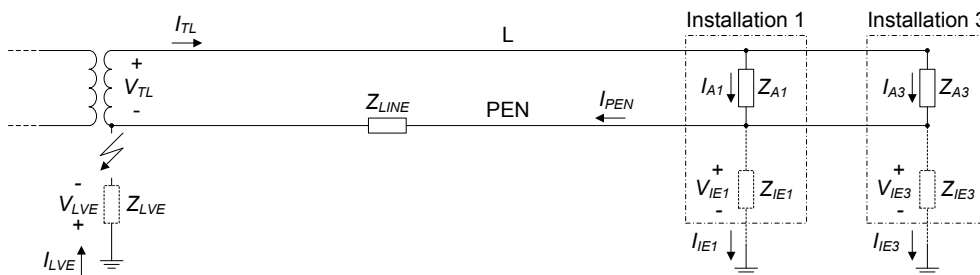


Figure 92: Experimental setup used for LV earth electrode high impedance failure

Figure 92 shows the experimental setup used to simulate a transformer LV earth electrode failure. Two loads were located at installation 1 and 3 respectively. The load at installation 1, represented by  $Z_{A1}$ , is a resistive load consisting of 12x 100 W globes connected in series with a combined impedance of 44  $\Omega$ . The load connected at installation 3, represented by  $Z_{A3}$ , is an electrical heater with a maximum power consumption of 2 kW. The heater consists a low and high setting with the current consumption is halved on the low setting. No loads were connected at installation 2. Incidental earths of 1 k $\Omega$  were added as shown is the figure. The

impedance of an LV feeder was represented by a  $1 \Omega$  impedance represented by  $Z_{LINE}$ . A  $70 \Omega$  earth electrode was used which is represented by  $Z_{LVE}$ .

The live current at the transformer  $I_{TL}$  was measured in conjunction with the current returning to the transformer via the transformers earth electrode  $I_{LVE}$ . Figure 93 shows a graph of the measurement results obtained. The current is split between the  $1 \Omega$  PEN conductor resistor and the parallel combination of the incidental earths. The expected return current can therefore be calculated as in equation 8.4.1:

$$I_{LVE} = \frac{Z_{LINE}}{Z_{IE1} || Z_{IE2}} I_{TL} = \frac{1}{500} I_{TL} \quad (8.4.1)$$

During stage 1 the circuit is under normal conditions with the loads varied to draw between 8 A and 13 A by switching loads on and off. The earth return current directly follows the live current with a ratio of 500 as expected for this setup. The earth return current is shown in milliampere in Figure 93. During stage 2 the earth return path becomes an open circuit at the location shown in Figure 93. The measured earth return current drops to zero, while the live current remains constant. During stage 3 the circuit is restored to normal conditions.

Figure 94 shows the ratio between the live and earth return current. A significant increase in the ratio is seen during stage 2 with the return path becoming an open circuit. The 0 A earth return current measured is changed in software to  $1 \mu\text{A}$  to avoid division by zero when calculating the ratio.

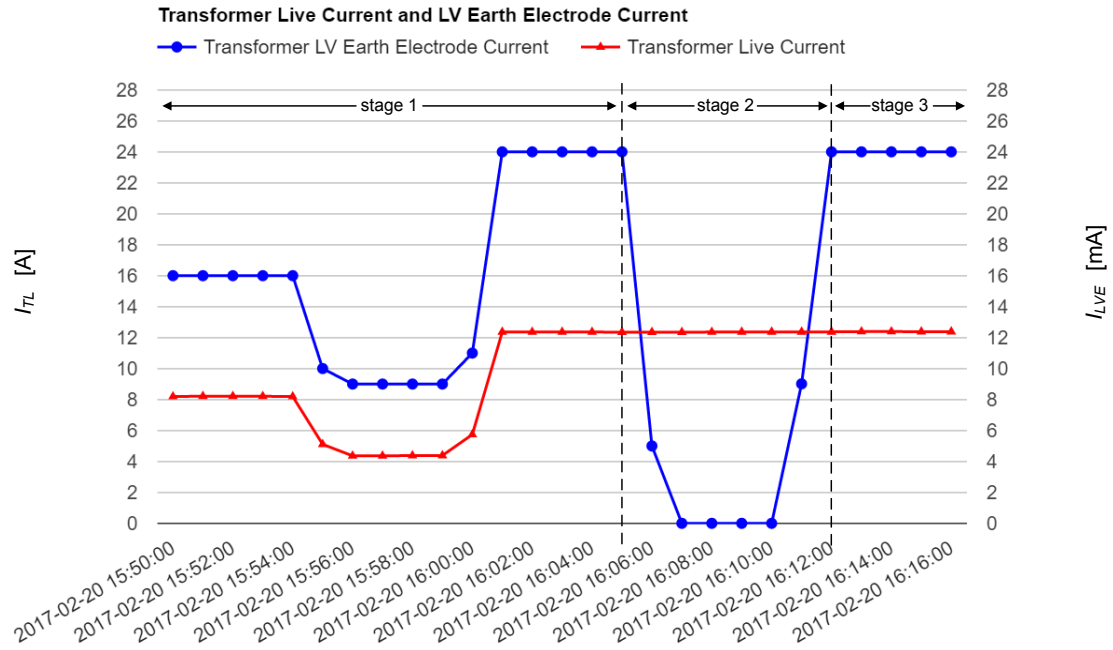


Figure 93: Transformer secondary live current and transformer LV earth electrode current

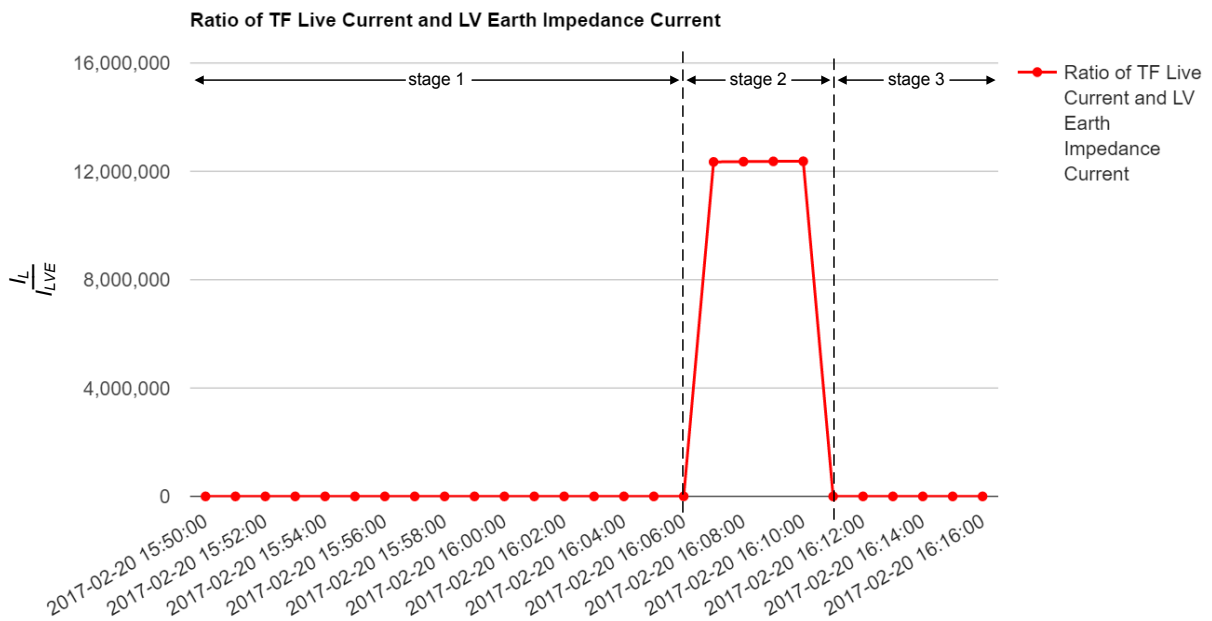


Figure 94: Ratio between transformer live current and transformer LV earth electrode current

## 8.5. UNACCOUNTED CURRENT FLOW

The experimental results for hazards grouped under unaccounted current flow are discussed together as they all involve the same detection method. All these hazards are detected by applying current balancing between the live current measured at the transformer and the sum of the currents measured at the customers as it will not be possible to distinguish between these hazards.

Figure 95 shows the experimental setup used to simulate the unaccounted current flow condition. Two houses were used with loads attached represented by  $Z_{A1}$  and  $Z_{A2}$  respectively. A 1 k $\Omega$  hazard impedance is located as shown in the figure. The impedance can represent a human touching the live and PEN conductor or a live and PEN conductor short circuited with a high impedance. The resultant current flow through the hazard is detected by performing current balancing between the cumulative current drawn by the houses and the transformer live current.

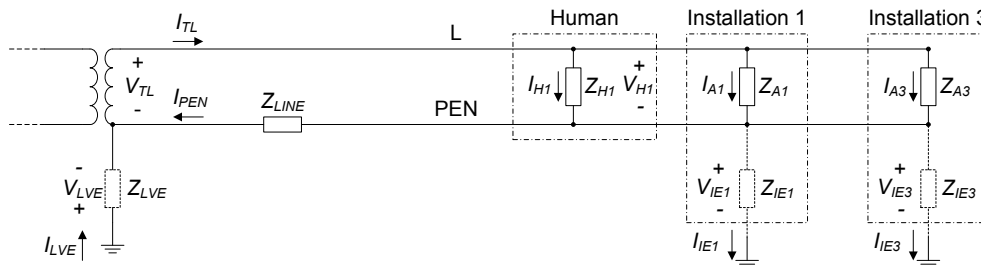


Figure 95: Experimental Setup used for phase conductor and PEN conductor exposed and reachable

Figure 96 shows the results captured on the experimental setup. Figure 97 shows the total current unbalance percentage in the system. During stage 1 no hazard is present and the total current unbalance is 0 A. A small current unbalance percentage of below 0.5% can be seen in Figure 97. This can be explained due to small measurement differences between the smart meters.

During stage 2 the 1 k $\Omega$  hazard resistor is inserted into the circuit. An unbalance current of 0.252 A is measured as expected, resulting in a 5.45% unbalance in the system with a total load current of 4.4 A. The unbalance current value in conjunction with the unbalance percentage is used to detect a possible hazard on the feeder. The percentage unbalance will greatly reduce as the load on the transformer is increased. For example, a transformer with a load current of 70 A and an unbalance current of 0.252 A will result in an unbalance percentage of 0.36%. This causes an increased difficulty to detect the unbalance by monitoring only the unbalance percentage. The total unbalance current will, therefore, have to be the primary value in the detection of this hazard. During stage 3 the hazard is removed and the system returns to its normal state with zero unbalance.

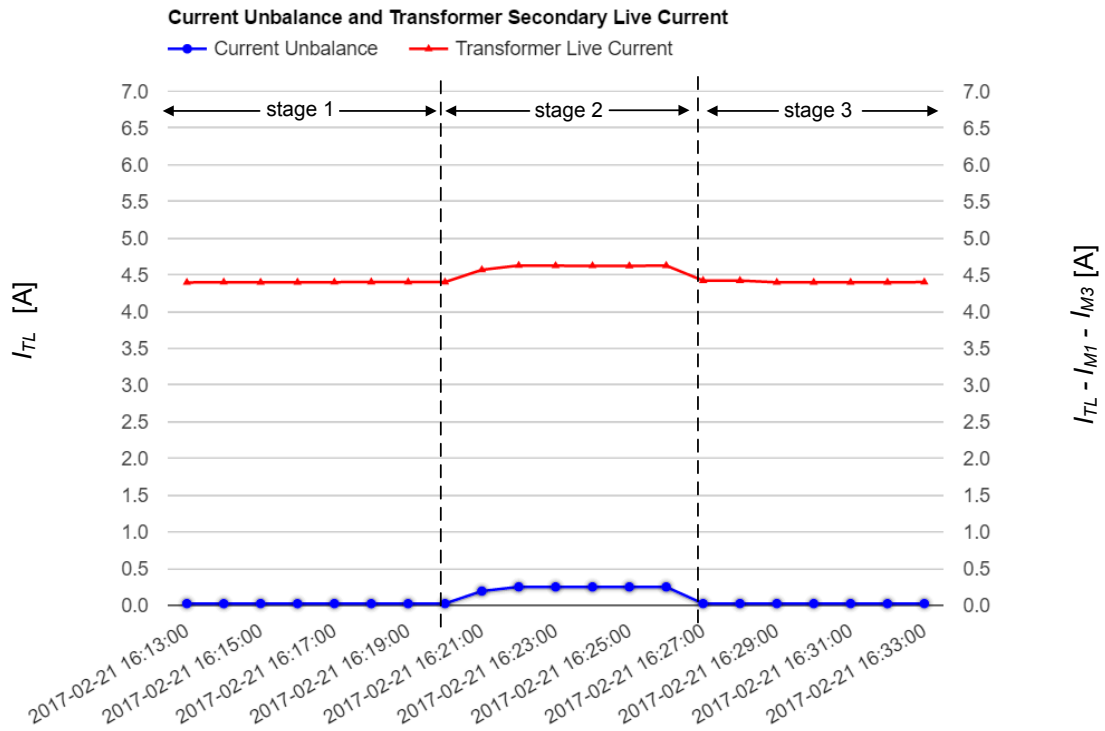


Figure 96: Transformer live current and current unbalance

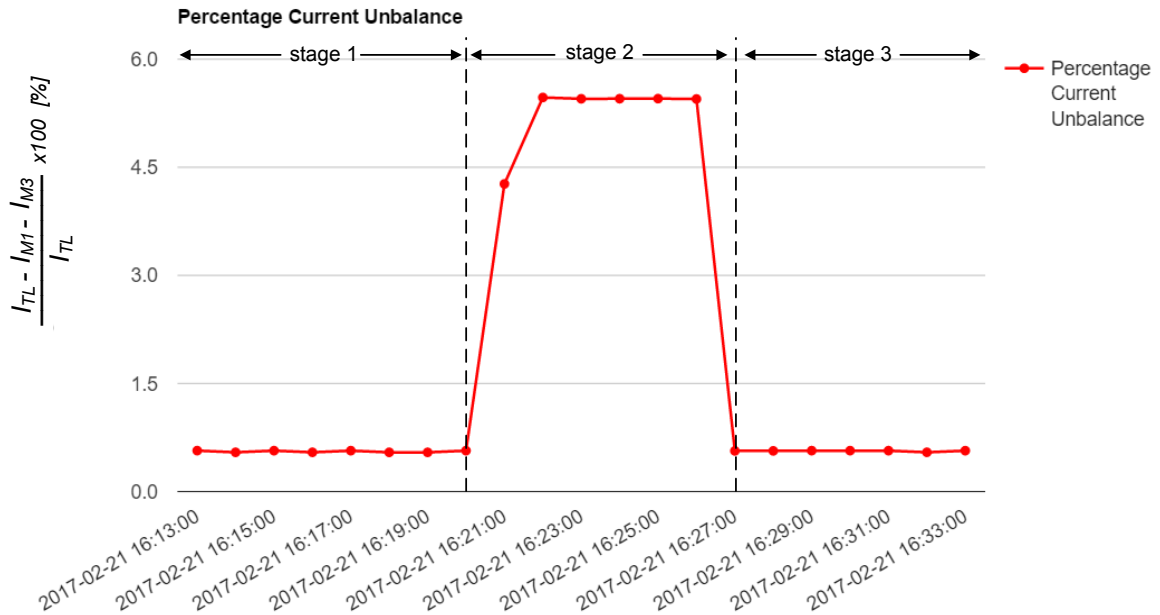


Figure 97: Percentage current unbalance

## 8.6. EARTH LEAKAGE PROTECTION NOT OPERATIONAL

The earth leakage protection not operational can possibly be detected by a meter not reporting data at a regular 1-minute interval. This is detected by continually monitoring the data inserted into the meter specific database tables. The meter watchdog Python script monitors the time elapsed as discussed in section 7.6.6.

The LV safety website displays the time elapsed since data was last received from a specific meter. If the meter is bypassed completely the loss in communications for a certain time could be used as an indicator. Other factors such as a power outage in the area will also result in the loss of communications.

It is suggested that an automated monitoring system be implemented in the data concentrator to detect if data is not received from a specific meter in a certain time period. This is currently done by manually monitoring the time elapsed since last meter communications data on the LV Safety website. An automated indication should be sent via the DNP3 protocol over a GPRS network to a remote station to notify of such an event.

## 8.7. CONCLUSION

This chapter presented the practical results obtained using the lab experimental model as discussed in section 8.2. It is shown that a PEN conductor failure can be detected by measuring an undervoltage at a customer on a single-phase feeder or an over or undervoltage at a customer on a dual-phase feeder. Chapter 9 will however introduce an additional detection method by continually measuring the line loop impedance to detect a deteriorating PEN conductor.

It is also shown that a broken LV earth electrode can be detected by measuring a drop in the earth return current to the transformer. On a real feeder the trend in the earth return current should be monitored, over time, to establish an expected earth return current. The ratio between the transformer phase and earth currents should also be monitored to distinguish between false positives as in sudden increase in phase current would lead to an increase in transformer earth current.

A simple result is shown that the data concentrator is able to detect unaccounted current flow. On a real feeder it would however be difficult to detect small differences between transformer current and that measured by all the meters.

The chapter concludes with a result obtained for the earth leakage protection hazard not operational. It is shown that a loss of supply to a meter could be a possible indication of an earth leakage not operational.

## **CHAPTER 9**

# **PERMANENT LOOP IMPEDANCE ASSESSMENT AND EXPERIMENTAL RESULTS**

### **9.1. INTRODUCTION**

Knowledge of loop impedance at particular locations in low voltage electrical systems can provide information on the adequacy of protection settings, deteriorating infrastructure, damaged infrastructure, etc. Loop impedance measurements are normally taken after an installation is constructed and handed over to the operator. Modern technology in the form of smart meters provides the opportunity to know loop impedance at the meter location at all times. By knowing the loop impedance to the transformer, it will be possible to detect a possible deteriorating live or PEN conductor. This method will have the advantage of detecting a possible failing PEN conductor before it completely fails as in most cases the PEN conductor becomes high impedance over time and does not necessarily instantly fail. For more information on the effects of a high impedance PEN conductor see Section 2.5.1.

This application of smart meters to measure loop impedance has not been proposed in literature. Smart meters have only been used for fault location detection as in [64] and [65], but have never been used to detect high loop impedance.

The feasibility of using the smart meters for loop impedance assessment is investigated below by considering two options. The first method requires all meter current and voltage measurements on a feeder while the second method only considers changes in current and voltage at each meter.

### **9.2. LOOP IMPEDANCE CALCULATION USING COMPLETE FEEDER CURRENT AND VOLTAGE MEASUREMENTS**

The complete measurement technique requires that all branch currents and node voltages are known to calculate loop impedance at each node as shown in Figure 98.

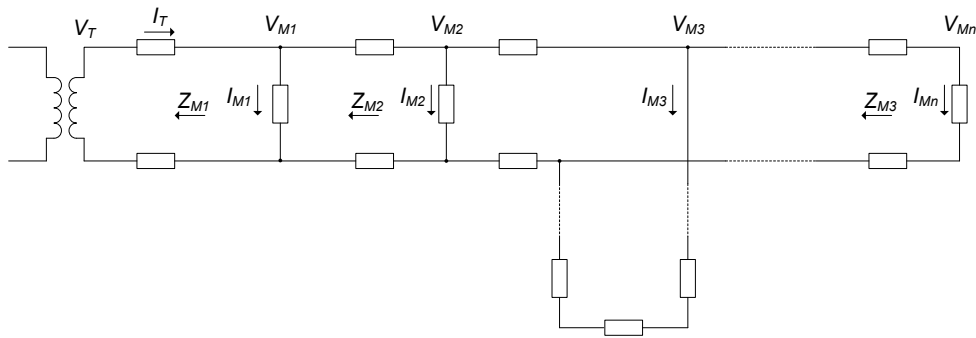


Figure 98: Line diagram illustrating the complete measurement technique

The loop impedance at the location of the first meter can be calculated as follows:

$$Z_{M1} = \frac{V_T - V_{M1}}{I_T} \quad (9.2.1)$$

The loop impedance seen by the other downstream meters can be calculated using the following generalized equation:

$$Z_{M1} = \frac{V_{n-1} - V_n}{I_T - \sum_{i=1}^{n-1} I_i} \quad (9.2.2)$$

From this equation, it is important to realize that all shunt currents upstream should be known at the time of the calculation. The voltage at the previous node is also required. For synchronous assessment of all nodal voltages and branch currents, GPS time synchronization and reliable communication is required. A single measurement failure would cause inaccurate results. In practice this technique, therefore, would be difficult to implement.

### 9.3. LOOP IMPEDANCE CALCULATION USING CURRENT AND VOLTAGE CHANGES AT METERS

The second method considered is to assess the effect that current changes have on voltage changes measured by the meters. Commercial devices that measure loop impedance work on the principle of applying a known load to the system and measure voltage changes. Instead of applying a load to the system to cause current steps, it was decided to rather use measured current steps caused by load changes and measure the effect they have on the voltage at the same time instant. That means the built in smart meter sensors can be used to calculate the loop impedance at the meter and communicate that value to the data concentrator.

The smart meter calculates 1 second averages of r.m.s. currents and voltages that is processed by the foreground loop in the MCU. The strategy followed is to compare each 1 second sample of current with the previous value. When the value of the current sample in meter  $n$  is more than a set threshold higher than the previous value, the difference between these two values are calculated.

$$\Delta I_{Mn}(k) = I_{Mn}(k) - I_{Mn}(k - 1) \quad (9.3.1)$$

The corresponding difference in voltage samples is also calculated as follows:

$$\Delta V_{Mn}(k) = V_{Mn}(k - 1) - V_{Mn}(k) \quad (9.3.2)$$

The loop impedance can then be calculated as follows:

$$Z_{Mn}(k) = \frac{\Delta V_{Mn}(k)}{\Delta I_{Mn}(k)} \quad (9.3.3)$$

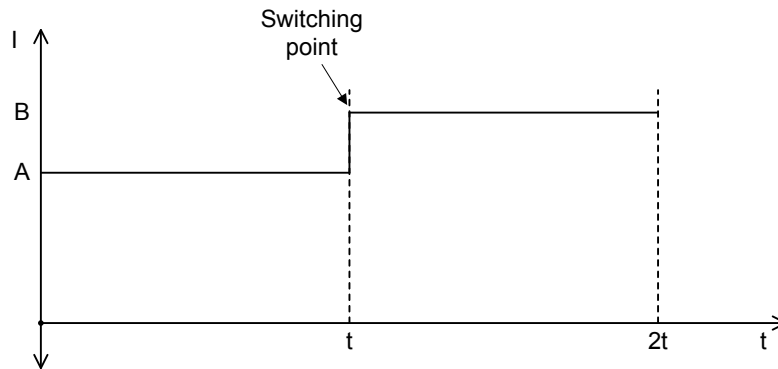


Figure 99: Graphical representation of delta current calculation

A graphic representation of the delta current measurement strategy can be seen in Figure 99. Each time instant  $t$  represents a 1 second average r.m.s. sample of the current measured by the meter. In this specific case the switching of a load falls exactly at the end of a 1 second sampling window. In this case the method yields the correct delta current calculated as follows:

$$\begin{aligned} \Delta I_{Mn}(k) &= I_{Mn}(k) - I_{Mn}(k - 1) \quad (9.3.4) \\ &= B - A \end{aligned}$$

The method however yields incorrect results if the switching event falls inside a 1 second sampling window. Figure 100 shows a graphical representation of this case.

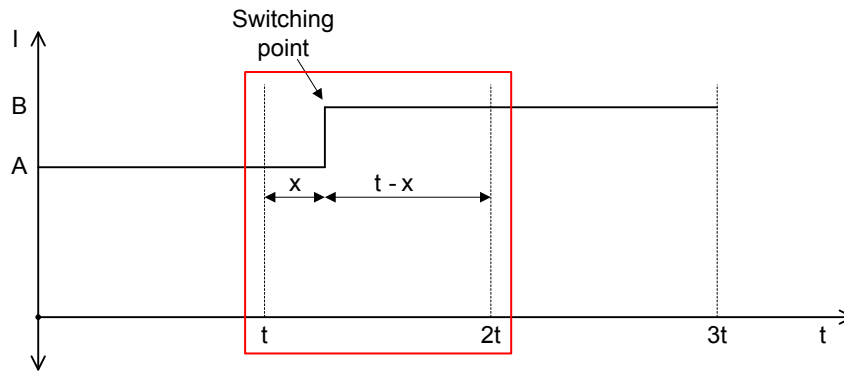


Figure 100: Graphical representation of delta current calculation ignoring the sample in which the switching event falls

To overcome this problem, it was decided to ignore the 1 second sample in which the switching event occurred as shown in red in Figure 100. The strategy involved keeping the previous three 1 second samples in the memory of the meter and should a positive current change be detected, to wait for another sample second before calculating the delta current. The delta current is then calculated as follows:

$$\begin{aligned}\Delta I_{Mn}(k) &= I_{Mn}(k) - I_{Mn}(k-2) \\ &= B - A\end{aligned}\quad (9.3.5)$$

The same voltage samples are used to calculate the voltage change. The delta voltage is calculated as follows:

$$\Delta V_{Mn}(k) = V_{Mn}(k-2) - V_{Mn}(k) \quad (9.3.6)$$

Lastly, the impedance is still calculated as follows:

$$Z_{Mn}(k) = \frac{\Delta V_{Mn}(k)}{\Delta I_{Mn}(k)} \quad (9.3.7)$$

### 9.3.1. Mathematical Proof

From Figure 101 it can be mathematically proven that the delta current can be calculated using equation 9.3.5. In Figure 101 a one second sample of the r.m.s. current is divided into ten samples. Ten samples are arbitrarily chosen and could have been any number as it is only used to proof the concept mathematically.

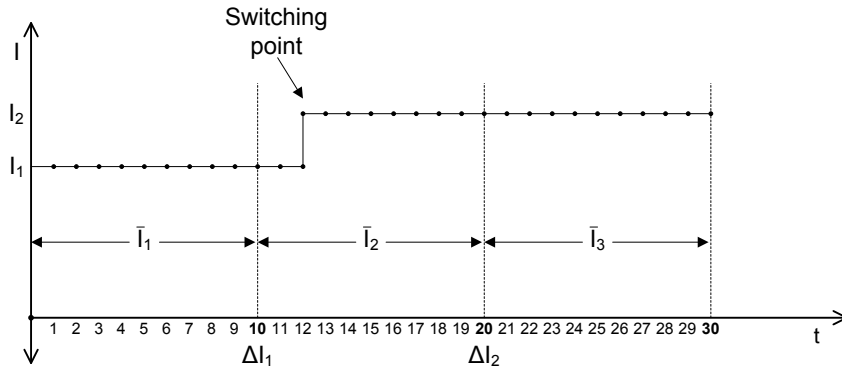


Figure 101: Mathematical representation

The average of each one second is represented by  $\bar{I}_n$  in equation 9.3.8 Each one second average is calculated by summing all the individual samples

$$\bar{I}_n = \frac{1}{10} \sum_{1}^{10} i(n) \quad (9.3.8)$$

where  $i(n)$  is the sampling value at each sampling instance.

The average of each of the three one second samples in Figure 101 is calculated as follows:

$$\begin{aligned} \bar{I}_1 &= \frac{1}{10} (10I_1) \\ &= I_1 \end{aligned} \quad (9.3.9)$$

$$\bar{I}_2 = \frac{1}{10} (2I_1 + 8I_2) \quad (9.3.10)$$

$$\begin{aligned} \bar{I}_3 &= \frac{1}{10} (10I_2) \\ &= I_2 \end{aligned} \quad (9.3.11)$$

To prove the delta current is not dependent on the one second average r.m.s. value in which the switching event occurred an expression for the initial and final ( $I_1$  and  $I_2$ ) r.m.s. currents are determined in terms of the individual delta currents,  $\Delta I_1$  and  $\Delta I_2$  as shown in Figure 101.

$$\begin{aligned} \Delta I_1 &= \bar{I}_2 - \bar{I}_1 \\ &= \frac{1}{10} (2I_1 + 8I_2) - I_1 \\ I_1 &= \frac{1}{10} (2I_1 + 8I_2) - \Delta I_1 \end{aligned} \quad (9.3.12)$$

$$\begin{aligned}\Delta I_2 &= \bar{I}_3 - \bar{I}_2 & (9.3.13) \\ &= I_2 - \frac{1}{10}(2I_1 + 8I_2) \\ I_2 &= \Delta I_2 - \frac{1}{10}(2I_1 + 8I_2)\end{aligned}$$

Finally, it is proven that by subtracting the initial and final r.m.s. currents ( $I_1$  and  $I_2$ ) the result is equal to the difference between individual delta currents,  $\Delta I_1$  and  $\Delta I_2$ .

$$\begin{aligned}\Delta I &= I_2 - I_1 & (9.3.14) \\ &= \Delta I_2 - \frac{1}{10}(2I_1 + 8I_2) - \Delta I_1 + \frac{1}{10}(2I_1 + 8I_2) \\ &= \Delta I_2 - \Delta I_1\end{aligned}$$

It proves that the difference in current is not dependant on the average value of the one second sample in which a switching event occurred.

#### 9.4. LOOP IMPEDANCE CALCULATION ERRORS AND SIMULATION RESULTS

The calculation of the loop impedance using changes in voltage and current introduces measurement errors. The first is caused by leakage current flowing through parallel loads at the same customer or on the same feeder.

Figure 102 shows a simplified circuit model. The LV side of the transformer is represented by voltage source  $V_{TL}$  and the impedance of the feeder by  $Z_{LINE}$ . Impedance  $Z_s$  represents a switched load at the customer which is used to calculate the impedance of the feeder and  $Z_L$  represents parallel loads either at the specific customer or at other customer installations on the same feeder.

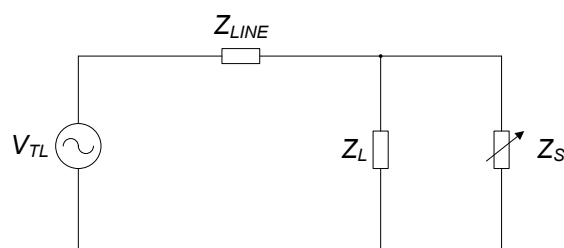


Figure 102: Simple circuit model to illustrate measurement error

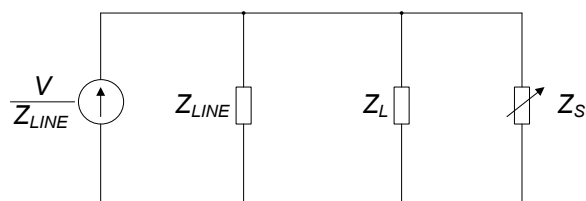


Figure 103: Norton equivalent circuit of simple circuit model in Figure 102

Figure 103 shows the Norton equivalent of the circuit in Figure 102. From Figure 103 it is evident that since  $Z_L$  is usually much larger than  $Z_{LINE}$  it will have a negligible effect on the current drawn, and can be ignored as shown in equation 9.4.2.

$$\begin{aligned} Z_{LINE} \parallel Z_L &= \frac{Z_{LINE} Z_L}{Z_{LINE} + Z_L} \\ &\approx \frac{Z_{LINE} Z_L}{Z_L} \\ &\approx Z_{LINE} \end{aligned} \quad (9.4.2)$$

The circuit now reduces to the circuit shown in Figure 104, with the assumption that  $Z_L$  is usually much larger than  $Z_{LINE}$ , thus ignoring the effect of parallel loads.

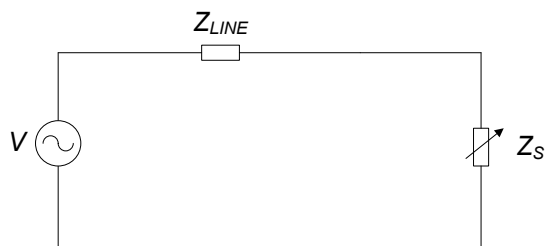


Figure 104: Reduces simplified circuit model with  $Z_L$  removed

A second error is introduced as only the absolute value of current and voltage is measured and used to calculate impedance, it is not possible to distinguish between reactance and resistance in the impedance calculation. Due to the resistive nature of most residential loads, they draw power close to unity power factor. Another important aspect of LV feeders is that they are more resistive than inductive. A typical conductor used for overhead LV lines is FOX conductor with resistance (R) of 0.86  $\Omega$ /km and reactance of 0.45  $\Omega$ /km in both the phase and neutral conductors. That equates to a X/R ratio of approximately 0.5. Figure 105 (a-c) shows the meter current and voltage phasors of a unity power factor load connected to a FOX line. Since the voltage phase shift, caused by the line reactance, is not measured, it is impossible to know what the line reactance is. Due to the low X/R ratio and the close to unity power factor, it can be assumed that the line voltage drop is purely resistive. By doing this a small error of typically a few percentage points is made as illustrated in (c). If the reactive component of the line impedance is increased, a larger error would be experienced as shown in (d), where the X/R ratio is greater than unity. This error is still small and might be acceptable for illustrative purposes.

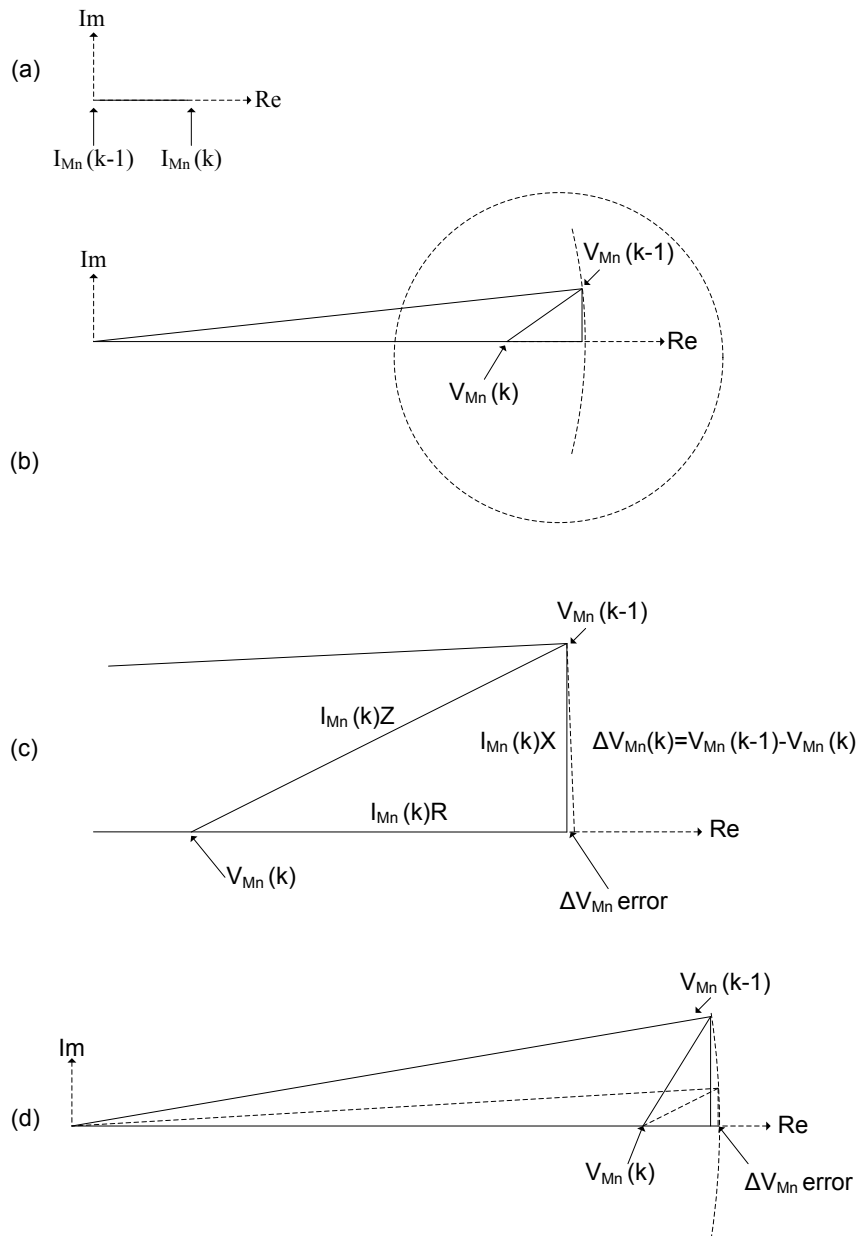


Figure 105: Phasor diagrams illustrating the simplified measurement technique

The technique is demonstrated using a simple model of an LV network in Digsilent Powerfactory as illustrated in Figure 106. The network consists of a 22 kV to 230 V dual phase transformer rated at 32 kVA. It feeds a dual phase feeder that uses Fox conductor with resistance (R) of 0.86  $\Omega/\text{km}$  and reactance (X) of 0.45  $\Omega/\text{km}$  in both the phase and neutral conductors. The network consists of two 200 m sections of Fox conductors, line 1 and line 2. After line 1, two houses are connected at pole top box 1 (PTB1) and after line 2, another two houses feed from PTB2. Meter 1 (M1) and meter 3 (M3) are connected to phase 1 and meters 2 and 4 are connected to phase 2. The loop impedance calculation is done at the fourth house using meter 4 (M4) measurements.

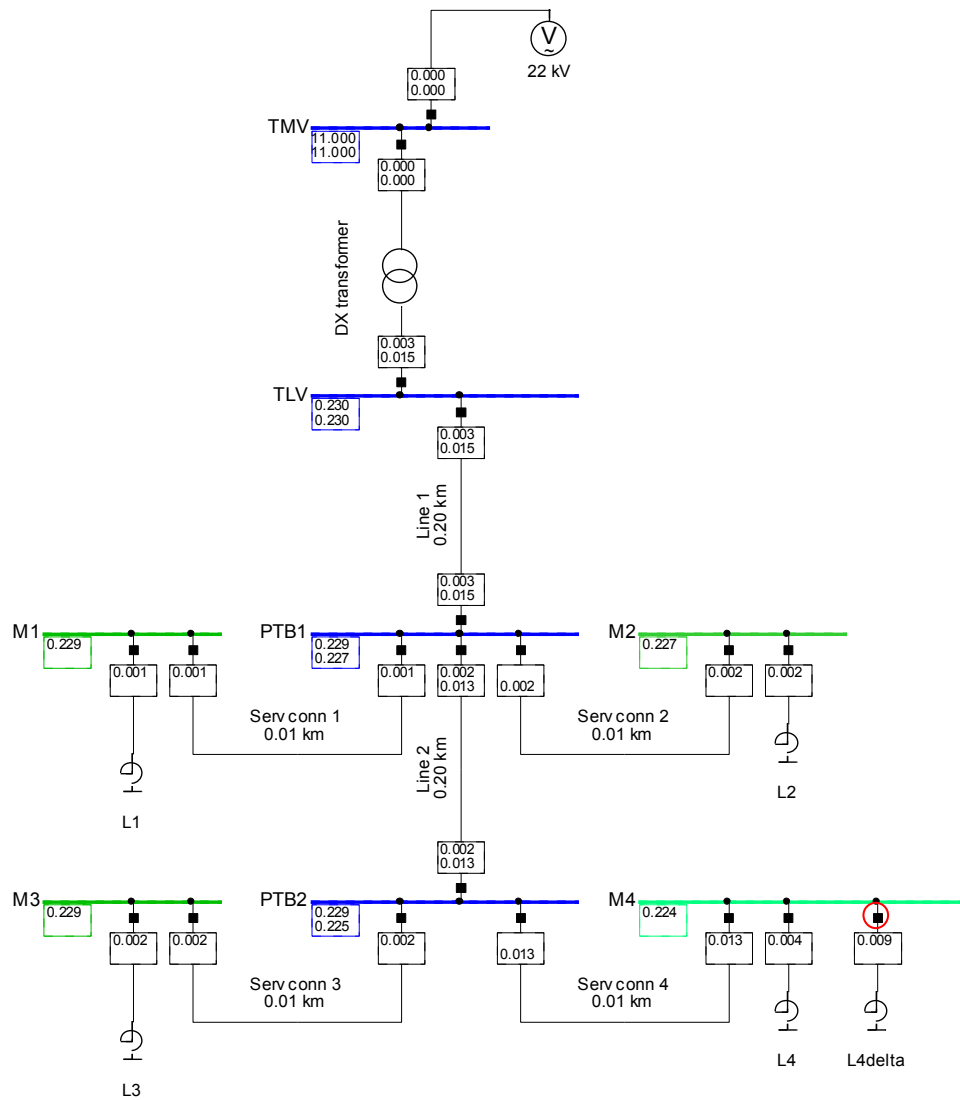


Figure 106: Power Factory single-line diagram to simulate the current and voltage change technique

The top graph in Figure 107 shows the measured r.m.s. current, delayed current and voltage. The bottom graph shows the  $\Delta V_{M4}(k)$ ,  $\Delta I_{M4}(k)$ , and  $Z_{M4}(k)$  waveforms when a load is switched. It shows that the algorithm calculated a loop impedance of 0.805  $\Omega$ . The loop impedance can manually be calculated by adding the impedances of line 1, line 2 and the service connection:

$$Z_{M4} = \sqrt{(0.86 * 0.2 * 4 + 0.58 * 0.01 * 2)^2 + (0.45 * 0.2 * 4)^2} \quad (9.4.1)$$

$$= 0.881 \Omega$$

This relates to an error of approximately 8%. A variety of loads were switched on at different houses to test the method's immunity against system loading. Each time the impedance calculated was in the order of 8%.

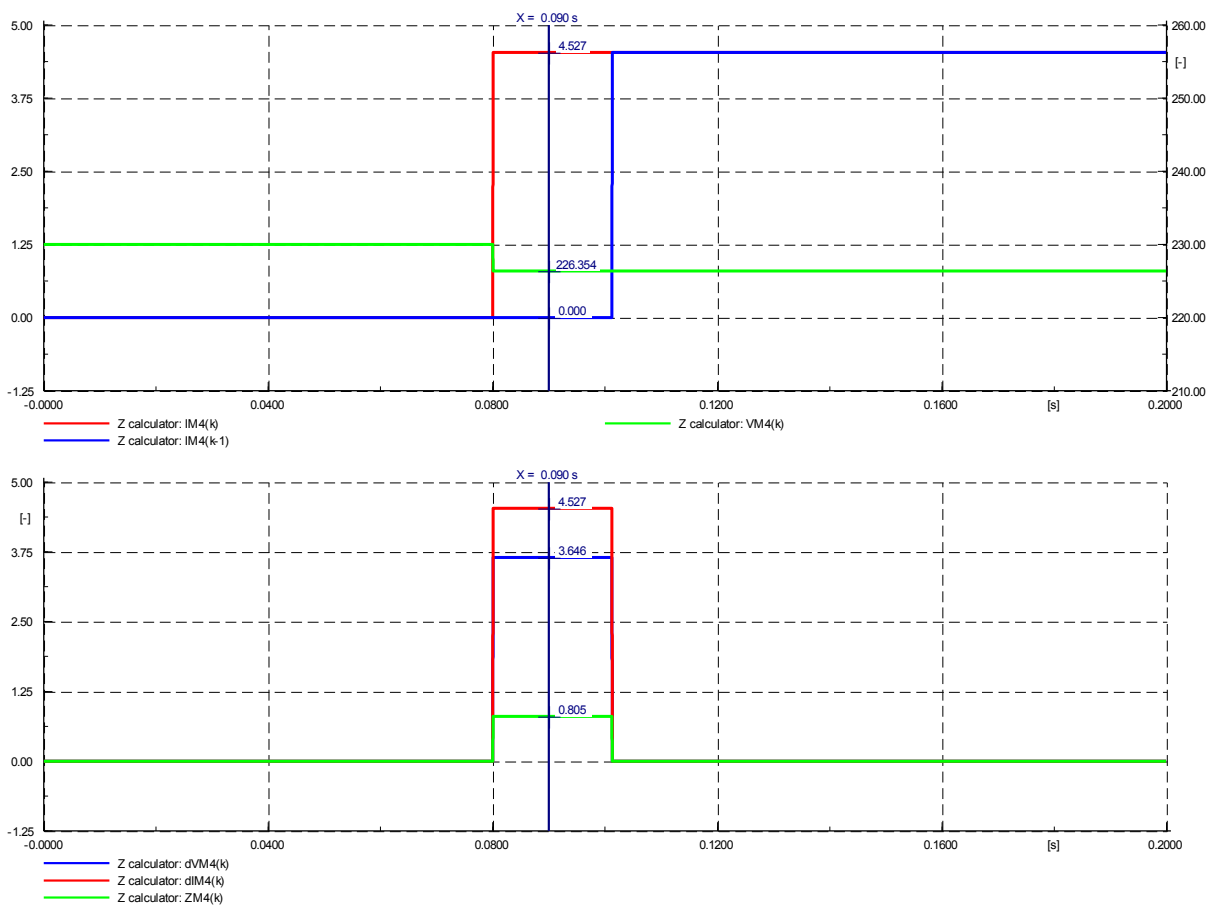


Figure 107: Power Factory outputs for calculating the impedance from current and voltage changes at meter 4

A high damaged line was simulated by increasing the impedance of line section 1. The results are shown in Figure 108. The impedance increased from  $0.8 \Omega$  to  $5.6 \Omega$ .

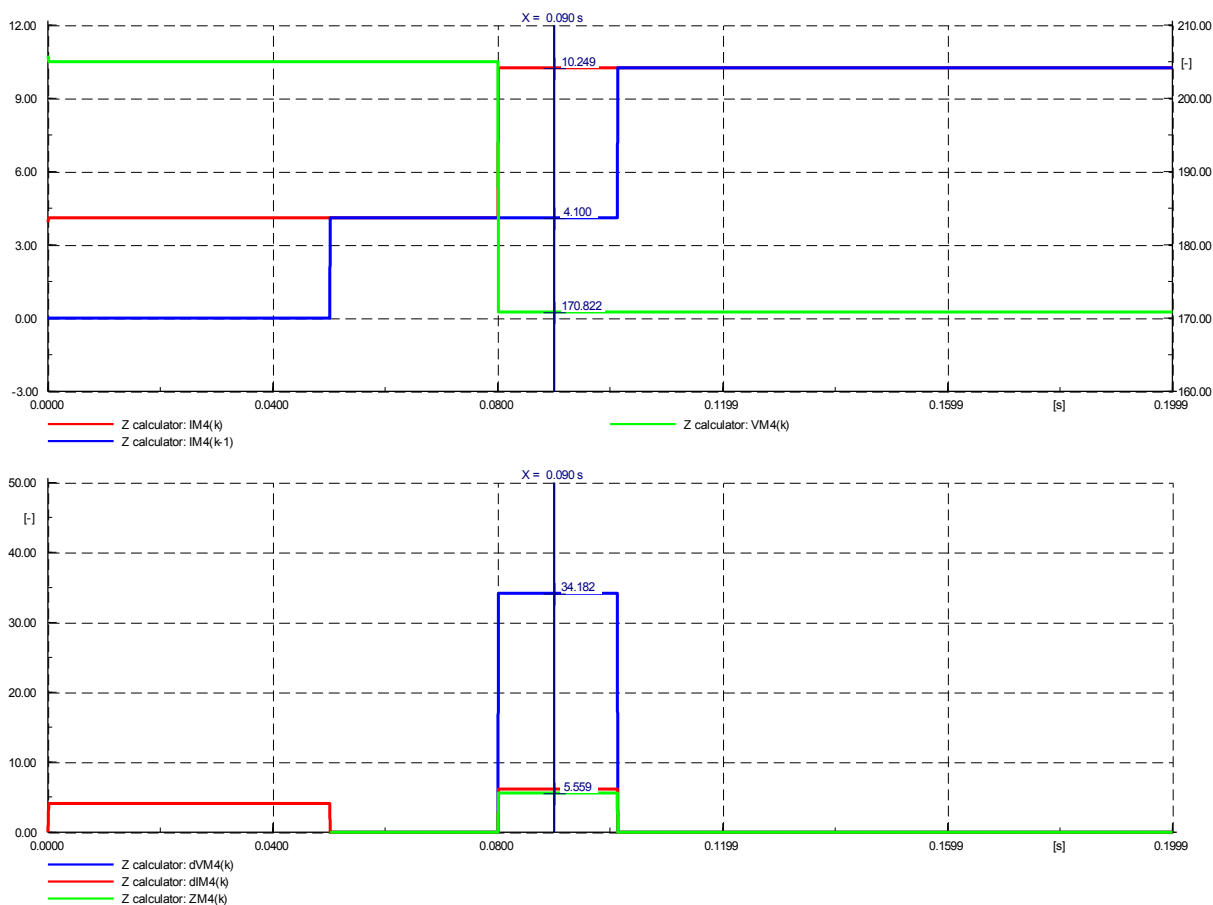


Figure 108: Power Factory outputs for calculating the loop impedance from current and voltage changes at meter 4 with damaged conductor

If, for some reason, a more accurate loop impedance calculation is required, the method can be extended by measuring phase as well.

### 9.5. LOOP IMPEDANCE SOFTWARE IMPLEMENTATION

A great advantage of the loop impedance calculation is that it can be solely implemented on a single meter and only an impedance value is sent to the data concentrator.

The impedance value is calculated in the main loop of the meter every second if a current change was detected as described in section 9.4. It was decided to react only on current changes greater than 0.2 A to avoid false readings. A buffer is used to hold the last three 1 second averaged current and voltage readings and is updated every second with the latest measurements.

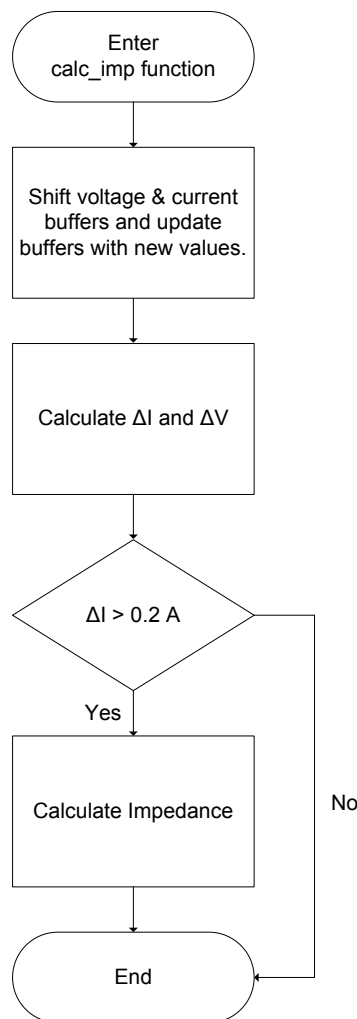


Figure 109: Loop impedance calculation flow diagram

## 9.6. PRACTICAL LOOP IMPEDANCE MEASUREMENTS

Figure 110 shows the experimental setup used to evaluate the impedance calculation strategy as described above. A  $1\ \Omega$  line impedance was added into the live conductor represented by  $Z_{L1}$ . A  $1\ \Omega$  line impedance was also placed into the PEN conductor represented by  $Z_{L2}$ , with a bypass switch,  $S_{L2}$ .  $Z_{L3}$  represents a variable line impedance ( $0\ \Omega - 28\ \Omega$ ) with a bypass switch,  $S_{L3}$ .

Two installations were used for the setup to evaluate the impact of multiple loads switching randomly. Both installations consisted of two loads, one constant load which remained switched on and a switched load which was switched on and off at random or at specific intervals.

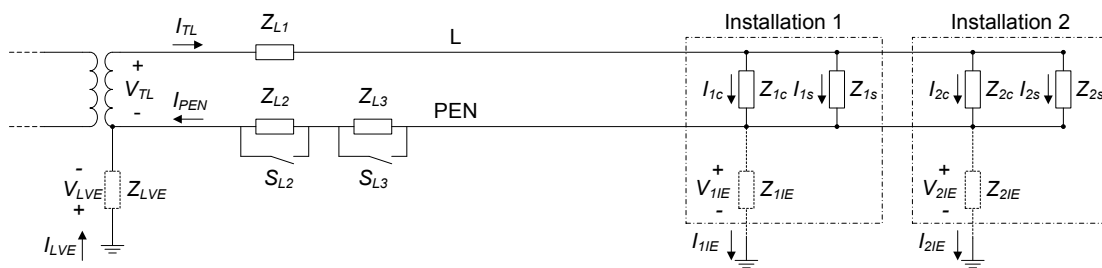


Figure 110: Experimental setup used to evaluate network impedance

The loads were switched using 24 VDC relays, capable of switching up to 10 A<sub>rms</sub>. The relays were in turn switched using smaller relays connected to I/O pins of a microcomputer. A Python script *load\_switch.py* was used to turn the loads on and off by changing the I/O pins to a logic high and low respectively.

### 9.6.1. Actual feeder loop impedance

The actual impedance of the feeder was determined to be able to verify the impedance measurements captured by the smart meters. Line impedances  $Z_{L2}$  and  $Z_{L3}$  were bypassed for this test with only line impedance  $Z_{L1}$  present in the loop. Figure 111 shows the voltage and current change that occurred when a load was switched at installation 2.

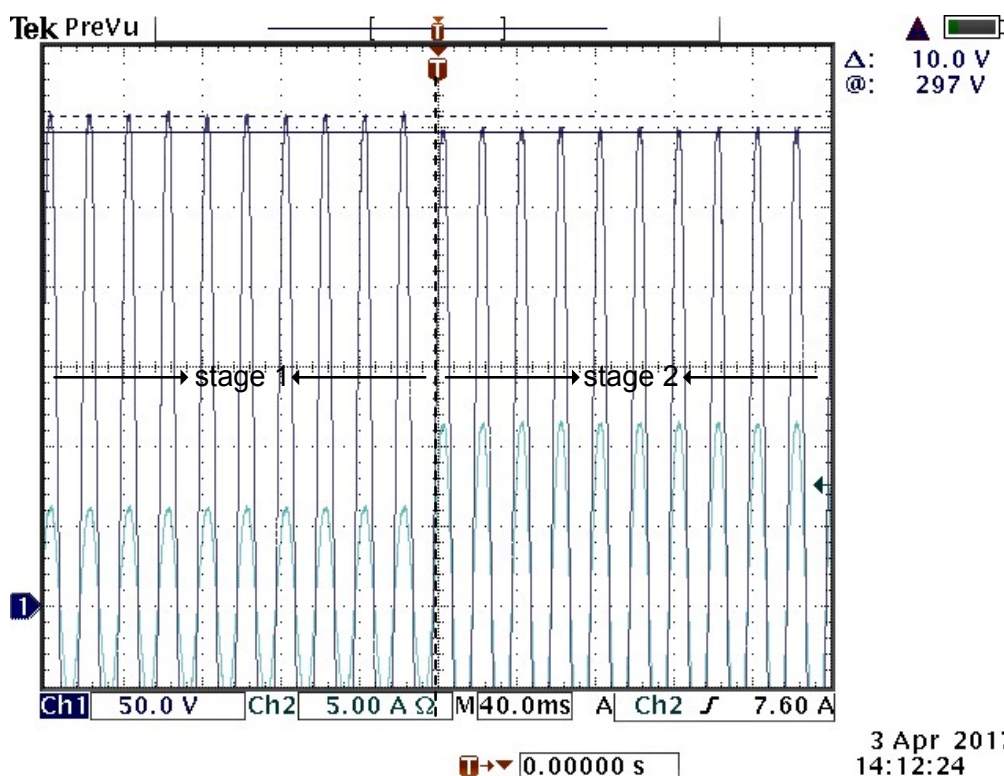


Figure 111: Voltage and current change used to calculate impedance of experimental feeder

A voltage change of 10 V<sub>p</sub> (7.07 V<sub>rms</sub>) with a current change of 7.48 A<sub>p</sub> (5.3 A<sub>rms</sub>) was measured on the oscilloscope. The impedance of the experimental network is then calculated as follows:

$$\begin{aligned} Z_{Feeder\ actual} &= \frac{\Delta V}{\Delta I} & (9.6.1) \\ &= \frac{7.07\ V}{5.3\ A} \\ &= 1.89\ \Omega \end{aligned}$$

The 1.89  $\Omega$  impedance value can be attributed to the 1  $\Omega$  line impedance ( $Z_{L1}$ ) and the impedance of the transformer.

## 9.7. FEEDER LOOP IMPEDANCE EXPERIMENTAL RESULTS

Practical results were obtained to evaluate the loop impedance as captured by the meters. Various loading scenarios were used. Firstly, a single load test was performed with only installation 2 present on the network. Installation 1 was then added to evaluate the effect on the line impedance measurement of an additional load switching. The data shown in the graphs were received by the data concentrator from the meters, and stored in a SQLite database table.

### 9.7.1. Experimental results - Single switching load

The following figures show the impedance results obtained for different variations of the switched load impedance ( $Z_{2s}$ ) and the constant load impedance ( $Z_{2c}$ ). The load at installation 1 was not switched in this case. Each impedance value does not necessarily represent a second passed as impedance values are only obtained when a switching event occurred. The load is switched at random between 3 to 5 second intervals.

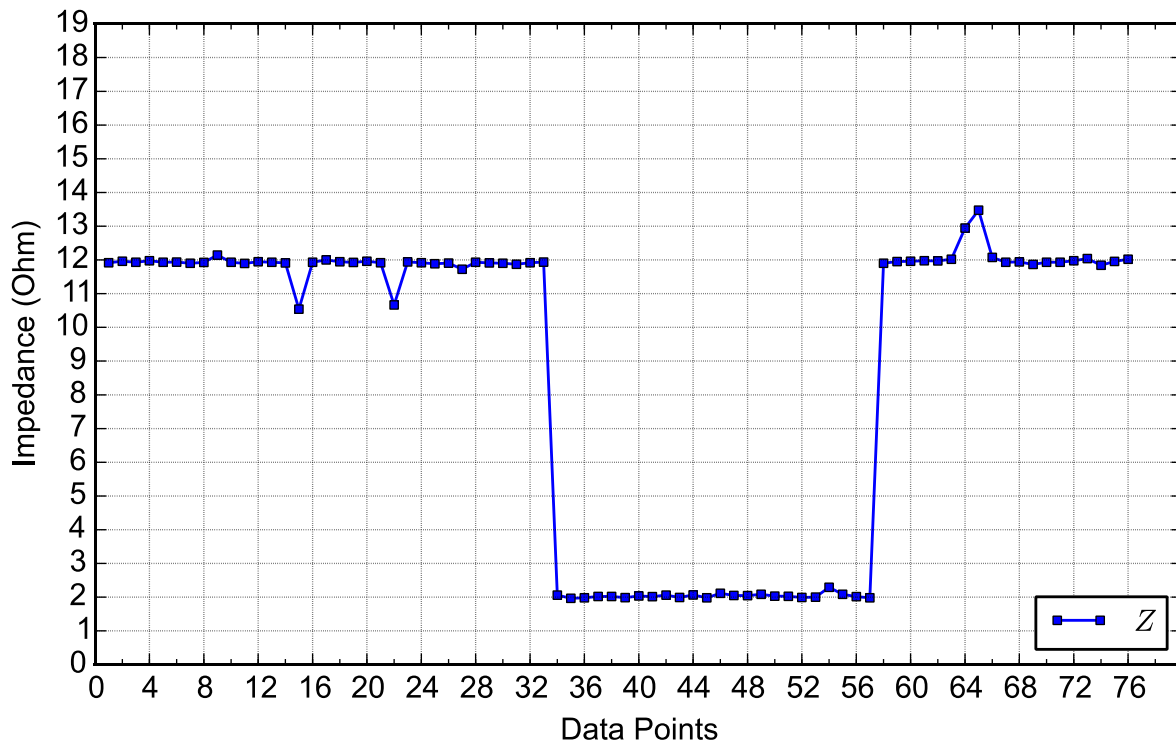


Figure 112: Line impedance of 10  $\Omega$  ( $Z_{L3}$ ) switched out and in of the feeder with a constant load of 0.43 A and a switching load of 4.78 A

Figure 112 shows the results obtained with a 10  $\Omega$  line impedance ( $Z_{L3}$ ) being switched out and in of the feeder. With the 10  $\Omega$  impedance in the line the total impedance measured is approximately 12  $\Omega$  which can be attributed to the 1  $\Omega$  line impedance ( $Z_{L1}$ ), the 10  $\Omega$  line impedance ( $Z_{L3}$ ) and the transformer impedance of approximately 1  $\Omega$ . With the 10  $\Omega$  impedance bypassed the feeder loop impedance falls back to close to 1.9  $\Omega$  as obtained in section 9.6.1. In this case a load drawing 4.78 A was switched with a constant load of 0.43 A.

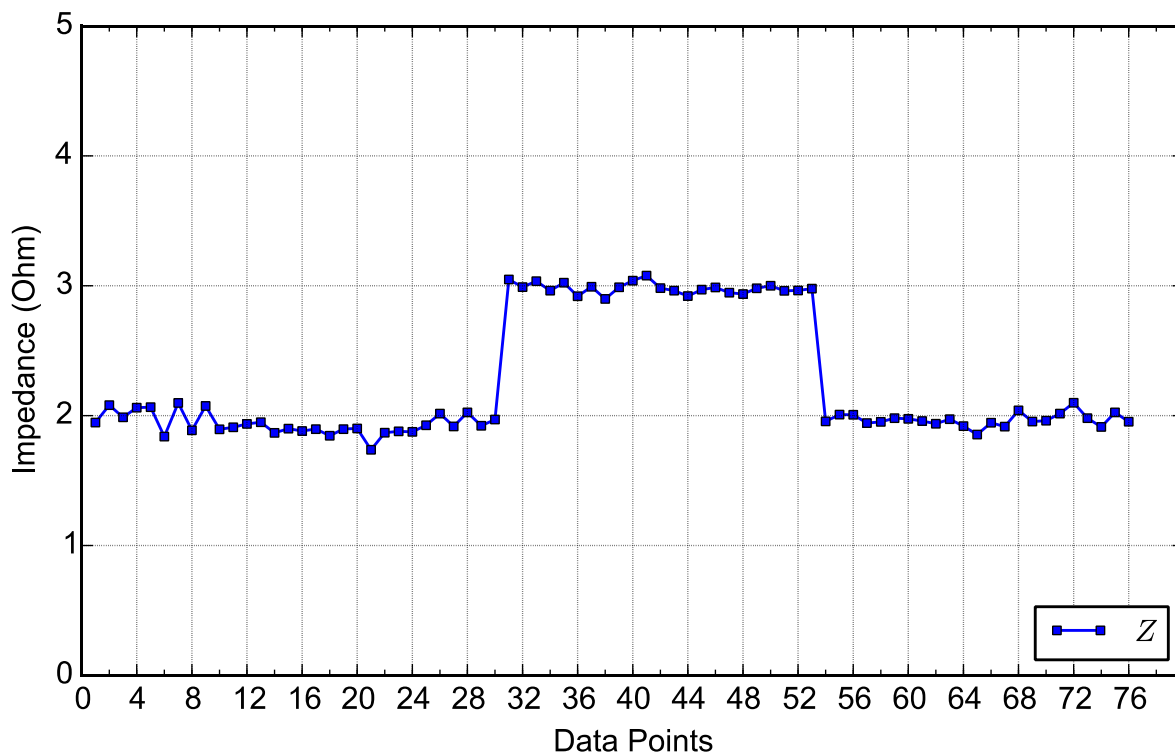


Figure 113: Line impedance of 1  $\Omega$  ( $Z_{L2}$ ) switched in and out of the feeder with a constant load of 0.43 A and a switching load of 4.78 A

In Figure 113 the 1  $\Omega$  line impedance ( $Z_{L2}$ ) was switched in and out of the feeder. The feeder loop impedance increased from close to 1.9  $\Omega$  to close to 2.9  $\Omega$ . The results show that a clear distinction can be made between a feeder impedance of 1.9  $\Omega$  and 2.9  $\Omega$ . The same load was switched (4.78 A) as in the previous case with a constant load of 0.43 A.

In Figure 114 the 1  $\Omega$  line impedance ( $Z_{L2}$ ) was bypassed and the variable impedance ( $Z_{L3}$ ) was increased from 0  $\Omega$  to 8  $\Omega$  in steps of approximately 1  $\Omega$ . The results show the steps in feeder loop impedance as expected, which resembles a deteriorating live or PEN conductor over time. Lastly, the variable impedance was decreased to 0  $\Omega$  and the feeder impedance falls back to 1.9  $\Omega$  as expected. The loading was the same as in the previous cases.

In Figure 115 the line impedance was increased to 2.9  $\Omega$  by switching in impedance ( $Z_{L2}$ ). In this case the constant load is increased to 4.4 A showing that the increase in constant load does not impact the results.

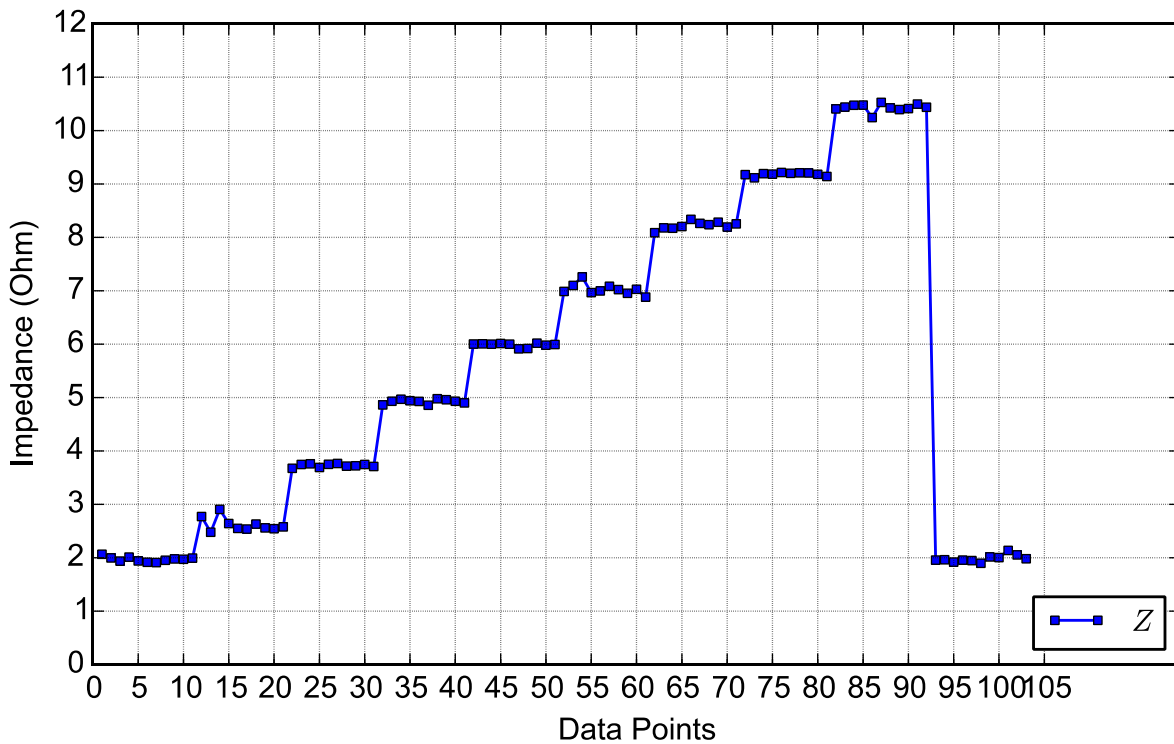


Figure 114: Line impedance increased in steps of approximately 1  $\Omega$  ( $Z_{L3}$ ) with a constant load of 0.43 A and a switched load of 4.78 A

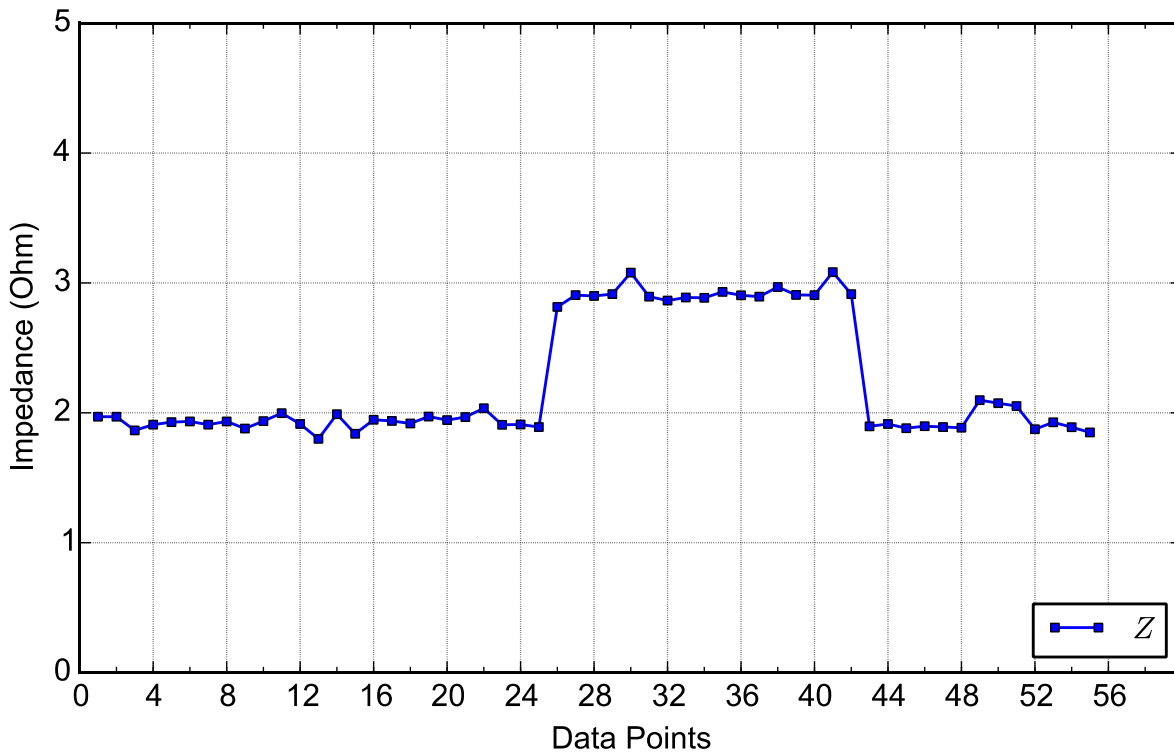


Figure 115: Line impedance of 1  $\Omega$  ( $Z_{L2}$ ) switched in and out of the feeder with a constant load of 4.4 A and a switched load of 4.78 A

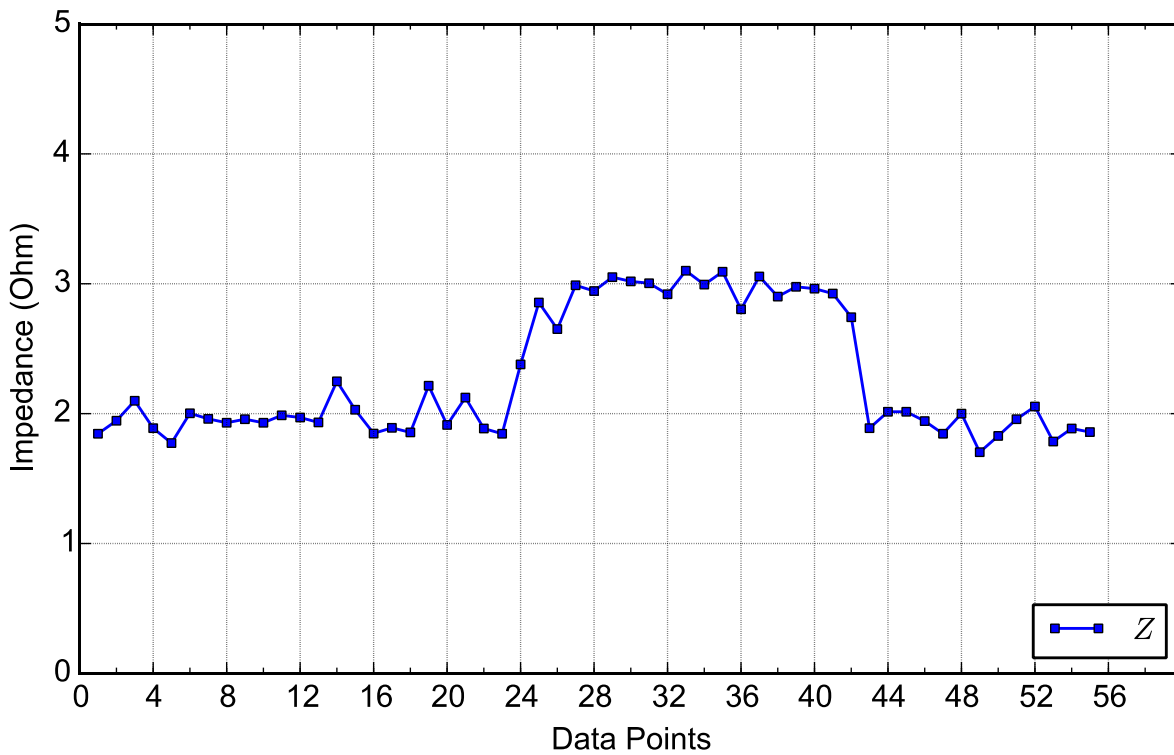


Figure 116: Line impedance of 1  $\Omega$  ( $Z_{L2}$ ) switched in and out of the feeder with a constant load of 4.4 A and a switched load of 0.7 A

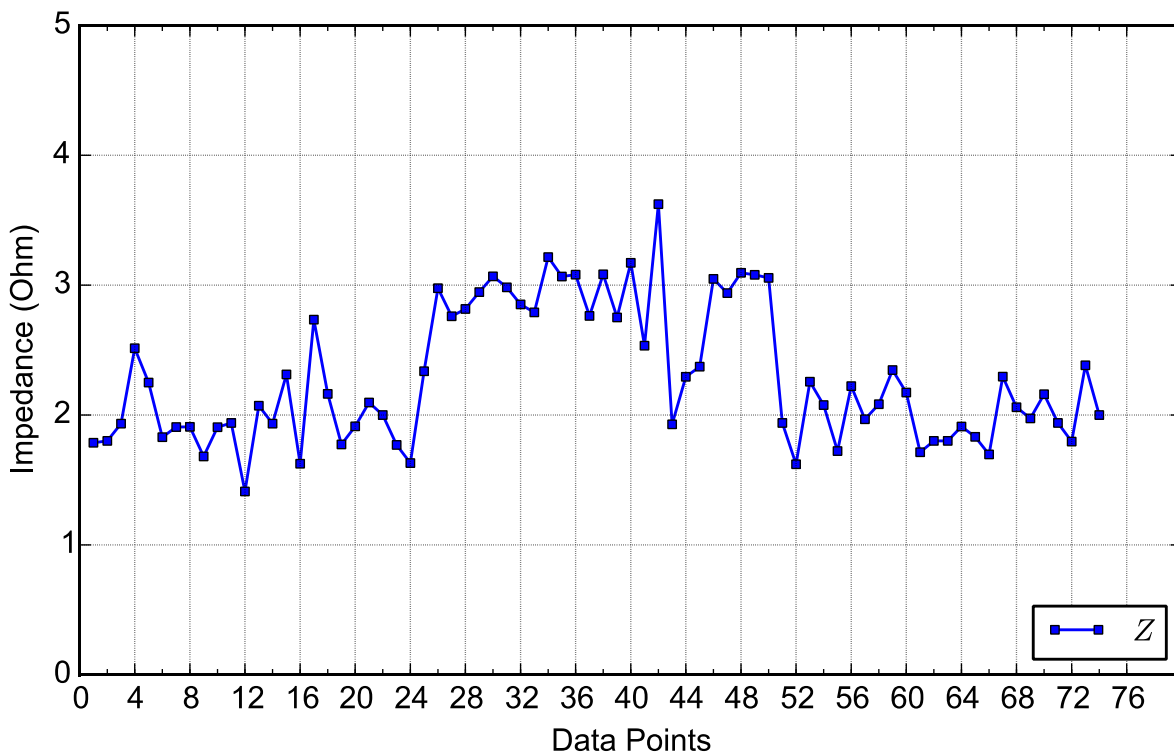


Figure 117: Line impedance of 1  $\Omega$  ( $Z_{L2}$ ) switched in and out of the feeder with a constant load of 4.4 A and a switched load of 0.3 A

In Figure 116 and Figure 117 a constant load drawing 4.4 A was used and the switching load was reduced to 0.7 A and 0.3 A respectively. As in Figure 115 the  $1 \Omega$  line impedance  $Z_{L2}$  was switched in and out of the line. As can be seen in the graphs the accuracy of the impedance measurement reduces as the switched load decreases.

It can be attributed to the 1 second average samples of the current and voltage used to calculate the impedance. Depending on where in the one second sample the current changed occurred, it will affect the accuracy of the impedance measurement. If the change in current occurred close to the end of the second sample, it will result in only a very small change in the average of the one second sample. Such a small change in both the current and voltage will lead to inaccuracies of the impedance calculation. It can be avoided by only reacting on substantial current changes, above 1 A, and ignoring small current changes.

Measurement inaccuracies do not contribute to the impedance inaccuracies as the current measurements are accurate to below 0.38% as can be seen in Table 6 and voltage measurements are accurate to below 0.01% as can be seen in Table 7 in section 4.10.

### 9.7.2. Experimental results - Multiple switching loads

Multiple loads switching at different customer installations on the same transformer feeder, at the same time instant, will result in a larger voltage drop measured at all the customer installations. Thus, the change in voltage measured at a specific customer installation is not exclusively due to the load switched at the specific customer but is a result of the combination of loads switched at other customers on the same feeder, resulting in inaccurate impedance measurements. Larger loads being switched at other customers will have a greater impact on the impedance measurement due to a larger voltage drop on the feeder.

The impedance measurement will also be affected if loads at other customers on a feeder are switched within 1 second before or after the 1 second window in which the switching event occurred. See section 9.3 for the method of calculating the current and voltage changes. In the following experimental results, the load at installation 1 was switched in addition to the load located at installation 2 to evaluate the effect on the line impedance as measured at installation 2.

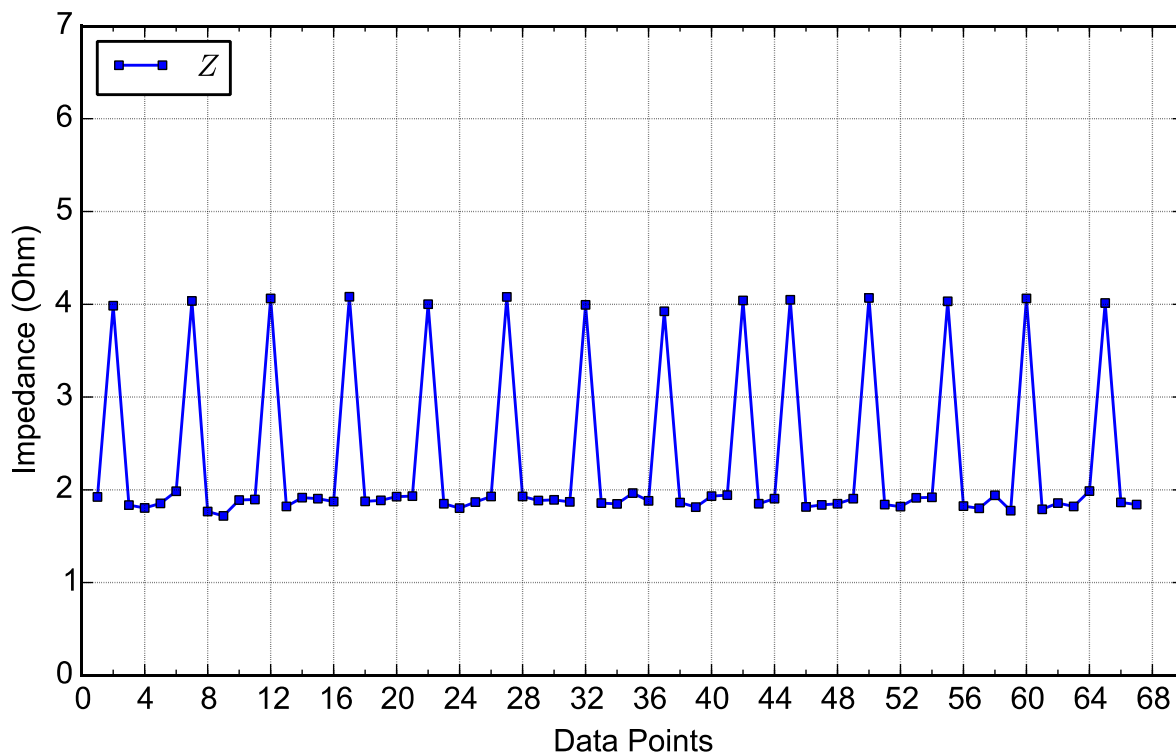


Figure 118: Impedance measured with  $Z_{2s}$  switching at 4 second intervals and  $Z_{1s}$  switching at 20 second intervals

In Figure 118 the load at installation 2 ( $Z_{2s} = 4.78 \text{ A}$ ) was switched at a fixed interval of 4 seconds. The load at installation 1 ( $Z_{1s} = 4.4 \text{ A}$ ) was switched at a fixed interval of 20 seconds. The switching of the loads was synchronised resulting in every 5<sup>th</sup> switching event of installation 2 falling on the same time instant as the switching event at installation 1. This was achieved by switching two relays using two Python scripts running concurrently. The impedance was calculated, as in section 9.7.1, at the meter located at installation 2.

The results obtained shown in Figure 118, shows a sequence of four valid impedance measurements close to  $1.9 \Omega$  and the 5<sup>th</sup> measurement approximately double the actual impedance of the feeder. It can be attributed to almost double the current drawn from the transformer at the specific time instant with only the current measured due to the load change at installation 2. The following shows the resultant impedance measurement for every 5<sup>th</sup> impedance measurement:

$$\begin{aligned}
 Z &= \frac{\Delta V_2}{\Delta I_2} & (9.7.1) \\
 &= \frac{19.69 \text{ V}}{4.78 \text{ A}} \\
 &= 4.12 \Omega
 \end{aligned}$$

As seen above the impedance measured at every 5<sup>th</sup> impedance measured is approximately double the actual impedance value as expected.

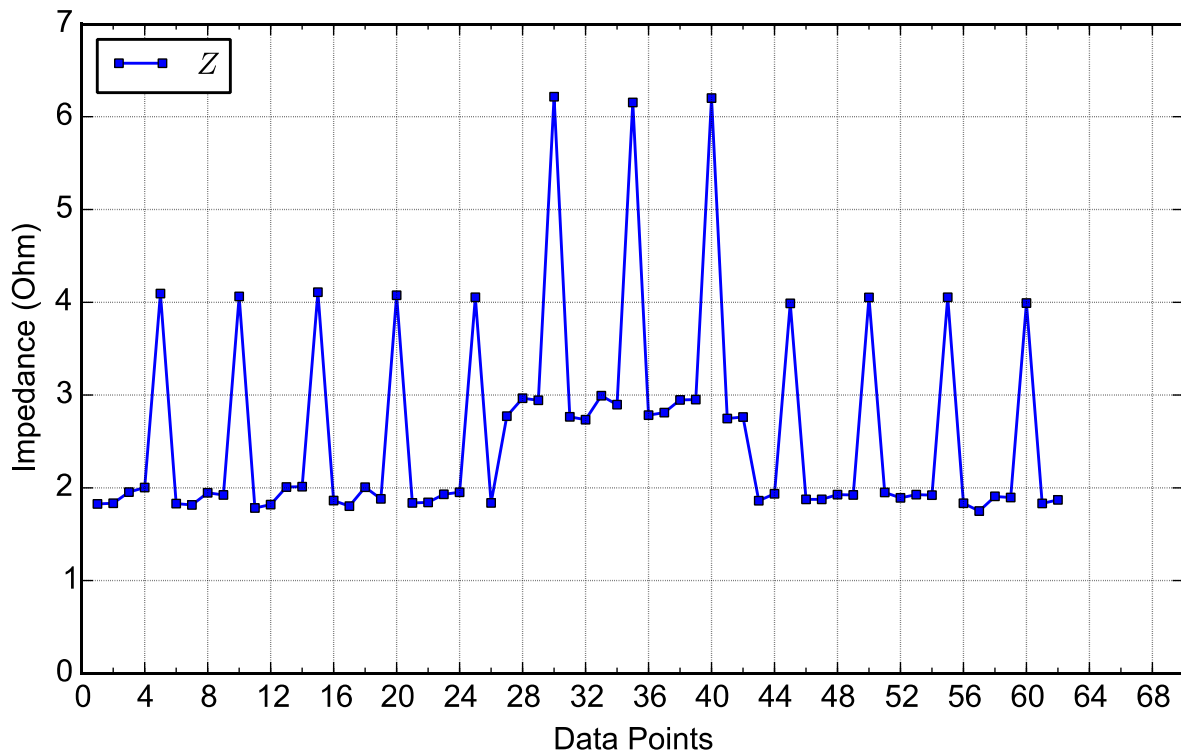


Figure 119: Impedance measured with  $Z_{2s}$  switching at 4 second intervals and  $Z_{1s}$  switching at 20 second intervals

In Figure 119 the same experiment is done as in Figure 118 but with line impedance  $Z_{L2}$  switched in and out of the PEN conductor at data points 27 and 43 respectively. As expected the impedance measured increases to approximately 2.9  $\Omega$  and with every 5<sup>th</sup> measurement almost double the actual impedance. Figure 119, however shows that for this switching case a clear distinction can be made between a line impedance of 1.9  $\Omega$  and a line impedance 2.9  $\Omega$ .

These precisely timed switching sequences will rarely, if ever, occur on a practical feeder. To recreate a practical feeder as closely as possible the switching events for the following two experiments were randomised with the loads at installation 1 and 2 switched randomly between 5 and 15 second intervals.

Figure 120 shows the results obtained with only line impedance  $Z_{L1}$  in the feeder, again the impedance is measured at installation 2. Most impedance values measured are as expected, approximately 1.9  $\Omega$ . The scattered measurements are a result of switching events at installation 1 falling in the 1 second interval before or after the 1 second interval in which the load at installation 2 was switched.

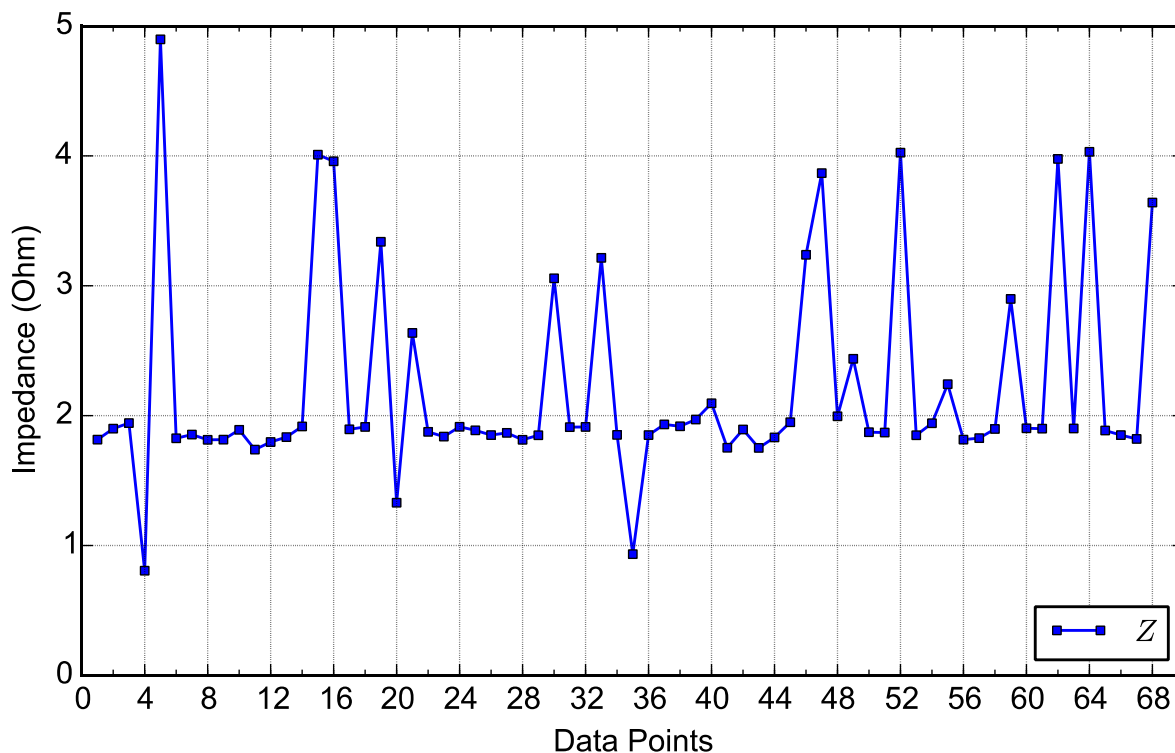


Figure 120: Impedance measured with loads  $Z_{2s}$  and  $Z_{1s}$  switching at random intervals between 5 and 15 seconds

The results provide a more accurate representation of what actual feeder impedance measurements of a feeder will look like in the field. Determining the precise feeder impedance now becomes a statistical problem. Most loads on a rural feeder with limited customers connected to a single MV/LV transformer will have mostly single switching events, but loads being switched 1 second of one another is inevitable.

By plotting the data from Figure 120 in a histogram, the bars representing the number of data points lying in a  $0.1 \Omega$  range, it can be seen that most the data points lie around  $1.9 \Omega$ . Approximately 64 % of the measurements lie between  $1.8 \Omega$  and  $2 \Omega$  as expected. The mean of the data points is  $2.2 \Omega$ .

Standard deviation in the statistical field is a measurement used to show the amount of variation or spread of a set of data points. A low standard deviation indicates that most of the data lie close to the mean and a high standard deviation indicates the data is widely spread around the mean. The standard deviation is therefore basically the average distance of the data from the mean.

The standard deviation can be calculated using the following formula:

$$\sigma = \sqrt{\sum_{i=1}^n \frac{(x_i - \bar{x})^2}{n - 1}} \quad (9.7.2)$$

where  $n$  is the number of data points,  $x_i$  a specific data point and  $\bar{x}$  the mean of the data.

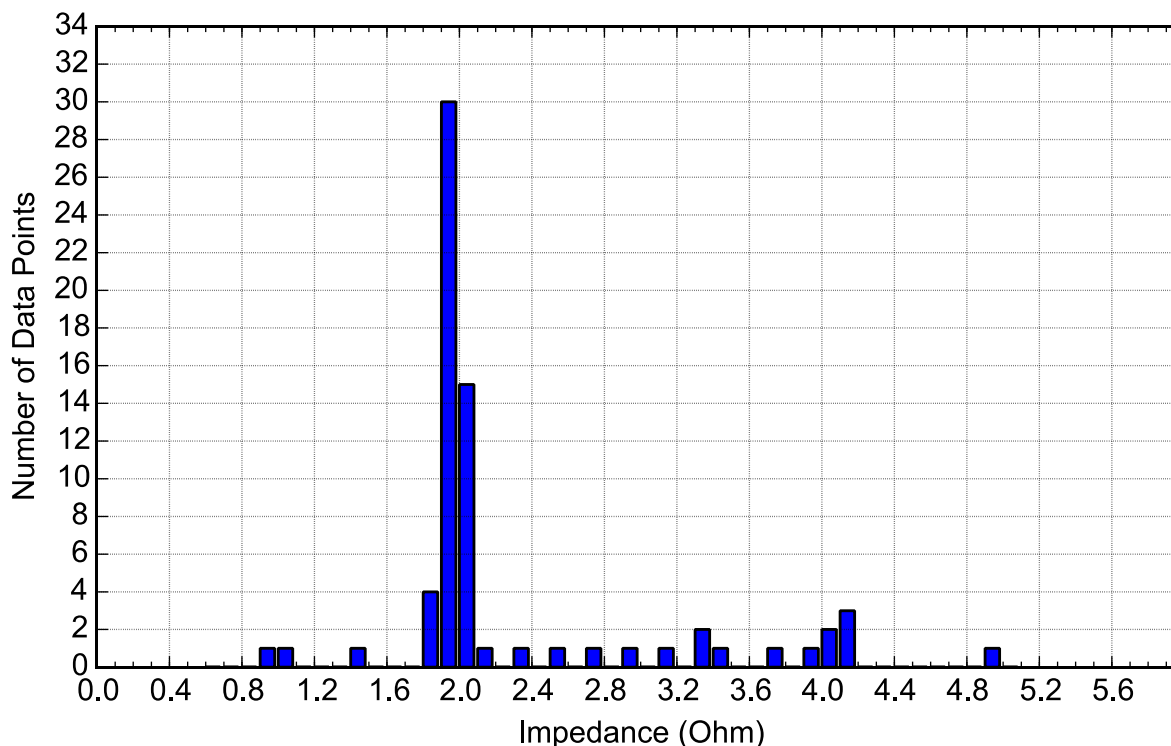


Figure 121: Statistical representation of impedance data in Figure 120. 64% of the data measured lies between 1.8  $\Omega$  and 2  $\Omega$

The standard deviation for the data represented in Figure 121 is 0.79  $\Omega$  and 76.8 % of the data lie within one standard deviation from the mean of 2.2  $\Omega$ . If a normal distribution would however be used to approximate the spread of the impedance data points we can assume that the 68 % of the impedance measurement data lie between 1.41  $\Omega$  and 2.99  $\Omega$ .

Over a long duration the mean and standard deviation will provide an indication if the impedance measured is an expected value or an outlier. An outlier in this case is an impedance measurement taken while two or more loads were switched within 1 second of the switching event used to calculate the impedance. If a live or PEN conductor starts to deteriorate and become a high impedance the mean will increase over time as well as the standard deviation of the data set.

An example can be seen in Figure 122, where line impedance  $Z_{L2}$  was switched into the line at data point 48 increasing the feeder impedance from 1.9  $\Omega$  to 2.9  $\Omega$ . The same random switching sequence with the same loads was used as in Figure 120. Figure 123 shows the histogram of the data similar to Figure 121. As expected most of the data points lie around 1.9  $\Omega$  and 2.9  $\Omega$  with 34.4% of the data points between 1.8  $\Omega$  and 2  $\Omega$  and 22.2% of the data points between 2.8  $\Omega$  and 3  $\Omega$ . The mean of the data lies between these two sets at 2.47  $\Omega$  and the standard deviation is 0.84  $\Omega$ . Comparing these values to the mean and standard deviation

of the data of Figure 120 both values increased as expected. The increase in standard deviation shows that the data is spread wider from the mean.

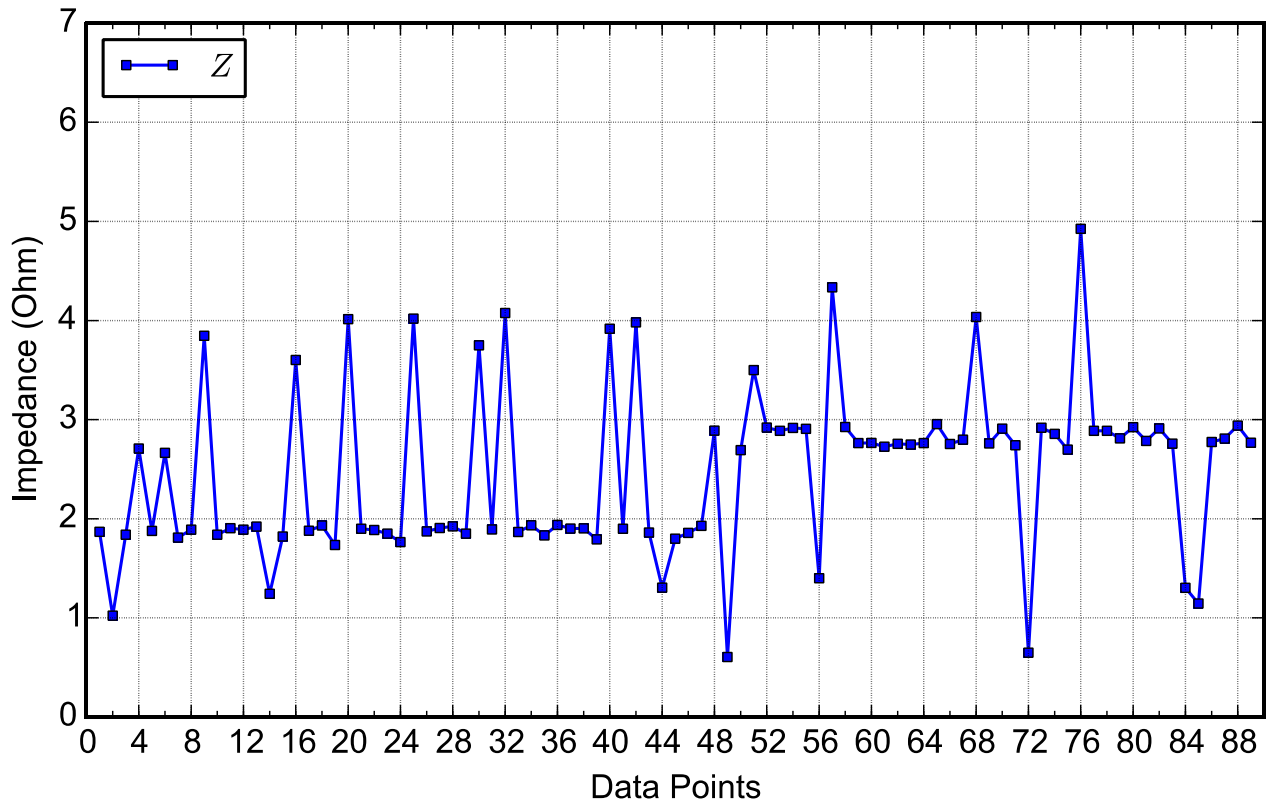


Figure 122: Impedance measured with loads  $Z_{2s}$  and  $Z_{1s}$  switching at random intervals between 5 and 15 seconds. Line impedance  $Z_{L2}$  was switched in to the feeder

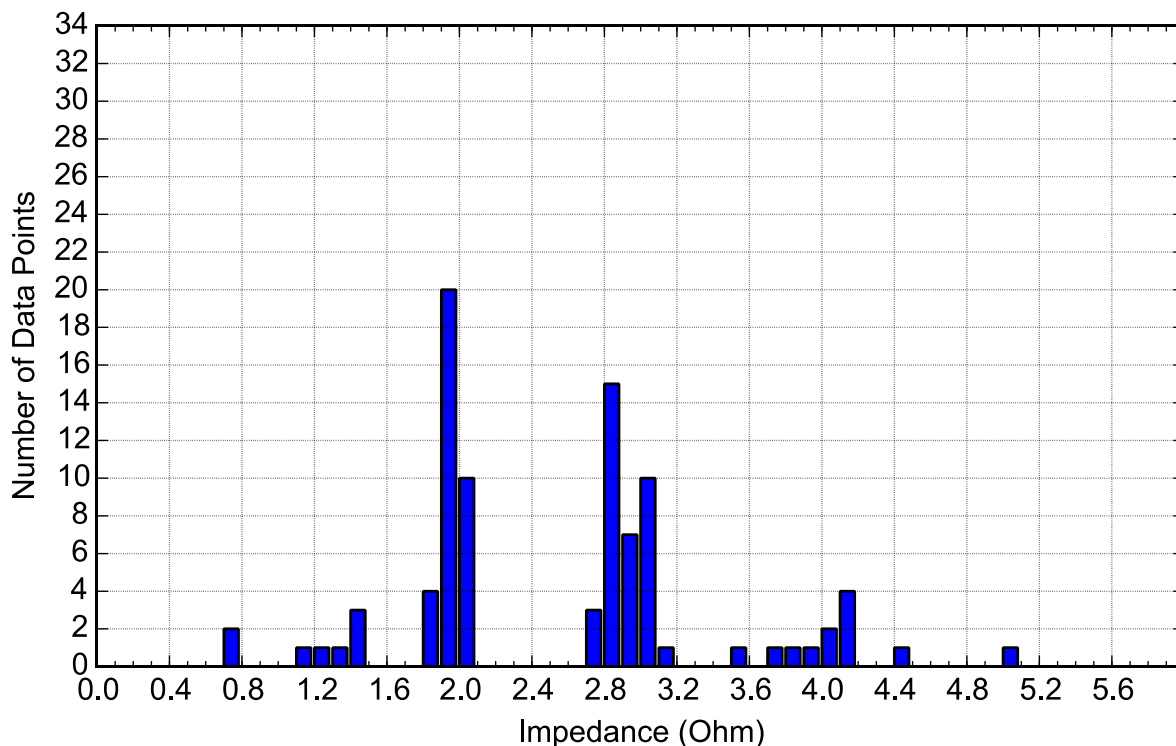


Figure 123: Statistical representation of impedance data in Figure 122. As expected most data points lie around 1.9  $\Omega$  and 2.9  $\Omega$

compared to the previous data points and gives an indication that the live or PEN conductor is deteriorating over time increasing the feeder impedance. The indication of the *health* of a feeder can therefore be determined by the continually monitoring the mean of a set of impedance measurements and its corresponding standard deviation value.

## 9.8. CONCLUSION

This chapter presented the possibility of determining the loop impedance, using the smart meters, of an LV feeder to detect possible failed infrastructure. Two techniques were discussed with the first making use of complete feeder current and voltage measurements. This technique posed the problem of being difficult to practically implement as a single measurement failure would cause inaccurate results.

The latter technique makes use of change in current and voltage to determine the impedance of the feeder loop. The smart meter calculates 1 second averages of r.m.s. currents and voltages. The strategy followed is to compare each 1 second sample of current and voltage with the previous values. The loop impedance could then be calculated on a specific meter and does not require communication of data, only the final impedance measurement is sent to the data concentrator.

Experimental results with a single load switching on a feeder proved that the impedance could be measured accurately using the smart meters. With a single load switching at random, the

impedance measured is a true reflection of the actual impedance of the feeder. Multiple loads switching at specific time instances created additional voltage drops on the feeder resulting in inaccurate impedance measurements at a specific customer installation. Rural feeders with low customers per transformer will provide better impedance results as multiple switching events will be less.

Statistical measures such as mean and standard deviation should be used to gain an indication of the impedance of a feeder where multiple switching events occur regularly. Due to most failures in the field occurring over time, the increase in both the mean and standard deviation of a set of impedance measurements will provide an indication of the live or PEN conductor becoming high impedance.

## CHAPTER 10

# CONCLUSIONS

### 10.1. SUMMARY

This thesis presented the possibility of enabling visibility on rural LV networks to detect identified hazards. Smart metering and smart grids are currently only used for system monitoring and revenue purposes. The concept investigated and presented in this thesis is to use smart metering to increase visibility into the LV grid to detect possible hazards.

Fatalities occur each year because of these hazardous conditions. Rural networks are more susceptible to these conditions due to more overhead conductors being used. This thesis presented an overview of the rural network topology and earthing schemes used in South Africa.

An Eskom LV safety working group identified four hazard categories as having the highest likelihood of occurring and posing the greatest risk to human life. Basic models of each hazardous condition were used to identify the hazard that exists. Proposed detection methods, using measurements taken by smart meters located at customer installations, are discussed. Only detection methods are proposed and the ability to act on such conditions should be done in future work.

Smart meters from Texas Instruments with ZigBee capabilities were used to construct an experimental model of a LV feeder. The software development done on the meter and the ZigBee communication implementation was discussed in this thesis. An experimental data concentrator was designed and built to receive the measurements from the various meters using a ZigBee RF connection.

Experimental results were obtained for each hazardous condition. The hazardous condition was simulated on an experimental LV feeder. The data concentrator was used to capture, store, manage and visualize data gathered from the smart meters. Currently, the data captured by the data concentrator is displayed using graphs on a website. This enables a user to monitor the data and identify a specific hazardous condition.

### 10.2. CONCLUSIONS

It was shown that a PEN conductor failure will lead to under or overvoltage conditions on dual phase feeders and undervoltage conditions on single phase systems. It was confirmed with the experimental setup that the hazard is detectable using phase voltage measurements. Existing solutions were examined which include changing the firmware of existing prepaid meters to act as a voltage comparator with an added dual-pole contactor to completely isolate the customer.

It was found that the best solution is to completely disconnect the feeder at the transformer should a PEN conductor failure occur. The concept of measuring the LV feeder loop impedance using the smart meters at customer installations was also explored as an additional detection method for detecting a PEN conductor failure. By continually monitoring the loop impedance a deteriorating PEN conductor can be detected before it fails. It was found that the LV feeder loop impedance can be successfully measured during the switching of load, but becomes a statistical problem once multiple loads are switched simultaneously on the same feeder. It will, however, not be possible to distinguish between a deteriorating live or PEN conductor by solely relying on the loop impedance measurement. Voltage monitoring in conjunction with loop impedance measurement should be used to detect a broken PEN conductor.

This thesis also showed that an earth electrode failure is detectable by monitoring the transformer LV earth electrode current with respect to the transformer live current. It was found that the ratio between the transformer phase and earth electrode current will provide a clearer indication of a broken earth electrode as a sudden spike in phase current will lead to a sudden spike in earth return current.

Unaccounted current flow conditions such as illegal connections and contact made with low hanging conductors was also detectable on the experimental setup, but small unaccounted currents might prove difficult to detect on real feeders.

### **10.3. RECOMMENDATIONS AND FUTURE WORK**

The following aspect should be further explored in future work:

- Improve understanding of how the hazardous conditions present itself in the field. Real measurement data from the field should be collected and analysed to fully understand the various hazardous conditions and re-evaluate the detection methods.
- Automated fault/hazard reporting should be added to the data concentrator, it would require the use of techniques such as machine learning.
- Send fault conditions to a head end system.
- Field test the ZigBee communication used.

## References

- [1] O. H. & Safety, "What Is Hazardous?," 17 2011. [Online]. Available: <https://ohsonline.com/Articles/2011/07/01/What-Is-Hazardous.aspx>.
- [2] Africa, Department of Energy: Republic of South, "A survey of energy-related behaviour and perceptions in South Africa: The residential Sector," Pretoria, 2012.
- [3] D. H. Geldenhuys, "Earthing of MV and LV Distribution Lines".
- [4] South African National Standard, *Earthing of Low-voltage (LV) distribution systems (SANS 10292:2013)*, Pretoria: SANS, 2013.
- [5] International Electrotechnical Commission, *Low-voltage electrical installations - Part 1: Fundamental principles, assessment of general characteristics, definitions*, IEC, 2005.
- [6] Eskom Distribution, "Pole-Mounted Service Distribution Boxes for Split Prepayment Metering," 2010.
- [7] Electrical Technology, "Electrical Technology: HRC fuse and its types," 12 December 2014. [Online]. Available: <http://www.electricaltechnology.org/2014/12/hrc-fuse-high-rupturing-capacity-fuse-types.html>. [Accessed 15 January 2017].
- [8] South African National Standard, *Low-voltage fuses Part2: Supplementary requirements for fuses for use by authorised persons. (SANS 60269-2:2016)*, Pretoria: SANS, 2016.
- [9] South African National Standards, *The wiring of premises - Part 1: Low voltage installations (SANS 10142-1)*, Pretoria: SANS, 2012.
- [10] British Standards Institution, *Code of practice for protective earthing of electrical installations (BS 7430:2011)*, BSI Standard Publication, 2011.
- [11] South African National Standards, *Protection against lightning - Part 4: Electrical and electronic systems within structures*, Pretoria: SANS, 2011.
- [12] V. Cohen, "Loss of neutral in LV distribution systems: consequences and solutions," *Vector Magazine*, pp. 46-50, Nov/Dec 2012.
- [13] NRS, *NRS Electricity supply- Quality of supply Part 2 (NRS 048-2:2007)*, Pretoria: NRS, 2007.
- [14] South African National Standards, *Electricity payment systems - Part 1-1: Mounting and terminal requirements for prepayment meters (SANS 1524-1-1:2013)*, Pretoria: SANS, 2013.
- [15] T. Vijayapriya, "Smart Grid: An Overview," *Smart Grid and Renewable Energy (SGRE)*, no.

November 2011, pp. 305-311, 2011.

- [16] Office of Electricity Delivery & Reliability, "Energy.gov," [Online]. Available: <https://energy.gov/oe/services/technology-development/smart-grid>. [Accessed 18 January 2017].
- [17] M. Kuzlu, "Communication network requirements for major smart grid applications in HAN, NAN and WAN," *Elsevier*, no. 67, pp. 74-88, 2014.
- [18] J. Calmeyer, "ZigBee as a technology platform for advanced metering infrastructure (AMI)," in *AMEU Convention*, Ekurhuleni, 2012.
- [19] Nersa, "NRS 049," 2016. [Online]. Available: <http://www.nersa.org.za/>. [Accessed 20 January 2017].
- [20] Eskom, "Standard for adopted open protocols for eskom advanced meters," Eskom, 2015.
- [21] G3-PLC Alliance, "G3-PLC Overview," G3-PLC Alliance, 2016. [Online]. Available: <http://www.g3-plc.com/what-is-g3-plc/g3-plc-overview/>. [Accessed 6 February 2017].
- [22] Landis & Gyr, "G3-PLC Smart Communications for the future," [Online]. Available: <http://eu.landisgyr.com/g3-plc>. [Accessed 6 February 2017].
- [23] G3-PLC, "G3-PLC Unique Features," G3-PLC Alliance, 2016. [Online]. Available: <http://www.g3-plc.com/what-is-g3-plc/g3-plc-unique-features/>. [Accessed 6 February 2017].
- [24] A. K. e. a. Kaveh Razazian, *G3-PLC Field Trials in U.S. Distribution Grid: Initial Results and Requirements*, IEEE Conference Publications, 2011.
- [25] Digi, "ZigBee stack layers," Digi, 28 9 2017. [Online]. Available: [https://www.digi.com/resources/documentation/Digidocs/90002002/Default.htm#Reference/r\\_zb\\_stack.htm%3FTocPath%3DZigbee%2520networks%7C\\_\\_\\_\\_\\_3](https://www.digi.com/resources/documentation/Digidocs/90002002/Default.htm#Reference/r_zb_stack.htm%3FTocPath%3DZigbee%2520networks%7C_____3).
- [26] Texas Instruments, "Texas Instruments ZStack," 2011. [Online]. Available: <http://www.ti.com/lit/ug/swru208b/swru208b.pdf>.
- [27] EETIMES, "EETimes," 10 06 2008. [Online]. Available: [http://www.eetimes.com/document.asp?doc\\_id=1276377](http://www.eetimes.com/document.asp?doc_id=1276377). [Accessed 04 05 2016].
- [28] Texas Instruments, "Implementation of a Three-Phase Electronic Watt-Hour Meter," August 2015. [Online]. Available: <http://www.ti.com/lit/an/slaa577g/slaa577g.pdf>.
- [29] Omnicron, "Omnicron," 2016. [Online]. Available: <https://www.omicronenergy.com/en/products/all/secondary-testing-calibration/cmc-256plus/>.

[Accessed 17 May 2016].

- [30] Texas Instruments, *Implementation of a three-phase electronic watt-hour meter using the MSP430F677x(A)*, Texas Instruments, 2015.
- [31] E. Moulin, *Measuring reactive power in energy meters*, Metering International, 2002.
- [32] Scriptoriumdesigns, "Introduction to Embedded Programming," W3, [Online]. Available: <http://www.scriptoriumdesigns.com/embedded/interrupts.php>. [Accessed 1 January 2017].
- [33] Texas Instruments, "CC2530EM Reference Design," Texas Instruments, 2016. [Online]. Available: <http://www.ti.com/tool/CC2530EM>.
- [34] Texas Instruments, "CC2530EM Schematics," 2016. [Online]. Available: <http://www.ti.com/general/docs/lit/getliterature.tsp?baseLiteratureNumber=swrc144&fileType=zip>.
- [35] Texas Instruments, "A True System-on-Chip Solution for 2.4-GHz IEEE 802.15.4 and ZigBee Applications," February 2011. [Online]. Available: <http://www.ti.com/lit/ds/symlink/cc2530.pdf>.
- [36] Texas Instruments, *ZigBee Interface Specifications*, TI, 2012.
- [37] T. Instruments, *Enhanced Universal Serial Communication Interface (eUSCI) - SPI mode*, TI, 2015.
- [38] Texas Instruments, "Battery Board for System-on-Chips," 2016. [Online]. Available: <http://www.ti.com/tool/soc-bb>.
- [39] Texas Instruments, "Texas Instruments CC-Debugger," [Online]. Available: <http://www.ti.com/lit/ug/swru197h/swru197h.pdf>.
- [40] Texas Instruments, "SmartRf flash programmer," 2016. [Online]. Available: <http://www.ti.com/tool/flash-programmer>. [Accessed 23 March 2016].
- [41] Texas Instruments, "A fully compliant ZigBee 3.0 stack," January 2016. [Online]. Available: <http://www.ti.com/tool/z-stack>. [Accessed 10 March 2016].
- [42] Raspberry PI, "Compute Module," [Online]. Available: <https://www.raspberrypi.org/products/compute-module/>. [Accessed 25 May 2016].
- [43] Raspberry PI, "RASPBerry PI 1 MODEL B+," [Online]. Available: <https://www.raspberrypi.org/products/model-b-plus/>. [Accessed 25 May 2016].
- [44] Raspberry PI, "IO Board," [Online]. Available: <https://www.raspberrypi.org/blog/tag/compute-module-io-board/>.

- [45] Diodes, "Diodes PAM2306," [Online]. Available: [http://www.diodes.com/\\_files/datasheets/PAM2306.pdf](http://www.diodes.com/_files/datasheets/PAM2306.pdf).
- [46] Microchip, "Microchip LAN9514," [Online]. Available: <http://www.microchip.com/wwwproducts/en/LAN9514>.
- [47] Fairchild, [Online]. Available: <https://www.fairchildsemi.com/datasheets/FS/FSUSB42.pdf>.
- [48] Raspberry PI, "Raspberry PI Hardware Design Guide," [Online]. Available: <https://www.raspberrypi.org/documentation/hardware/computemodule/cm-designguide.md>.
- [49] R. Faludi, Building Wireless Sensor Networks, Sebastopol: O'Reilly Media, Inc, 2010.
- [50] CINTERION, "Cinterion TC63i," [Online]. Available: <http://uk.farnell.com/cinterion/tc63i/mod-gsm-gprs-quad-band-tcp-ip/dp/1718876>.
- [51] Fairchild Semiconductor, "74LCX541 - Low Voltage Octal Buffer," [Online]. Available: <https://www.fairchildsemi.com/datasheets/74/74LCX541.pdf>.
- [52] ON Semiconductor, "NCP582," [Online]. Available: [http://www.onsemi.com/pub\\_link/Collateral/NCP582.PDF](http://www.onsemi.com/pub_link/Collateral/NCP582.PDF).
- [53] Adafruit, "Adafruit GPS," [Online]. Available: <https://www.adafruit.com/product/746>.
- [54] Raspi, "Raspberry Pi Headers," [Online]. Available: <http://raspi.tv/wp-content/uploads/2014/07/Raspberry-Pi-GPIO-pinouts.png>.
- [55] Texas instruments, "Texas Instruments MAX3232E," [Online]. Available: <http://www.ti.com/lit/ds/symlink/max3232e.pdf>.
- [56] Microchip, "Microchip MCP25625," [Online]. Available: <ww1.microchip.com/downloads/en/DeviceDoc/20005282A.pdf>.
- [57] Raspbian.org, "Raspbian," [Online]. Available: <https://www.raspbian.org/>.
- [58] Hobby Electronics, "XBee Explorer USB," 2016. [Online]. Available: <http://www.hobbytronics.co.uk/xbee-explorer-usb>. [Accessed 28 11 2016].
- [59] D. XBEE, "XCTU Software," DIGI , [Online]. Available: <https://www.digi.com/products/xbee-rf-solutions/xctu-software/xctu>. [Accessed 10 07 2016].
- [60] SQLite, "SQLite," 24 10 2017. [Online]. Available: <https://www.sqlite.org/>.
- [61] G. v. Rossum, "The history of Python," 13 January 2009. [Online]. Available: <http://python-history.blogspot.co.za/2009/01/introduction-and-overview.html>. [Accessed 18 11 2016].

- [62] E. DeBill, "Modules Count," 2016. [Online]. Available: <http://www.modulecounts.com>. [Accessed 18 11 2016].
- [63] Tutorialspoint, "Tutorialspoint," 2017. [Online]. Available: [https://www.tutorialspoint.com/python/python\\_cgi\\_programming.htm](https://www.tutorialspoint.com/python/python_cgi_programming.htm). [Accessed 10 January 2017].
- [64] A. A. M. Majidi, *Fault Location in Distribution Networks by Compression Sensing*, IEEE, 2015.
- [65] M. O. F. J. Cordova, *Fault Location Identification in Smart Distribution Networks with Distributed Generation*, IEEE.
- [66] Eskom Holdings SOC Ltd., *Distribution Standard - Part 2: Earthing (Rev.0)*, 2010.
- [67] *Electricity Supply - Quality of Supply Part 2: voltage characteristics, compatibility levels, limits and assessment methods (NRS 048-2:2015)*, Pretoria, 2015.
- [68] South African National Standards, *Electricity payment systems Part1-1: Mounting and terminal requirements for payment meters (SANS1524-1-1:2015)*, Pretoria: SANS, 2013.
- [69] Government Regulation Gazette, No. 8928, "Regulation Paper," Pretoria, 2008.
- [70] H. Madhoo, "Investigating the value proposition of Advanced Metering Infrastructure in developed and emerging economies with a focus on South Africa," University of Witwatersrand, Johannesburg, 2014.
- [71] EssayBoost, "Research Essay Papers," 9 August 2016. [Online]. Available: <http://essayboost.com/an-analysis-of-the-history-of-coal-its-burning-and/>. [Accessed 18 November 2016].
- [72] South African National Standard, *The wiring of premises. Part 1: Low-voltage installations (SANS 10142:2017)*, SANS, 2017.

## APPENDIX A.

### GPS NMEA DATA

#### A.1 BACKGROUND

The NMEA specification was developed by the national marine electronics association (NMEA) as a specification that defines the interface between various pieces of marine electronic equipment. This includes global positioning system (GPS) receivers.

GPS devices send position data to a computer or microcontroller using the NMEA 0183 standard. The NMEA 0183 standard uses an ASCII, serial communications protocol that defines how data is sent from one “talker” to one or more “listeners”. The NMEA standard was created in 1983 and has since undergone several revision updates. The latest standard, NMEA 0183, replaced the earlier 0180 and 0182 standards.

#### A.2 NMEA MESSAGE SENTENCES

The NMEA protocol consist of data sentences. Each sentence starts with a data type defining the type of sentence and its data structure. The data types are defined in the NMEA standard and the most commonly used types for GPS applications can be found in Table 24.

Table 24: Commonly used NMEA Data Types

Data Type Identifier	Notes
GPRMC	Recommended Minimum data for GPS
GPGGGA	Fix Information
GPGSA	Overall Satellite data
GPVTG	Vector track and Speed over Ground
GPGLL	Latitude/Longitude data
GPGSV	Detailed Satellite data

#### A.3 HARDWARE INTERFACE

The NMEA standard defines a GPS hardware interface to conform to the EIA-422 standard or most commonly known as RS422. They are also compatible with most serial ports on microcontrollers and computers. The NMEA standard defines an interface speed of 4800 b/s but on some newer GPS models it can be increased to 9600 b/s. Devices can seem to be unresponsive at a baud rate of 4800 b/s as only 480 characters can be sent in a second. This correlates to about 6 NMEA messages in a second. A car travelling at 120 km/h moves 33 m in

one second, resulting in GPS devices to seem unresponsive at a baud rate of 4800 b/s. Faster baud rate helps to overcome this problem.

#### A.4 NMEA MESSAGE DATA STRUCTURE

All NMEA sentence types have the same basic structure adhering to the following conditions:

- All NMEA sentences have a maximum length of 82 characters.
- The start character for each sentence is the “\$” symbol.
- All data fields are comma-delimited.
- If no data is available for a certain field, the field is left blank. This usually occurs if the GPS device has lost satellite reception.
- The first character to follow the last data field is an asterisk, which is followed by a checksum.
- The checksum is the bitwise exclusive OR of ASCII characters of all the characters between the \$ and \*.

#### A.5 NMEA MESSAGE EXAMPLE

The following shows an example of the GPRMC (recommended minimum sentence) message. This NMEA sentence is used in the smart meter GPS implementation.

```
$GPRMC,183045.000,A,3351.9759,S,1838.4299,E,1.49,111.67,040117,003.1,W,A*74
```

**\$GPRMC:** Specifying the sentence type.

**183045.000:** Represents the coordinate universal time (UTC). The example 183045.000 represents 18:30:45 in UTC.

**A:** Status of the signal. A = Active, V = Void

**3351.9759,S:** Latitude in degrees minutes (ddmm.mmmm) format in the southern hemisphere.

**01838.4299,E:** Longitude in degrees minutes (ddmm.mmmm) format in the eastern hemisphere.

**1.49:** Speed over the ground in knots.

**111.67:** Track angle measured clockwise from True North.

**040117:** Represents the date 04 January 2017.

**003.1,W:** Magnetic Variation

**\*74:** Checksum data, always begins with \*.

# APPENDIX B. SCHEMATICS OF TEXAS INSTRUMENTS SMART METER

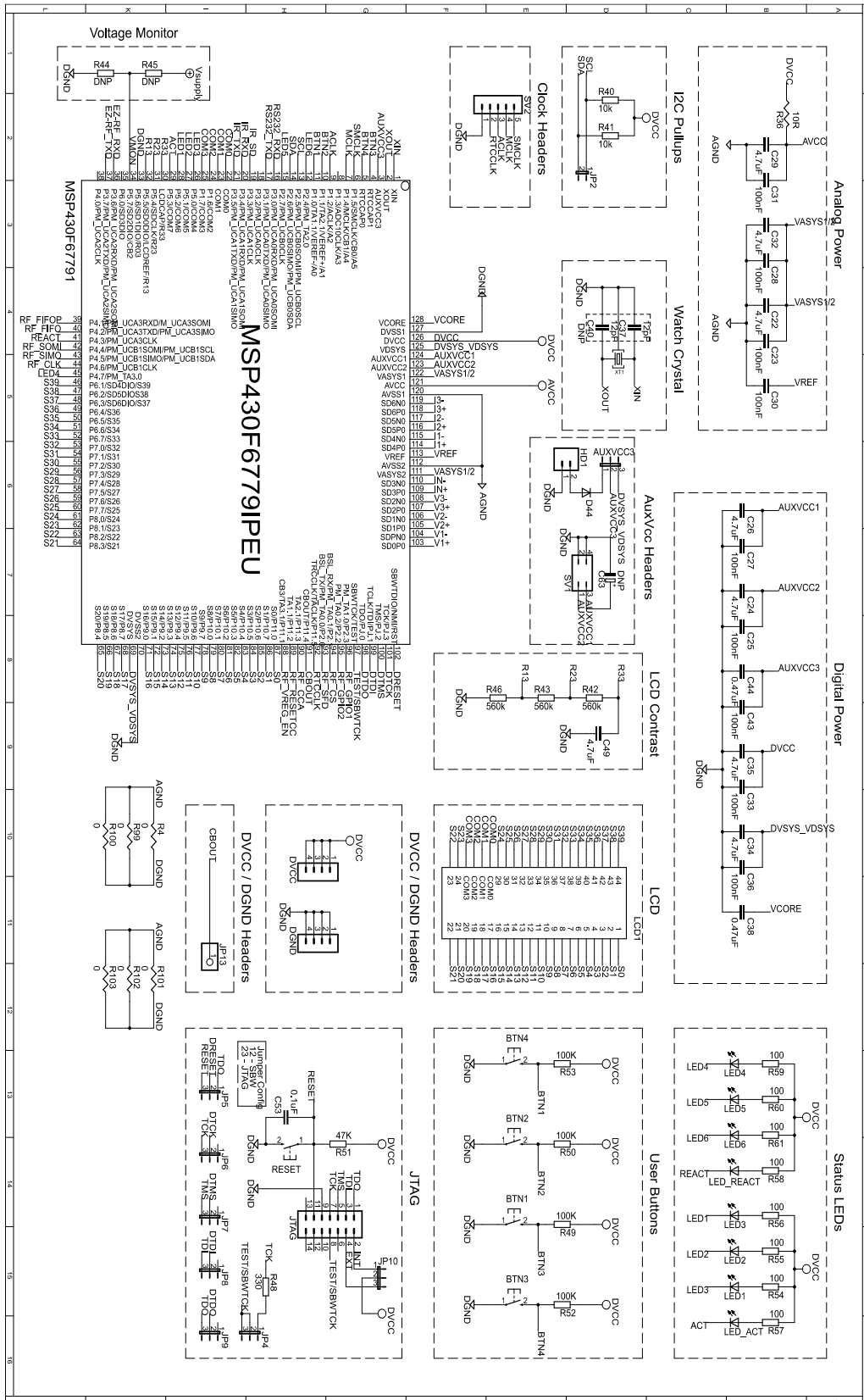
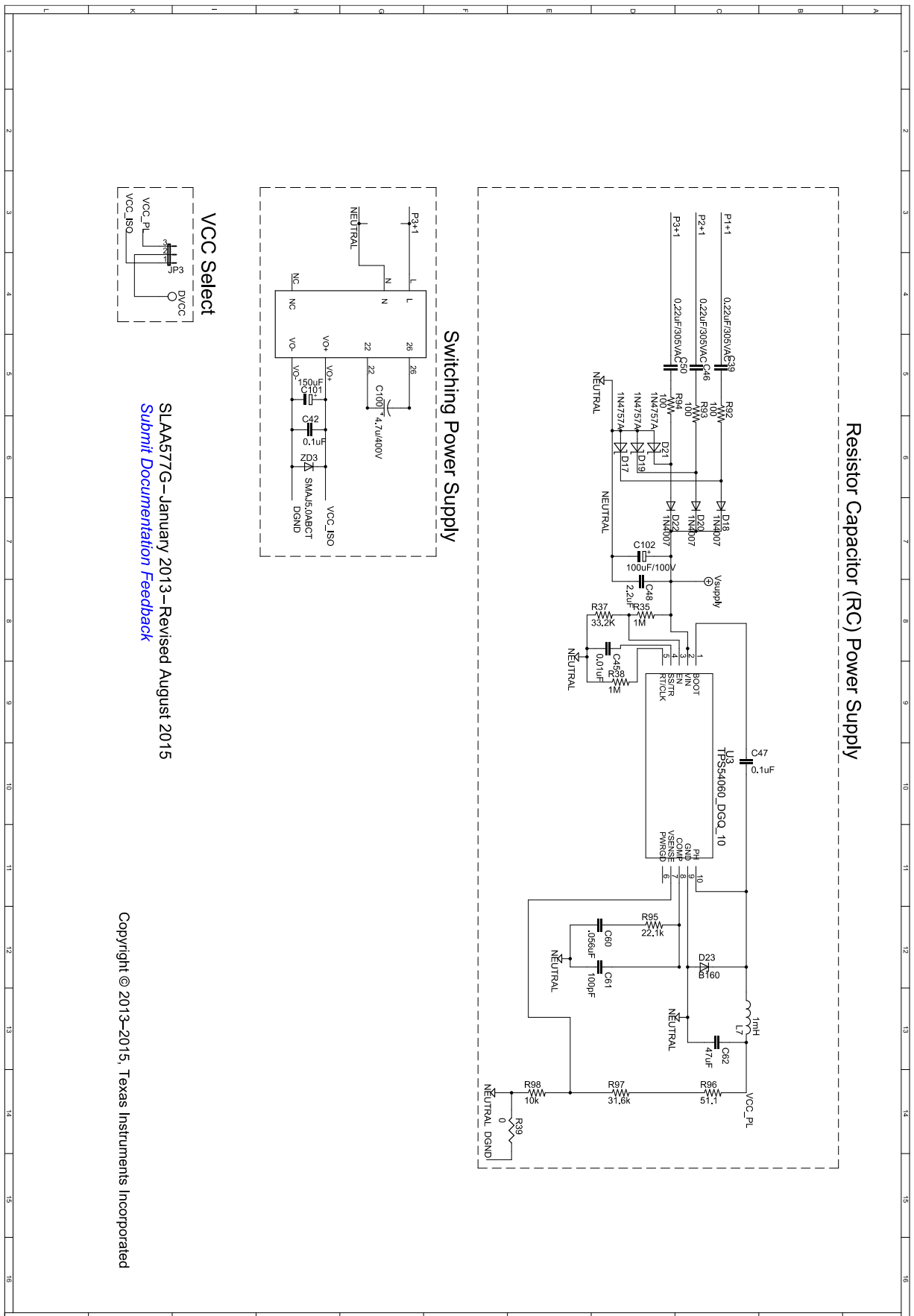


Figure 124: Smart Meter Schematics (1 of 4) [28]





SLAA577G—January 2013—Revised August 2015  
 Submit Documentation Feedback

Copyright © 2013–2015, Texas Instruments Incorporated

Figure 126: Smart Meter Schematics (3 of 4) [28]

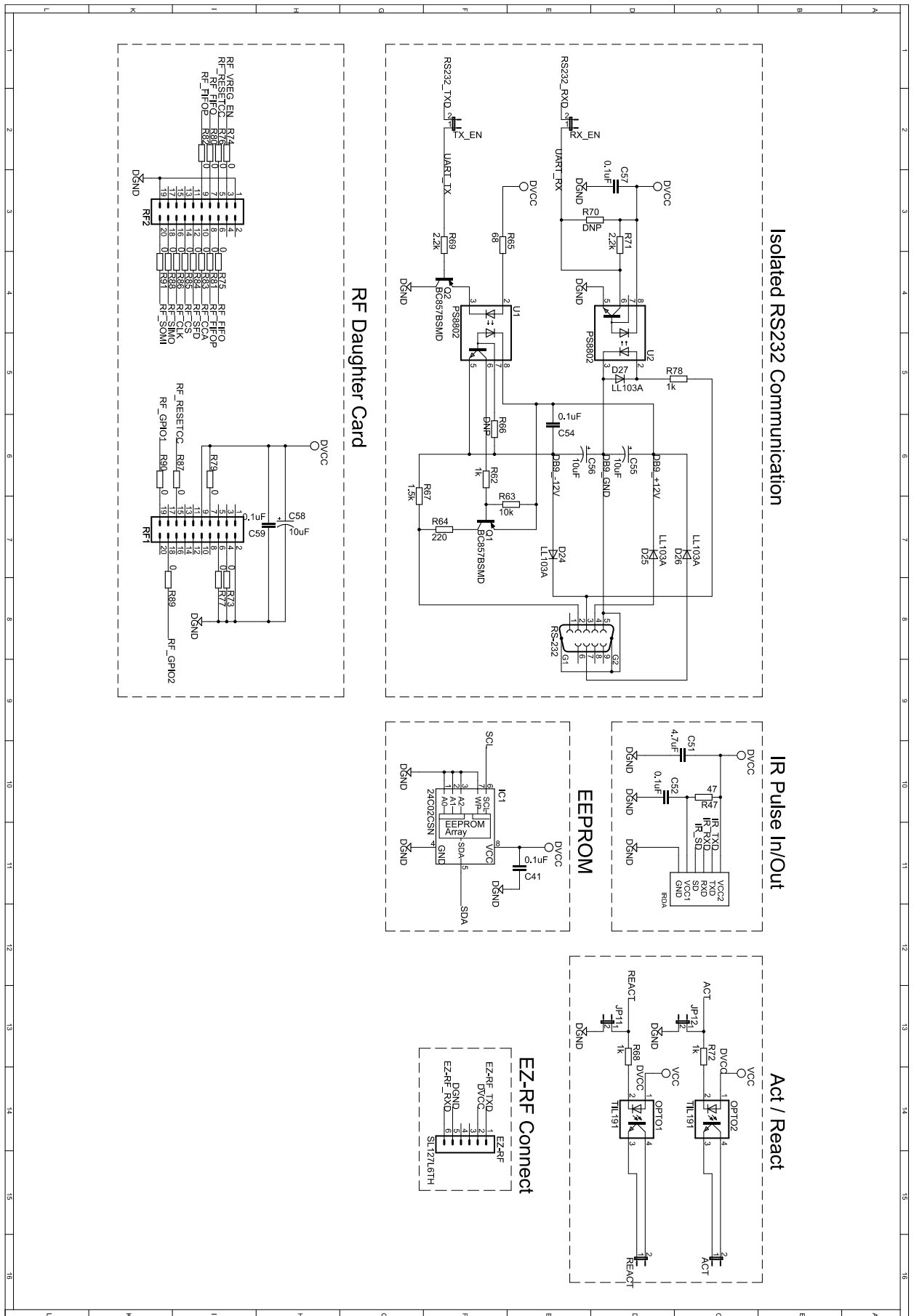
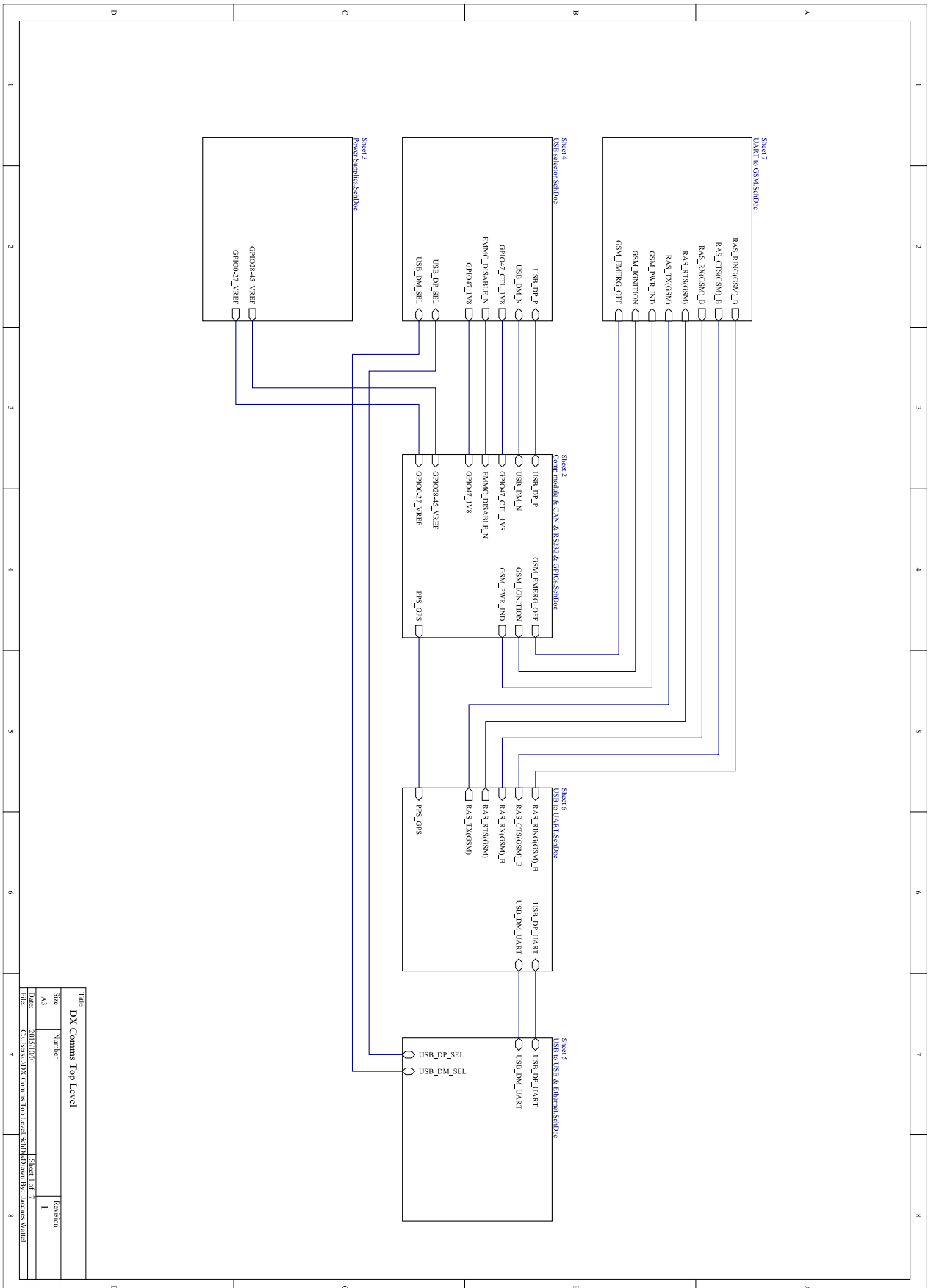


Figure 127: Smart Meter Schematics (4 of 4) [28]



Title		DX Commis Top Level	
Size	Number	Revision	
A3	1	1	
Date:	2015/04/01	Sheet of	7
File:	C:\Users\jdx\Documents\DX Commis Top Level\SCH3\Sheet3.dwg	Drawn by:	Ismael Ward

Figure 128: Data Concentrator Schematics (1 of 7)



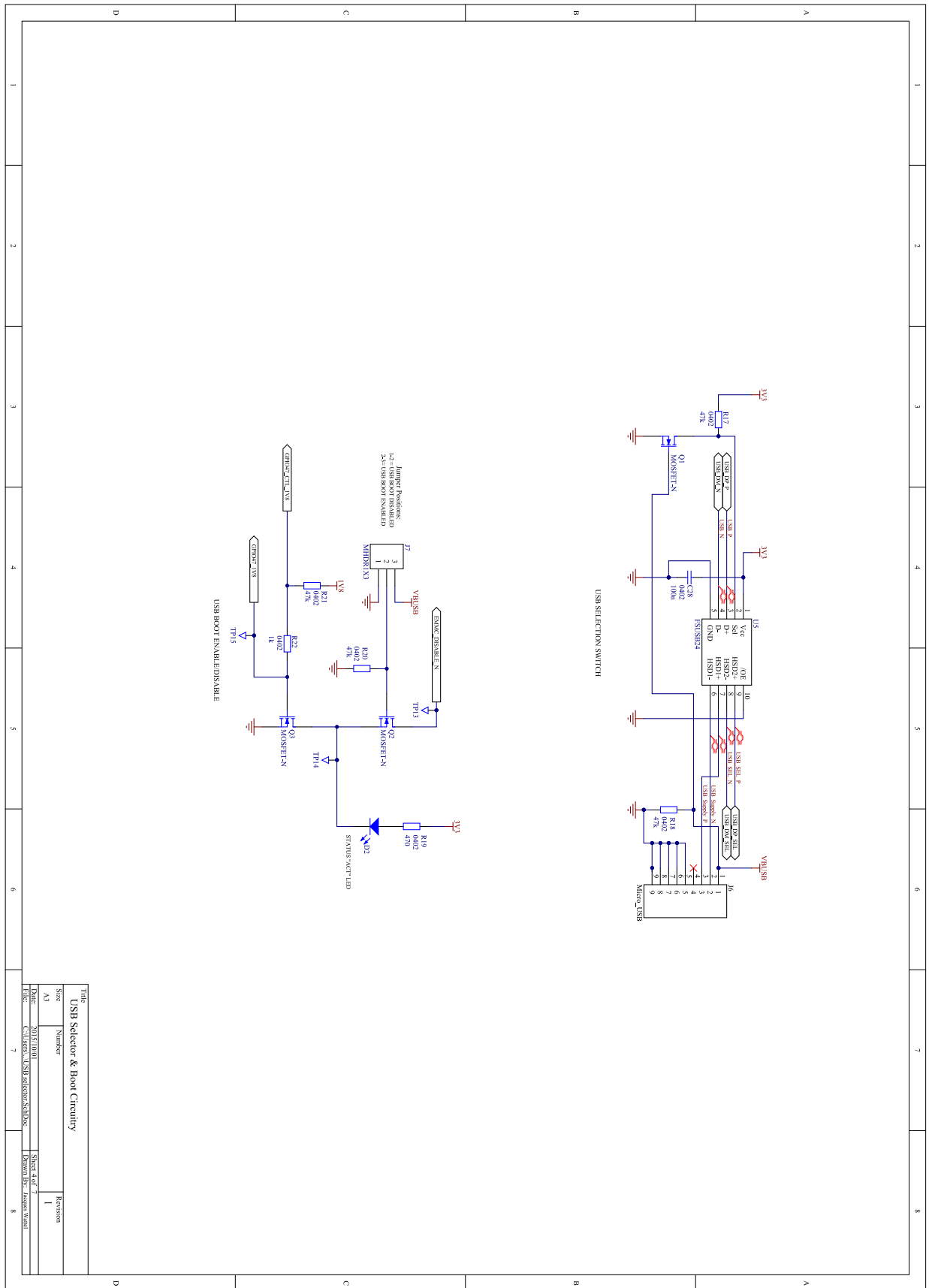


Figure 130: Data Concentrator Schematics (3 of 7)

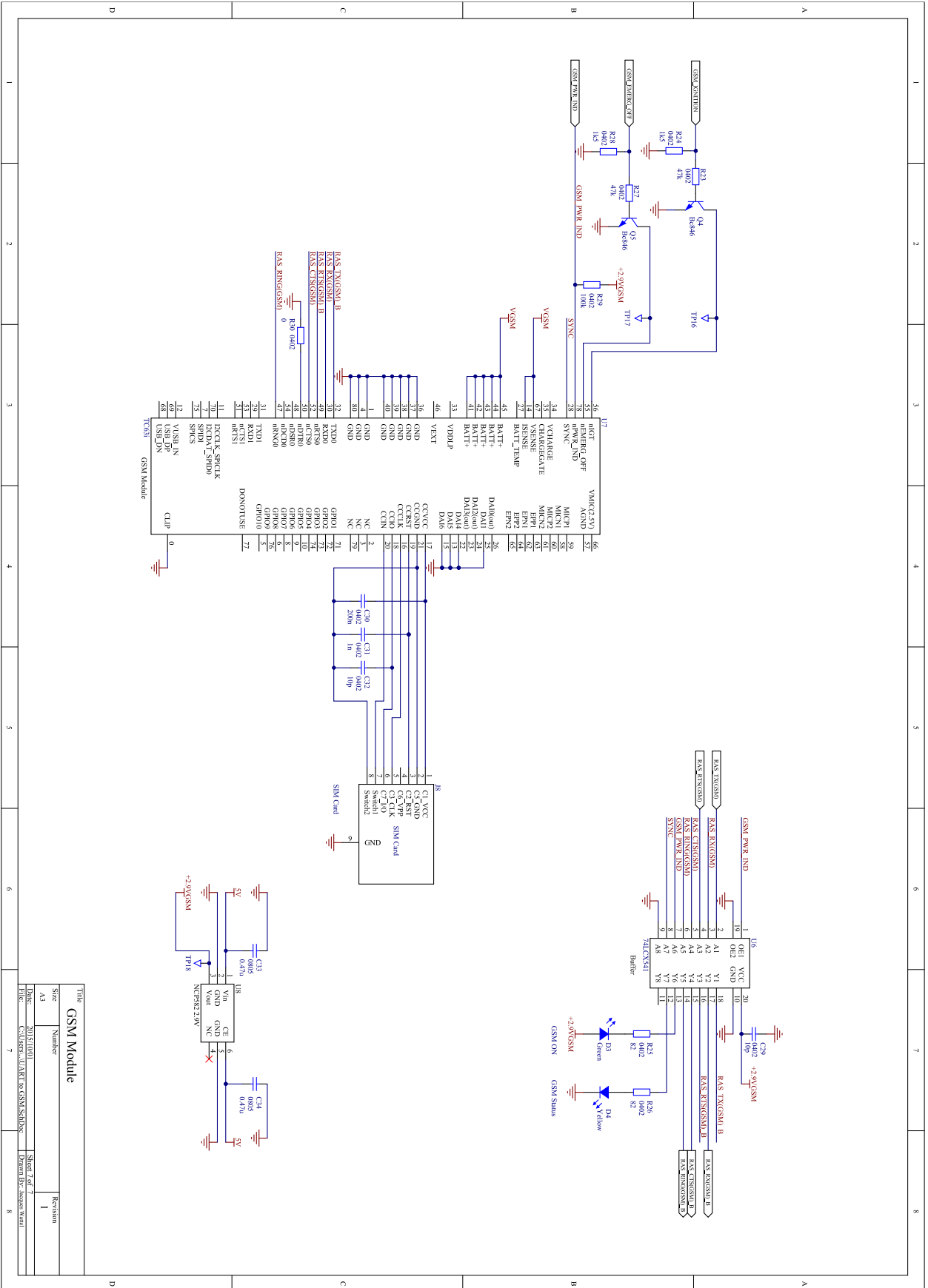


Figure 131: Data Concentrator Schematics (4 of 7)



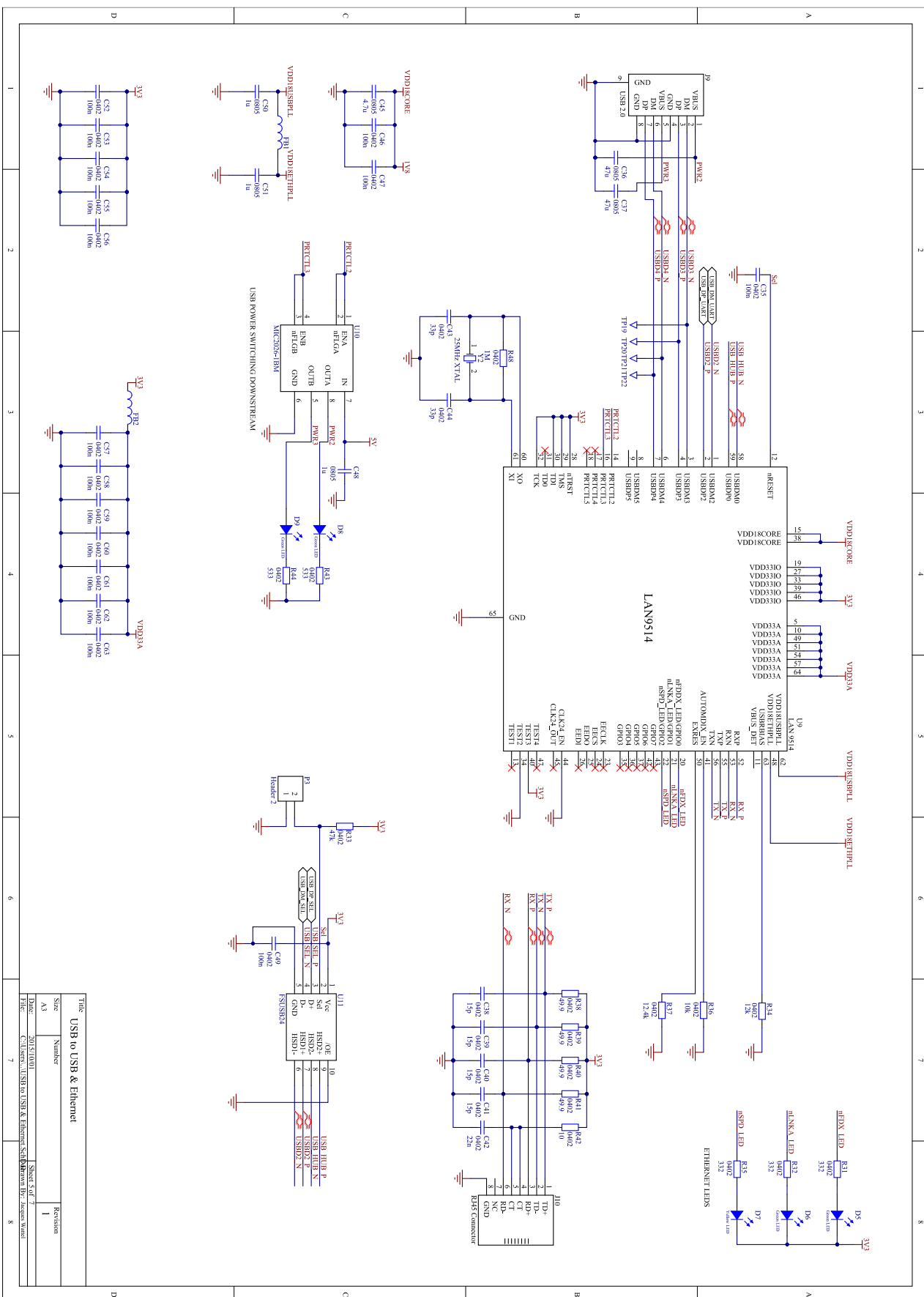


Figure 133: Data Concentrator Schematics (6 of 7)

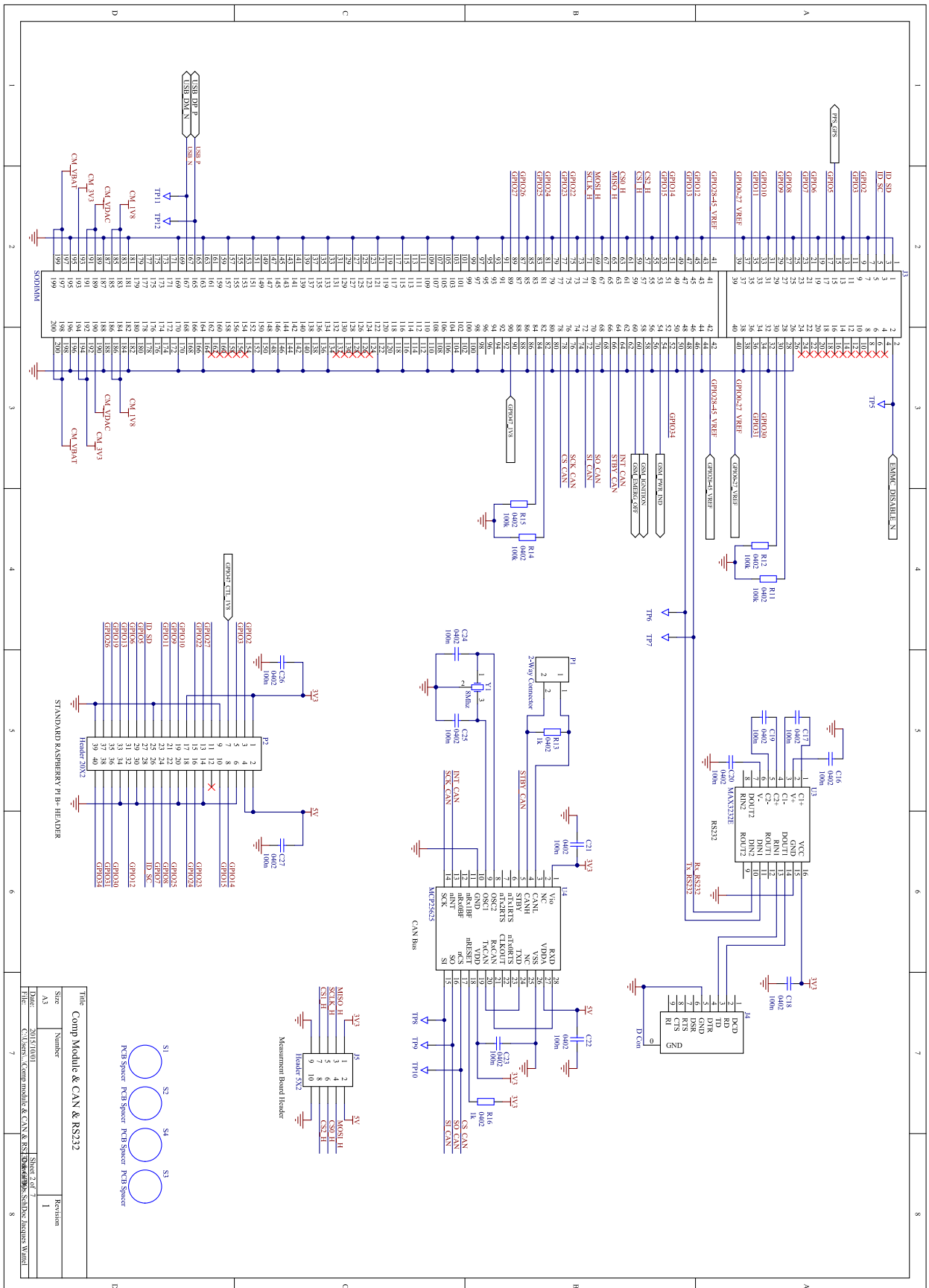


Figure 134: Data Concentrator Schematics (7 of 7)